

Electrical and Electronic Materials Science

By:

Bijay_Kumar Sharma

Electrical and Electronic Materials Science

By:

Bijay_Kumar Sharma

Online:

< <http://cnx.org/content/col11615/1.14/> >

OpenStax*CNX*

This selection and arrangement of content as a collection is copyrighted by Bijay_Kumar Sharma. It is licensed under the Creative Commons Attribution License 4.0 (<http://creativecommons.org/licenses/by/4.0/>).

Collection structure revised: May 1, 2014

PDF generated: May 1, 2014

For copyright and attribution information for the modules contained in this collection, see p. 229.

Table of Contents

1	Crystal Growth-Bulk and Epitaxial Film-Part 1	1
2	Crystal Growth-Bulk and Epitaxial Film-Part 2	9
3	Crystal Growth-Bulk and Epitaxial Film-Part 3	13
4	Crystal Growth-Bulk and Epitaxial Film-Part 4	17
5	Tutorial on Chapter 1-Crystal and Crystal Growth.	27
6	Syllabus of EC1419A_Electrical and Electronic Materials Science	35
7	Chapter 2. Solid State of Matter.	37
8	Chapter 2. Section 2.3.2. Application of Inert Gases.	53
9	Chapter 2. Solid State of Matter. Section.2.5. Bohr Model of Hydrogen Atom.	63
10	Tutorial on Chapter 2: Insulator, Semi-conductor and Metal.	75
11	SSPD_Chapter 1_Part 12_Quantum Mechanical Interpretation of Resistance	79
12	SSPD_Chapter 1_Part 11_Solid State of Matter	91
13	Chapter 3. Special Classification of Semiconductors.Sec3.1.Compund Semiconductors	101
14	Chapter 4.Light and Matter – Dielectric Behaviour of Matter	107
15	Section 4.2. Dielectric and its Physics.	119
16	Section 4.3. Dielectric Loss.	127
17	Section 4.5. Piezo-electricity and Ferro-electricity.	133
18	Chapter 5_Introduction-Nanomaterials.	139
19	Section 5.4. Nano-Size Effect on various opto-electronic-magnetic properties of nano materials.	157
20	EVEN SEMESTER2014-MidSemester Examination Answers	169
21	Chapter 5. Section 5.6. Metamaterials.	177
22	Chapter 7. Magnetic Materials.	181
23	Chapter 7. Section 7.6.3. Hysteresis Loops of Hard Iron and Soft Iron.	207
24	Chapter 8. Superconductors.	221
	Index	228
	Attributions	229

Chapter 1

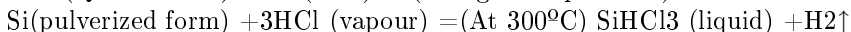
Crystal Growth-Bulk and Epitaxial Film-Part 1¹

CRYSTAL GROWTH

- (1)Preparation of polycrystalline Electronic Grade Silicon material in *Siemens Reactor*.
- (2)Bulk Crystal preparation or Pure,Electronic Grade, Single Crystal Silicon ingot preparation by *Czochralski method* and by *Float Zone Method*.
- (3)Diamond cutting of Silicon Ingot into Silicon Wafers and *lapping, polishing and chemical etching* of the Wafers to obtain mirror finished Substrates for IC preparation.
- (4)Epitaxial Film Growth-*Chemical Vapour Phase Deposition(CVD)* or *Liquid phase Epitaxy(LPE)*.
- (5)For Photonic Application , compound Semiconductor Epitaxial Film Growth is achieved by *Molecular Beam Epitaxy (MBE)*.

PREPARATION OF POLYCRYSTALLINE ELECTRONIC GRADE SILICON MATERIAL.

Quartz Sand (SiO₂) plus Coke are put in a container with submerged electrode **Arc Furnace**. Electric energy is consumed at the rate of 13 kWhr per kg and SiO₂ is reduced to Silicon by Coke. This silicon is of 98% purity. The solid silicon is pulverized and kept in an oven where Hydrogen Chloride vapour is passed at 300°C. Silicon is converted into SiHCl₃ (liquid) which is called Trichloro Silane.



¹This content is available online at <<http://cnx.org/content/m34199/1.1/>>.

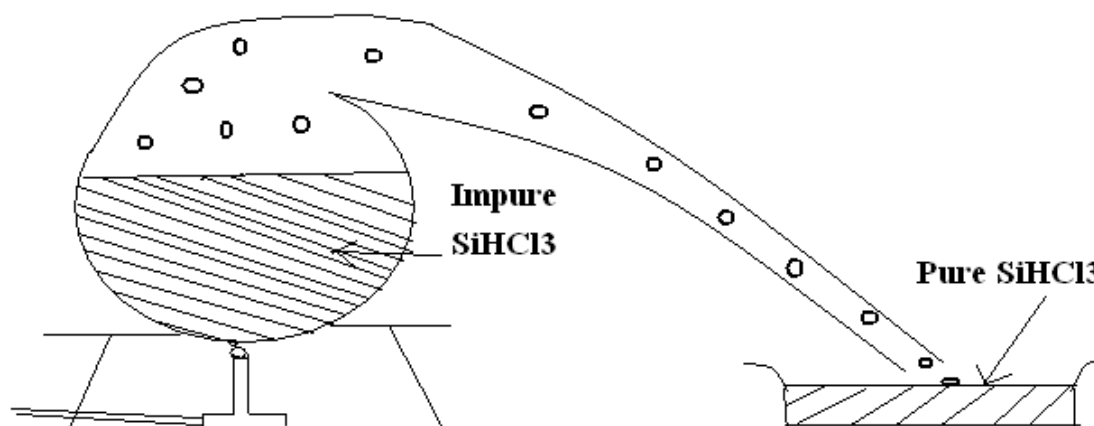
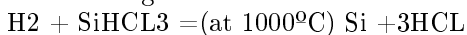


Figure 1. Multiple Distillation Set-up for preparing electronic grade TriChloroSilane.

Figure 1.1

SiHCl_3 (liquid) has B.P 31.8°C . Whereas most impurities are less volatile. Therefore by multiple distillation electronic grade TriChloroSilane is obtained which eventually is used in SIEMEN'S REACTOR.



(Hydrogen reduction)

(a form of CVD of Silicon on slim rod of Silicon on Tantalum wire)

Slim rod contains Tantalum Wire surrounded by Silicon as shown in Figure 2. Slim rod can be formed either by CVD on hot Tantalum wires or can be pulled from the melt.

(When Si deposited by CVD on hot Tantalum wires then there can be thermal runaway due to negative temperature coefficient of resistance(t.c.r) of surrounding silicon deposit dominating over positive t.c.r of the Tantalum wires. The thermal runaway has to be prevented by controlling the current.)

The resulting fattened slim rod has considerable metal contamination at the core of the rod. This can be removed by dissolving the central metallic core with acid. A Nitric/Hydrofluoric acid mixture is then pumped through the hollow core. This cleaning method widens the hollow core by removing silicon and metal contamination(1mm/hr). First nitric acid is used to dissolve the metallic core. Next Hydrofluoric acid is passed through the hollowed core to dissolve the inner layer of silicon and in the process removing the metal contamination. The fattened, purified rod of silicon thus obtained will be used as the feedstock for crystal pulling. Hydrofluoric acid is very corrosive and it can effect our bones even. Therefore Teflon gloves, Teflon Aprons, Teflon tweezers and Teflon beakers have to be used while working with HF acid.

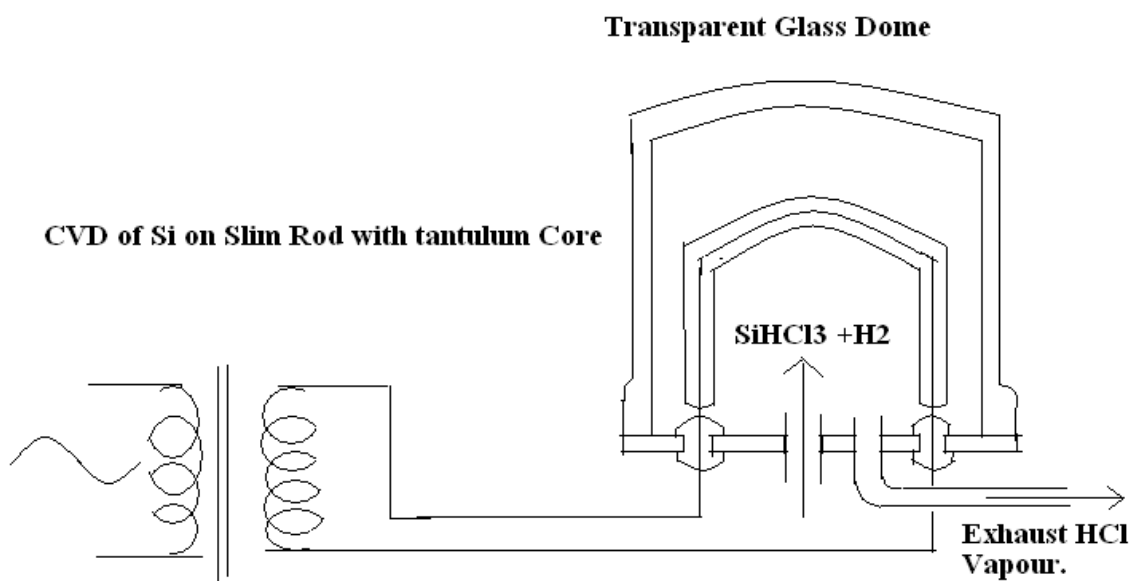


Figure 2. Siemens' Reactor for Chemical Vapour Deposition of Electronic Grade Si on Tantalum Wire Core which is heated at 1000 degree centigrade.

Figure 1.2

FLOW CHART OF SIEMEN'S REACTOR

Reduction of sand with carbon gives impure polycrystalline Silicon
↓
Reaction of pulverized raw silicon with HCl gaseous vapour to form TriChloroSilane
↓
Multiple distillation of TriChloroSilane to obtain purified electronic grade TriChloroSilane
↓
Thermal decomposition of SiHCl₃ at 1000 degree centigrade in Sieman's reactor to obtain fattened rods of electronic grade Silicon

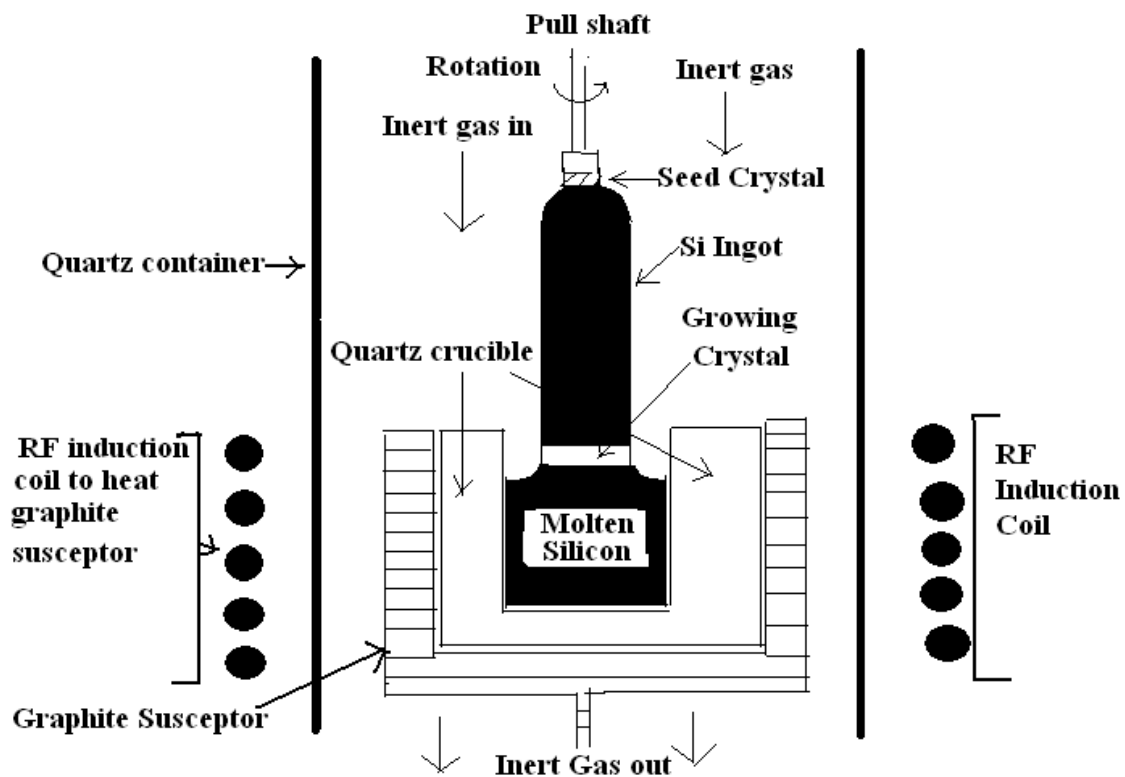


Figure 3. The schematic illustration of the growth of a single crystal Si Ingot by Czochralski Technique.

Figure 1.3

Figure 3. The schematic illustration of the growth of a single crystal Si ingot by the Czochralski technique.

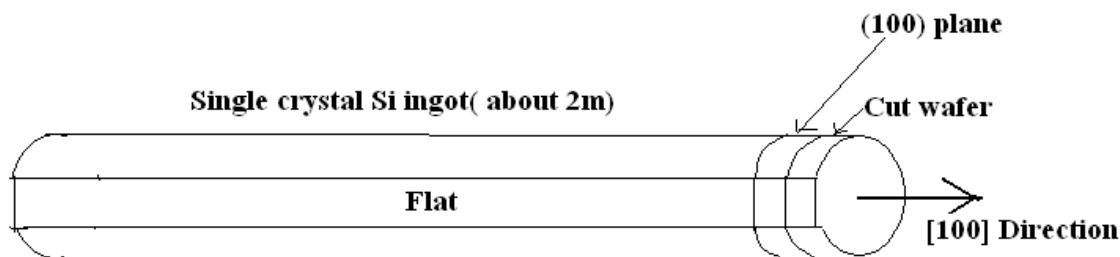


Figure 4. The crystallographic orientation of the Silicon Ingot is marked by grinding a Flat. The ingot can be as long as 2 meter. Wafers are cut using a rotating annular diamond saw. Typical wafer thickness is 0.6-0.7 mm.

Figure 1.4

The crystallographic orientation of silicon ingot is marked by grinding a flat as shown in Figure 4. The ingot can be as long as 2m. Wafers are cut using a rotating annular diamond saw. Typical wafer thickness is 0.6-0.7mm

CZOCHELSKI METHOD OF SINGLE CRYSTAL PULLING

Polycrystalline silicon is not suitable for Electronic Device preparation. Polycrystals have grain boundaries which make mobility unpredictable because of unpredictable amount of defect scattering. Grain boundaries cause uneven distribution of dopants. Along the grain boundaries there is more rapid diffusion of dopant as compared to that in the bulk. Hence we opt for single crystal silicon

Czochralski Equipment, as shown in Figure 3 and Figure 5, has a graphite lining. Graphite is of Nuclear Reactor Grade. Within the Graphite lining, Quartz crucible of high purity is placed for holding the silicon melt. Induction heating is used for maintaining the silicon melt at 1420°C. Induction heating is eddy current heating. The eddy currents are induced in the graphite lining by alternating magnetic field caused by RF induction coil. Crystal pulling is carried out in inert atmosphere of argon to prevent oxidation and to suppress evaporation.

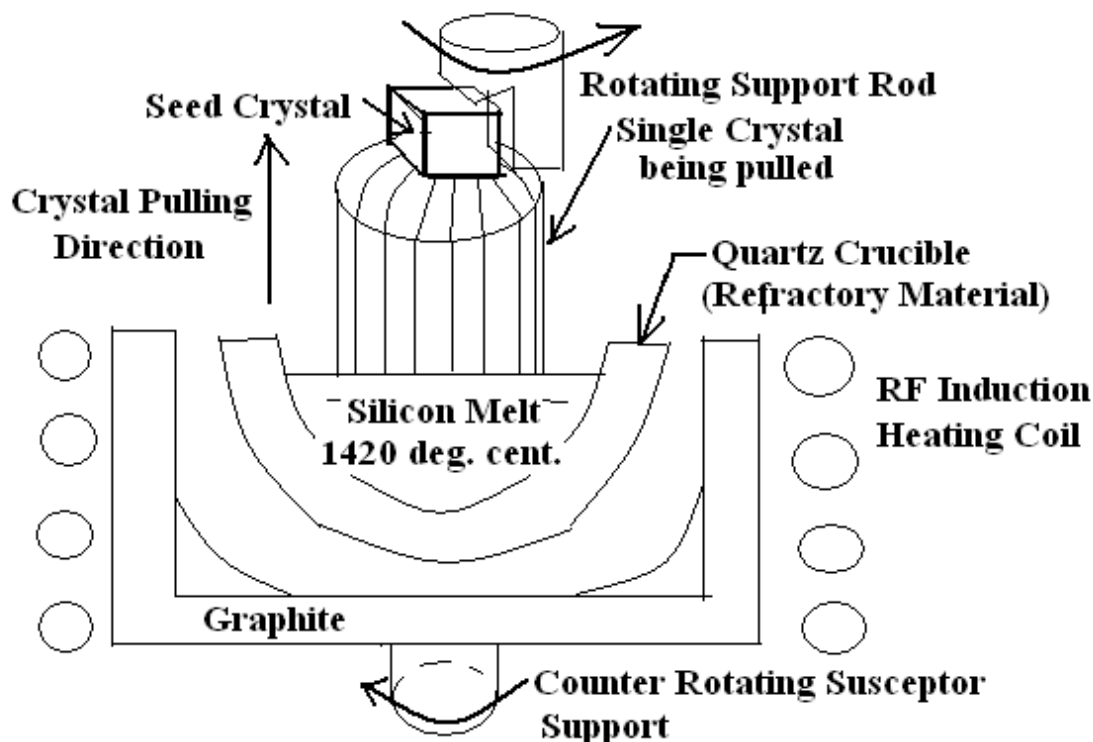


Figure 5. Czochralski Equipment.

Figure 1.5

Seed crystal determines the perfection and the orientation of the single crystal being pulled. Hence seed is dislocation free and of desired crystal orientation.

The total length of Si ingot is $L=2\text{m}$ & $\Phi =15\text{cm}, 20\text{cm}, 25\text{cm}$, Optimum pulling rate is 2 mm per min. In 24 hr period the total length of ingot is pulled. Silicon being highly refractive (m.p.1410 c) is highly contaminable. The Quartz of the containment vessel undergoes dissolution into Si during its growth. The result is the inclusion of O₂ as a donor impurity into Silicon. Carbon is another impurity that finds its way into Silicon. These contaminants are particularly harmful for powerful devices.

Counter rotation and rotation are produced to provide uniformity, homogeneity of thermal effects and dopants. This minimizes the defects also.

In spite of these homogenizing effects there are swirl effect which lead to non-uniform distribution of desired and undesired contaminants. This leads to non-uniform resistivity distribution across a silicon wafer. The spatial variation is such that these non-uniformities are not particularly important in I.C. or in miniature devices. However in power devices, which are large area devices, local variation in doping can lead to non-uniform heating and hence to hot spots and failures. For example 3" diameter Thyristor carries 3000 amps. Even one defect per slice will be catastrophic to such a device but is inconsequential to I.C. Fabrication.

This implies that for applications in which contaminants are critical, crystal, wafers produced by CZOCHRALSKI METHOD are not suitable.

One way to avoid the contaminants is to be avoid contact with quartz crucible. This is achieved by FLOAT ZONE METHOD of Crystal Growth.

FLOAT ZONE METHOD OF CRYSTAL GROWTH

An electronic grade , pure polycrystalline silicon rod is held vertically as shown in Figure 6 in inert atmosphere .thus no crucible is used and hence contaminations are avoided.

A seed crystal is held at the bottom of the rod to determine the crystallographic orientation

Through R.F induction heating a narrow zone of vertical, purified, poly crystalline bar is melted. Dimensions of the molten zone are such that surface tension hold it in place. Because of less than unity segregation coefficient , $a(m)=(\text{concentration } M \text{ in solid phase})/(\text{concentration of } m \text{ in liquid phase})$, impurities prefer to stay in liquid phase.

As the R.F. coil is sifted from bottom to top , the impurities of the region are swept to the top and the recrystallized portion is relatively pure and single crystalline with orientation that of seed crystal. If high purity is required then several passes can be made and ends containing impurities can be sliced off leaving behind very pure single crystal silicon ingot. Pure crystal of very high resistivity can be achieved by repeated recrystallization through several passes.

Table 1. Segregation Coefficient for different dopents in different hosts.

Semiconductor	N Type	P type
Silicon	$a(\text{P}) = 0.35$, $a(\text{As}) = 0.3$	$a(\text{B}) = 0.8$
Gallium Arsenide	$a(\text{Se}) = 0.10$	$a(\text{Zn}) = 0.42$

Table 1.1

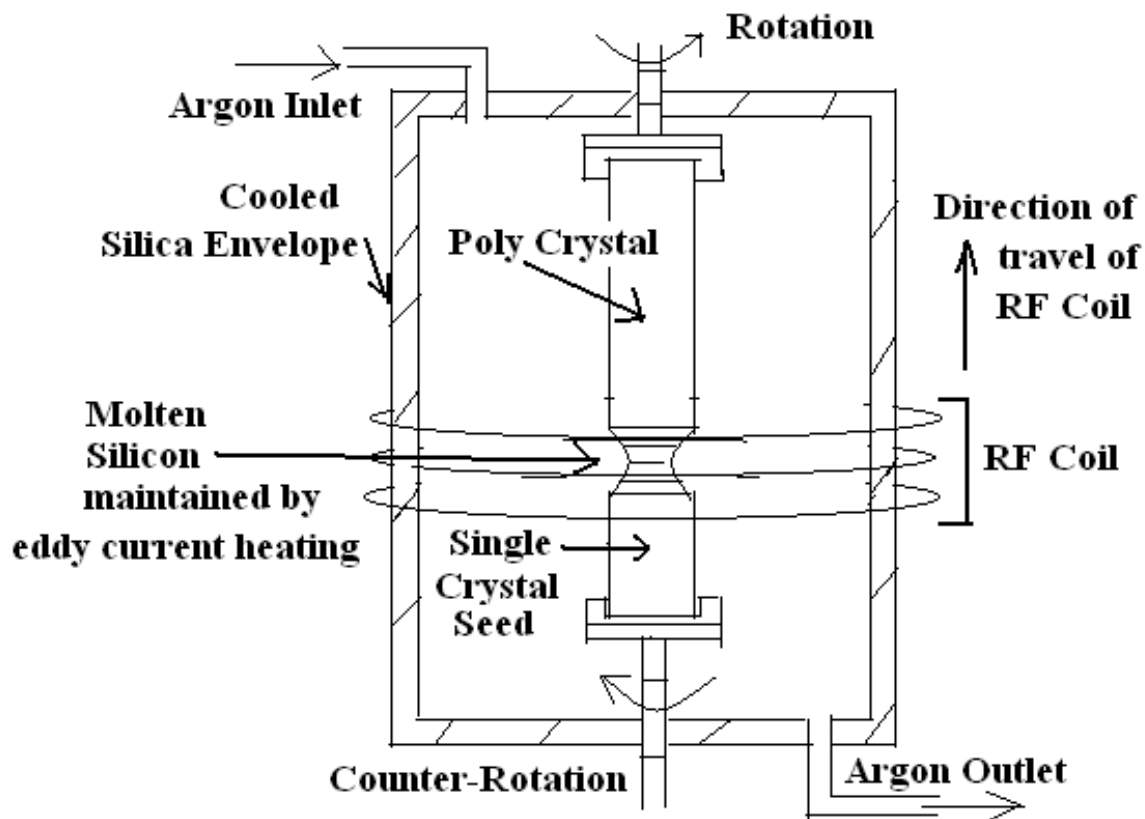


Figure 6. Float Zone Method of Crystal Growth.

Figure 1.6

Chapter 2

Crystal Growth-Bulk and Epitaxial Film-Part 2¹

Crystal Growth- Bulk and Epitaxial Film- Part2.

SLICING OF SINGLE CRYSTAL INGOT INTO SILICON WAFERS

Slicing of the Si ingot into Si wafers is achieved by circular saw blade. The circular saw blade is illustrated in Figure 7.

¹This content is available online at <<http://cnx.org/content/m34200/1.2/>>.

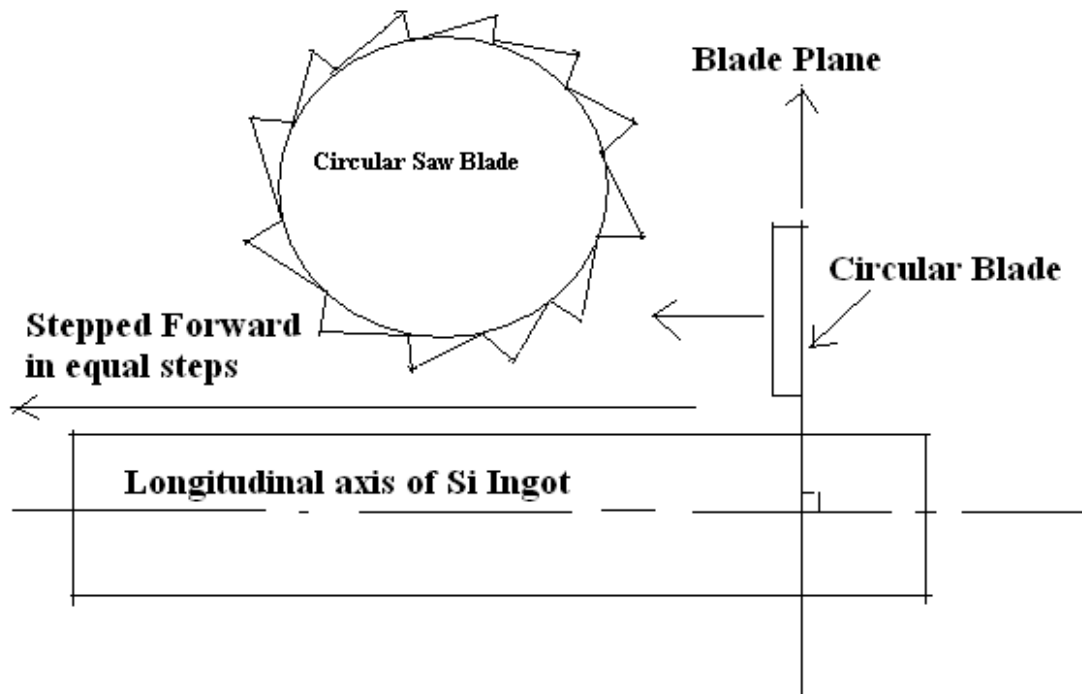
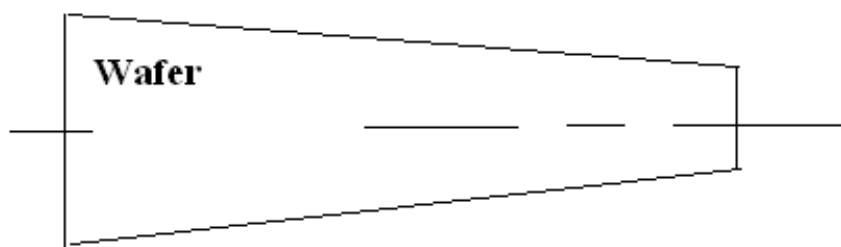


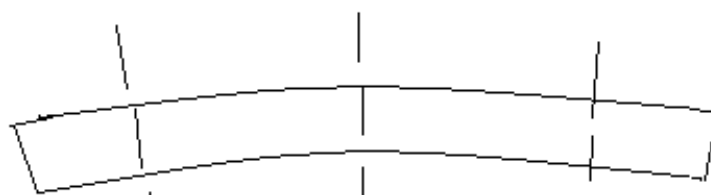
Figure 7. Circular Saw Blade with diamond impregnation. Saw Blade must be kept perpendicular to the longitudinal axis of the ingot to avoid taper in the wafer.

Figure 2.1

Circular saw blade consists of stainless steel impregnated with diamond dust at the cutting edge. On the hardness scale diamond is the hardest. 500 micrometres thick Si wafers are sliced out through damage free and parallel sawing. The ingot should be sawed in parallel planes to avoid taper of the wafer.



Non-uniform thickness of the wafer gives rise to TAPER defect



By BOW or CURVATURE of Wafer , flatness is effected.

Figure 8. TAPER & FLATNESS of Wafer

Figure 2.2

In the process of sawing , mechanical, defects are inevitable. To remove the mechanical defects and to achieve taper-free, flat, mirror finish wafers we do lapping, chemical etching and polishing.

LAPPING: For removing mechanical scratches and abrasions encountered during sawing, lapping is essential. A batch of wafers are placed between two parallel plain steel discs which describe planetary motion in relation to each other. A slurry of cutting compound (generally alumina) is used and as lapping progresses, the grade of abrasion is refined. Smoothness is within $10\ \mu\text{m}$ and flatness is within $2\ \mu\text{m}$.

CHEMICAL ETICHING: To remove edge damages which had been caused due to sawing and grinding, the wafers is dipped in HF acid using Teflon beakers. Chemical Vapor etching can also be done as described in epitaxy section.

POLISHING: A slurry of silica in NaOH is used for polishing to mirror smoothness. Lapping , Chemical Etching and Polishing removes $100\ \mu\text{m}$ thick substrate leaving behind $400\ \mu\text{m}$ thick silicon substrate on which I.C. Fabrication can be carried out..

FLOW CHART OF WAFER PREPARATION

Starting Material - Sand, Sand reduced to Silicon, Silicon converted to TriChloroSilane, through multiple distillation TrichloroSilane is purified to Electronic Grade and reduced in Siemen's Reactor to Pure Electronic Grade Polycrystalline Si.

↓

From purified Silicon Melt, single crystal ingot is pulled out by Czochralski Method or Poly Si ingot is purified re-crystallized by Float Zone Method. Required Dopant (Phosphorous for N Type ingot and Boron for P Type ingot) is added to the melt in calculated manner to form single crystal ingot of specific impurity type doping and of given resistivity.

↓
Sawing, Lapping, Grinding and Polishing
↓

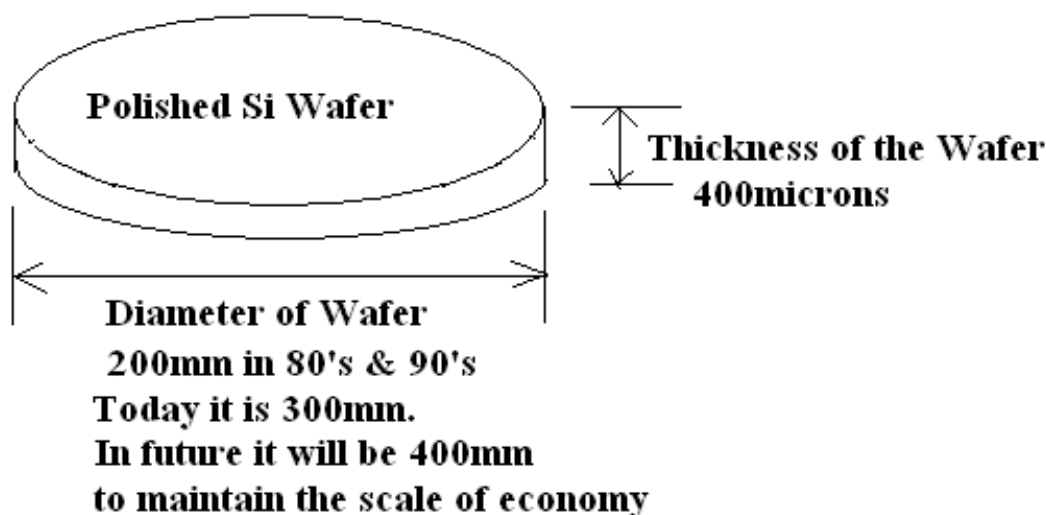


Figure 2.3

In early days when IC Technology had just started i.e. in the year 1961 the wafer size was only 1 inch. Then it was: * 2 inch (50.8 mm). Thickness 275 μm . * 3 inch (76.2 mm). Thickness 375 μm . * 4 inch (100 mm). Thickness 525 μm . * 5 inch (127 mm) or 125 mm (4.9 inch). Thickness 625 μm . * 150 mm (5.9 inch, usually referred to as "6 inch"). Thickness 675 μm . * 200 mm (7.9 inch, usually referred to as "8 inch"). Thickness 725 μm . * 300 mm (11.8 inch, usually referred to as "12 inch" or "Pizza size" wafer). Thickness 775 μm . * 450 mm ("18 inch"). Thickness 925 μm (expected). By all these technique , high purity (99.999%) single crystal ingots with a controlled amount of N or P type dopant can be produced. The maximum resistivity obtained in Si ingot is $10^4 \Omega\text{-cm}$ whereas in Ga As and InP the $\rho_{\text{max}} = 10^8 \Omega\text{-cm}$. That is almost semi-insulating ingot of GaAs and InP can be obtained. Semi-insulating GaAs and InP wafers are suitable for reduction of parasitics, for isolation of active devices from one another, for reduction of power drain and for achieving high speed.

Presently because of technical constraints we have the option of Si, GaAs and InP substrate only. Therefore we have a very limited choice of overlay films also. This severely constrains the photonic device design.

Chapter 3

Crystal Growth-Bulk and Epitaxial Film-Part 3¹

CRYSTAL GROWTH

Silicon, (Si):The most common semiconductor, atomic number 14, energy gap $E_g = 1.12$ eV- indirect bandgap; crystal structure- diamond, lattice constant 0.357 nm, atomic concentration 5×10^{22} atoms/cm³, index of refraction 3.42, density 2.33 g/cm³, dielectric constant 11.7, intrinsic carrier concentration 1.02×10^{10} cm⁻³, bulk mobility of electrons and holes at 300 °K: 1450 and 500 cm²/V-s, thermal conductivity 1.31 W/cm °C, thermal expansion coefficient 2.6×10^{-6} °C⁻¹, melting point 1414 °C; excellent mechanical properties (MEMS applications); single crystal Si can be processed into wafers up to 300mm in diameter. In future this diameter will be 450mm.

P type= Always Boron (B) Doped N type= Dopant typically as follows:Res: .001-.005 Arsenic (As)Res: .005-.025 Antimony (Sb)Res: >.1 Phosphorous (P)

EPITAXIAL CRYSTAL GROWTH

The substrate or the wafer only constitutes the strong base of the integrated circuit. The actual active and passive components fabrication and there integration are carried out in overlay films which are grown by epitaxial technique.

EPITAXY is a Greek word meaning : ‘epi’ (upon) & ‘taxy’ (ordered). That is an epitaxial film, a few μm thick, is an orderly continuation of the substrate crystal. It grows very slowly layer by layer. Hence the dimension , defects and doping magnitude as well as uniformity can be precisely and accurately controlled in the crystal growth direction.

This precise control is obtained in Molecular Beam Epitaxy (MBE) but not in Liquid Phase Epitaxy(LPE) or in Chemical Vapour Phase Epitaxy (CVPE). The thickness accuracy is within $\pm 3\text{\AA}$ which is essential for growing Quantum Photonic Devices namely Quantum Dots, Quantum Wells and Super-lattices

¹This content is available online at <<http://cnx.org/content/m34202/1.4/>>.

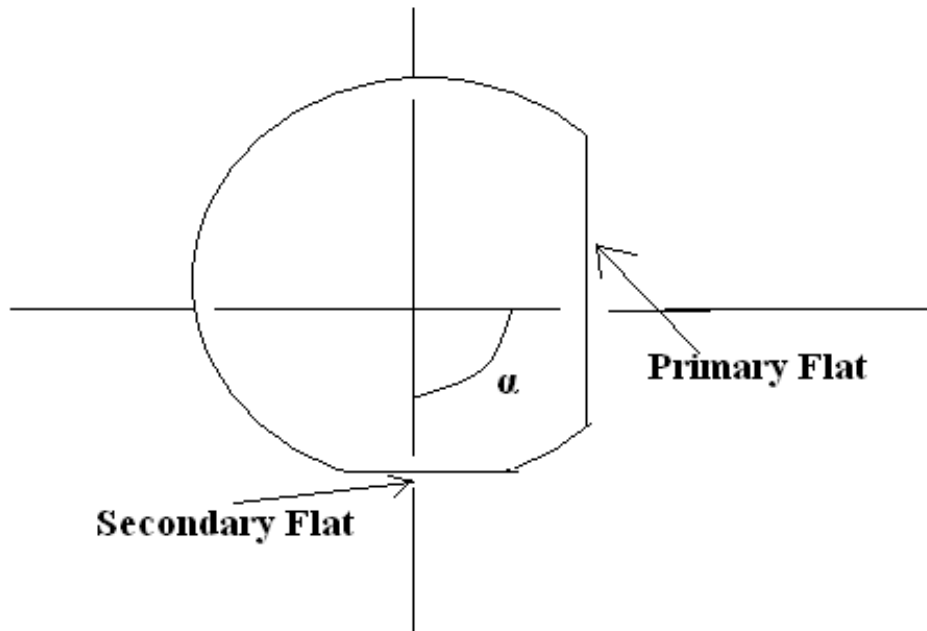


Figure 9 Silicon Wafer Identity Marks.

Figure 3.1

Table 2. Identity marks of the Wafer to identify its orientation and semiconductor type.

α (angle between primary and secondary flats as indicated in Figure 9)	Type	Orientation
45°	N	$\langle 111 \rangle$
90°	P	$\langle 100 \rangle$
180°	N	$\langle 100 \rangle$
0°	P	$\langle 111 \rangle$

Table 3.1

The normal to the plane along which crystals cleaves is the cleavage plane orientation. Suppose the cleavage plane orientation is $\langle 111 \rangle$. Miller Index is being used to define the planes and their normal. Figure 10 illustrates the Plane's Miller Index and how the normal to the plane is represented. If the exposed surface of the Si wafer, which is known as major flat, is parallel to cleavage plane then the given wafer has a crystal orientation $\langle 111 \rangle$.

If the cleavage plane orientation is $\langle 100 \rangle$ and the wafer major flat is parallel to YZ plane then the crystal orientation is $\langle 100 \rangle$. In this case cleavage plane lies in YZ plane i.e. $[100]$ plane and its orientation is perpendicular to YZ plane i.e. x-axis. Hence Wafer Crystal Plane orientation is $\langle 100 \rangle$

Scribing the wafer along cleavage planes allows it to be easily diced into individual chips ("die") so that billions of individual circuits or systems on an average wafer can be separated into individual dies. Each individual die is eutectic ally bonded on ceramic substrate. The substrate is bonded to the header. The gold wire is connected to the bonding pads of the die on one end and to the chip terminals on the header by Thermo-compression bonding or by Ultra-sonic bonding. Next the die is hermetically sealed into Dual-in-Line(DIP) package or TO5 package

In $\langle 100 \rangle$ crystal orientation, scribed pieces form rectangle whereas in $\langle 111 \rangle$ crystal orientation, scribed pieces form triangles. Here we have to scribe from the base of the triangle to the apex.

For MOS fabrications, wafers with crystal orientation $\langle 100 \rangle$ are used. This helps achieve a lower threshold voltage. For BJT and other applications wafers with orientation $\langle 111 \rangle$ are preferred.

Silicon Crystal Bulk is isotropic to diffusion of dopants and to etchants used for etching the oxide layer. This is because of the symmetric property of Cubic Structure of Si. But real devices are built near the surface hence the orientation of the crystal does matter.

In 111 crystal terminates on 111 plane and in 100 it terminates on 100 plane. 111 plane has largest number of Si atoms per cm^2 whereas 100 has the least number of atoms per cm^2 . Because of this difference 111 planes oxidize much faster because the oxidation rate is proportional to the Silicon atoms available for reaction.

But because the atom surface density is the highest the dangling bond surface density is also the highest in 111 hence Si/SiO₂ has superior electrical properties in terms of interface states in 100. Interface states give rise to 1/f noise or flicker noise. Because of this superiority all MOS devices use 100 crystal orientation. But historically BJT have used 111 because 111 crystal growth is easier to grow by Czochralski method. But as we move to sub-micron and deep and ultra-deep sub-micron BJT, 100 crystal orientation seems to be the crystal orientation of choice for BJT also.

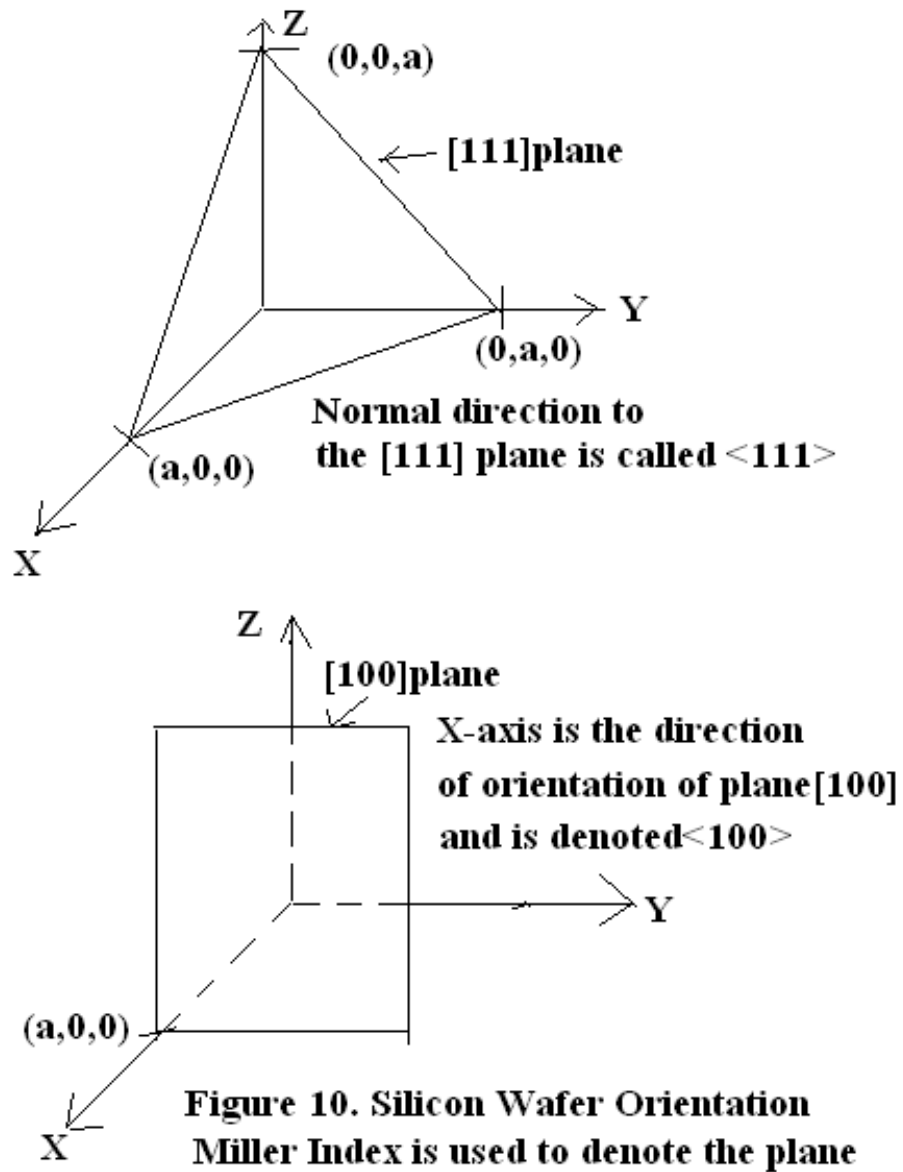


Figure 3.2

Chapter 4

Crystal Growth-Bulk and Epitaxial Film-Part 4¹

Crystal Growth-Bulk and Epitaxial Film_Part 4

EPITAXIAL FILM GROWTH.

There are two major epitaxial film growth technologies:

Silicon Epitaxial Film Growth Technology (Low End Technology hence economical) and Compound Semiconductor Epitaxial Film Growth Technology (High End Technology hence expensive and suitable for niche applications).

Silicon Epitaxial Film Growth Technology are further divided into:

Chemical Vapour Phase Deposition(CVPD) Technology and Liquid Phase Epitaxy(LPE). LPE is relatively cheaper but very toxic.

Compound Semiconductor Epitaxial Film Growth is achieved by Molecular Beam Epitaxy System which is inordinately expensive and in India in a few places only we have MBE systems namely TIFR(Mumbai), Solid State Physics Laboratory(Delhi), Central Electronics Engineering Research Institute (Pilani), IIT(Madras) and CSIO(Chandigarh).

In Table 3 we make a comparative study of LPE, CVPD and MBE. Molecular Beam Epitaxy is carried out under Ultra High Vacuum Conditions. This means we are working at 10^{-10} Torr where 1 Torr is 1mm of Hg. For achieving Ultra High Vacuum we have to work in three stages: Rotary Pump is used for achieving 10^{-3} Torr. Silicon Oil Vapour Pump is used to achieve 10^{-5} Torr and Ion Pump is used to achieve Ultra High Vacuum of 10^{-10} Torr. This ultra high vacuum requirement makes MBE equipment inordinately expensive. This equipment is imperative for Photonic Devices.

CHEMICAL VAPOUR PHASE DEPOSITION(CVPD) OF EPITAXIAL FILMS or Chemical Vapour Phase Epitaxy(CVPE).

In Figure 11 , we describe CVPD system for obtaining Si Epitaxial Films. A controlled chemical vapour of precise chemical composition at a precisely controlled flow rate is passed over silicon substrates. Si Substrates act as the seed crystals. They are kept at precisely controlled temperature of 1270°C by RF induction heating hence they are placed on Graphite Susceptors. This gives a precise control of Si molecules, in vapour phase of partial pressure P, impinging upon Si Substrate:

(Impingement Rate) F =

¹This content is available online at <<http://cnx.org/content/m34203/1.1/>>.

$$F = \frac{P}{\sqrt{(2\pi mkT)}} = \left[\frac{3.5 \times 10^{22} P(\text{Torr})}{\sqrt{m(\text{gm}) T(\text{Kelvin})}} \right]$$

Figure 4.1

$$\frac{\text{molecules}}{\text{cm}^2 \text{-sec}}$$

Figure 4.2

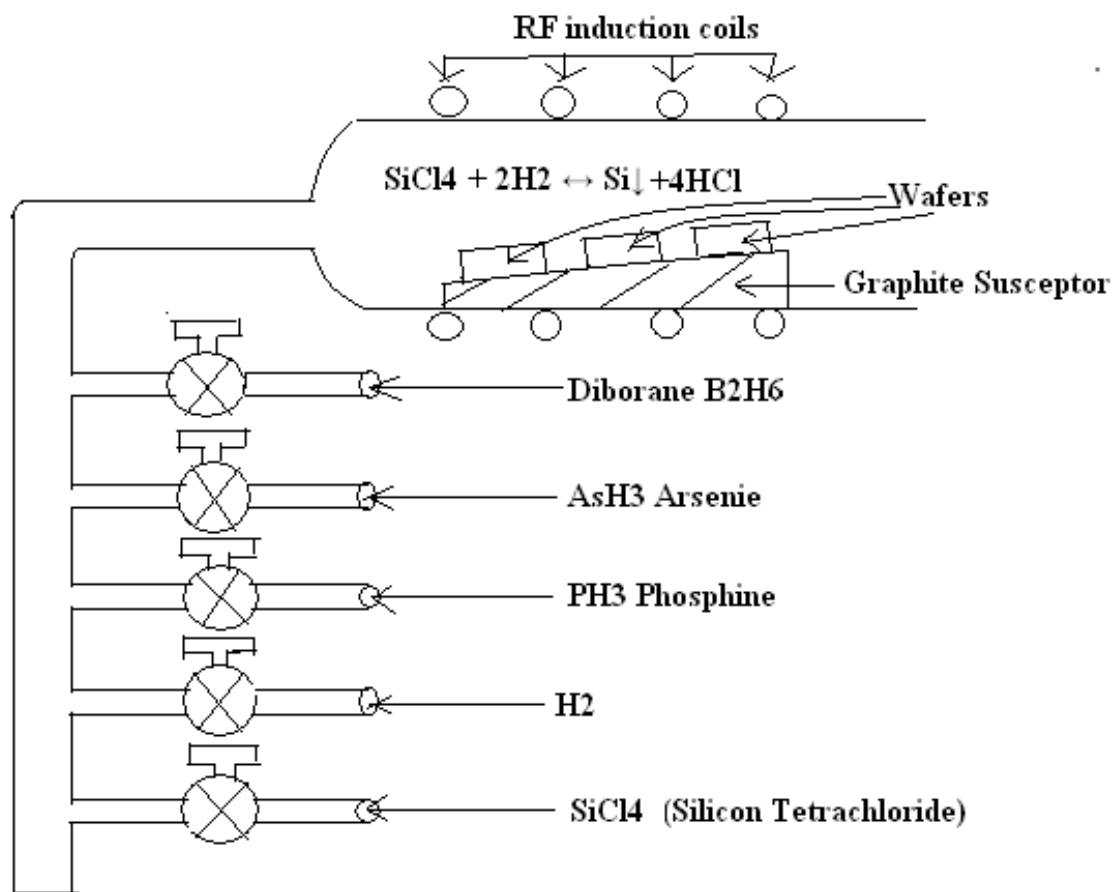


Figure 11. Chemical Vapour Phase Epitaxy for growing epitaxial films of Silicon.

Figure 4.3

Table 3. Comparative study of LPE, CVPD and MBE

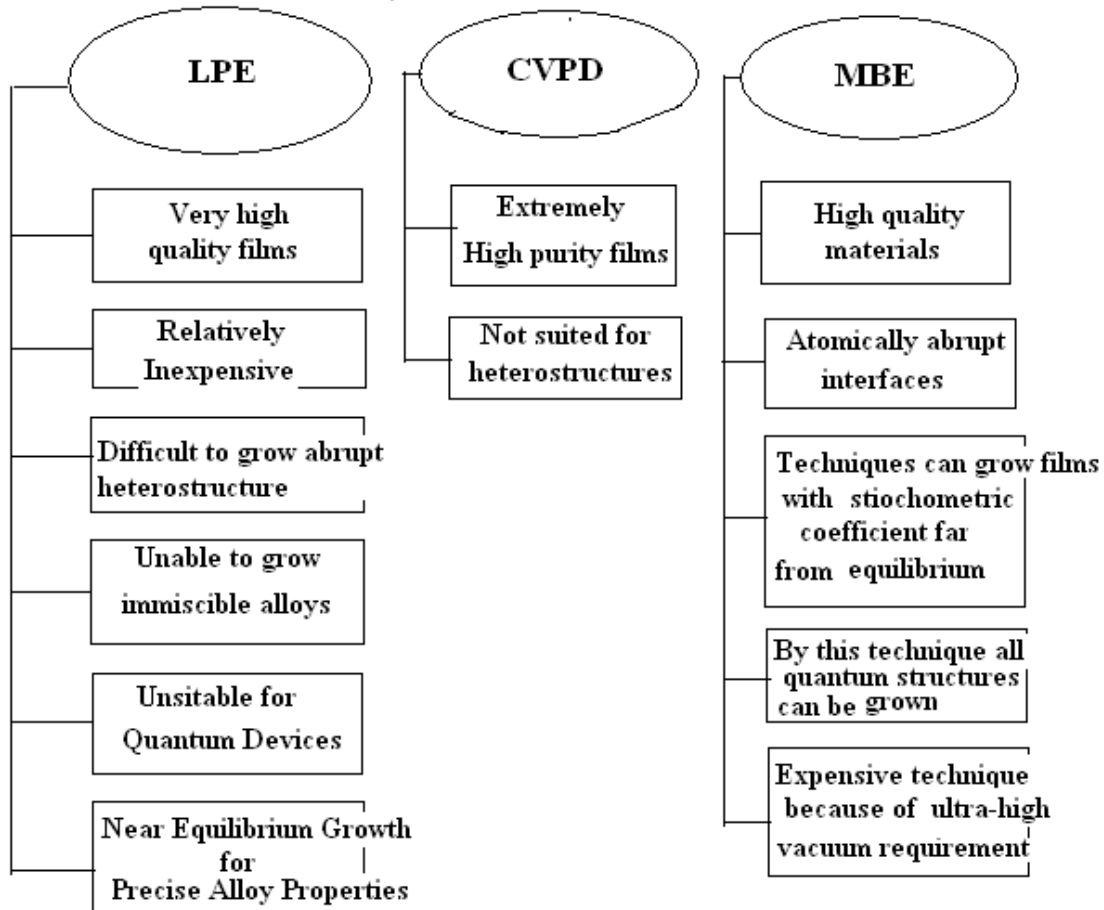
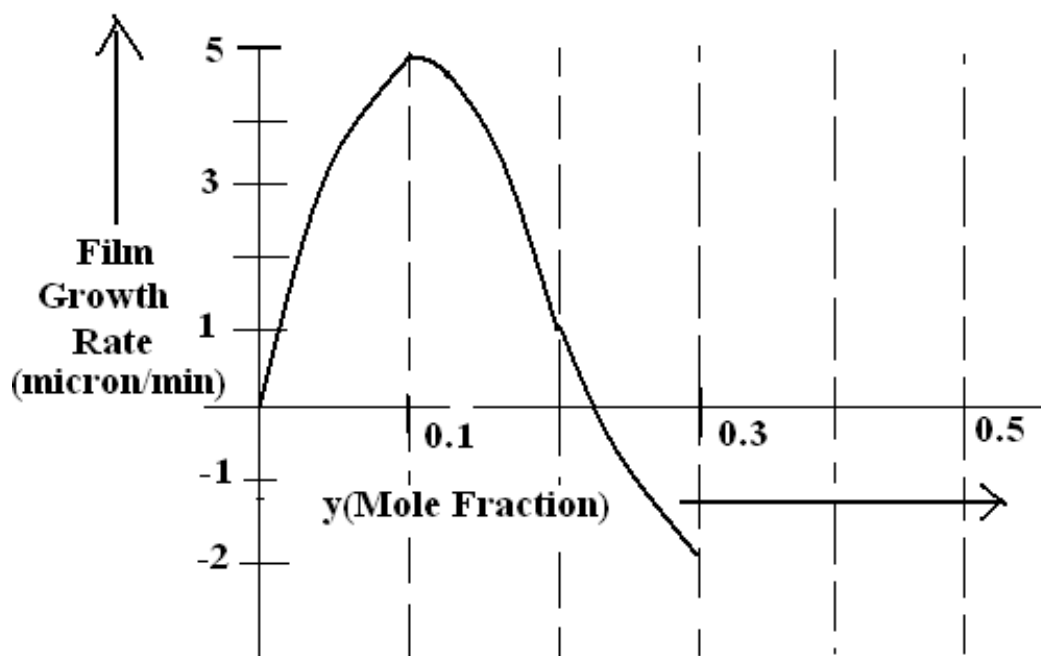


Figure 4.4

CPVD is suitable for Homo-epitaxy but not for hetero-epitaxy. The byproduct of this reaction is HCl as seen from the chemical equation of reaction:



This byproduct HCl can attack the Silicon Substrate and cause chemical etching. Hence Chemical Reaction as depicted Eq.(1) is reversible.



Graph 1. Film growth rate vs y(Mole Fraction)

Figure 4.5

If y (mole fraction = SiCl_4 conc./Total conc) is greater than 0.23 as seen from Graph 1, growth rate is negative. This means chemical etching of Silicon Wafer. The negative growth rate is used for in-situ cleaning of Silicon Wafers. This is one of the ways of chemical etching while preparing Silicon Wafers from Silicon Ingot.

If $y < 0.23$ we have positive growth rate and Si vapour deposition takes place as an epitaxial film. The growth rate is maximum at $y = 0.1$. The maximum growth rate is $5\mu\text{m}/\text{minute}$.

Since CVPD is carried out at 1270°C , there is the problem of out-diffusion of Arsenic from the substrate into the epitaxial layer. Arsenic is used as buried layer to reduce the series collector resistance of Vertical NPN transistor. Arsenic has very low diffusion coefficient still at the elevated temperature of 1270°C , some out-diffusion is inevitable. To prevent this out-diffusion altogether, we use Liquid Phase Epitaxy which is shown in Figure 12.

LIQUID PHASE EPITAXY.

The Liquid Phase Epitaxy set up is shown in Figure 12. This is carried out at 900°C hence the problem of out-diffusion is completely prevented but Silane which is used for LPE is highly toxic. As seen in Figure 12, there is a super saturated solution of Silane kept at 900°C . By Graphite Slider, the silicon substrate is brought directly underneath the well containing Silane. As Substrate comes in contact with Silane, latter is dissociated into Silicon and Hydrogen and Silicon precipitates onto the substrate forming an epitaxial film on the substrate.

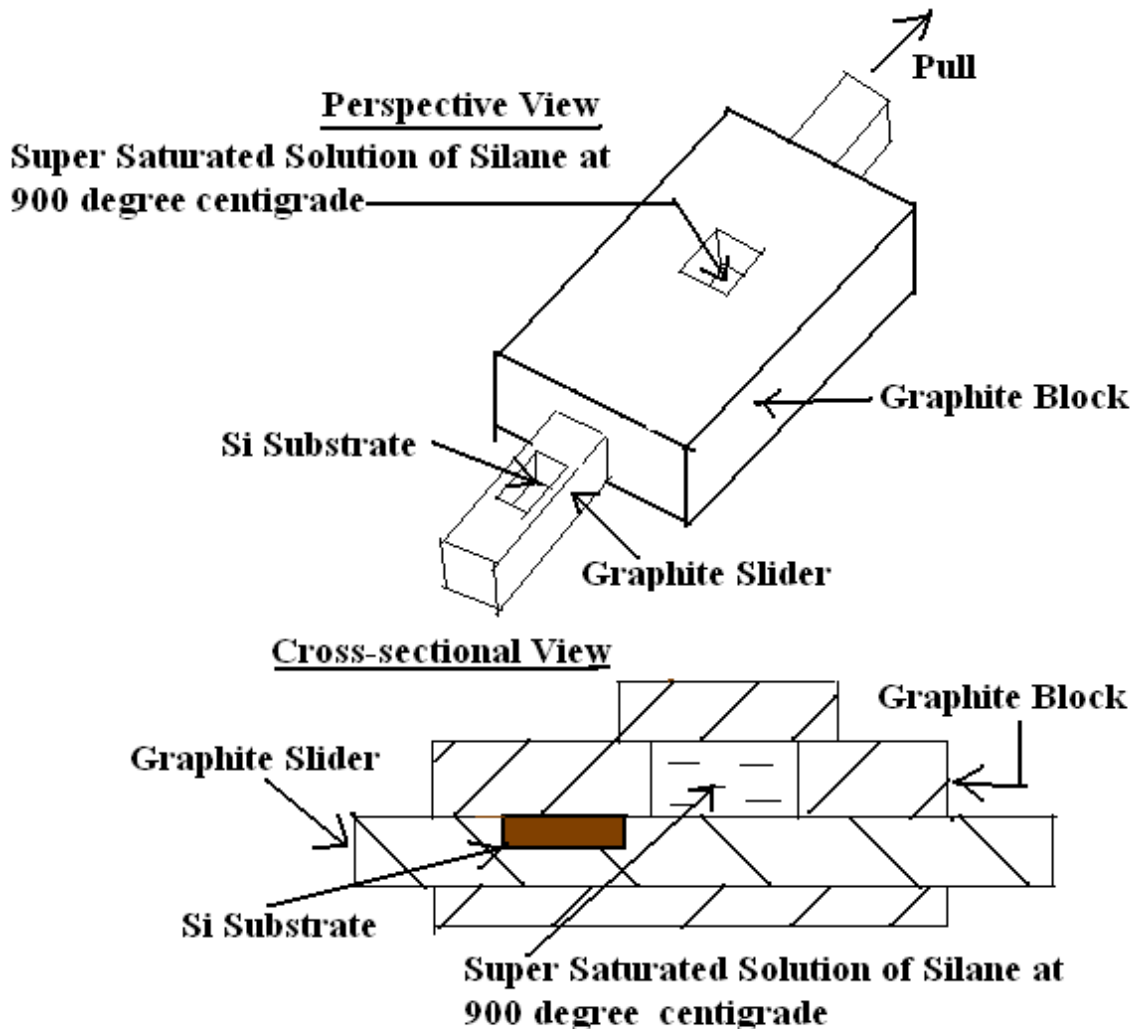


Figure 12. Liquid Phase Epitaxy Setup.

Figure 4.6

MOLECULAR BEAM EPITAXY

Due to explosive demand of Wireless Communication Equipment there has been a sudden spurt in demand of MBE equipments particularly of multiple wafer MBE equipment which can give a high throughput of epitaxially prepared wafers.

There are two kinds of epitaxial film growth: **Homoepitaxy** (same composition) and **Heteroepitaxy** (different composition). By Molecular Beam Epitaxy, multi-layered thin films of single crystals of different compositions and of atomic dimension can be grown. In effect we can achieve heteroepitaxy which is the hallmark of compound semiconductor devices such as Photonic Devices and GaAs MESFET.

MBE is a process for making compound semiconductor materials with great precision and purity. These

materials are layered one on top of the other to form semiconductor devices such as transistors and lasers. These devices are used in such applications as fiber-optics, cellular phones, satellites, radar systems, and display devices. MBE is used for fabrication of Super-lattices and hetero-junction MESFET. Super lattices are periodic structures of alternating Ultra-thin layers of compound semiconductor.

MBE growth produces complex structures of varying layers which are further processed to produce a range of electronic and optoelectronic devices, including high speed transistors, light-emitting diodes, and solid state lasers. MBE is a powerful technique both for research into new materials and layer structures, and for producing high-performance devices.

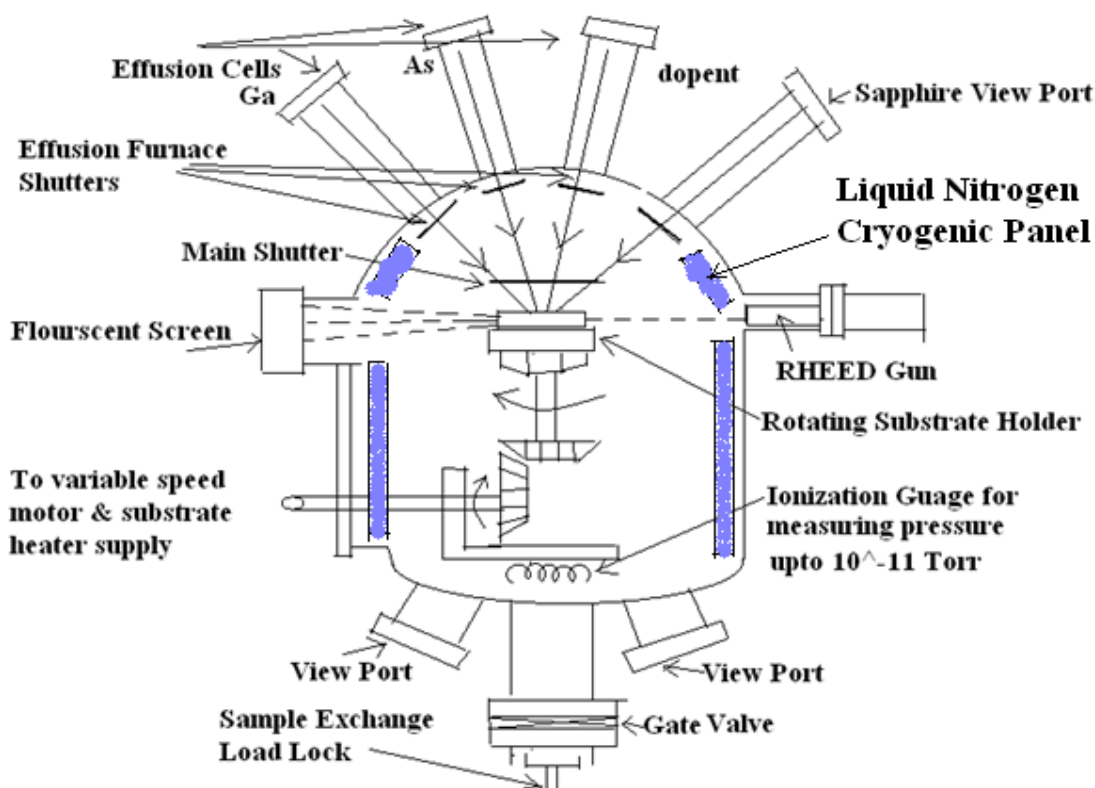


Figure 13. Molecular Beam Epitaxy Set Up.

Figure 4.7

Referring to Figure 13:

The walls of the chamber cooled with liquid nitrogen. This cryogenic screening around the substrate minimizes the spurious flux of contaminating atoms and

Sample Exchange Load Lock-this permits maintenance of Ultra High Vacuum while changing the substrate.

Effusion Cells- this contains the solid source to be evaporated and deposited on the substrate. Temperature of the effusion oven is adjusted to give desired evaporation rate.

Rotating Substrate Holder- rotation of substrate ensures less than $\pm 1\%$ doping variation and $\pm 0.5\%$ in thickness variation.

RHEED Gun-Reflection High Energy Electron Diffraction Gun gives a beam of electron which can be made incident on the epitaxially grown film. The diffraction pattern of electrons is studied on the fluorescent screen. This shows a maximum when there is a completed monolayer and a minimum when there is a partial layer as this produces more scattering. Thus RHEED Gun is used for in-situ monitoring of the growth of the epitaxial film mono-layer by mono-layer.

Computer controlled shutters of each furnace allows precise control of the thickness of each layer, down to a single layer of atoms.

Substrate Heating- to obtain high quality epitaxial layer, growth temperature must be relatively high. The substrate wafer must be heated to allow the atoms to move about the surface and reach the proper ordered site. Growth must be at a temperature where growth rate is insensitive of minor temperature variation. Atoms arriving at the substrate surface may undergo absorption to the surface, surface migration, incorporation into the crystal lattice, and thermal desorption. Which of the competing pathways dominates the growth will depend strongly on the temperature of the substrate. At a low temperature, atoms will stick where they land without arranging properly - leading to poor crystal quality. At a high temperature, atoms will desorb (reevaporate) from the surface too readily - leading to low growth rates and poor crystal quality. In the appropriate intermediate temperature range, the atoms will have sufficient energy to move to the proper position on the surface and be incorporated into the growing crystal.

The Inventors of MBE are : J.R. Arthur and Alfred Y. Chuo (Bell Labs, 1960).

MBE is a technique for epitaxial growth of single crystal atomic layer films on single crystal substrate. It gives precise control in chemical composition and doping profiles. To avoid contamination of the epitaxial films, Ultra High Vacuum within MBE chamber is imperative. It requires Very/Ultra high vacuum (10^{-8} Pa or 10^{-11} Torr). This implies that Epitaxial film is grown at slow deposition rate (1 micron/hour). This permits epitaxial growth of single atomic layer if desired. Slow deposition rates require proportionally better vacuum. Ultra-pure elements are heated in separate quasi-knudson effusion cells (e.g., Ga and As) until they begin to slowly sublimate. Gaseous elements then condense on the wafer, where they may react with each other (e.g., GaAs). The term "beam" in MBE means the evaporated atoms do not interact with each other or with other vacuum chamber gases until they reach the wafer. Each gas beam may be turned on and off rapidly with a shutter or a valve. Beam intensity (called the flux) is adjusted for precise control of layer composition. A collection of gas molecules moving in the same direction constitute the molecular beam. Simplest way to generate a molecular beam is Effusion cell or Knudsen cell . Oven contains the material to make the beam. Oven is connected to a vacuum system through a hole. The substrate is located with a line-of-sight to the oven aperture. From kinetic theory, the flow through the aperture is simply the molecular impingement rate on the area of the orifice. Impingement rate is: The total flux through the hole. The spatial distribution of molecules from the orifice of a knudsen cell is normally a cosine distribution. The intensity drops off as the square of the distance from the orifice. Intensity is maximum in the direction normal to the orifice and decreases with increasing θ , which causes problems. Use collimator, a barrier with a small hole; it intercepts all of the flow except for that traveling towards the sample.

During the MBE process, growth can be monitored in situ by a number of methods:

Reflection high energy electron diffraction (RHEED), using forward scattering at grazing angle, which shows a maximum when there is a completed monolayer and a minimum when there is a partial layer as this produces more scattering;

Low energy electron diffraction (LEED), takes place in backscattering geometry and can be used to study surface morphology, but not during growth;

Auger electron spectroscopy (AES), records the type of atoms present;

Modulated beam mass spectrometry (MBMS), allows the chemical species and reaction kinetics to be studied.

Computer controlled shutters of each furnace allows precise control of the thickness of each layer, down to a single layer of atoms.

Intricate structures of layers of different materials can be fabricated this way e.g., semiconductor lasers, LEDs.

Before starting the epitaxial growth, in-situ cleaning of substrate is required. This is achieved by High

Temperature Baking of the substrate. This decomposes and vaporizes the oxide layer over the substrate. The second method of in-situ cleaning is low energy ion beam of inert gas is used to sputter clean the surface. After the sputtering , low temperature annealing is required to reorder the surface lattice system.

If there is a lattice mismatch between the substrate and the growing film, elastic energy is accumulated in the growing film. At some critical film thickness, the film may break/crack to lower the free energy of the film. The critical film thickness depends on the Young's moduli, mismatch size, and surface tensions. Hence under heteroepitaxy, we must keep the thickness lower than critical film thickness.

Figure 14 shows the physics of epitaxial growth in MBE system. . The aim of this process is to enable sharp interfaces to be formed between one type of alloy and the next e.g. GaAs and AlAs, and thus create structures which may confine electrons and exhibit 2-dimensional² l behaviour. Molecular Beam Epitaxy (MBE³) is basically a sophisticated form of vacuum evaporation.

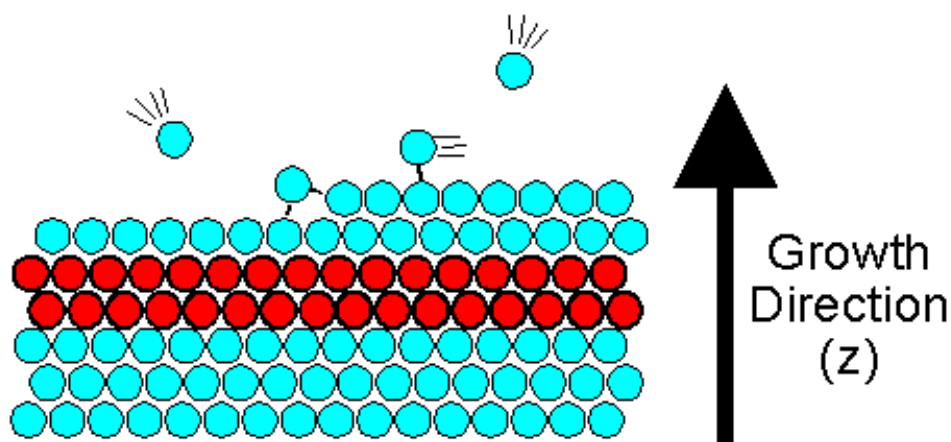


Figure 14. Molecular Beam Epitaxy growth mono-layer by layer or atom layer by layer.

Figure 4.8

METAL ORGANIC CHEMICAL VAPOUR PHASE DEPOSITION>

The growth process in MOCVD (metal-organic CVD, also known as MOVPE metal-organic vapour phase epitaxy) is similar to MBE, but the atoms are carried in gaseous form to the substrate. GaAlAs growth is achieved by using a mixture of hydrogen as a carrier gas and organometallic precursors such as trimethyl gallium and/or trimethyl aluminium together with arsine. The growth rate can be 10 times greater than in MBE, the process does not require ultra high vacuum and it can be scaled up from research to production of commercial devices relatively easily. However, the preparation of the gaseous mixtures has to be very carefully controlled so that as yet it is unclear which technique will eventually dominate. One advantage MOVPE has over MBE is in the ability to grow phosphorous containing alloys, once phosphorous has been

²<http://www.warwick.ac.uk/%7Ephsbn/2deg.htm>

³<http://www.warwick.ac.uk/%7Ephsbn/mbe.htm#mbe>

introduced into an MBE chamber it is almost impossible to grow anything else! One disadvantage is that in situ monitoring is more difficult.

Chapter 5

Tutorial on Chapter 1-Crystal and Crystal Growth.¹

Tutorial on Chapter 1-Crystal and Crystal Growth.

1. Give the percentage packing of Face-Centered-Cube ? [Ans.74%]

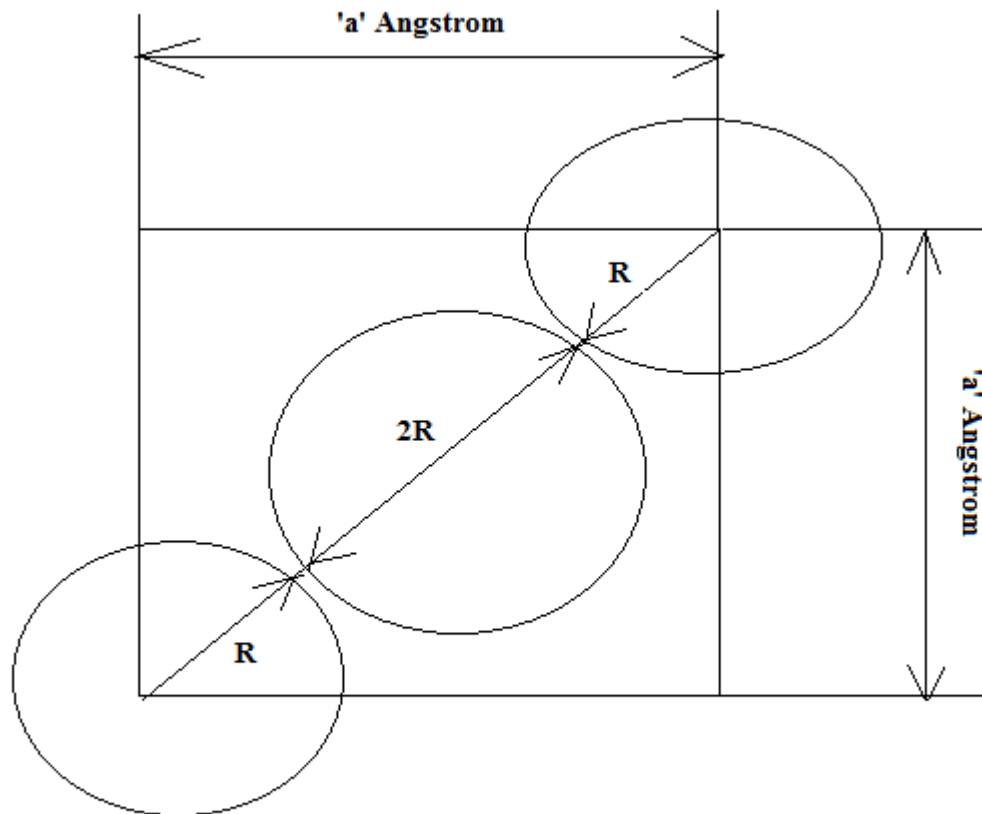
Method:

FCC crystal has 8 atoms at the 8 corners of the cube and 6 atoms on the 6 faces (4 on side faces+2 on the upper and lower faces].

Therefore $N = \text{the coordination Number} = \text{the number of atoms per unit cell} = (8 \times 1/8 + 6 \times 1/2) = 4$ atoms per unit cell.

The atoms are solid spheres and are closely packed so that the atom at the center of the face are touching the 4 atoms on the four corners of the face as shown in the Figure I.

¹This content is available online at <<http://cnx.org/content/m48918/1.1/>>.



Arrangement of the corner spheres and face centered sphere.

Figure 5.1

Inspecting the Figure we find that:

$4R = \text{diagonal of the face} = a\sqrt{2}$.

Therefore $R/a = \sqrt{2}/4 = 1/(2\sqrt{2})$

$$\text{packing ratio} = \frac{4V_{\text{sphere}}}{a^3} = \frac{4}{a^3} \times \frac{4}{3} \pi R^3 = \frac{16}{3} \pi \times \left(\frac{R}{a}\right)^3 = \frac{16}{3} \pi \left(\frac{1}{2\sqrt{2}}\right)^3 = \pi \times \frac{1}{3\sqrt{2}} = 0.74$$

Figure 5.2

Therefore packing percentage in FCC crystals is 74%.

1. Give the percentage packing of Body-Centered-Cube ? [Ans.68%]

Method:

BCC crystal has 8 atoms at the 8 corners of the cube and 1 atom at the center of the Cube. Therefore $N =$ the coordination Number = the number of atoms per unit cell = $(8 \times 1/8 + 1) = 2$ atoms per unit cell.

The atoms are solid spheres and are closely packed so that the atom at the center of the Cube is touching the 2 atoms on the two corners of the cross diagonal of the cube as shown in the Figure 2.

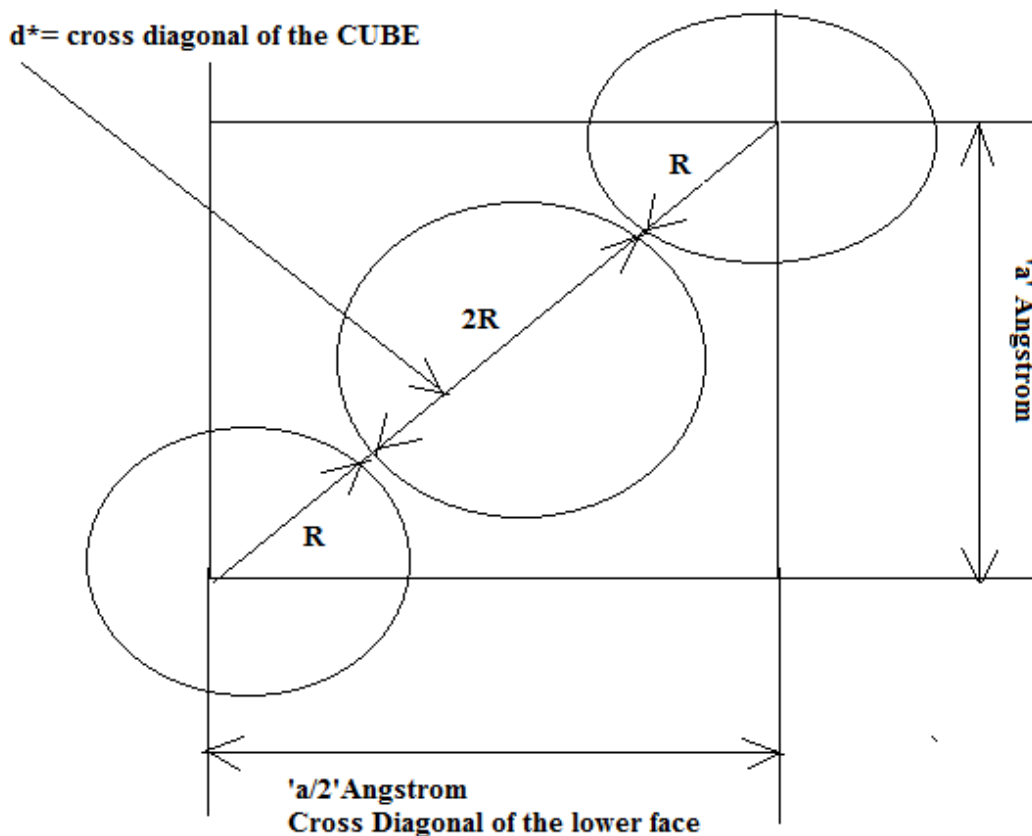


Figure 5.3

Inspecting the Figure we find that:

$$4R = \text{cross diagonal of the Cube} = a\sqrt{3}.$$

$$\text{Therefore } R/a = \sqrt{3}/4;$$

$$\text{packing ratio} = \frac{2V_{\text{sphere}}}{a^3} = \frac{2}{a^3} \times \frac{4}{3} \pi R^3 = \frac{8}{3} \pi \times \left(\frac{R}{a}\right)^3 = \frac{8}{3} \pi \left(\frac{\sqrt{3}}{4}\right)^3 = \frac{8}{3} \pi \times \frac{3\sqrt{3}}{64} = \pi \frac{\sqrt{3}}{8} = 0.64$$

Figure 5.4

Therefore packing percentage in FCC crystals is 68%.

1. Determine the conducting electrons density in FCC Cu where the lattice parameter is 3.6 Angstrom ?
[Ans. $8.5734 \times 10^{28} / \text{m}^3$]

Copper is univalent crystal hence each atom contributes one electron. Therefore atomic density gives the conducting electron density.

Coordination Number of Cu = N = 4 atoms per unit cell.

Unit cell volume is a^3 .

Therefore atomic density = conducting electron density = $4 / (a^3) = 8.5734 \times 10^{28} / \text{m}^3 = 8.5734 \times 10^{22} / \text{cc}$.

1. Si, Ge and GaAs are all diamond crystal structure. Diamond structure is two interpenetrating FCC crystals with one sub-lattice displaced w.r.t. the other along the cross diagonal of the cube by a quarter of the cross diagonal length. In case of Ga As it is ZincBlende cubic structure which has one sub-lattice of Ga and the other sub-lattice of As.

Find the weight density of Si, Ge and GaAs. Given Avogadro Number = $N_{\text{Avo}} = 6.02 \times 10^{23}$ atoms/gm-mole, Si, Ge and GaAs have atomic weight of 28.1, 72.6 and 144.63 (mean = 72.315 respectively and the lattice parameters are 5.43 \AA , 5.646 \AA and 5.6533 \AA respectively.

[Ans. 2.33 gm/cc , 5.37 gm/cc and 5.32 gm/cc respectively]

Method:

Coordination Number = N = 8 corner atoms + 6 face center atoms + 4 body center atoms = $(1/8 \times 8 + 1/2 \times 6 + 4) = 8$ atoms per unit cell.

Therefore Number density = $N^* = 8/a^3 = 4.9967 \times 10^{22}$ atoms/cc, 4.445×10^{22} atoms/cc, 4.4277×10^{22} atoms/cc, of Si, Ge and GaAs respectively.

Weight of one atom = (AW gm/mole) \div (N_{Avo} atoms/mole) = 4.66×10^{-23} gm/atom, 1.157×10^{-22} gm/atom, 1.244×10^{-22} gm/atom of Si, Ge, GaAs respectively.

Therefore weight density = Wt of one atom \times N^* = Weight Density = ρ

Therefore density of Si = 4.9967×10^{22} atoms/cc \times 4.6677×10^{-23} gm/atom = 2.33 gm/cc .

Therefore density of Ge = 4.4495×10^{22} atoms/cc \times 1.206×10^{-22} gm/atom = 5.366 gm/cc .

Therefore density of GaAs = 4.42776×10^{22} atoms/cc \times 1.2012×10^{-22} gm/atom = 5.318 gm/cc gm/cc.

1. A Silicon Ingot should have a P-Type doping of 10^{16} Boron Atoms/cc. In a Czocharlaski Crystal Growth set-up what amount of Boron element by weight should be added to a Si melt of 60Kg. Given: Atomic Weight of Boron = 10.8, Segregation Coefficient = 0.8.

[Answer; About 6 milli gm]

Method:

Let Solid Phase concentration of Boron = C_S ;

Let Liquid Phase concentration of Boron = C_L ;

By Definition, segregation coefficient = $C_S / C_L = 0.8$.

Therefore $C_L = (10^{16} / \text{cc}) / 0.8 = 1.25 \times 10^{16}$ atoms/cc.

Volume of the Melt = $V_0 = (\text{Weight of the Si-Melt}) / \rho_{\text{Si}} = (60 \times 10^3 \text{ gm}) / (2.33 \text{ gm/cc})$.

Therefore $V_0 = 25.75 \times 10^3$ cc.

No. of Boron atoms to be added = $V_0 \times C_L = 25.75 \times 10^3$ cc $\times 1.25 \times 10^{16}$ atoms/cc = N_0 .

Therefore $N_0 = 32.2 \times 10^{19}$ Boron atoms to be added to the whole melt.

Number of gm-moles of Boron required = $N_0 / N_{\text{Avogadro}}$

= 32.2×10^{19} Boron Atoms / 6.02×10^{23} Boron Atoms/gm-mole = 5.349×10^{-4} gm-mole.

Weight of Boron required =

gm-mole \times Atomic Weight = 5.349×10^{-4} gm-mole $\times 10.8$ gm/gm-mole = 5.78 milligm.

1. A layer of $10 \mu\text{m}$ thick epitaxial film is to be deposited on a Si Substrate by CVD method. For how long should the substrate stay in the CVD oven at 1270°C if the gas mixture of gases is in the following concentrations in atoms/cc: H_2 is 2.94×10^{19} and SiCl_4 is 6×10^{17} .

Given:

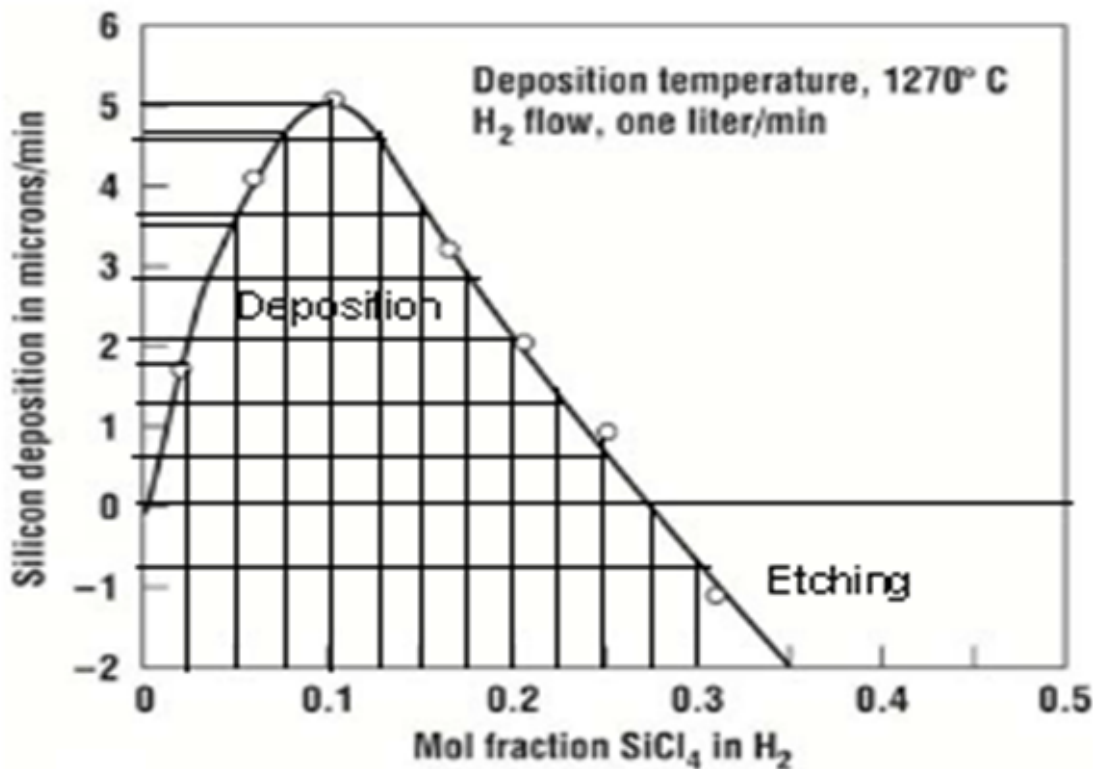


Figure 5.5

The above figure gives Growth Rate (microns/min) vs the Mole Fraction (y) of SiCl_4 . At higher concentrations of HCl i.e. at mole fraction > 0.275 in-situ etching occurs.

From the Figure the following Table is generated:

Mole Fraction	Growth Rate(microns/min)
0.025	1.6
0.050	3.8
0.075	4.6
0.100	5.0
0.125	4.5
0.150	3.6
0.175	2.9
0.200	2.1
0.225	1.3
0.250	0.6
0.275	0
0.300	-0.8

Table 5.1

In the above table the growth rate is the net result of two competing reactions:

Forward reaction where SiCl_4 is decomposing at 1270°C and aiding the Si epitaxial growth and Backward reaction where HCl vapour is etching the Si surface in-situ.

From low mole fraction to 0.275, forward reaction dominates. At 0.275 the two competing reactions are balanced. Above mole fraction 0.275 backward reaction prevails resulting into etching of the Si surface of the substrate.

In our problem the Mole Fraction is :

$$\text{Mole Fraction} = \frac{\text{Conc. of SiCl}_4}{\text{Conc. of H}_2 + \text{Conc. of SiCl}_4} = 0.02$$

Figure 5.6

From the Graph, corresponding to $y = 0.02$, the growth rate is 1.5microns per minute. Therefore 10 microns will require 6.7 minutes of exposure in CVD Furnace.

1. In a Molecular Beam Epitaxy System, find the time required to form a monolayer of O_2 at pressure 1 Torr, 10^{-6} Torr and 10^{-10} Torr. Given Oxygen Molecular Weight = $M=32$ and Oxygen Molecular Diameter = 3.45\AA . Assume that the mono-layer is a close pack structure.

[Answer: 2.43×10^{-6} sec, 2.43 sec, 6 hours]

Method:

Surface Concentration of the closely packed monolayer of Oxygen Molecules = N_S .

$$N_s = \frac{1 \text{ cm}^2}{\frac{\pi}{4} d^2 \text{ cm}^2} = \frac{1 \text{ cm}^2}{\frac{\pi}{4} (3.45 \times 10^{-8})^2 \text{ cm}^2} = 1 \times 10^{15} / \text{cm}^2$$

Figure 5.7

Let the time required for monolayer of Oxygen formation be t_0 where $t_0 = N_s / \Phi$
 Where Φ = Impingement Rate of Oxygen molecules on Substrate Surface in MBE Bell Jar.

$$\Phi = \frac{P}{\sqrt{2\pi M k T}} = \frac{3.51 \times 10^{22} \times P^*(\text{Torr})}{\sqrt{M \times T(\text{Kelvin})}} \text{ molecules}/(\text{cm}^2 \cdot \text{sec})$$

Figure 5.8

Here $M=32$ and $T=300\text{K}$ and P is the corresponding pressure in Torr at which the time for monolayer growth is to be calculated.

P (Torr)	Φ (impingement rate)	t_0 (units of time)
1	3.58×10^{20}	$2.8 \mu\text{s}$
1×10^{-6}	3.58×10^{14}	2.8sec
1×10^{-10}	3.58×10^{10}	27914s = 7.75hours

Table 5.2

This problem clarifies why MBE requires a super Vacuum to fabricate stable and reproducible devices. This is precisely why using Compound Semiconductors is prohibitively costly and we are looking for alternatives to Compound Semiconductors.

Chapter 6

Syllabus of EC1419A _ Electrical and Electronic Materials Science¹

EC 1x19A Electrical & Electronic Material

Revised Syllabus with effect from session 2011-12

L-T-P: 3-0-0 Credit: 3

1. Band Theory of Solids- Energy Band Diagram, E-k diagram, reduced E-k diagram, insulators, semi-conductors and conductors [6 lectures]
2. Dielectric Behaviour of Materials: polarization, dielectric constant at low frequency and high frequency, dielectric loss, piezo electricity and ferro electricity [6 lectures];
3. Magnetic Behaviour of Materials- diamagnetism, para magnetism, ferromagnetism and ferrimagnetism; soft and hard magnetic materials and their applications [6 lectures]
4. Semiconductor- single crystal, polycrystal and amorphous; Fermi-Dirac Distribution; Hall Effect; Intrinsic and Extrinsic; N-type and P-type; Crystal Growth-(1) preparation of electronic grade polycrystal in Siemen's Reactor (2) Czochralski Method and Float Zone Method of bulk single crystal ingot preparation(3) mirror finished wafer preparation (4) Epitaxial Film Growth- Chemical Vapour Phase Deposition & Liquid Phase Epitaxy (5) Molecular Beam Epitaxy [12 lectures]
5. Concept of Phonons- quantization of lattice vibration [2 lectures]
6. Special classification of Semiconductor Materials- degenerate (semi-metal) and non-degenerate semiconductor; elemental and compound semiconductor; direct and indirect band gap material [3 lectures]
7. Superconductors- low and high temperature (YBaCuO) superconductors; Meissner Effect, applications [3 lectures]
8. Special Materials: Nano materials (ZnO, TiO₂, buckyball carbon and graphene), semiconducting polymers, flexible electronic materials, meta materials, smart materials.

Text Book:

References:

1. Principles of Electric Engineering Materials and Devices by S.O. Kasp, McGraw Hill;
2. Structures and Properties of Materials Vol VI, electronic properties by Robert M. Rose, Lawrence A. Shepherd and John Wulf, Wiley Eastern ltd;

¹This content is available online at <<http://cnx.org/content/m48856/1.1/>>.

Chapter 7

Chapter 2. Solid State of Matter.¹

Chapter 2. Solid State of Matter.

"It is evident that many years of research by a great many people, both before and after the discovery of the transistor effect has been required to bring the knowledge of semiconductors to the present development. We were fortunate to be involved at a particularly opportune time and to add another small step in the control of Nature for the benefit of mankind.

- John Bardeen, 1956 Nobel Lecture.

Figure 7.1

We were taught in our high school that there are three states of matter:

Solid- it has a fixed volume and fixed shape.

Liquid- it has fixed volume but it takes the shape of the vessel it is kept in.

Gas-it has no fixed volume and no fixed shape. It takes the volume and shape of the vessel it is kept in.

From this we concluded that in Gaseous State inter-molecular distance is not fixed and the arrangement of the molecules is not fixed. Whereas in Liquid State inter-molecular distance is fixed but the arrangement of the molecules is not fixed. In contrast in Solid State inter-molecular distance is fixed and as well as the arrangement of the molecules is fixed. In fact every elemental or compound solid has a well defined crystalline structure. Every Solid has a characteristic Unit Cell and this is periodically repeated at an spatial distance known as Lattice Parameter.

The most commonly found Unit Cell structures are: Cubic Cell, FCC Cell and BCC Cell.

A large mm range spatial periodicity is called Single Crystal.

Micron range spatial periodicity is known as Poly-crystal.

Nanometer range spatial periodicity is known as Amorphous.

In Figure 2.1. single crystal, poly crystal and amorphous solids are shown .

¹This content is available online at <<http://cnx.org/content/m49804/1.1/>>.

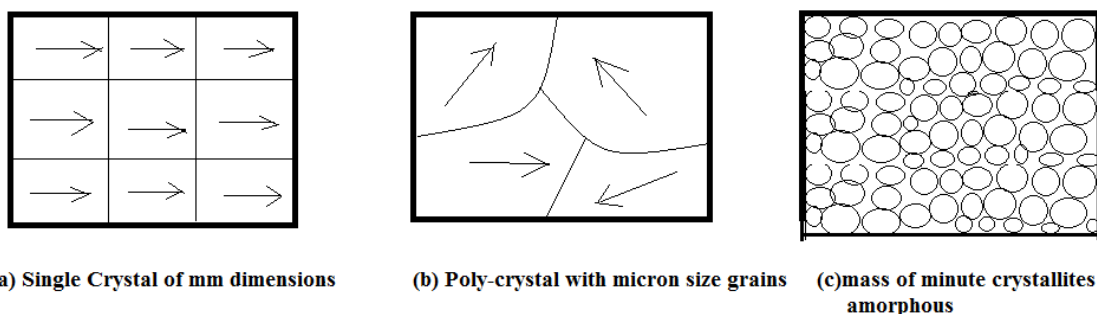


Figure 2.1. Comparative Study of Single crystal, Poly-crystal and Amorphous Solid State of Matter

Figure 7.2

We subsequently learnt that there was a **FOURTH STATE** of Matter namely **PLASMA**. Matter above 4000K is in plasma state. The whole Universe was in a state of plasma up to 380,000 years after the Big-Bang. Now we know a **FIFTH STATE** of matter called **Bose-Einstein Condensate** at a fraction of Kelvin.

Section 2.1. Alloy- Solid Solutions.

Only a few elements are widely used commercially in their pure form. Generally, other elements are present to produce greater strength, to improve corrosion resistance, or simply as impurities left over from the refining process. The addition of other elements into a metal is called alloying and the resulting metal is called an alloy. Even if the added elements are nonmetals, alloys may still have metallic properties.

Copper alloys were produced very early in our history. Bronze, an alloy of copper and tin, was the first alloy known. It was easy to produce by simply adding tin to molten copper. Tools and weapons made of this alloy were stronger than pure copper ones. The typical alloying elements in some common metals are presented in the table below.

Table 2.1. Some Important Alloys and their constituent elements.

Alloys	Composition
Brass	Copper, Zinc
Bronze	Copper, Zinc, Tin
Pewter	Tin, Copper, Bismuth, Antimony
Cast Iron	Iron, Carbon, Manganese, Silicon
Steel	Iron, Carbon (plus other elements)
Stainless Steel	Iron, Chromium, Nickel

Table 7.1

The properties of alloys can be manipulated by varying composition. For example steel formed from iron and carbon can vary substantially in hardness depending on the amount of carbon added and the way in which it was processed.

Section 2.2. General Material Classification.

Based on atomic bonding forces, matter is classified in three classes namely: metallic, ceramic and polymeric. These three classes can be further combined together to form composites. In Figure 2.2. we illustrate the three classes and their composites.

<p>Metals: (1) Ferrous Metals and Alloys. (2) Non-ferrous Metals and Alloys- Nickel, Titanium, precious metals, refractory metals, superalloys. Refractory Metals are highly resistant to temperature for example: Niobium, Molybdenum, Tantalum, Tungsten, Rhenium.</p>	<p>Polymeric: (1) Thermoplastics, (2) Thermoset Plastics, (3) Elastomers.</p> <p>Composite: (1) Re-inforced Plastics, (2) Metal-matrix composites, (3) Ceramic-matrix composites, (4) Sandwich Structure, (4) Concrete.</p>
<p>Ceramics: (1) Glasses, (2) Glass Ceramic, (3) Graphite, (4) Diamond.</p>	

Figure 2.2. The three classes of matter and their composites.

Figure 7.3

Section 2.2.1. Metals.

Metals account for about two thirds of all the elements and about 24% of the mass of the planet. Metals have useful properties including strength, ductility, high melting points, thermal and electrical conductivity, and toughness. From the periodic table, it can be seen that a large number of the elements are classified as being a metal. A few of the common metals and their typical uses are presented below.

Common Metallic Materials:

- (1) Iron/Steel - Steel alloys are used for strength critical applications
- (2) Aluminum - Aluminum and its alloys are used because they are easy to form, readily available, inexpensive, and recyclable.
- (3) Copper - Copper and copper alloys have a number of properties that make them useful, including high electrical and thermal conductivity, high ductility, and good corrosion resistance.
- (4) Titanium - Titanium alloys are used for strength in higher temperature ($\sim 1000^\circ \text{F}$) application, when component weight is a concern, or when good corrosion resistance is required
- (5) Nickel - Nickel alloys are used for still higher temperatures ($\sim 1500\text{-}2000^\circ \text{F}$) applications or when good corrosion resistance is required.

(6) Refractory materials are used for the highest temperature ($> 2000^\circ \text{F}$) applications.

In metal, the lattice centers are immersed in a sea of conducting electrons. These conducting electrons give metallic bonding which is malleable and ductile. It does not have brittleness. Plus it is conductive.

Section 2.2.2. Ceramics.

A ceramic has traditionally been defined as "an inorganic, nonmetallic solid that is prepared from powdered materials, is fabricated into products through the application of heat, and displays such characteristic properties as hardness, strength, low electrical conductivity, and brittleness." The word ceramic comes from the Greek word "keramikos", which means "pottery." They are typically crystalline in nature and are compounds formed between metallic and nonmetallic elements such as aluminum and oxygen (alumina- Al_2O_3), calcium and oxygen (calcia - CaO), and silicon and nitrogen (silicon nitride- Si_3N_4).

The two most common chemical bonds for ceramic materials are covalent and ionic. Covalent and ionic bonds are much stronger than in metallic bonds and, generally speaking, this is why ceramics are brittle and metals are ductile.

Section 2.2.3. Polymers.

A polymeric solid can be thought of as a material that contains many chemically bonded parts or units which themselves are bonded together to form a solid. The word polymer literally means "many parts." Two industrially important polymeric materials are plastics and elastomers. Plastics are a large and varied group of synthetic materials which are processed by forming or molding into shape. Just as there are many types of metals such as aluminum and copper, there are many types of plastics, such as polyethylene and nylon. Elastomers or rubbers can be elastically deformed a large amount when a force is applied to them and can return to their original shape (or almost) when the force is released.

Polymers have many properties that make them attractive to use in certain conditions. Many polymers:

- (1) are less dense than metals or ceramics,
- (2) resist atmospheric and other forms of corrosion,
- (3) offer good compatibility with human tissue, or
- (4) exhibit excellent resistance to the conduction of electrical current.

The polymer plastics can be divided into two classes, thermoplastics and thermosetting plastics, depending on how they are structurally and chemically bonded. Thermoplastic polymers comprise the four most important commodity materials – polyethylene, polypropylene, polystyrene and polyvinyl chloride. There are also a number of specialized engineering polymers. The term 'thermoplastic' indicates that these materials melt on heating and may be processed by a variety of molding and extrusion techniques. Alternately, 'thermosetting' polymers can not be melted or remelted. Thermosetting polymers include alkyds, amino and phenolic resins, epoxies, polyurethanes, and unsaturated polyesters.

Rubber is a natural occurring polymer. However, most polymers are created by engineering the combination of hydrogen and carbon atoms and the arrangement of the chains they form. The polymer molecule is a long chain of covalent-bonded atoms and secondary bonds then hold groups of polymer chains together to form the polymeric material. Polymers are primarily produced from petroleum or natural gas raw products but the use of organic substances is growing. The super-material known as Kevlar is a man-made polymer. Kevlar is used in bullet-proof vests, strong/lightweight frames, and underwater cables that are 20 times stronger than steel.

Section 2.2.4. Composites.

A composite is commonly defined as a combination of two or more distinct materials, each of which retains its own distinctive properties, to create a new material with properties that cannot be achieved by any of the components acting alone. Using this definition, it can be determined that a wide range of engineering materials fall into this category. For example, concrete is a composite because it is a mixture of Portland cement and aggregate. Fiberglass sheet is a composite since it is made of glass fibers imbedded in a polymer.

Composite materials are said to have two phases. The reinforcing phase is the fibers, sheets, or particles that are embedded in the matrix phase. The reinforcing material and the matrix material can be metal, ceramic, or polymer. Typically, reinforcing materials are strong with low densities while the matrix is usually a ductile, or tough, material.

Some of the common classifications of composites are:

- Reinforced plastics
- Metal-matrix composites
- Ceramic-matrix composites
- Sandwich structures
- Concrete

Composite materials can take many forms but they can be separated into three categories based on the strengthening mechanism. These categories are dispersion strengthened, particle reinforced and fiber reinforced. Dispersion strengthened composites have a fine distribution of secondary particles in the matrix of the material. These particles impede the mechanisms that allow a material to deform. (These mechanisms include dislocation movement and slip, which will be discussed later). Many metal-matrix composites would fall into the dispersion strengthened composite category. Particle reinforced composites have a large volume fraction of particle dispersed in the matrix and the load is shared by the particles and the matrix. Most commercial ceramics and many filled polymers are particle-reinforced composites. In fiber-reinforced composites, the fiber is the primary load-bearing component. Fiberglass and carbon fiber composites are examples of fiber-reinforced composites.

If the composite is designed and fabricated correctly, it combines the strength of the reinforcement with the toughness of the matrix to achieve a combination of desirable properties not available in any single conventional material. Some composites also offer the advantage of being tailorable so that properties, such as strength and stiffness, can easily be changed by changing amount or orientation of the reinforcement material. The downside is that such composites are often more expensive than conventional materials.

Section 2.3. The atomic bonding in Matter.

It should be clear that all matter is made of atoms. From the periodic table, it can be seen that there are only about 100 different kinds of atoms in the entire Universe. These same 100 atoms form thousands of different substances ranging from the air we breathe to the metal used to support tall buildings. Metals behave differently than ceramics, and ceramics behave differently than polymers. The properties of matter depend on which atoms are used and how they are bonded together.

There are 4 kinds of atomic bonding:

- i. Metallic Bonding.
- ii. Covalent Bonding.
- iii. Ionic Bonding.
- iv. Van-der-Waal Bonding.

All chemical bonds involve electrons. Atoms will stay close together if they have a shared interest in one or more electrons. Atoms are at their most stable and chemically inert form when they have no partially-filled electron shells such as Inert Gases /Noble Gases/Rare Gases such as He, Ne, Ar, Kr, Xe and Rn . These are odourless, colorless, monoatomic gases with very little reactivity hence they are called Inert Gases.

In Table 2.2 and Table 2.3. the salient parameters and the electronic shell configurations of the Noble Gases are given.

Table 2.2. The salient parameters of Noble Gases

Gas	B.P(K)	M.P.(K)	Z*	Atomic radius(pm)	Ionization Energy(eV)
He	4.4 Below 4.4K He exhibits superfluidity	0.95 Solid He found in the Core of Jupiter. It Behaves like metal	2	31	24.8
Ne	27.3	24.7	10	38	21.5
Ar	87.4	83.6	18	71	16
Kr	121.5	115.8	36	88	14
Xe	166.6	161.7	54	108	12
Rn	211.5	202.2	86	120	11

Table 7.2

*Z = Atomic Number.

Table 2.3. Shell Structure of Inert Gas Atoms.

Gas	Z	K-Shell(n=1)	L-Shell(n=2)	M-Shell(n=3)	N-Shell(n=4)	O-Shell(n=5)	P-Shell(n=6)
He	2	1s ²					
Ne	10	1s ²	2s ² , 2p ⁶				
Ar	18	1s ²	2s ² , 2p ⁶	3s ² , 3p ⁶			
Kr	36	1s ²	2s ² , 2p ⁶	3s ² , 3p ⁶ , 3d ¹⁰	4s ² , 4p ⁶		
Xe	54	1s ²	2s ² , 2p ⁶	3s ² , 3p ⁶ , 3d ¹⁰	4s ² , 4p ⁶ , 4d ¹⁰	5s ² , 5p ⁶	
Rn	86	1s ²	2s ² , 2p ⁶	3s ² , 3p ⁶ , 3d ¹⁰	4s ² , 4p ⁶ , 4d ¹⁰ , 4f ¹⁴	5s ² , 5p ⁶ , 5d ¹⁰	6s ² , 6p ⁶

Table 7.3

Table 2.4. Simplified Shell Structure of Inert Gas Atoms.

Gas	Z				
He	2	1s ²			
Ne	10	He	2s ² , 2p ⁶		
Ar	18	Ne	3s ² , 3p ⁶		
Kr	36	Ar	3d ¹⁰	4s ² , 4p ⁶	
Xe	54	Kr	4d ¹⁰	5s ² , 5p ⁶	
Rn	86	Xe	4f ¹⁴	5d ¹⁰	6s ² , 6p ⁶

Table 7.4

K, L, M, N, O and P-Shell are major Shells corresponding to the Principal Quantum Number $n = 1, 2, 3, 4, 5$ and 6.

Within each Shell there are Sub-Shells s, p, d and f.

Here we will briefly discuss the Periodic Table.

Principal Quantum Number: $n \rightarrow$ gives the energy quantization as well as the complete ONE period of elements.

Azimuthal Quantum Number: $l \rightarrow$ gives the orbital angular momentum quantization.

Magnetic Quantum Number: $m \rightarrow l, (l-1), \dots, 0, \dots, -(l-1), -l$. This gives the orientation quantization. When a magnetic field B_{external} is applied in Z-axis, Orbital Angular Momentum L will align so as to give an Integral Projection of l on Z-axis as shown in Figure 2.2.

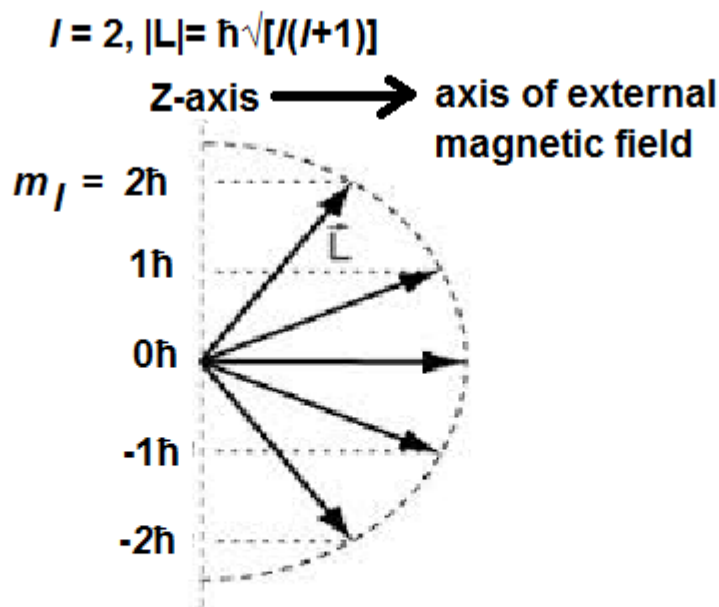


Figure 2.2. The Projection of the orbital angular momentum $|L|$ along the Z-axis along which an external Magnetic Field is applied.

Figure 7.4

Here for K-Shell, corresponding to Principal Q.N. $n=1$, l can be only 0. There is only s-subshell.

For L-Shell, corresponding to Principal Q.N. $n=2$, l can be 0 and 1. Here there are two subshells namely: s-subshell and p-subshell.

For M-Shell, corresponding to Principal Q.N. $n=3$, l can be 0, 1 and 2. Here there are three subshells namely: s-subshell, p-subshell and d-subshell.

For N-Shell, corresponding to Principal Q.N. $n=4$, l can be 0, 1, 2 and 3. Here there are four subshells namely: s-subshell, p-subshell, d-subshell and f-subshell.

For O- Shell, corresponding to Principal Q.N. $n=5$, l can be $0, 1, 2, 3$ and 4 . Here there are five subshells namely: *s-subshell*, *p-subshell*, *d-subshell*, *f-subshell* and *g-subshell*.

For P- Shell, corresponding to Principal Q.N. $n=6$, l can be $0, 1, 2, 3, 4$ and 5 . Here there are six subshells namely: *s-subshell*, *p-subshell*, *d-subshell*, *f-subshell*, *g-subshell* and *h-subshell*.

In nut-shell, the above information can be summarized by Table 2.5.

Table 2.5. Electron Distribution among the Sub-Shells.

***m l* Permissible statesw/o spin Orbitalshape Name**

s 0 0 1 SPHERE sharp

p 1 -1,0,+1 3 TWODUMB BELLS principal

d 2 -2,-1,0,+1,+2 5 FOURDUMB BELLS diffuse

f 3 -3,-2,-1, 0,+1,+2,+3 7 EIGHTDUMB BELLS fundamental

***m l* Permissible statesw/o spin Orbitalshape Name**

s 0 0 1 SPHERE sharp

p 1 -1,0,+1 3 TWODUMB BELLS principal

d 2 -2,-1,0,+1,+2 5 FOURDUMB BELLS diffuse

f 3 -3,-2,-1, 0,+1,+2,+3 7 EIGHTDUMB BELLS fundamental

m l Permissible statesw/o spin Orbitalshape Name

s 0 0 1 SPHERE sharp

p 1 -1,0,+1 3 TWODUMB BELLS principal

d 2 -2,-1,0,+1,+2 5 FOURDUMB BELLS diffuse

f 3 -3,-2,-1, 0,+1,+2,+3 7 EIGHTDUMB BELLS fundamental

Sub-Shell Or Orbital	l	m_l	Permissible states w/o spin	Orbital shape	Name
s	0	0	1	SPHERE	sharp
p	1	-1, 0, +1	3	TWO DUMB BELLS	principal
d	2	-2, -1, 0, +1, +2	5	FOUR DUMB BELLS	diffuse
f	3	-3, -2, -1, 0, +1, +2, +3	7	EIGHT DUMB BELLS	fundamental

Table 7.5

The ORBITAL SHAPES of electron cloud for s-orbital, p-orbital, d-orbital and f-orbital are illustrated in Figure 2.3.

$n = 1$	$l = 0$		s orbital
$n = 2$	$l = 0$		s orbital
	$l = 1$		p orbital
$n = 3$	$l = 0$		s orbital
	$l = 1$		p orbital
	$l = 2$		d orbital
$n = 4$	$l = 0$		s orbital
	$l = 1$		p orbital
	$l = 2$		d orbital
	$l = 3$	complex shape	f orbital

Figure 2.3. Electronic Configuration or the shape of the Electron Cloud surrounding the Nucleus for different values of azimuthal quantum number.

Figure 7.5

Spin Quantum Number: $s = \pm(1/2)$. This gives the quantization of the spin angular momentum. This Quantum Number 's' has been illustrated in Figure 2.4.

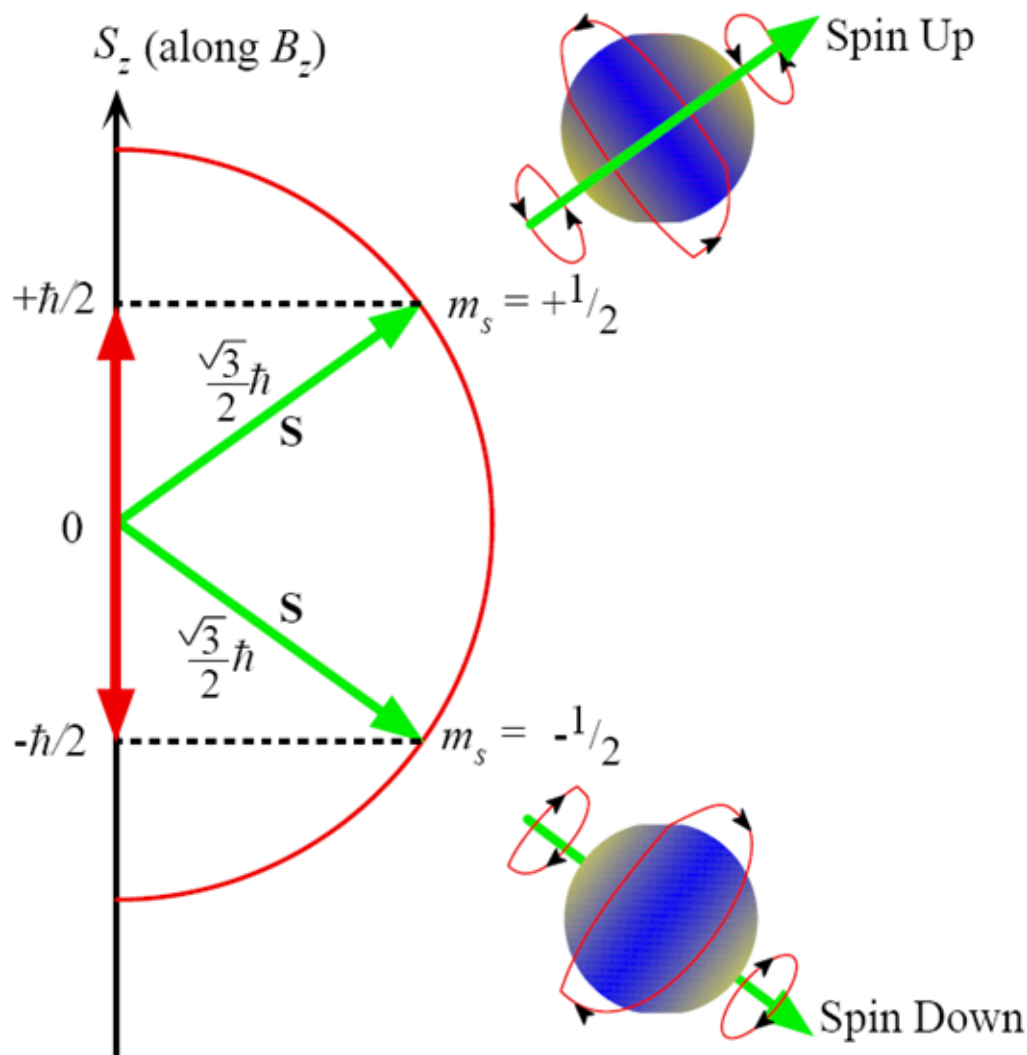


Figure 2.4. Electron, being a FERMION, has an axial spin angular momentum $(\sqrt{3}/2)\hbar$ which has a projection of $\pm(\hbar/2)$ on Z-axis. Z-axis is the axis of externally applied Magnetic Field.

Figure 7.6

For each unique set of (n, L, m) there can be two permissible electronic states: one corresponding to $+(1/2)$ and the second anti-parallel $-(1/2)$.

Pauli Exclusion Principle clearly states that no two electrons can have the same four quantum numbers. At least one quantum number should differ.

For $n = 1$, l can only be 0 . This marks the First Period. This means spherically symmetrical electron

cloud surrounding the nucleus. This means Orbital Angular Momentum will be always ZERO in first period.

Therefore in First Period, $n=1$, $l = 0$, $m = 0$, $s = \pm (1/2) \rightarrow$ this correspond to TWO elements H and He.

H is the first Group and He is the last Group in First Period. This is illustrated in Table 2.6.

Table 2.6. Elements of FIRST Period.

First Period	1 st Gr	2 nd Gr	3 rd Gr	4 th Gr	5 th Gr	6 th Gr	7 th Gr	8 th Gr
Elements	H	-	-	-	-	-	-	He
s-orbital being filled	$1s^1$	-	-	-	-	-	-	$2s^2$
K-Shell is being Filled up	s-subshell in K-Shell	-	-	-	-	-	-	s-subshell in K-Shell is Full

Table 7.6

For $n=2$, l can be 0 and 1. This marks the Second Period.

Here we have K Shell which is already FULL and corresponds to He configuration and L-Shell is in the process of getting filled as shown in Table 2.7.

Table 2.7. Elements of SECOND Period.

Second Period	1 st Gr	2 nd Gr	3 rd Gr	4 th Gr	5 th Gr	6 th Gr	7 th Gr	8 th Gr
Elements	Li	Be	B	C	N	O	F	Ne
He corresponds to K-Shell	$He2s^1$	$He2s^2$	$He2s^22p^1$	$He2s^22p^2$	$He2s^22p^3$	$He2s^22p^4$	$He2s^22p^5$	$He2s^22p^6$
L-Shell is being filled up.	s-subshell in L-Shell	s-subshell in L-Shell is Full	p-subshell in L-Shell is Full					

Table 7.7

For $n=3$, l can be 0, 1 and 2. This marks the Third Period.

Here we have K Shell which is already FULL and L-Shell is also filled and this K and L filled Shell corresponds to Neon. M-Shell is in the process of getting filled up as shown in Table 2.8.

Table 2.8. Elements of THIRD Period.

Third Period	1 st Gr	2 nd Gr	3 rd Gr	4 th Gr	5 th Gr	6 th Gr	7 th Gr	8 th Gr
<i>continued on next page</i>								

Elements	Na	Mg	Al	Si	P	S	Cl	Ar
Ne corresponds to K-Shell and L-Shell	Ne3s ¹	Ne3s ²	Ne3s ² 3p ¹	Ne3s ² 3p ²	Ne3s ² 3p ³	Ne3s ² 3p ⁴	Ne3s ² 3p ⁵	Ne3s ² 3p ⁶
M-Shell is being filled up.	s-subshell in M-Shell	s-subshell in M-Shell is Full	p-subshell in M-Shell	p-subshell in M-Shell is Full				

Table 7.8

For $n=4$, l can be 0, 1, 2 and 3 This marks the Fourth Period.

Here we have K Shell and L-Shell are filled up. But M-Shell is partially filled up. K, L, and M (partially) corresponds to Ar. Partially filled M-Shell and empty N-Shell is in the process of getting filled up as shown in Table 2.9.

Table 2.9. Elements of FOURTH Period.

Fourth Period	1 st Gr	2 nd Gr	†	3 rd Gr	4 th Gr	5 th Gr	6 th Gr	7 th Gr	8 th Gr
Elements	K	Ca		Ga	Ge	As	Se	Br	Kr
Ar corresponds to K, L-Shell filled up and M-Shell partially filled up.	Ar4s ¹	Ar4s ²		Ar3d ¹⁰ 4s ² 4p ¹	Ar3d ¹⁰ 4s ² 4p ²	Ar3d ¹⁰ 4s ² 4p ³	Ar3d ¹⁰ 4s ² 4p ⁴	Ar3d ¹⁰ 4s ² 4p ⁵	Ar3d ¹⁰ 4s ² 4p ⁶

continued on next page

N-Shell, s-orbital is first filled up. † Then M-Shell d-orbital is filled up. Then N-Shell p-orbital is filled up	s-subshell in N-Shell getting filled	s-subshell in N-Shell is Full		d-subshell in M-Shell is fullp-subshell in N-Shell	d-subshell in M-Shell is full p-subshell in N-Shell	d-subshell in M-Shell is fullp-subshell in N-Shell is Full			
---	--------------------------------------	-------------------------------	--	--	---	--	--	--	--

Table 7.9

† Sc, Ti, V, Cr, Mn, Fe, Co, Ni, Cu, Zn are the d-Block Transition elements which are there due to belated filling up of d-orbitals in M-Shell which has 10 electron states permissible from $3d^1$ to $3d^{10}$.

For $n=5$, l can be 0, 1, 2, 3 and 4. This marks the Fifth Period.

Here we have K Shell, L-Shell and M-Shell are filled up. But N-Shell is partially filled up. K, L, M and N (partially) corresponds to Kr. Partially filled N-Shell and empty O-Shell is in the process of getting filled up as shown in Table 2.10.

Table 2.10. Elements of FIFTH Period.

Fifth Period	1 st Gr	2 nd Gr	†	3 rd Gr	4 th Gr	5 th Gr	6 th Gr	7 th Gr	8 th Gr
Elements	Rb	Sr		In	Sn	Sb	Te	I	Xe
Kr corresponds to K, L, M-Shell filled up. And N-Shell partially filled up.	$Kr5s^1$	$Kr5s^2$		$Kr4d^{10}5s^2 5p^1$	$Kr4d^{10}5s^2 5p^2$	$Kr4d^{10}5s^2 5p^3$	$Kr4d^{10}5s^2 5p^4$	$Kr4d^{10}5s^2 5p^5$	$Kr4d^{10}5s^2 5p^6$
<i>continued on next page</i>									

O-Shell s-orbital Is first filled.† Then N-Shell is filled up and then O-Shell is being filled up.	s-subshell in O-Shell getting filled	s-subshell in O-Shell is Full		d-subshell in N-Shell is fullp-subshell in O-Shell	d-subshell in N-Shell is full p-subshell in O-Shell	d-subshell in N-Shell is fullp-subshell in O-Shell is Full			
--	--------------------------------------	-------------------------------	--	--	---	--	--	--	--

Table 7.10

† Y,Zr,Nb,Mo,Tc,Ru,Rh,Pd,Ag,Cd are the d-Block Transition elements which are there due to belated filling up of d-orbitals in N-Shell which has 10 electron states permissible from $4d^1$ to $4d^{10}$.

For $n=6$, l can be $0, 1, 2, 3, 4$ and 5 . This marks the Sixth Period.

Here we have K Shell, L-Shell, M-Shell are filled up and N-Shell and O-Shell is partially filled up. K,L, M full and N(partially) and O(partially) corresponds to Xe. Partially filled N-Shell and partially filled O-Shell is in the process of getting filled along with empty P-Shell up as shown in Table 2.11.

Table 2.11. Elements of SIXTH Period.

Fifth Period	1 st Gr	2 nd Gr	†	3 rd Gr	4 th Gr	5 th Gr	6 th Gr	7 th Gr	8 th Gr
Elements	Cs	Ba		Th	Pb	Bi	Po	At	Rn
Xe corresponds to K, L, M-Shell filled up. N-Shell and O-Shell partially filled up.	$Xe6s^1$	$Xe6s^2$		$Xe4f^{14}5d^{10}6p^1$	$Xe4f^{14}5d^{10}6p^2$	$Xe4f^{14}5d^{10}6p^3$	$Xe4f^{14}5d^{10}6p^4$	$Xe4f^{14}5d^{10}6p^5$	$Xe4f^{14}5d^{10}6s^26p^6$
<i>continued on next page</i>									

P-Shell s-orbital Is first filled. † Then N-Shell is filled up and then O-Shell is being filled up. Then P-Shell p-orbital is filled up.	s-subshell in P-Shell getting filled	s-subshell in P-Shell is Full		f-subshell in N-Shell is full. The d-orbital in O-Shell is full and p-orbital in P-Shell has started filling up	f-subshell in N-Shell is full. The d-orbital in O-Shell is full and p-orbital in P-Shell has started filling up	f-subshell in N-Shell is full. The d-orbital in O-Shell is full and p-orbital in P-Shell has started filling up	f-subshell in N-Shell is full. The d-orbital in O-Shell is full and p-orbital in P-Shell has started filling up	f-subshell in N-Shell is full. The d-orbital in O-Shell is full and p-orbital in P-Shell has started filling up	f-subshell in N-Shell is full. The d-orbital in O-Shell is full and p-orbital in P-Shell is Full.
--	--------------------------------------	-------------------------------	--	--	--	--	--	--	--

Table 7.11

†La,Hf,Ta,W,Re,Os,Ir,Pt,Au,Hg are the d-Block Transition elements which are there due to belated filling up of d-orbitals in O-Shell which has 10 electron states permissible from $5d^1$ to $5d^{10}$.

Ce,Pr,Nd,Pm,Sm,Eu,Gd,Tb,Dy,Ho,Er,Tm,Yb,Lu are f-Block Transition elements which are due to belated filling up of N-Shell f-orbital belated fillings from $4f^1$ to $4f^{14}$.

Section 2.3.1. Applications of Noble Gases

Argon is used in glass chambers to provide inert atmosphere as for instance in Incandescent Lamp and in Siemen's Reactor. Helium is used as breather gas. He-O₂ is used as breathing gas for deep-sea divers at a depth of 55m. This prevents oxygen toxemia. This also prevents Nitrogen narcosis. Helium gases have replaced highly inflammable Hydrogen gases in lighter than air applications.

Noble gases have multiple stable isotopes except Radon which is radio-active. Radon has a half-lifetime of 3.8days. It decays to Helium and Polonium which further decays to lead.

In each PERIOD of the periodic table, Noble gas has the highest first Ionization Energy and the Group I alkali metal has the lowest Ionization energy. There is only weak Vander Waal's force acting between Noble gas atoms. Hence they have very low Melting Point and Boiling Point.

Noble Gases are nearly Ideal Gases and their deviations from Ideal Gas Law give important clues regarding the inter-atomic distances of the gas atoms.

If an atom has only a under-populated sub-shell, it will tend to lose them to become positively ionized as it happens in alkali metal. When metal atoms bond, a metallic bond occurs. When an atom has a nearly full electron sub-shell, it will try to find electrons from another atom so that it can fill its outer sub-shell and become electro-negative. These elements are usually described as nonmetals. The bond between two nonmetal atoms is usually a covalent bond. Whereas metal and nonmetal atom come together and an ionic bond occurs. There are also other, less common, types of bond but the details are beyond the scope of this material. On the next few pages, the Metallic, Covalent and Ionic bonds will be covered in detail.

Chapter 8

Chapter 2. Section 2.3.2. Application of Inert Gases.¹

Chapter 2. Section 2.3.2. Application of Inert Gases.

Helium- Helium is used as a component of breathing gases due to its low solubility in fluids or lipids. For example, gases are absorbed by the blood and body tissues when under pressure during scuba diving. Because of its reduced solubility, little helium is taken into cell membranes, when it replaces part of the breathing mixture, helium causes a decrease in the narcotic effect of the gas at far depths. The reduced amount of dissolved gas in the body means fewer gas bubbles form decreasing the pressure of the ascent. **Helium** and **Argon** are used to shield welding arcs and the surrounding base metal from the atmosphere during welding.

Helium is used in very low temperature cryogenics, particularly for maintaining superconductors at a very low temperature. Superconductivity is useful for creating very strong magnetic fields. Helium is also the most common carrier gas in gas chromatography².

Neon- Neon is used for many applications that we see in daily life. For examples: Neon lights, fog lights, TV cine-scopes, lasers, voltage detectors, luminous warnings and also advertising signs. The most popular applications of Neon would be the Neon tubes that we see for advertisement or elaborate decorations. These neon tubes consist with neon and helium or argon under low pressure submitted to electrical discharges. The color of emitted light shown is dependent on the composition of the gaseous mixture and also with the color of the glass of the tube. Pure Neon within a colorless tube can obtain a red light, which reflects a blue shine. These reflected light are also known as fluorescent light.

Argon- Argon is used for a diverse group of applications in the growing industries of : electronics, lighting, glass, and metal fabrications. Argon is used in electronics to provide a protective heat transfer medium for ultra-pure semiconductors from silicon crystals and for growing germanium. Argon can also fill fluorescent and incandescent light bulbs; creating the blue light found in neon type lamps. By utilizing argon's low thermal conductivity, window manufacturers can provide a gas barrier needed to produce double-pane insulated windows. This insulation barrier improves the windows' energy efficiency. Argon also creates an inert gas shield during welding; to flush out melted metals to eliminate porosity in casting; and to provide an oxygen-and-nitrogen free environment for annealing and rolling metals and alloys.

Krypton- Just like argon, krypton can be found in energy efficient windows. It is also found in fuel sources, lasers and headlights. It is estimated that 30% of energy efficient windows sold in Germany and England are filled with krypton; approximately 1.8 liters of krypton. Being more thermally efficient, krypton is sometimes chosen over argon as a choice for insulation. Krypton can be found in lasers which works as a control for a desired optic wavelength. It is usually mixed with a halogen (most likely fluorine) to produce typically called "excimer" lasers. Krypton is sometimes used within halogen sealed beam headlights. These headlights produces up to double the light output of standard headlights for a brighter gleam. Also, Krypton is used

¹This content is available online at <<http://cnx.org/content/m49811/1.1/>>.

²http://chemwiki.ucdavis.edu/Analytical_Chemistry/Instrumental_Analysis/Chromatography/Gas_Chromatography

for high performance light bulbs which have higher color temperatures and efficiency because it reduces the rate of evaporation of the filament.

Xenon- Xenon is used for various applications. From incandescent lighting, to development in x-rays, to plasma display panels (PDPs) and much more. Incandescent lighting uses Xenon because less energy can be used to produce the same amount of light output as a normal incandescent lamp. Xenon has also made it possible to obtain better x-rays with reduced amounts of radiation. When mixed with oxygen, it can enhance the contrast in CT imaging. The revolutionize the health care industries. Plasma display panels (PDPs) using xenon as one of the fill gases may one day replace the large picture tube in television and computer screens. This promises a revolution in the television and computer industries.

Nuclear Fission products may include a couple of radioactive isotopes of xenon, which also absorb neutrons in nuclear reactor cores. The formation and elimination of radioactive xenon decay products can be a factor in nuclear reactor control.

Radon- Radon has been said to be the second most frequent cause of lung cancer, after cigarette smoking. However, it can be found in various beneficial applications as well. For examples through: radiotherapy, relief from arthritis, and bathing. In radiotherapy, radon has been used in implantable seeds, made of glass or gold, primarily used to treat cancers. For arthritis, its been said that exposure to radon mitigates auto-immune diseases such as arthritis. Those who have arthritis have actually sought limited exposure to radioactive mine water and radon to relief their pain. However, radon has nevertheless found to induce beneficial long-terms effect. Some places actually have "Radon Spas". For examples: Bad Gastern, Austria and Japanese Onsen in Misasa, Tottori. "Radon Spa" is a relieving therapy where people sit for minutes to hours in a high-radon atmosphere, believing that low doses of radiation will boost up their energy.

Section 2.4. Covalent bonding, ionic bonding, metallic bonding and Van-der-Wal's Weak Force bonding.

In this Universe all subsystems and this Universe itself is always moving to minimum energy configuration because this is the stable equilibrium condition. So is the case with atomic configurations known as molecules or with atomic periodic configuration in a single crystal solid. How the atoms, identical or dissimilar, will stably configure will be decided by the minima energy configuration. Minima energy configuration will decide the type of bond in a given molecule or in a solid state crystalline structure.

Covalent, Ionic and Metallic bonds are primary bonds and require more than 1eV/atom dissociation energy.

Van-der-Waal's Weak Force Bonding is secondary bonding and requires less than 0.1eV/atom dissociation energy.

2.4.1. Ionic Bonding.

In a chemical compound of first group Alkali metal (Li,Na,K,Rb,Cs) and seventh group Halogen element (F,Cl,Br,I) minimum energy configuration is obtained through ionic bonded alkahalide salts namely KF, LiF,MgO, CsCl and ZnS. Figure 2.5 illustrates the minimum energy configuration of NaCl .

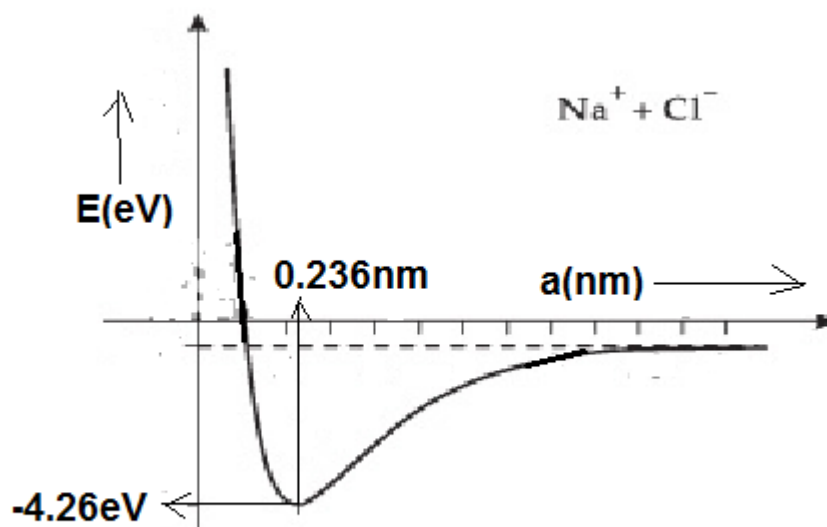


Figure 2.5. Potential Energy vs Interatomic Distance in NaCl molecule

Figure 8.1

1. In ionic bonded crystalline solids, the electrons are tightly bound to both cations and anions nuclei hence these solids are good insulators.

2. Ionic crystals do not absorb light hence they are transparent to light.

3. Ionic salts are hard owing to strong ionic bonds,

4. These have high M.P.

5. These are brittle. One layer cannot slip past the other. They tend to cleave and not deform.

6. Ionic salts are good IR absorbers because ionic salts electron-cloud system has natural frequency or resonance frequency at IR. Therefore IR are strongly absorbed by ionic salts.

7. These are non-directional and hence isotropic.

NaCl has fcc structure with coordination number of 6. CsCl has bcc structure with coordination number of 8. In water, because of very high DC relative permittivity ($\epsilon_r = 70$), ionic salt is very soluble and cations and anions easily dissociate and NaCl aqueous solution is a strong electrolytic solution and will allow electricity to flow through. But ionic salts are insoluble in covalent organic solvents such as Benzene (C_6H_6) and Carbon Tetrachloride (CCl_4). This is because the organic solvent has a very low dielectric constant therefore ionic salts do not dissociate hence do not dissolve in organic solvent.

2.4.2. Covalent Bond.

In an ionic bond there is 100% transfer of electrons from alkali metals to halogen elements, in the process both fulfill their octaves as well they create a strong electrostatic attractive force. But in Silicon, Germanium or Diamond the four electrons are shared with four neighbouring atoms in a tetrahedral crystalline structure which leads to complete fulfillment of octaves for all atoms except those on the boundaries which have incomplete bonds or dangling bonds. This is 100% covalent bond and occurs only for Group IV elements. [$\text{CH}_4, \text{SiC}, \text{F}_2, \text{Cl}_2, \text{H}_2$]

Group III and Group V, lead to 75% covalent and 25% ionic. [GaAs]

Group II and Group VI, lead to 25% co-valent and 75% ionic.

Group I and Group VII, lead to 100% ionic.

Materials, elements or compounds, having 100% covalent bonding has the following properties:

1. Highly directional bond therefore anisotropic.
2. It can be non-polar as in Si, Ge and Diamond or it can be Polar as in Water molecule.
3. Good insulator.
4. These solids are brittle or it can be soft also. If brittle they are transparent and they cleave.
5. Low latent heat of fusion and evaporation.

The covalent bonds between atoms in a given molecule are very strong, as strong as ionic bonds. However, unlike ionic bonds, there is a limit to the number of covalent bonds to other atoms that a given atom can form. For example, carbon can make four bonds - not more. Oxygen can form two bonds. As a result, once each atom has made all the bonds it can make, as in all the molecules shown above, the atoms can no longer interact with other ones. For this reason, two covalent molecules barely stick together. Light molecules are therefore **gases**, such as methane or ethane, above, hydrogen, H_2 , nitrogen, N_2 (the main component of the air we breathe, etc. Heavier molecules, such as e.g. the isooctane molecule, are liquids at room temperature, and others still, such as cholesterol, are solids.

In Figure 2.6. we see that Hydrogen Molecule achieves minimum PE configuration through sharing its lone electron as a pair. The dissociation energy is 4.5eV.

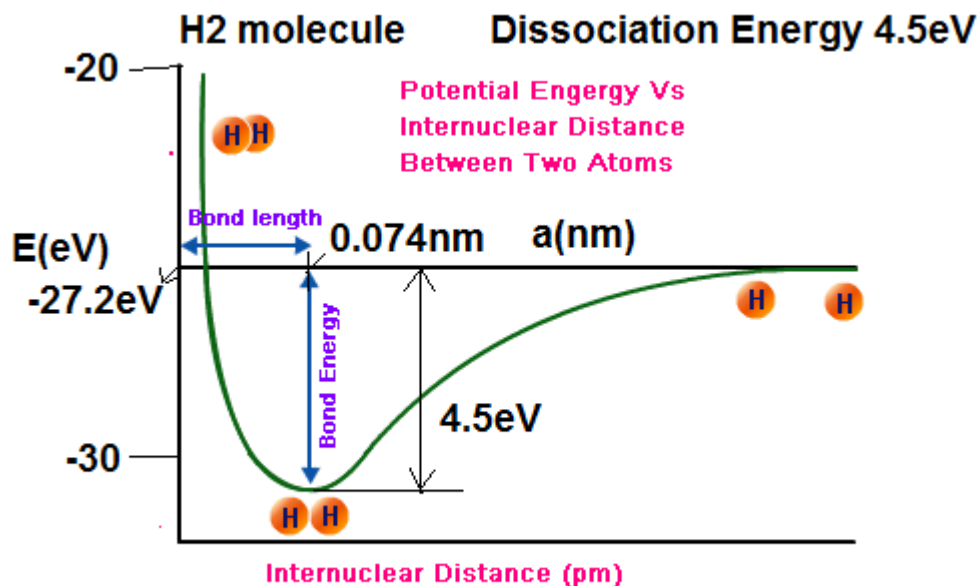


Figure 2.6. Potential Energy vs Internuclear distance

Figure 8.2

alt.

Section 2.4.3. Metallic Bond.

Group I and Group II form strong metallic bond whereas Gr III form weak metallic bonds. The conducting electrons are weakly held by their host atoms. Therefore at room temperature they easily become delocalized and belong to the whole lattice. This sea of delocalized electrons keep the (+)ve charged lattice centers

together. The metallic bonds are non-directional and allow ionic centers to go past each other. Hence they are ductile, malleable and have metallic luster. In Figure 2.7, metallic bond is illustrated. This sea of de-localized electrons give high electrical conductivity and high thermal conductivity attributes to metals.

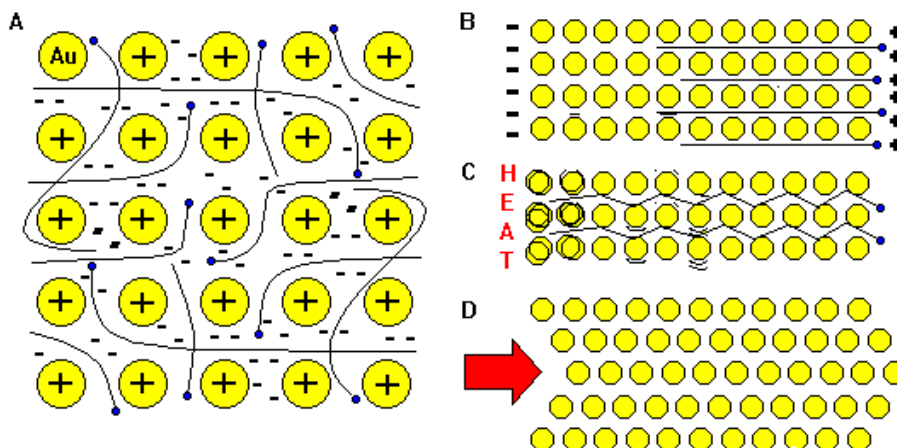


Figure 2.7. Illustration of Metallic Bond. The positively charged lattice centers are submerged in a sea of delocalized conduction band electrons. These delocalized electrons allow high thermal conductivity as well as high electrical conductivity.

Figure 8.3

Section 2.4.4. The secondary or Van-der-Waal's weak force bonding.

This is Bond-induced bonding. Noble Gases are chemically inert and consist of monoatomic molecule. But still have an attractive force because of which they liquefy when cooled.

In absence of the three primary bonds, Van-der-Waal Bonding provides the fourth kind of bonding mechanism which provides the cohesive force for liquefaction and solidification. Macroscopic behavior such as Surface Tension, Friction, Viscosity, Adhesion and Cohesion have their physical basis in this mechanism.

Here there is no sharing of electrons or physical transfer of electron still because of distortion of the electron cloud there may be a fluctuating dipole or they may be a permanent dipole. In either case a weak attraction is created among the molecules and this becomes the physical basis for Van-der-Waal's weak force bonding as shown in Figure 2.8.

In non-polar molecules it is by induction or by electronic polarization due to close proximity. It is polarized and synchronized so that it is always attractive as shown in Figure 2.8. In polar substances dipole to dipole creates the electrostatic attraction.

It is this force which crystallizes Argon Crystals at -187°C and liquefies He at 4K.

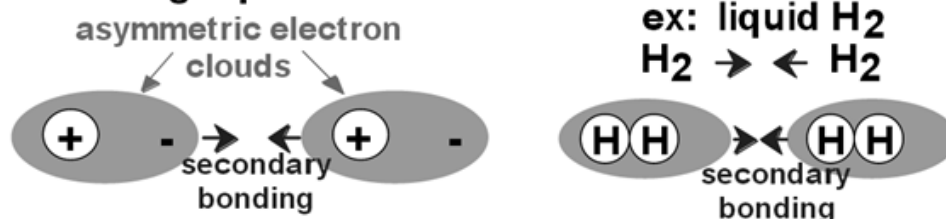
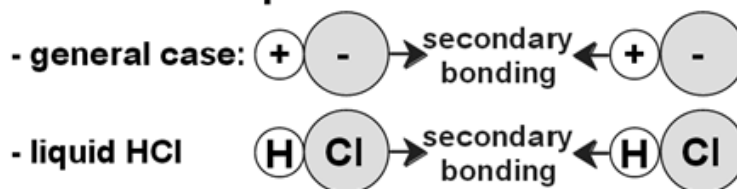
Arises from interaction between dipoles**• Fluctuating dipoles****• Permanent dipoles-molecule induced****Figure 2.8. Fluctuating dipoles or permanent dipoles are the basis for weak Van-der-Waal bonding.**

Figure 8.4

Van-der-Waal force is much weaker than co-valent bond, ionic bond and metal bond hence where this secondary bond is at work M.P is very low as is evident from Table 2.12.

Table 2.12. M.P. of Solid Argon, Solid H and Solid Methane where secondary bonding is at play.

Material	Melting Point	Bond Strength (eV/molecule)
Solid Argon	-189 °C	0.08
Solid Hydrogen	-259 °C	0.01
Solid Methane	-183 °C	0.1

Table 8.1

Section 2.4.5. Anomalous behaviour of Water-Ice.

Animal-life is able to survive in a frozen lake essentially because of the anomalous behavior of Water below 4 °C. Below 4 °C, the cooling should make water denser but instead it makes water lighter as seen in Figure 2.10 as a result there is inverse Temperature Gradient as shown in Figure 2.11 and warmer water remains at lower layers well insulated from freezing cold and provides favourable habitat for the marine world even though the surface of the lake is frozen. This anomalous behavior occurs due to the transition from Close-Pack Structure of Water to Open Pack Structure of Ice as seen in Figure 2.9.

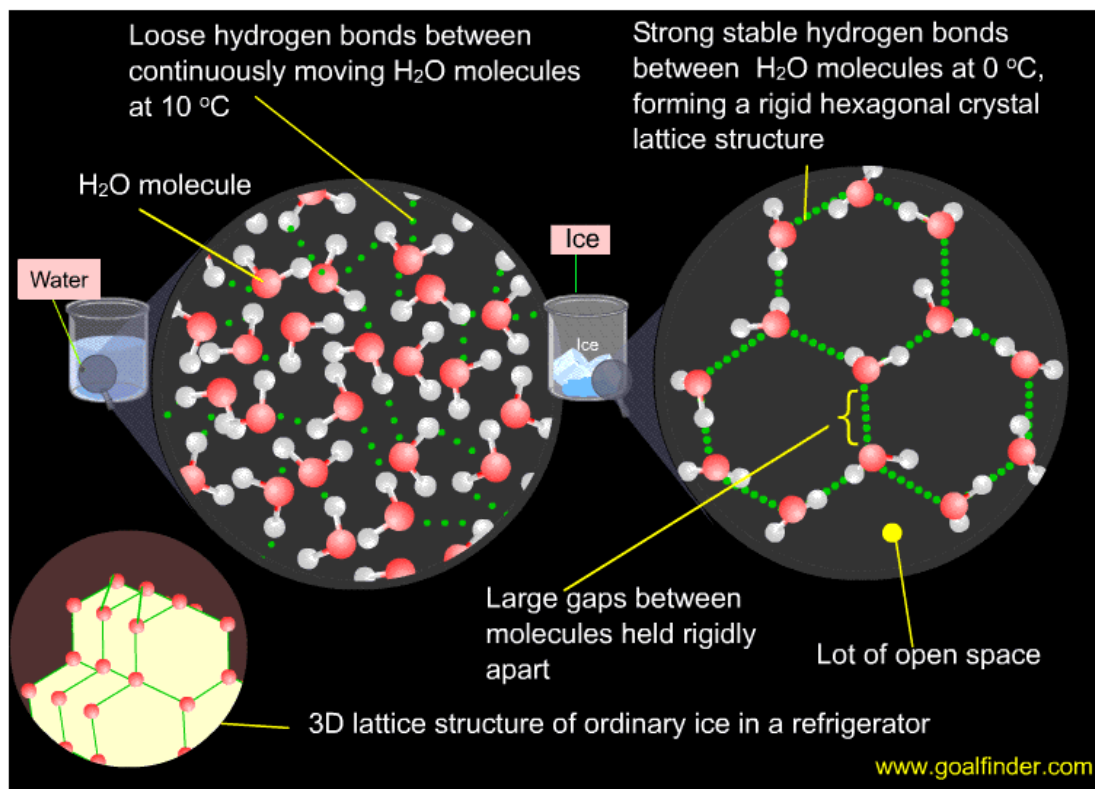


Figure 2.9. Close-Pack Tetrahedral Structure of Water Molecule above 4°C . Open-pack hexagonal channel-like crystalline structure of ICE below 0°C .

Figure 8.5

Anomalous expansion of 1cc water between 4deg C and 0deg C due to phase transition from CLOSE PACK to OPEN PACK crystalline structure.

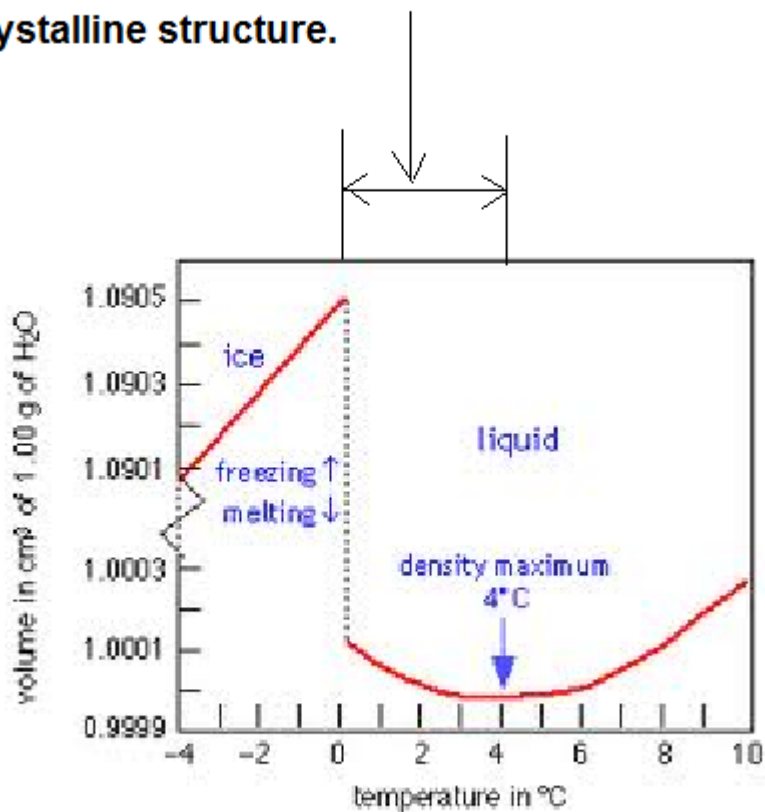


Figure 2.10. Anomalous behaviour of Water below 4deg C.

Figure 8.6

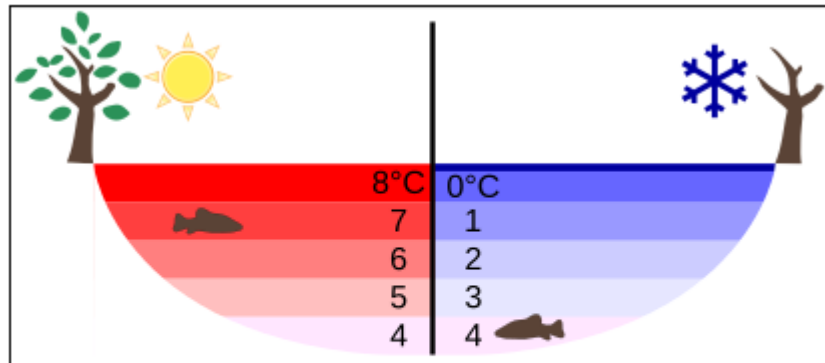


Figure 2.11. Inverse Temperature Gradient below 4deg C in a freezing lake.

Figure 8.7

Chapter 9

Chapter 2. Solid State of Matter.

Section.2.5. Bohr Model of Hydrogen Atom.¹

Chapter 2. Solid State of Matter.

Section.2.5. Bohr Model of Hydrogen Atom.

According to Maxwell's Equation an accelerated electron must give off radiation and lose energy. An electron in an atom in a circular orbit is continuously accelerated towards the center. The acceleration towards the center is:

$$a = \frac{v^2}{r} \text{ where } v$$

= *tangential velocity of electron, tangential to the circle of orbital rotation*

Figure 9.1

and r = radius of the orbit.

2.1

Figure 9.2

This centripetal force is supplied by the electrostatic force of attraction by the nucleus of the Atom given by the following expression:

¹This content is available online at <<http://cnx.org/content/m49815/1.1/>>.

$$m_e \frac{v^2}{r} = \frac{q \times Zq}{4\pi\epsilon_0 r^2} \quad \text{where } Z = \text{Atomic Number} = \text{number of electrons}$$

= number of protons, 4π comes because in Rationalized MKS Units 1 Coulomb of charge

Figure 9.3

gives 1 Coulomb of flux hence at a distance r the electric flux density $D = \frac{q}{4\pi r^2}$

Figure 9.4

$$q = |\text{charge}| \text{on an electron} = |\text{charge}| \text{on proton} \quad 2.2$$

Figure 9.5

Therefore:

$$m_e v^2 = \frac{q \times Zq}{4\pi\epsilon_0 r} \quad 2.3.$$

Figure 9.6

A circularly orbiting electron is continuously being accelerated towards the center hence it should be giving of SYNCHROTRON Radiation. Synchrotron radiation has the same frequency as the rate at which electron is orbiting the nucleus of the Atom. Infact this principle is being utilized in modern day Synchrotrons and Betatrons. If this is to occur then electron must spiral into the nucleus and atom must collapse. But all around us the atoms are stable. Hence Bohr made the following Postulates:

Postulate 1. Electrons are in Stationary States. There are some discrete energy states in which electrons are permitted to stay.

Postulate 2. In the stationary states:

$$\text{Angular Momentum} = I \times \omega = m_e r^2 \times \frac{v}{r} = m_e v r = \text{Integral Multiple of } \frac{h}{2\pi} = n\hbar \quad 2.4$$

Figure 9.7

In a few years de Broglie in France gave his hypothesis of matter wave and that:

$$\text{Wavelength of the matter wave of electron} = \lambda = \frac{h}{p} = \frac{h}{mv} \quad 2.5$$

Figure 9.8

Combining Bohr's Law (2.4) and de Broglie hypothesis (2.5) we get the following:

$$2\pi r = \text{circumference of the orbit} = n\lambda \quad 2.6$$

Figure 9.9

Equation (2.6) implies that only the electrons which form a standing wave along their respective orbital paths as shown in Figure 2.12. are permitted to stay in stationary orbits. If the electron does not form a standing wave it starts radiating and it spirals in as shown in Figure 2.13.

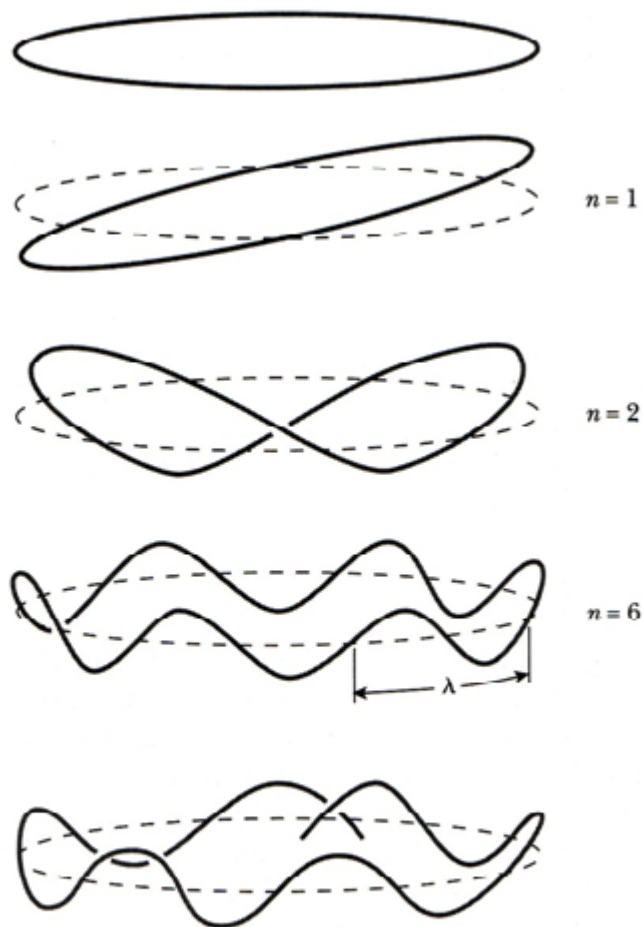


Figure 2.12. Electron's matter wave forms a standing wave corresponding to every principle Quantum Number.

Figure 9.10

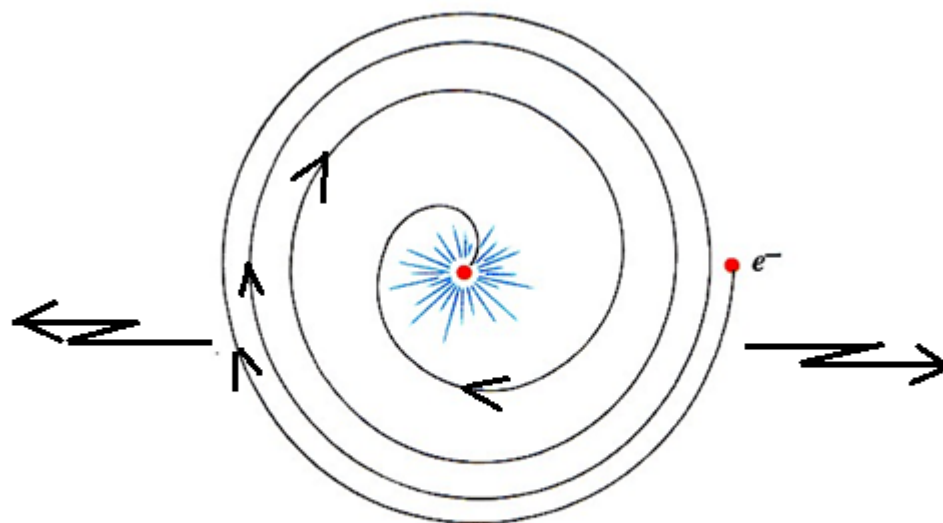


Figure 2.13. Electron in a radiative orbit spirals in as shown and atom collapses.

Figure 9.11

From (2.4) squaring both sides we get:

$$v^2 = \frac{(n\hbar)^2}{(m_e r)^2} \quad 2.7$$

Figure 9.12

Multiplying both sides by the mass of electron we get:

$$m_e v^2 = \frac{(n\hbar)^2}{m_e (r)^2} \quad 2.8$$

Figure 9.13

Both (2.3) and (2.8) give twice the Kinetic Energy of the orbiting electron. In (2.3) the KE has been

obtained from Newtonian Mechanics consideration whereas from Bohr's postulate (2.8) has been obtained. But the two are equal. Based on this equality we obtain:

$$\frac{q \times Zq}{4\pi\epsilon_0 r} = \frac{(n\hbar)^2}{m_e(r)^2} \quad 2.9.$$

Figure 9.14

Rearranging the terms we obtain the radius of the orbits as follows:

$$r_n(\text{radius of the } n^{\text{th}} \text{ Orbit around an atom of Atomic Number } Z)$$

Figure 9.15

$$= \frac{4\pi\epsilon_0(n\hbar)^2}{m_e q^2 Z} = \left(\frac{n^2}{Z}\right) \times \frac{\epsilon_0(h)^2}{\pi m_e q^2} = \left(\frac{n^2}{Z}\right) \times a_0 \text{ where } a_0 = \text{Bohr Radius} = \frac{\epsilon_0(h)^2}{\pi m_e q^2} \quad 2.10$$

Figure 9.16

Calculating the Bohr Radius we get : $a_0 = 52.9459$ picometer(pm).

Here we have taken the Universal Constants and electron charge and mass as follows:

$$q = \text{charge of electron} = 1.6 \times 10^{-19} \text{ C}, m_e = \text{rest mass of electron} = 9.1 \times 10^{-31} \text{ Kg},$$

Figure 9.17

$$\text{Planck's Constant} = h = 6.62 \times 10^{-34} \text{ J} \cdot \text{s}, \quad \epsilon_0 (\text{abs. permittivity}) = \frac{1}{36\pi \times 10^9} \text{ F/m.}$$

Figure 9.18

According to Quantum Mechanics, the maximum probability density occurs at Bohr Radius but the total probability within a sphere of Bohr Radius is less than 65%.

Section 2.5.1. Total Energy of Electron in n th Orbit of an Atom of Atomic Number Z.

Total Energy TE is given as follows:

$$TE = \text{Kinetic Energy} \left(\frac{1}{2} m_e v^2 \right) + \text{Potential Energy} \left(-\frac{q \times Zq}{4\pi\epsilon_0 r} \right) \quad 2.11$$

Figure 9.19

From (2.3) we find that $2 \times \text{KE} = \text{magnitude of PE}$ hence TE simplifies to:

$$TE = \frac{1}{2} \left(-\frac{q \times Zq}{4\pi\epsilon_0 r} \right) = -\frac{q \times Zq}{8\pi\epsilon_0 r} \quad 2.12$$

Figure 9.20

Substituting the nth Orbit Radius (r_n) as given in (2.10) we get TE as follows:

$$TE = -\frac{q \times Zq}{8\pi\epsilon_0} \times \frac{1}{\left(\frac{n^2}{Z}\right) \times a_0} = \left(\frac{Z^2}{n^2}\right) \times \left(\frac{1}{a_0}\right) \times \left(\frac{q^2}{8\pi\epsilon_0}\right) \quad 2.13$$

Figure 9.21

From (2.10) and (2.13) gives the orbital radius and the corresponding energy for any atom of Atomic Number Z.

Section 2.5.2. Calculation of the orbital radii and Total Energy of different principle Orbits of Hydrogen Atom.

We use (2.10) and (2.13) to determine the orbital radii and total energy of the discrete energy states of Hydrogen. Here $Z=1$ is taken since H atom has 1 electron and 1 proton. In (2.13) the results are obtained in Joules. To obtain results in eV we must divide Joules by $(qC \times 1V)$. The results of calculations is given in Table 2.13.

Table 2.13. Radii and total Energy of Hydrogen Atom Principal electronic Orbits.

(Principal Quantum Number)n	r_n (Angstrom)	Total Energy(eV)
1	0.529	-13.6
2	2.12	-3.4
3	4.76	-1.5
4	8.47	-0.85

Table 9.1

Based on the above Table a correct theoretical basis of the Spectral Lines of Hydrogen Atom was provided by Neil Bohr as explained in Figure 2.14.

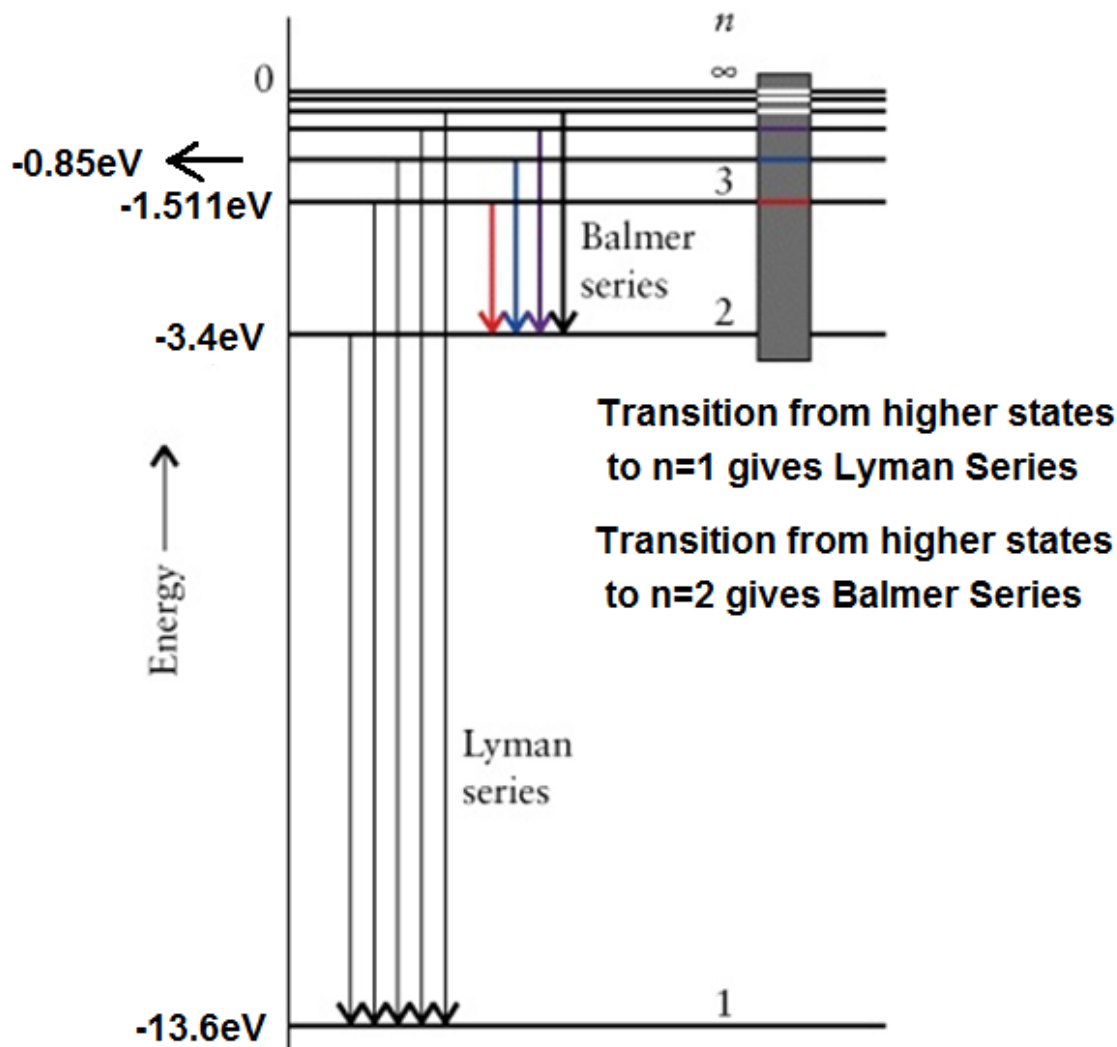


Figure 2.14. Theoretical Basis of the Spectral Lines observed in Hydrogen Atom.

Figure 9.22

As seen in Figure 2.14:

Transition from higher states to ground state namely $n = 1$ gives Lyman Series.

Transition from higher states to next excited state namely $n = 2$ gives Balmer Series.

Transition from higher states to third excited state namely $n = 3$ gives Paschen Series.

Transition from higher states to fourth excited state namely $n = 4$ gives Brackett Series.

Transition from higher states to fifth excited state namely $n = 5$ gives Pfund Series.

Section 2.5.3. Problems with Bohr Theory.

Bohr's Model is unable to show that apart from Principal Quantum Numbers(n) there are azimuthal/orbital quantum number (l), magnetic quantum numbers (m) and spin quantum numbers (s).

In 1925, Erwin Schrodinger proposed Wave Mechanics applicable to matter wave.

His proposition was the following:

$$H\psi = E\psi$$

2.14

Figure 9.23

H is the Hamiltonian Operator which includes KE plus PE operator. The Hamiltonian Operator operating on Matter Wave yields the Eigen Values of Hamiltonian Operation.

This equation was applied to an electron orbiting a proton in a Hydrogen atom. Since it had spherical symmetry hence Spherical Coordinates or Spherical Frame of Reference was adopted. The solution of Schrodinger Equation yielded the three non-relativistic quantum numbers namely:

Principal Quantum Number 'n' which gives the quantization of Energy of Orbital Electrons.

Azimuthal/Orbital Quantum Number 'l' which gives the quantization of the orbital angular momentum L.

Magnetic Quantum Number 'm' which gives the quantization of the orientation of L with a special frame of reference Z axis.

(2.14) is non-relativistic equation hence only non-relativistic Quantum Numbers are predicted.

Relativistic treatment yields the Spin Quantum Numbers.

These four Quantum Number have been explained Section 2.4.

Bohr Theory could not be used to determine energies of atoms with more than one electron. It was unable to explain fine structure observed in H atom spectra. It cannot be used to understand bonding in molecules, nor can it be used to calculate energies of even the simplest molecules. Bohr's model based on classical mechanics, used a quantization restriction on a classical model.

Section 2.5.3. Calculation of Outermost Orbital Radii and Total Energy associated with Outermost Electron in Noble Gases He, Ne, Ar, Kr, Xe and Rn.

Equations (2.10) and (2.13) cannot be directly applied to atoms heavier than Hydrogen. This is because in complex atoms while studying the outermost orbit we have to account for the screening effect of the intervening electron cloud.

The Inert Gases and their electronic configurations are tabulated in Table 2.3

Table 2.3. Shell Structure of Inert Gas Atoms.

Gas	Z	K-Shell(n=1)	L-Shell(n=2)	M-Shell(n=3)	N-Shell(n=4)	O-Shell(n=5)	P-Shell(n=6)
He	2	1s ²					
Ne	10	1s ²	2s ² , 2p ⁶				

continued on next page

Ar	18	1s ²	2s ² , 2p ⁶	3s ² , 3p ⁶			
Kr	36	1s ²	2s ² , 2p ⁶	3s ² , 3p ⁶ , 3d ¹⁰	4s ² , 4p ⁶		
Xe	54	1s ²	2s ² , 2p ⁶	3s ² , 3p ⁶ , 3d ¹⁰	4s ² , 4p ⁶ , 4d ¹⁰	5s ² , 5p ⁶	
Rn	86	1s ²	2s ² , 2p ⁶	3s ² , 3p ⁶ , 3d ¹⁰	4s ² , 4p ⁶ , 4d ¹⁰ , 4f ¹⁴	5s ² , 5p ⁶ , 5d ¹⁰	6s ² , 6p ⁶

Table 9.2

From Table 2.3 it is evident that in Neon, K-shell electrons and L Shell s-orbital electrons will have a screening effect to the extent that p-orbital in L-Shell will experience only the pull of (10-4) protons and screening factor (S) is 4.

In Argon, K-shell, L-Shell and M-Shells s-orbital electrons will have a screening effect to the extent that p-orbital in M-Shell will experience only the pull of (18-12) protons and screening factor (S) is 12.

In Krypton, K-shell, L-Shell, M-Shell and N-Shell s-orbital electrons will have a screening effect to the extent that p-orbital in N-Shell will experience only the pull of (36-30) protons and screening factor (S) is 30.

In Xeon, K-shell, L Shell, M-Shell, N-Shell and O-Shell s-orbital electrons will have a screening effect to the extent that p-orbital in O-Shell will experience only the pull of (54-48) protons and screening factor (S) is 48.

In Radon, K shell, L Shell, M-Shell, N-Shell, O-Shell and P-Shell s-orbital electrons will have a screening effect to the extent that p-orbital in P-Shell will experience only the pull of (86-80) protons and screening factor (S) is 80.

In 1964, J.C.Slater empirically measured the covalent bonds of all the elements and published their outer orbital radii by the title "Atomic Radii in Crystals" in *Journal of Chemical Physics*, Volume 41, No.10, pp 3199-3205.

I used these empirical values of atomic radii and the modified formula for (2.10) namely:

$$r_n(\text{radius of the } n^{\text{th}} \text{ Orbit around an atom of Atomic Number } Z)$$

Figure 9.24

$$= \left(\frac{n^2}{Z - S} \right) \times a_0 \quad 2.15$$

Figure 9.25

Using the empirical values of the radii and using (2.15) I determined the actual screening effect in each case.

The magnitude of the total energy of the outermost orbital electron directly gives the First Ionization Energy and this has been experimentally measured by .

Table 2.4. Empirical Radii(R), Z, calculated S* , experimentally measured First Ionization Energy of the 6 Inert Gases.

Inert Gas	R(pm)	Z	S*	n(P.Q.N of outermost orbit)	First Ionization Energy(eV)†
He	31	2	0.292068	1	24.8
Ne	38	10	4.42675	2	21.5
Ar	71	18	11.2885	3	16.0
Kr	88	36	26.3735	4	14.0
Xe	108	54	41.744	5	12.0
Rn	120	86	70.1162	6	11.0

Table 9.3

S*- calculated value of Screening effect by me.

E*- calculated value of total energy of the outermost orbital electron.

P.Q.N- Principal Quantum Number.

†Experimentally determined by Greenwood(reference not available)

Chapter 10

Tutorial on Chapter 2: Insulator, Semi-conductor and Metal.¹

Tutorial on Chapter 2: Insulator, Semi-conductor and Metal.

1. Q.1. Fermi-level in Metal :

$$E_F = \frac{h^2}{2m_e} \times \left(\frac{3n}{8\pi}\right)^{\frac{2}{3}} \text{ where } n = \text{density of conduction electrons in the metal}$$
$$= 6.62606876 \times 10^{-34} \text{ J} - \text{s}$$

Figure 10.1

Determine the Fermi-level of Sodium and Copper where $n = 2.5 \times 10^{22}$ electrons/cc and $n = 8.5 \times 10^{22}$ electrons/cc.

Metals	E_F (eV)	n (#/cc)	W_F (eV)	Light absorbed and re-emitted
Li	4.72			
Na	3.12	2.5×10^{22}	2.3	
K	2.14	-	2.2	
Rb	1.82		-	

continued on next page

¹This content is available online at <<http://cnx.org/content/m49555/1.2/>>.

Cs	1.53		1.8	
Cu	7.04	8.5×10^{22}	2	Orange
Ag	5.51		4	Appears White because reflects the visible spectrum
Au	11.7		2.3	Yellow
Ca			3.2	
Ba			2.5	
Pt			5.3	
Ta			4.2	
W			4.5	
StBaCuO			1	Most suitable as Cathode material in Thermoionic Tubes.

Table 10.1

1. Q.2. Density of States $[N(E)]$ is defined as number of permissible states per unit volume per unit energy level:

$$N(E) = \frac{\sqrt{2}m_e^{3/2}E^{1/2}}{\pi^2\left(\frac{h}{2\pi}\right)^3};$$

Figure 10.2

Show that mean energy of electron in conduction band is $(3/5)E_F$.

- Q.3. Determine $P(E_F + kT)$ in Fermi-Dirac Statistics. Determine Temperature T at which $P(E_F + 0.5eV) = 1\%$. [Answers: 0.27, 1262Kel]
- Q.4. Determine the density of occupied states at $(E_F + kT)$ at $T=300K$. Find the energy E below (E_F) which will yield the same density of occupied states. [Answer 0.92eV]

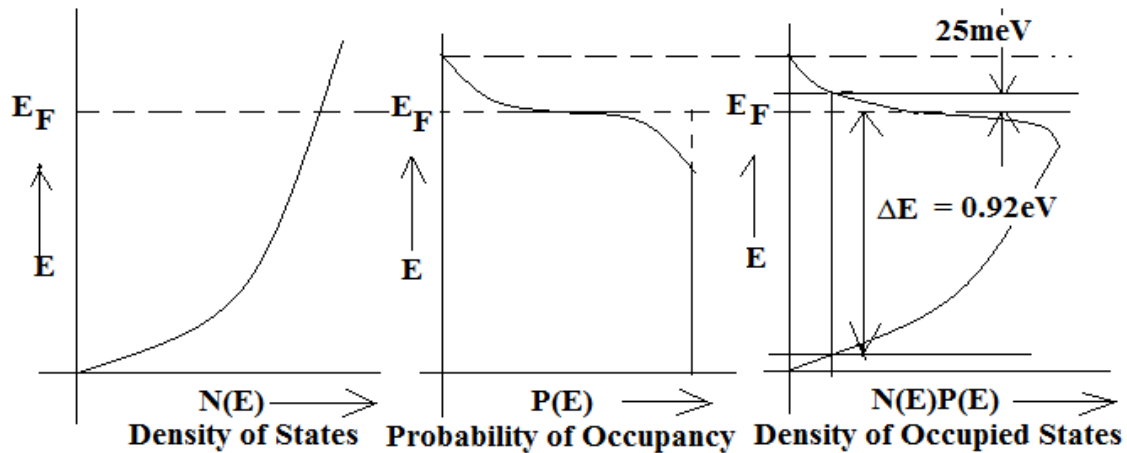


Figure 10.3

1. Q.5. Determine the Fermi Velocity of conduction electron in Metal Copper and Thermal Velocity of conduction electron or hole in Semi-conductor.

[Hint:

$$\text{In Metal } \frac{1}{2}m_e v_F^2 = \frac{3}{5}E_F \text{ and in Semi-conductor } \frac{1}{2}m_e v_{\text{Thermal}}^2 = \frac{3}{2}kT;$$

Figure 10.4

] {Answer : Fermi Velocity in Metal Copper is $2.7256 \times 10^6 \text{m/s}$ and in semi-conductor Thermal Velocity is $1.17 \times 10^5 \text{m/s}$ }

1. Q.6. In Copper, ρ (resistivity) = $1.67 \times 10^{-8} \Omega\text{-m}$ and σ (conductivity) = $6 \times 10^7 \text{S/m} = q\mu n$. Where $n = 8.5 \times 10^{28} \text{electrons/m}^3$. Determine conduction electron mobility. [$40 \text{cm}^2/(\text{V-s})$]
2. Q.7. 3 m long Copper wire of $R = 0.03 \Omega$ and the current I through the wire is 15A.
 - a. Determine Voltage Drop across the Wire. [0.45V]
 - b. Determine the Electric Field within the Wire. [0.15V/m]
 - c. Determine the drift velocity of electron within the wire. [$0.6 \times 10^{-3} \text{m/s}$]
 - d. Determine the Fermi Velocity. [$2.7256 \times 10^6 \text{m/s}$]
 - e. Determine the Mean Free Time or Relaxation Time. [$2.27 \times 10^{-14} \text{s}$]
 - f. Determine the Mean Free Path and compare with the lattice parameter of Copper. [618\AA]

- Q.8. Typical Resistivity of N-Type Silicon is $1 \Omega\text{-cm}$ and typical current density is $100\text{A}/\text{cm}^2$. Calculate the applied Electric Field in Silicon Sample and calculate the drift velocity. Assume mobility of electron to be $1400\text{cm}^2/(\text{V-s})$ [Answer: $100\text{V}/\text{cm}$ and $140 \times 10^3 \text{cm}/\text{s}$]
- Q.9. Calculate the intrinsic resistivity of Ge, Si and GaAs. [$107\Omega\text{-cm}$; $3.4 \times 10^5 \Omega\text{-cm}$; $7 \times 10^8 \Omega\text{-cm}$].
- Q.10. In all the calculations above we have assumed that the effective mass of electron or hole within the solid is the same whereas it is not true. The effective mass in Metals are generally higher than the free space mass and in semiconductors it is lighter as seen from the Table below.

Material	Si	Ge	GaAs	InAs	AlAs
m_e^*/m_e	0.26	0.12	0.068	0.023	0.88
m_{hole}^*/m_e	0.39	0.3	0.5	0.3	0.3
$E_g(\text{eV})$	1.12	0.67	1.42	0.35	2.2

Table 10.2

Electrons and holes in a crystal interact with the periodic potential field in the crystal. They surf over the periodic potential variation of the crystal developing roller coaster effect which leads to drastic reduction in effective mass. If effective mass is considered the thermal velocity comes to be much higher.

For electron with effective mass of $0.26m_e$ the thermal velocity is $2.3 \times 10^5 \text{m}/\text{s}$.

For hole with effective mass of $0.39m_e$ the thermal velocity is $2.2 \times 10^5 \text{m}/\text{s}$.

- Q.11. Find the drift velocity, mean free time and mean free path in a P-Type Sample with hole mobility = $470\text{cm}^2/(\text{V-s})$ and applied Electric Field $E = 10^3 \text{V}/\text{cm}$. All calculations will have to be carried out in Rationalized MKS units that is mobility will be taken as $0.047\text{m}^2/(\text{V-s})$. Thermal Velocity at Room Temperature is approximately $10^5 \text{m}/\text{s}$. [$4.7 \times 10^5 \text{cm}/\text{s}$, $\tau = 0.1\text{ps}$, $\text{MFP} = 100\text{\AA}$]

Chapter 11

SSPD _ Chapter 1 _ Part 12 _ Quantum Mechanical Interpretation of Resistance¹

SSPD _ Chapter 1 _ Part 12 _ Quantum Mechanical Interpretation of Resistance in a conductor.

1.12. SCATTERING OF CONDUCTING ELECTRONS AND RESISTIVITY OF SOLIDS.

Here we are dealing with a 3-D orderly configuration of atoms arranged as a single crystal of infinite dimensions. We have already seen that electron has all the properties of light wave namely: Bragg reflection, refraction, interference and diffraction. Therefore scattering of electrons cannot be understood in a classical manner.

Liquid state of matter causes fifty times more scattering of electron as compared to the gaseous state of matter where as liquid is thousand times more dense. Therefore extent of scattering does not depend on the density of scattering centers but on the disorderly arrangement of the scattering centers. Here it will be proper to point out as to exactly what the difference is between scattering and reflection.

A smooth plane reflects light whereas a rough plane scatters light. In reflection the angles of incidence are identical hence angles of reflection are identical. As a result the total incident beam of light is reflected. In a rough plane, the constituent rays of the light beam are reflected in different directions since the angles of incidence are different for different rays. This is known as scattered light. These two phenomenon are shown in Figure(1.68).

¹This content is available online at <<http://cnx.org/content/m34450/1.1/>>.

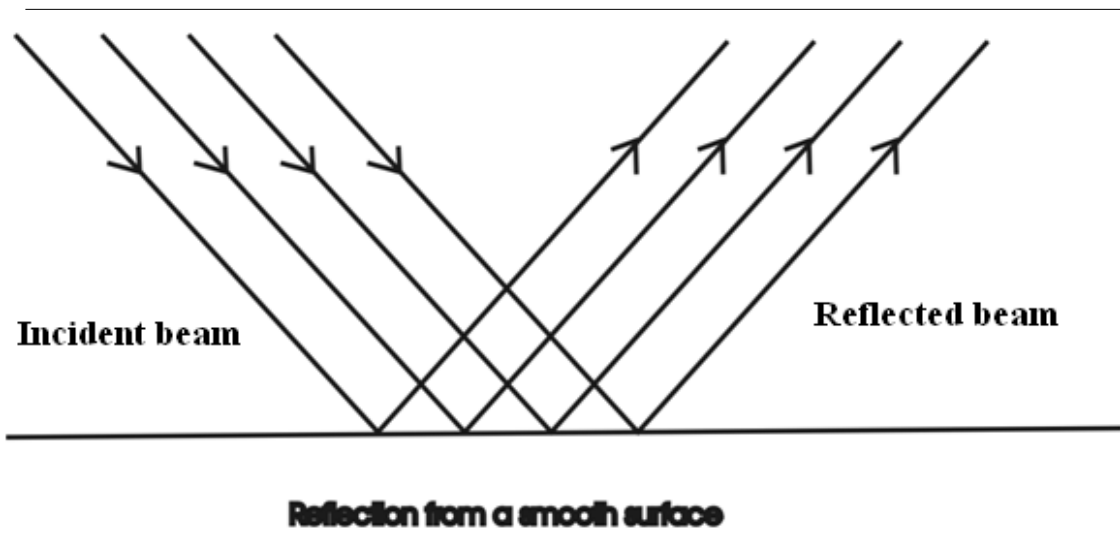


Figure 1.68.a. Reflection from a smooth surface keeps the reflected rays parallel. Hence incident beam is parallel and reflected beam is parallel.

Figure 11.1

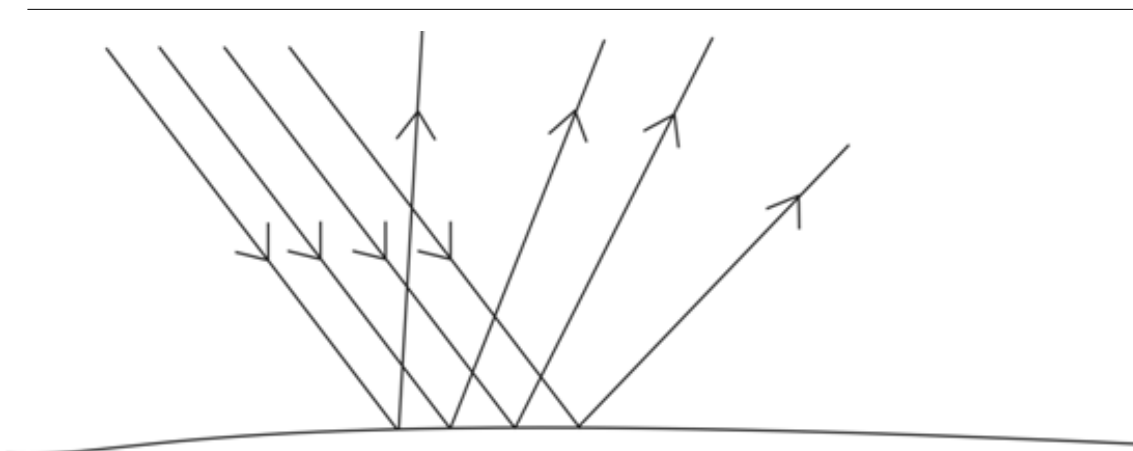


Figure 1.68.b. Parallel beam incident on an irregular and rough surface causes scattering. The reflected rays are no more collimated. They scatter out in all directions. Hence the reflected beam is diffused in nature.

Figure 11.2

Figure 1.68. Reflection and Scattering.

Electron is a matter wave probability amplitude matter wave. In 3-D orderly crystalline solid the propagation of electron causes the interaction with and vibration of all the intervening lattice centers. The lattice centers become the emitters of secondary wavelets.

The secondary wavelets interfere and propagate forward in the direction of constructive interference.

- If the crystal is at 0 Kelvin then there is no thermal vibration. Also assume that there are no crystal defects and that there are no impurities.
- Also the crystalline lattice is not bounded by surfaces and is infinite in the three directions.
- Also electrons are in the outer partially filled conduction band well removed from the upper edge of the conduction band.

If all these conditions are fulfilled then the direction of constructive interference will be the direction of incidence and electron will propagate forward as if there is no obstacle in its path. The first impulsive energy will sustain the electron in a straight line propagation path with uniform velocity with no dissipation of energy. This propagation will continue for infinite time and till infinite distance. This is exactly as Newton had predicted about the inertness of bodies: A body at rest will continue to be at rest and a body in motion will continue to be in motion in a straight line with an uniform velocity unless made to act otherwise by the application of force.

This is what is more popularly known as SUPERCONDUCTIVITY.

Near the upper edge of the conduction band, electrons will suffer Bragg Reflection and this will be decided by the direction of orientation of the lattice plane from where the specular reflection takes place.

Lattice thermal vibration or/and lattice defects or/and lattice impurities cause the disorderliness and this disorderliness leads to change of direction of propagation or the change of direction of constructive

interference. This change of direction is called scattering of electron. The change of direction is random and the distance over which this happens is statistically varying. The mean distance over which a straight line motion is maintained before scattering occurs is called the mean free path and the mean time taken to cover the mean free path is called mean-free time. The electron scattering within a real crystalline lattice which suffers from all defects and imperfections and which is at Room Temperature has been illustrated in Figure(1.69).

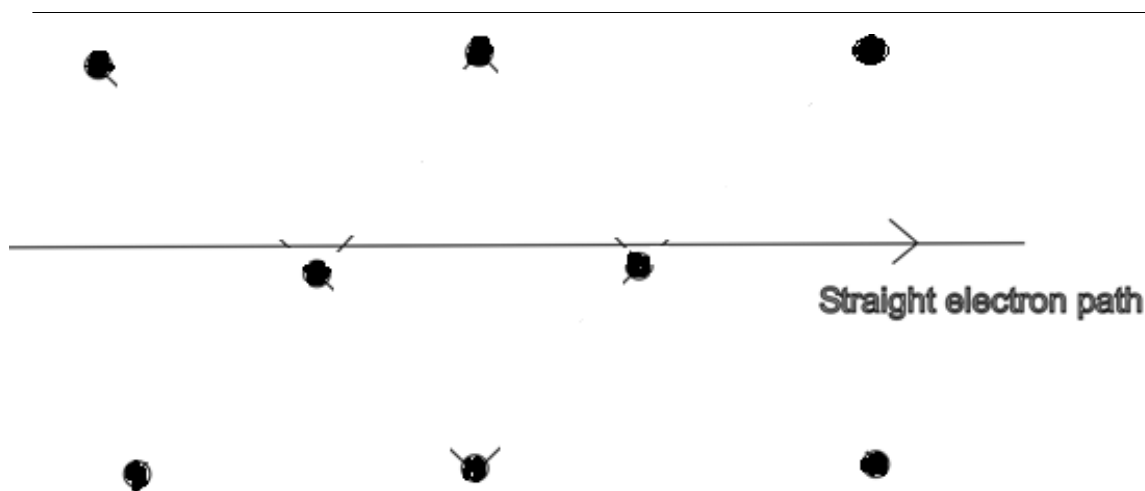


Figure 1.69.a. Electron is moving along a straight path in an ideal crystalline lattice. An ideal crystalline lattice has no defects, no imperfections and no thermal vibrations. Electron experiences a no scattering.

Black Circles are Lattice Centers arranged in a perfect orderly pattern.

Figure 11.3

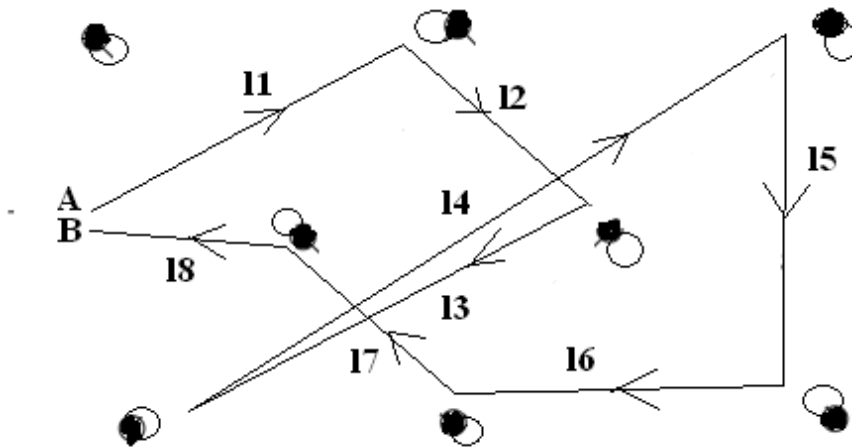


Figure 1.69.b. A real crystalline lattice is shown with lattice centers randomly displaced with respect to orderly arrangement of lattice centers due to thermal vibration. This perturbation in the orderly arrangement leads to random motion of electron with no net displacement in time. As we see that after eight scattering electron initially starting from 'A' finally ends at 'B' which is more or less in the same location as 'A'.

**Black circles denote the orderly pattern of crystal.
Open circle represent the perturbation in the regular orderly arrangement of the lattice centers.**

Figure 11.4

Figure 1.69. Scattering Phenomena of electron in a real crystalline lattice where lattice thermal vibration, lattice defect, lattice impurities and lattice boundaries are present.

This scattering of electron does not depend on the density of lattice centers but on the degree of disorderliness of the lattice centers and this degree of disorderliness depends on thermal vibration, lattice defects and lattice impurity density.

By increasing the temperature, the amplitude of lattice thermal vibrations is increased ;

During the growth of the crystal, lattice defects are increased;

During doping and diffusion, impurities are introduced in the crystal.

All these factors contribute towards disorderliness which in turn contribute towards the scattering of the conduction electrons. It is this scattering which creates resistance in a conducting solid. There are two parameters which describe the scattering phenomena:

Mean free path($\langle l \rangle$) and mean free time(τ).

As seen in Figure(1.69.b), at $l_1, l_2, l_3, l_4, \dots$ distances the direction changes.

Therefore mean free path:

$$\langle l \rangle = \frac{\sum l_n}{N} \dots \dots \dots \mathbf{1.100}$$

If the time taken is $t_1, t_2, t_3, t_4, \dots$ along the randomly varying paths then the mean free time:

$$\tau = [\sum \mathbf{t} \mathbf{n}] / N \dots\dots\dots \mathbf{1.101}$$

$$\text{And } \langle \mathbf{v} \rangle / \tau = \text{average thermal velocity} = \mathbf{v} \text{ thermal } \dots\dots\dots \mathbf{1.102}$$

By Equipartition Law of Energy, every degree of freedom has an average thermal energy = $(1/2)kT$. Since conducting electron has three degrees of freedom(x, y, z) hence the total average thermal energy of a conducting electron is equal to $(3/2)kT$.

$$\text{Therefore } (1/2)m_e \cdot \mathbf{v} \text{ thermal }^2 = (3/2)kT \dots\dots\dots \mathbf{1.103}$$

Where k = Boltzman's constant = $1.38 \times 10^{-23} \text{ J/Kelvin} = 8.62 \times 10^{-5} \text{ eV/Kelvin}$

And T is temperature at Kelvin scale. m_e^* = effective mass of electron.

Temperature in Celsius scale is added to 273 to obtain temperature in Kelvin Scale. The zero of Kelvin scale occurs at $-273^\circ \text{Celsius}$. At this temperature i.e. at 0 Kelvin the amplitude of thermal vibrations of lattice centers is zero and if there is no lattice defect and no doping then we have a perfect orderly lattice which will behave like a superconductor.

1.12.1. Quantum Mechanical basis of Resistance in a conducting Solid.

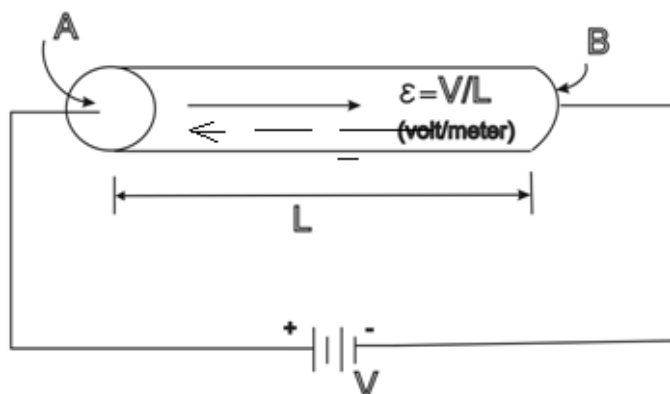
An ideal crystal with no lattice defects, no dopents and at zero Kelvin temperature behaves like a superconductor.

In a normal metal, resistance is always present.

Let us consider a cylindrical metal of length L cm and $A(\text{cm})^2$ cross-sectional area. A potential difference of V volts is applied across it as shown in Figure(1.70).

The electric field along the longitudinal axis is:

$$\varepsilon = (V/L) \text{ Volt/meter } \dots\dots\dots \mathbf{1.104}$$



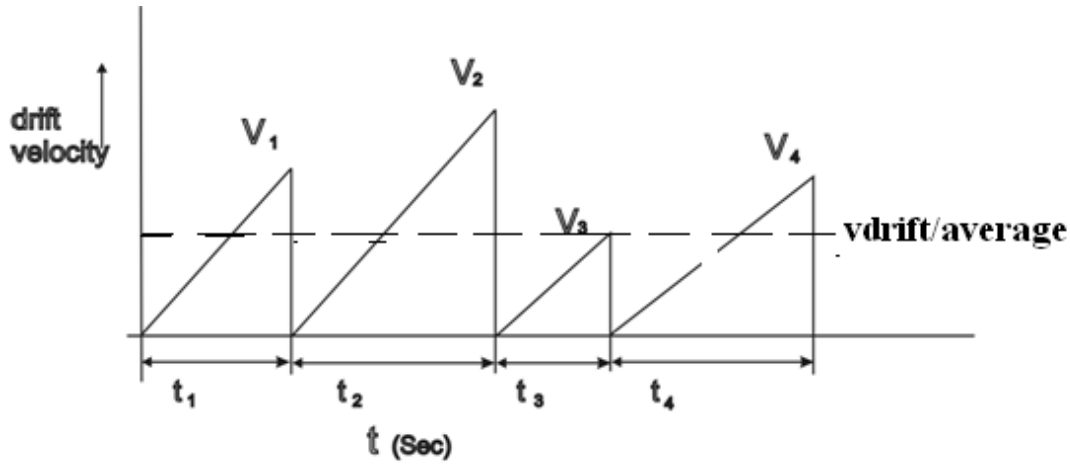
(a) The application of an electric field across cylindrical metal specimen

Figure 1.70.a. An electric field is applied along the positive z axis of a cylindrical metal conductor. Electrons move along the negative z axis causing an electric current $I = V / R$

where $R = (\text{resistivity}) \cdot (L) / A = R = \rho L / A$ according to Ohm's Law.

Electrons move along the negative z axis shown by the broken line.

Figure 11.5



(b) The instantaneous drift velocity of electron with respect to time

Figure 1.70.b. Instantaneous drift velocity profile with respect to time.

Figure 11.6

Figure 1.70. Electron drift in z direction(longitudinal axis of the cylinder) after the application of the z-axis electric field.

According to Kinematics, the electric field is applied in z direction. This will cause an acceleration in [-z] direction since electron is negative. This acceleration will continue until the electron gets scattered. At the point of scattering all the kinetic energy of the electron is imparted to the lattice and the electron starts anew from zero velocity. Since this is an statistical phenomena hence acceleration time periods are $t_1, t_2, t_3, t_4, \dots$ and the terminal velocities are $v_{t1}, v_{t2}, v_{t3}, v_{t4}, \dots$. Acceleration time periods

$t_1, t_2, t_3, t_4, \dots$ are the same as the transit periods along the randomly changing straight line segments as defined in Eq.(1.100)

From kinematics: $v_{tn} = u + at_n$

where $a = \text{acceleration} = \mathbf{F}/m_e^* = q\varepsilon / m_e^* = q(\mathbf{V}/L) / m_e^* \dots \dots \dots$
1.105

But $u = \text{initial velocity} = 0$ therefore $v_{tn} = at_n = (q\varepsilon / m_e^*) (t_n) \dots \dots \dots$
1.106

Therefore the average drift velocity over n^{th} acceleration period is:

$$v_n = (v_{tn} + 0)/2 = (q\varepsilon / 2m_e^*) (t_n) \dots \dots \dots \quad \mathbf{1.107}$$

Suppose during the flow of current from one end to the other, a given electron undergoes N scattering. This means it undergoes N acceleration periods.

The average drift velocity during N periods of acceleration which occur during the flow of the current is:

$$v_{\text{drift}} = [\sum v_n]/N = [\sum (q\varepsilon / 2m_e^*) (t_n)]/N$$

$$\text{Therefore } v_{\text{drift}} = (q\varepsilon / 2m_e^*) [\sum (t_n)]/N$$

$$\mathbf{v_{drift}} = (q\varepsilon / 2m_e^*) \tau = (q \tau / 2m_e^*) \cdot \varepsilon \dots \dots \dots \quad \mathbf{1.108}$$

where $\tau = [\sum (t_n)]/N = \text{mean free time as defined in Eq.(1.101)}$ and

$$\mu_n = \text{electron mobility} = (q \tau / 2m_e^*)$$

This relation was used to determine the electron mobility in Table 1.11, Part 11.

Now under low drift velocity condition, drift velocity varies directly as the applied field ϵ and the constant of proportionality is known as the drift mobility (μ (cm²/(v-sec)) as shown in Figure 1.72.

$$\mathbf{v}_{\text{drift}} = (\mathbf{q} \tau / 2\mathbf{m} \mathbf{e}^*) \epsilon = \mu \mathbf{n} \epsilon \dots\dots\dots \mathbf{1.109}$$

Current density = \mathbf{J} = number of Coulombs/second

Therefore $\mathbf{J} = \mathbf{q} \times$ number of electrons flowing through unit cross-sectional area per second.

If we assume that there is no diffusion of mobile carriers and we only have electric drift of the mobile carriers then number of electrons flowing through unit cross-sectional area per second = $(1\text{cm}^2)(v_{\text{drift}})(n)$

where n = number of conducting electrons per unit (cm)²

and v_{drift} = drift velocity of electrons;

$$\text{Therefore } \mathbf{J} = (\mathbf{q} \cdot \mathbf{v}_{\text{drift}} \cdot n) \text{ Coulombs}/(\text{sec-cm}^2) \dots\dots\dots \mathbf{1.110}$$

$$\text{Or } \mathbf{J} = \mathbf{q} \cdot \mu \cdot \epsilon \cdot n = \sigma \cdot \epsilon \dots\dots\dots \mathbf{1.111}$$

Where σ (conductivity) = $1/\rho$ (resistivity)

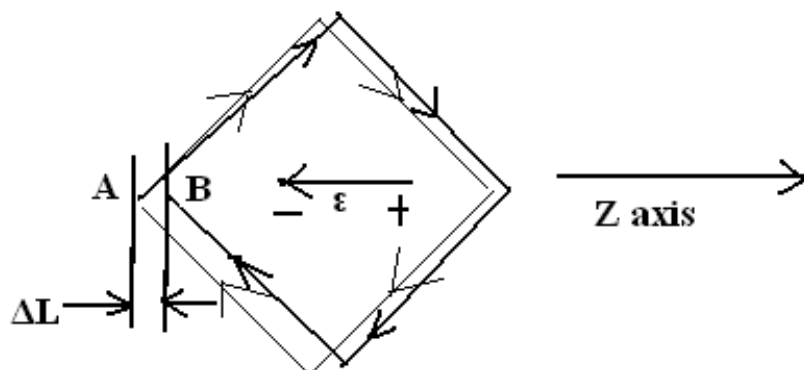
$$\mathbf{J} = \mathbf{q} \cdot \mu \cdot \epsilon \cdot n = \sigma \cdot \epsilon$$

$$\text{Or } \mathbf{J} = \mathbf{I}/\mathbf{A} = (1/\rho) \times (\mathbf{V}/\mathbf{L})$$

$$\text{Therefore } \mathbf{V}/\mathbf{I} = \mathbf{R} = (\rho \mathbf{L})/\mathbf{A} \rightarrow \text{Ohm's Law.} \dots\dots\dots \mathbf{1.112}$$

In Eq.(1.109), we find that drift mobility is directly dependent on the mean free time between two consecutive scatterings. Mean free time (τ) is dependent on scattering. Larger is the perturbation in the lattice network from the ideal lattice more frequent will be the scattering and hence shorter will be the mean free time. As the perturbation from the ideal condition or the disorderliness is reduced, so will the scattering phenomena be reduced and mean free time will become longer. Under ideal condition there will be no scattering and mean free time will become infinite. Here the mobility becomes infinite, conductivity becomes infinite and resistivity becomes zero. This is a superconductor. Here once an electron gets an impulsive push it continues to travel in a straight line for infinite distance and for infinite time without any energy dissipation. Hence initial kinetic energy imparted by the impulsive push is conserved forever by the conducting electron. This is tantamount to a current flow in a close loop superconductor without any battery connected to the circuit.

In a normal conductor even with no battery connected, the mobile carriers are undergoing random motion with no net displacement. When an electric field is applied then superimposed on this random motion there is a net displacement of electrons in the opposite direction to the electric field. This has been shown in Figure(1.71). The net displacement is given by ΔL in time Δt .



Thin line is the random motion with no electric field hence there no net displacement.
If an electric field is applied in -z direction then the scattering follows the bolder line and after four scatterings the electron is displaced with respect to the original position by by ΔL in time Δt in positive z direction and the electric field is applied in -z direction.

Figure 1.71. The net drift experienced by an electron under the influence of electric field.

Figure 11.7

As can be seen in Figure 1.71 electron is undergoing continuous random motion under the influence of thermal energy. As temperature increases electrons become more restless and start meandering along more zig zag path but they never make a net displacement in any direction as shown by 'thin line' zig zag path. But as an electric field(ϵ) is applied in $-z$ direction, electron follows bolder line and as seen in Figure 1.71 it experiences a net displacement of ΔL in $+z$ direction in Δt .

$$\Delta L/\Delta t = \text{average drift velocity} = v_{\text{drift}} = \mu_n \epsilon ;$$

In 1911, Kamerling Ons detected superconductivity and superfluidity in solid mercury at 4.3Kelvin.

In 1962 a Russian Scientist was awarded the Nobel Prize in Physics for his study on superfluidity and superconductivity in liquid Helium at 4Kelvin.

In 1987 Karl Alex Muller and Bednorz of Germany were awarded the Nobel Prize for discovering the superconductivity in ceramic Yttrium Barium Copper Oxide [$Y_1Ba_2(CuO)_3$] at liquid Nitrogen temperature 77Kelvin. Bednorz was a research student under Muller at that time.

Before we leave this Chapter on mobility and resistance it will be appropriate to introduce the reader to the concept of two kinds of mobilities:

First kind μ_{lattice} due to the scattering caused due to lattice thermal vibration and it is temperature

dependent;

Second kind μ_{impurity} due to the scattering caused due to the dopants and/or crystalline defects;

At liquid Helium temperature that is at less than 4Kelvin there is no scattering due to thermal vibrations but scattering due to impurity and/or crystal defect persist. Therefore semiconductors never become superconductors. Even at 0Kelvin residual resistivity persists due to impurity and/or crystal defect.

So the effective mobility is given by the following reciprocal relationship:

$$1/\mu = 1/\mu_{\text{lattice}} + 1/\mu_{\text{impurity}} \dots\dots\dots 1.113$$

The quantum-mechanical model of electron scattering, which has been presented in this chapter is valid only when drift velocity is much lower than the thermal velocity. When we reach high Electric Field region, the electric energy is directly transferred to the crystalline lattice and the drift velocity saturates at Scatter Limited Velocity as shown in Figure(1.72). The Scatter Limited Velocity is 10^7 cm/sec for Silicon and it can be derived from the following relation:

$$(1/2)(m_e^*)(v_{\text{scatter limited}})^2 = (1/2)(m_e^*)(v_{\text{thermal}})^2 = (3/2)kT \dots\dots\dots 1.114$$

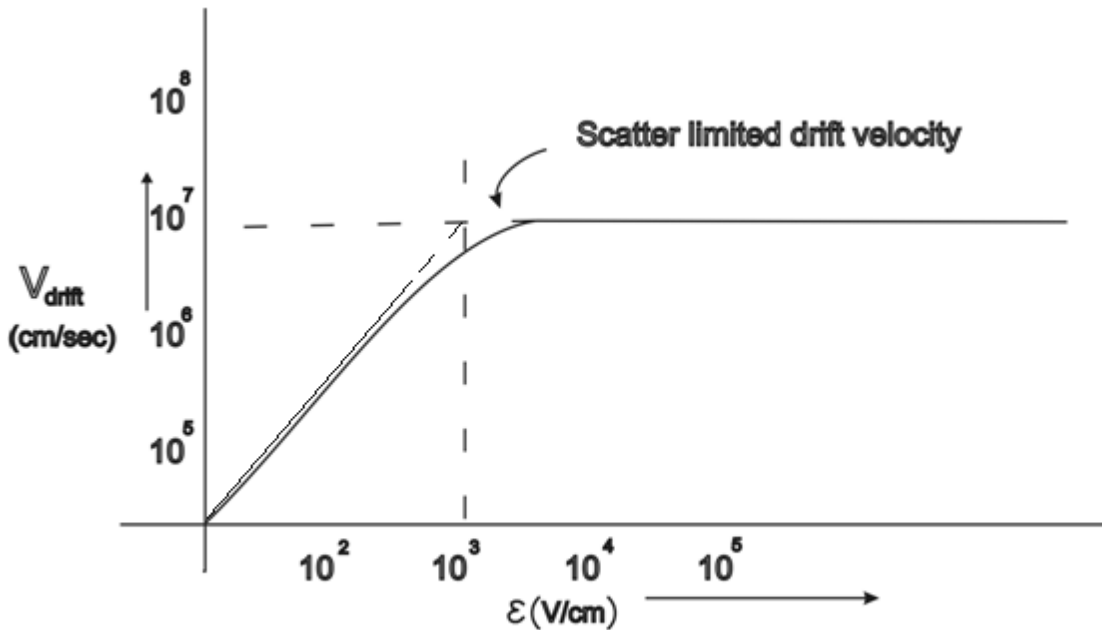


Figure 1.72. Vdrift versus Electric Field.

Figure 11.8

Figure 1.72. In high electric field region the drift velocity saturates at scatter limited velocity.

The Quantum Mechanical perspective tells us that electron is not impeded by the lattice centers. If the lattice centers are perfectly orderly at 0Kelvin then electron if imparted an impulsive energy will acquire a finite kinetic energy and with this KE it will continue to travel in a straight line through the crystalline lattice till infinity. What impedes the flow and causes the loss of KE is not lattice centers per se but the disorderliness of the lattice center network. This is the reason why Graphene is working out to be a wonder material with a very large drift mobility. Graphene is a sheet of orderly arrangement of hexagonal structure

which is unperturbed or unbroken over large distances hence mean free path in Graphene is of the order of micrometers as compared to the mean free path in GaAs where it is of the order of a fraction of micrometer.

Chapter 12

SSPD _ Chapter 1 _ Part 11 _ Solid State of Matter¹

SSPD _ Chapter 1 _ Part 11 _ Solid State of Matter

1.10.DEFINITION OF INSULATORS, SEMICONDUCTORS AND INSULATORS.

1.10.1. SIX STATES OF MATTER.

There are six states of matter: gas, liquid, solid, plasma, Bose-Einstein Condensate and Fermi-ionic Condensate.

Gas has no fixed shape or volume. They have the shape and volume according to the vessel they occupy. Inter molecular distances are large and molecules are independent of one another. This state of matter obeys the Ideal Gas Law.

Liquid has a fixed volume but no fixed shape. It takes the shape of the vessel it occupies. Intermolecular distances are fixed and molecules experience cohesive force with respect to one another.

Solids have a fixed volume and fixed shape. The molecules are arranged in an orderly fashion giving rise to a crystalline structure. Because of the variation in the range of orderliness, the crystalline structure is classified as Single Crystal, Poly-crystal and Amorphous. The range of orderliness is shown in Figure(1.39).

For 300,000 years after the Big-Bang, temperature of the Universe was above 4000K and all matter was in PLASMA STATE. This is a soup of electrons, protons and neutrons. As long as matter is in plasma state, RADIATION dominates. Gravitational attraction is dominated by electromagnetic forces and thus the gravitational accretion is prevented. As soon as temperature falls below 4000K, plasma recombines to form neutral mass of Hydrogen (70%), Helium(30%) and traces of Lithium. At this point radiation decouples and matter dominates. The decoupled radiation carries the imprint or profile of the matter distribution through out the Universe at the time of de-coupling. This decoupled radiation persists till today in almost its pristine state in which it decoupled from the matter. This decoupled radiation is known as Cosmic Microwave Background Radiation (CMBR). The latest study of CMB by WMAP show that indeed there are hot spots and cold spots in CMB implying that in the remote past matter distribution did contain the unevenness which would eventually become the seeds for the formation of clusters, galaxies, solar systems and planets.

Bose-Einstein Condensate and Fermi-ionic condensate are described in Section (1.15). They are closely related but Fermi-ionic Condensate formed at a lower temperature than the temperature at which Bose-Einstein Condensate is formed. It manifests a complex of spectacular behavior:

- i. It flows through tiny capillaries without experiencing any friction;
- ii. It climbs in the form of film over the edge of vessels containing it. This phenomena is referred to as 'film creep';
- iii. It spouts in a spectacular way when heated under certain conditions;

¹This content is available online at <<http://cnx.org/content/m34343/1.1/>>.

- iv. If it is contained in a rotating container, the content in He-II Phase never rotates along with the container.

1.10.2. SOLID STATE OF MATTER.

With the development of Quantum Mechanics, Band Theory of solid was proposed by Felix Bloch[Appendix XXXXIII]. As already seen in the last section, electrons in a single crystal solid occupy energy bands separated by forbidden zones known as Band Gaps as shown in Figure(1.40) , Figure(1.41) and in Figure(1.49).

The outer band is known as the conduction band and the band just below is valence band. In insulators and semiconductors, the energy band gap between valence and conduction is wide of the order of eV and conduction band is completely empty at low temperatures for both insulators and semiconductors. That is at 77K (liquid Nitrogen temperature) and below, semi-conductor is an insulator. Only near room temperature and by introduction of controlled amount of impurities that semiconductor acquires a certain degree of conductivity. As we will see in semiconductor chapter the effective density of states at the lower edge of conduction band (N_C)

and at the upper edge of the valence band (N_V) is nearly the same as shown in Table(1.10). This is of the order of 10^{19} permissible states per centimeter cube. Hence as soon as *doping approaches this order of magnitude, number of conducting electrons are comparable to the available energy states which is the criteria for degenerate systems. Hence at that order of magnitude of doping, semiconductor becomes degenerate and behaves like a semi-metal.*

So an INSULATOR can be defined as the solid which has an empty conduction band and a large band gap , of the order of 4eV or more. There electron- hole pair cannot be thermally generated . Hence it remains non-conducting at all temperature.

On the contrary, SEMICONDUCTORS are non conducting and hence insulator below liquid Nitrogen temperature and above liquid Nitrogen temperature they acquire conductivity either due to thermal generation of electron-hole pair or due to contribution of conducting electrons by net donor atoms or due to holes contributed by net acceptor atoms.

Metals have partially filled conduction band or overlapping conduction and valence bands. As a result, there are mobile electrons available in copious amount. This amount is of the order 10^{22} per centimeter cube. As we see in the Table(1.10), atomic concentration in Solids are of the order of 10^{22} per c.c. and each atom contributes an electron for conduction. Hence availability of conduction electrons is 12 orders of magnitude greater than intrinsic Silicon and 9 orders of magnitude greater than that of intrinsic Germanium. Because of this large number of mobile carriers present in metal that resistivity is so much lower in metal than that in semiconductor. This point will become clearer as we proceed with the quantum-mechanical interpretation of conducting electron in metal or in semi-conductor.

As seen in Table(1.10) , the mobility of conducting electrons in semiconductors is much higher than that in metal which is typically $44\text{cm}^2/(\text{V}\cdot\text{sec})$ for Copper.

Table(1.10) Characteristics of Ge, Si and GaAs at 300 K.

Characteristics	Symbol	Units	Ge	Si	GaAs	Cu
Effective Density of States	N_c	Cm^{-3}	1.04×10^{19}	2.8×10^{19}	4.7×10^{17}	
<i>continued on next page</i>						

	N v	Cm⁻³	6.1×10¹⁸	1.02×10¹⁹	7×10¹⁸	
Energy Gap	E g	eV	0.68	1.12	1.42	
Intrinsic Carrier concentration	n i	Cm⁻³	2.25×10¹³	1.15×10¹⁰	1.6×10⁶	8.5×10²²
Effective mass	m n (unit mass 9.11×10⁻³¹ Kg)		0.33	0.33	0.068	
	m p (unit mass 9.11×10⁻³¹ Kg)		0.31	0.56	0.56	
Mobility	μ n	Cm²/(V-s)	3900	1350	8600	44
	μ p	Cm²/(V-s)	1900	480	250	
Dielectric Constant	ε r		16.3	11.8	10.9	
Atomic Concentration		Cm⁻³	4.42×10²²	5×10²²	4.42×10²²	8.5×10²²
Breakdown Field	E BR	V/cm	10⁵	3×10⁵	3.5×10⁵	

Table 12.1

1.10.2.1. METALS (with special reference to the mobility of conducting electrons and its implications for particle accelerators).

Metal is a lattice of positive ions held together by a gas of conducting electrons. The conducting electrons belonging to the conduction band have their wave-functions spread through out the metallic lattice. The average kinetic energy per electron is $(3/5)E_F$ (This will be a tutorial exercise). Hence

$$\frac{1}{2} m^* v_e^2$$

Figure 12.1

=

$$\frac{3}{5} E_F$$

Figure 12.2

1.93

where m^* is the effective mass of the electron but we will assume it to be the free space mass. Therefore:

$$v_e = \sqrt{\left[\frac{6}{5} \times \frac{E_F}{m^*}\right]}$$

Figure 12.3

..... **1.94**

Where

$$v_e = \text{velocity of the mobile electron in conduction band}$$

Figure 12.4

This velocity is not thermal velocity but velocity resulting from Pauli's Exclusion Principle which essentially is the result of the ferm-ionic nature of electrons. Electrons tend to repel one another when confined in a small Cartesian Space. Electrons are claustrophobic.

Therefore mean free path =

$$L^* = v_e \times \tau$$

Figure 12.5

..... **1.95**

Where τ is mean free time.

Substituting the appropriate values for each metal, we get the mean free path for electron in their respective metals.

Table(1.10) Tabulation of the Fermi Energy, velocity, mean free time and mean free path of conducting electrons in their respective metals.

Metal	E F	Velocity($\times 10^5$ m/s)	τ (femtosec)	$L^*(\text{A}^\circ)$
Li	4.7	9.96	9	90
Na	3.1	8.08	31	250
K	2.1	6.65	44	293
Cu	7.0	12.15	27	328
Ag	5.5	10.77	41	441.6

Table 12.2

As we see from Table(1.10), the mean distance between two scatterers is 2 orders of magnitude greater than the lattice constant which is of the order of 5 \AA . Hence lattice centers per se are not the scatterers but infact the disorderliness is what causes the scattering. *The scatterers are thermal vibrations of lattice centers, the structural defect in crystal growth and the substitutional/interstitial impurities.* This implies that with reduction in temperature mobile electrons will experience less scattering hence the metal will exhibit less resistivity leading to positive temperature coefficient of resistance. We will dwell upon this in Section (1.12).

1.10.2.2. SEMICONDUCTORS

Semiconductors are insulators initially. At low temperatures, all electrons are strongly bonded to their host atoms. Only at temperatures above Liquid Nitrogen that thermal generation of electron-hole pairs take place. So in semiconductors the situation is quite different as compared to that in metal. The conducting electrons and holes owe their mobility to thermal energy they possess in contrast to the conducting electrons in metal. On an average by Equipartition Law of Energy, the mobile carriers possess $(1/2)kT$ thermal energy per carrier per degree of freedom. Since the carriers have 3 degrees of freedom hence they possess $(3/2)kT$ average thermal energy per carrier.

Therefore

$$\frac{1}{2} m^* v_e^2 = \frac{3}{2} kT$$

Figure 12.6

..... 1.96

Therefore

$$v_e = \sqrt{\left[\frac{3kT}{m^*}\right]}$$

Figure 12.7

..... 1.97

Therefore in semiconductors the mean free path will be the product of the thermal velocity and the mean free time. Mean free time is calculated from mobility of the mobile carriers which is determined experimentally.

From Table(1.10) we obtain the mobility values. In Table (1.11) the mobility, mean free time, thermal velocity and mean free paths are tabulated for Ge , Si and GaAs.

Table(1.11) Mobilities, Mean Free Times, Thermal Velocities and Mean Free Paths of Ge, Si and GaAs.

Semiconductor	$\mu(\text{cm}^2/(\text{V}\cdot\text{sec}))$	τ (femtosec)	v_e (m/sec)	L^* (\AA)
Ge	3900	2217	0.95×10^5	2106
Si	1350	767.6	0.95×10^5	729
GaAs	8600	4890	0.95×10^5	4645.5

Table 12.3

As we see electron has much larger mobility in semiconductors as compared to that in metals. This implies that the mean free path of electrons is greater by one order of magnitude in semiconductor as compared to that in metal. But why is the scattering less in semiconductors as compared to that in metal.? This answer is obtained by determining the de Broglie wavelength of electron and by using wave optics.

We will determine the velocity of a conducting electron in Electron Microscope, in metal and in semiconductor. In these three cases the conducting electron gains Kinetic Energy equal to the Potential Energy it loses while falling through a potential difference of 10kV in case of Electron Microscope(because 10kV is the accelerating voltage in Electron Microscope), through a potential difference of 4V in case of metal(because average kinetic energy associated with conducting electron is $(3/5)E_F$ and E_F is 7eV in copper) and through a potential difference 0.025V in case of semiconductor (since thermal voltage at 300K Room Temperature is $kT/q = 0.025\text{V}$). From the kinetic velocity the de Broglie wavelength is determined. The set of equations are: Kinetic Energy gained =

$$\frac{p^2}{2m^*} = q \times V_{acc}$$

Figure 12.8

Therefore momentum gained

$$p = \sqrt{2m^*qV_{acc}}$$

Figure 12.9

; Therefore de Broglie wavelength:

$$\lambda = \frac{h}{p} = \frac{h}{\sqrt{2m^*qV_{acc}}}$$

Figure 12.10

;

In Table (1.12) the de Broglie wavelengths are tabulated:

Table 1.12. de Broglie wavelengths of conducting electron in Electron Microscope, Metal and Semiconductor.

	V acc	v e (m/sec)	$\lambda(m)$	Implications
Electron Microscope	10kV	59×10^6	$10^{-11} \text{ m} = (1/50)(5\text{\AA})$	$\lambda \ll a$ (lattice constant)
	100kV	187.6×10^6	$4 \times 10^{-12} \text{ m}$	
Metal	4V	10^6	$6 \times 10^{-10} \text{ m} = (5\text{\AA})$	$\lambda \sim a$ (lattice constant)
Semiconductor	0.025V	10^5	$7.75 \times 10^{-9} \text{ m} = (78\text{\AA})$	$\lambda \gg a$ (lattice constant)

Table 12.4

As seen from Table(1.12), we see that de Broglie wavelength is much less than the lattice constant in case of Electron Microscope. For 100kV, theoretically the resolution should be $(1/100)(4\text{\AA})$. This is like Sunlight falling through a broad aperture. Sun-ray will pass in a straight line and shadow of the aperture should fall on the screen behind the aperture. Hence in an Electron Microscope, a regular lattice array does not scatter an electron beam. The shadow of the crystal lattice should be imaged. But this theoretical resolution is never achieved since we are using magnetostatic focusing. Only 1\AA is the resolution actually achieved. In case of 10kV, though the theoretical resolution $(1/50)(5\text{\AA})$ but in practice only 10\AA resolution is achieved. The electron beam can penetrate through a thin specimen and produce the image of its broad features without being influenced by the atomic details.

In electron microscope the electron can be accelerated to higher energy to obtain a finer resolution. It can resolve on the scale of molecules but can barely perceive the atoms.

To resolve at atomic and sub-atomic level we need to go to particle accelerators. *Particle Accelerators are gargantuan machines which can be regarded as giant microscopes for probing into the innermost recesses of matter - an awesome complement to the giant telescopes which probe to the edges of the Universe.*

To arrive at the resolving power of particle accelerator we must know Special Theory of Relativity and we must make relativistic corrections in order to arrive at the correct resolving power of the particle accelerators. These are described in the Appendix XXXIV. Here we will just use them to arrive at the resolving power of the particle accelerators.

Relativistic momentum is related to the total energy E by the following relation ship:

$$E^2 = p^2 c^2 + m_0^2 c^4$$

Figure 12.11

.....1.98
de Broglie wavelength associated with this particle is:

$$\lambda = \frac{h}{p} = \frac{hc}{\sqrt{[E^2 - (m_0c^2)^2]}}$$

Figure 12.12

1.99

Using Equation (1.99), the resolving power of various particle accelerators operational around the world is tabulated in Table(1.13).[Taken from Table(9.1), “Overview of Particle Physics”, by Abdus Salam, New Physics, edited by Paul Davies, Cambridge University Press, 1992]

Table 1.13. The resolution of the particle accelerators around the World.

Name & Location	Energy reached	Year	Resolution	Particle detected
Rutherford*Manchester, UK.	10MeV, alpha particle's velocity= 2×10^7 m/s, Alpha particle= 4He nucleus;	1911	4.5×10^{-15} m	Nucleus size= 10^{-14} m; Rutherford determined the size to be 30fm- But the correct estimate is 7fm;
		1919	1.24×10^{-15} m	Proton size= 10^{-15} m=1fm;
		1932	1.24×10^{-15} m	Neutron size= 10^{-15} m=1fm
	1GeV		1.24×10^{-15} m	
Bepc(e+e-)Beijing	4GeV	1987		
TRISTAN(e+e-)Japan	60GeV	1987		
	10GeV	1979	1.24×10^{-16} m	Quark size= 10^{-16} m
SLC(e+e-)Stanford, California, USA;	100GeV	1987	1.24×10^{-17} m	W-, W+ & Z0 detected
LEP(I) (e+e-)Large electron-positron colliderCERN, Geneva;	100GeV	1987	1.24×10^{-17} m	

continued on next page

LEP(II) (e+e-) CERN, Geneva	200GeV	1995	$6.2 \times 10^{-18} \text{ m}$	Top Quarks detected
HERA(ep)Hamburg	320GeV	1991	$3.87 \times 10^{-18} \text{ m}$	
SpSCERN, Geneva	900GeV	1986	$1.38 \times 10^{-18} \text{ m}$	
TevatronFermiLab, USA	4TeV	1987	$1.24 \times 10^{-18} \text{ m}$	No excited state of quarks or leptons detected size= 10^{-18} m
TevatronFermiLab, USA	4TeV	1987	$6.2 \times 10^{-19} \text{ m}$	
UNKSerpukhov, Russia	3TeV	1995	$4.13 \times 10^{-19} \text{ m}$	
EeSerpukhov, Russia	4TeV	?	$3 \times 10^{-19} \text{ m}$	
Large Hadron Collider (LHC), CERN, Geneva	16TeV	?	$7.75 \times 10^{-20} \text{ m}$	
SSC (super particle superconducting-Collider), USA;	40TeV	?	$3.1 \times 10^{-20} \text{ m}$	
	1PeV	?	$1.24 \times 10^{-21} \text{ m}$	
	1EeV	?	$1.24 \times 10^{-24} \text{ m}$	

Table 12.5

* the first particle accelerator was established at Cavendish Laboratory, Cambridge University. In 1919 Rutherford became the first Director and he was instrumental in establishing the particle accelerator.

In Metal the wavelength is comparable to the lattice constant. This is like light falling through a narrow aperture whose dimension is comparable to the wavelength. Incident light will form a circular diffraction pattern behind the aperture on the target screen. This implies that conducting electron in a metallic lattice is strongly scattered by the lattice centers. Hence it has a very low mobility.

In Semiconductor, the de Broglie wave length is much larger than the lattice constant. Hence lattice scattering is weak and only the gross imperfections cause the scattering. These gross imperfections could be phonons and dislocations extending over several lattice constants. This is what makes conducting electrons much more mobile in semiconductor as compared to that in metal.

In metal, conducting electrons behave like degenerate gas and not quite like ideal gas whereas in semiconductors they behave like non-degenerate gas which is more like ideal gas obeying ideal gas law.

In ideal gas the molecules are far apart, independent of one another and possessing average energy of $(3/2)kT$ whereas in degenerate gas the molecules are closely packed and average kinetic energy is much larger than $(3/2)kT$. In Table(1.14),

Metals and Semiconductors parameters have been tabulated in the same table.

Table(1.14). Conductivity(σ), Fermi Level(E_F), Mean Free Path(L^*) and Mean Free Time(τ) at 0°C for monovalent metals and semiconductors.

Metal	σ (10 ⁶ S/cm)	ρ (Ω -cm)	n ($10^{22}/\text{cm}^3$)	μ ($\text{cm}^2/(\text{Vs})$) $= \sigma / (nq)$	Φ (eV)	L^* (\AA)	τ (fs) = $me\mu/q \times 10^{-4}$
Li	0.12	8.3×10^{-6}	4.62	16.2	4.7	110	9
Na	0.23	4.35×10^{-6}	2.65	54.17	3.1	350	31
K	0.19	5.26×10^{-6}			2.1	370	44
Cu	0.64	1.67×10^{-6}	8.5	47	7.0	420	27
Ag	0.68	1.47×10^{-6}	5.9	72	5.5	570	41
Ge		47	$n_i = 2.25 \times 10^{10}$	3000		2106	2217
Si		300k	$n_i = 1.15 \times 10^{10}$	1300		729	767.6
GaAs		70.5M	$n_i = 2 \times 10^6$	8600		4645.5	4890

Table 12.6

Chapter 13

Chapter 3. Special Classification of Semiconductors. Sec 3.1. Compound Semiconductors¹

Chapter 3. Special Classification of Semiconductors.

Section 3.1. Compound - Semiconductors.

Compound Semiconductors are the basis of a whole new branch of Science and Technology known as Photonics. Light Sources and Light Detectors belong to this discipline. III-V elements give rise to Compound Semiconductors which are suitable for Light Generation or Light detection. These III-V elements form alloys across the whole range of concentration at their growth temperature. This wide miscibility range allows alloys to be grown with band structures adjusted for specific applications. This leads to Band structure manipulation according to our specific needs. This is known as Band-gap Engineering. The common Alloys used in Photonics are as given below:

- i. GaP(2.3eV, $a = 5.42 \text{ \AA}$) ----- GaAs_xP_(1-x) ----- GaAs(1.42eV, 5.65 \AA): here x is the stoichiometric coefficient and by adjusting 'x', band-gap can be tailored from 1.42eV to 2eV.
- ii. InP(1.3eV, 5.85 \AA) ----- InGaP ----- GaP(2.3eV, 5.42 \AA).
- iii. GaAs(1.42eV, 5.65 \AA) ----- GaAlAs ----- AlAs(2.2eV, 5.65 \AA).
- iv. GaAs(1.42eV, 5.65 \AA) ----- GaAsSb ----- GaSb(0.65eV, 6.1 \AA).
- v. GaAs(1.42eV, 5.65 \AA) ----- GaInAs ----- InAs(0.35eV, 6.05 \AA).
- vi. InP(1.3eV, 5.85 \AA) ----- InPAs ----- InAs(0.35eV, 6.05 \AA).
- vii. GaSb(0.7eV, 6.1 \AA) ----- GaInSb ----- InSb(0.15eV, 6.5 \AA).

The three element alloys are TERNARY ALLOYS. Two from Group III and two from Group IV combine to form QUATERNARY ALLOYS.

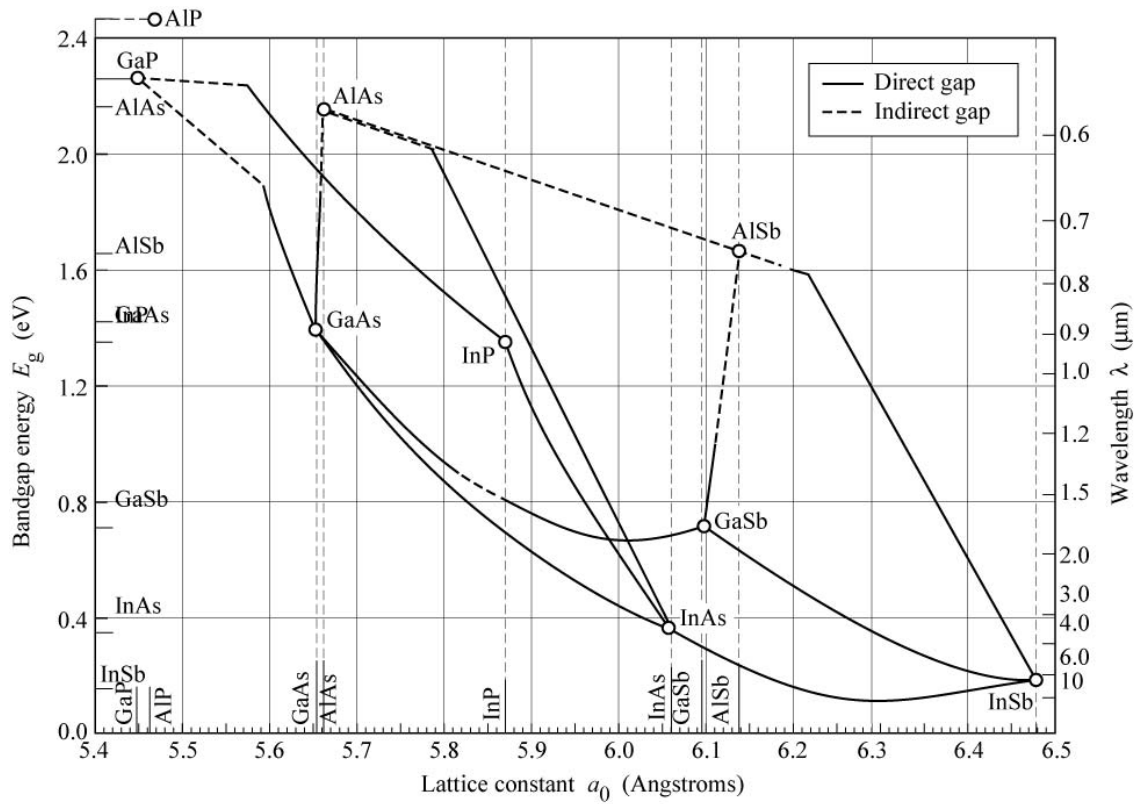
Wide miscibility shown above has been translated into a topological diagram Figure 3.1 where Band-Gap versus Lattice Constant is plotted for the seven major Compound Semiconductors namely GaP, GaAs, GaSb, InAs, InSb, InP, AlAs, and AlSb and their derived Ternary Alloys.

As seen from Figure 3.1, none of the pure compounds listed have a direct band-gap more than $1.65 \mu\text{m}$ for producing Visible Spectra Radiation. GaAs, InP, GaSb, InAs and InSb have direct band-gap but less than 1.65eV.

AlP, GaP, AlAs and AlSb all have Band-gap larger than 1.65eV but all are in-direct band-gap hence not suitable for optical generation. Hence for Optical LEDs we go for alloys of GaP and GaAs known as ternary alloy GaAs_(1-x)P_x. In Figure 3.2, the white light spectrum and the corresponding Band-gaps are shown.

¹This content is available online at <<http://cnx.org/content/m49543/1.1/>>.

Figure

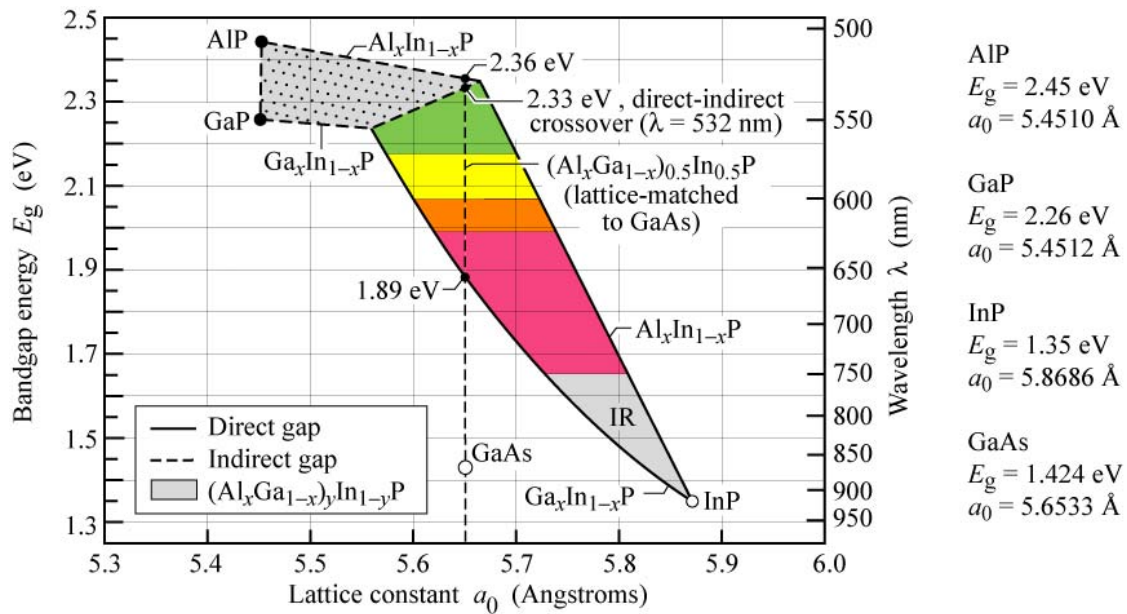


Bandgap energy and lattice constant of various III-V semiconductors at room temperature (adopted from Tien, 1988).

E. F. Schubert
Light-Emitting Diodes (Cambridge Univ. Press)
www.LightEmittingDiodes.org

Figure 13.1

Figure 3.1. Topological diagram for Compound Semiconductors and their Ternary Compounds. The Solid lines indicate Direct Band Gap materials and dashed lines show In-direct Band Gap materials.

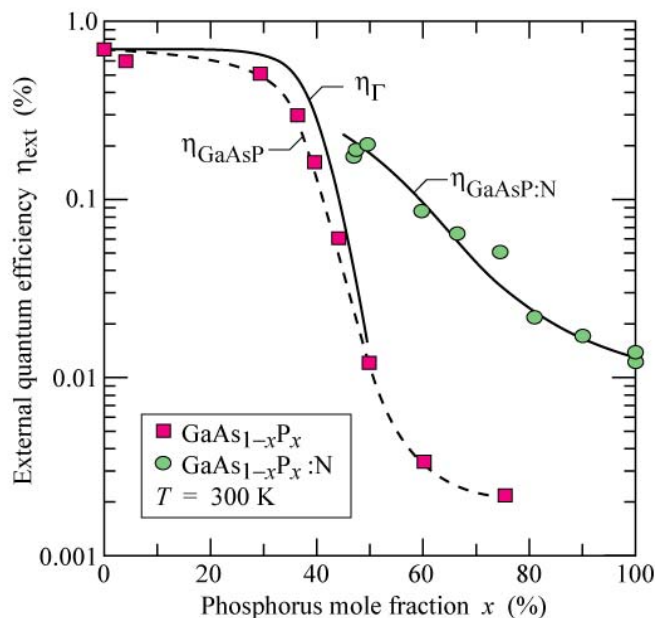


Bandgap energy and corresponding wavelength versus lattice constant of $(\text{Al}_x\text{Ga}_{1-x})_y\text{In}_{1-y}\text{P}$ at 300 K. The dashed vertical line shows $(\text{Al}_x\text{Ga}_{1-x})_{0.5}\text{In}_{0.5}\text{P}$ lattice matched to GaAs (adopted from Chen *et al.*, 1997).

E. F. Schubert
Light-Emitting Diodes (Cambridge Univ. Press)
www.LightEmittingDiodes.org

Figure 13.2

Figure 3.2. The plot of Band-Gap and the corresponding Wavelength versus Lattice Constant.



Experimental external quantum efficiency of undoped and N-doped GaAsP versus the P mole fraction. Also shown is the calculated direct-gap (Γ) transition efficiency, η_{Γ} , and the calculated nitrogen (N) related transition efficiency, η_N (solid lines). Note that the nitrogen-related efficiency is higher than the direct-gap efficiency in the indirect bandgap ($x > 50\%$) regime (after Campbell *et al.*, 1974).

E. F. Schubert
Light-Emitting Diodes (Cambridge Univ. Press)
www.LightEmittingDiodes.org

Figure 13.3

Figure 3.3. External Quantum Efficiency vs stoichiometric coefficient of Phosphorous in ternary alloy GaAs (1-x) P x .

For the manufacture of coloured LEDs we have to use GaAs_(1-x)P_x ternary alloy. This has a problem. Below $x = 0.45$ it is a direct band-gap material but at higher proportion of Phosphorous it becomes indirect and its performance becomes very poor as shown in Figure 3.3. By doping with Nitrogen it can be restored to Direct Band-gap material and utilized for LED manufacturing. Table 3.1 tabulates the different ternary alloys used for manufacturing the spectrum coloured LEDs.

Table 3.1. The Ternary Alloys (GaAs (1-x) P x) used in the manufacture of the whole range of spectrum coloured LED. Here $E_g = 1.424 + 1.15x + 0.176x^2$.

Colour	Wavelength(μm)	Energy Band-gap(eV)	'x'	Substrate
Red	0.64	1.9	0.4	GaAs
Orange	0.62	2	0.5	GaP
Yellow	0.58	2.15	0.58	GaP
Green	0.55	2.25	0.656	GaP
Blue	0.475	2.60	0.9	SiC

Table 13.1

3.1.1. The Crystal Structure of Compound Semiconductors and its Dopent.

GaP, GaAs, GaSb, InAs, InSb, InP, AlAs, and AlSb have the the same crystalline structure as Diamond but now it is called Zinc-Blende. It is two interpenetrating FCC sublattices with one sublattice made of

Group III element and the other FCC sublattice made of Group V element and one sub-lattice is displaced with respect to the other along the diagonal of the cube by a quarter of the diagonal length i.e. by $a\sqrt{3}/4$. The net result is that every Group III has FOUR Group V atoms as neighbours and similarly Group V has for Group III atoms as neighbours. This completes the co-valent bond requirement.

Table 3.2 tabulates the dopents of III-V Compound semiconductors.

Table 3.2. P and N type dopents for III-V Compunds.

Group	II	III	IV	V	VI
	Zn	Ga	Si	As	S
		In	Ge	P	Se
				N	
	Acceptor		Amphoteric Dopents		Donors

Table 13.2

Silicon and Germanium can either be Donor or Acceptor depending upon what they substitute. If Group III is substitute then they become DONOR and if they substitute Group V then they become acceptor. But since Si is smaller in size hence energetically it is favourable to replace Ga hence Si is Donor in GaAs and bigger Ge substitutes the bigger As atoms hence Ge is acceptor.

3.1.2. Band-gap Engineering.

The manipulation of Band Structure required for different kinds of applications is Band-gap Engineering. There are three techniques of Band-gap Engineering:

- i. Alloying;
- ii. Use of Heterojunctions and
- iii. Built-in strain via mismatched epitaxy.

The Aim of Band-gap Engineering is to tailor/customize the band-gap according to the wavelength at which we want to operate.

The second objective is to tailor the lattice constant according to our matching or our mis-matching requirements.

The wide miscibility range allows alloys to be grown with Band structures adjusted and finally tuned for specific applications.

3.1.3. Properties of Alloys.

In Alloys we have Lattice Parameter (a) Law called Vegard's Law. If we have two solid mixture $A_xB_{(1-x)}$ then the Alloy's Lattice Parameter is given as follows:

$$a_{\text{alloy}} = x \cdot a_A + (1 - x) \cdot a_B \quad 3.1.$$

Figure 13.4

Alloys are not perfect crystals even if they have perfect lattice structure. This because in solid mixture atoms donot have periodic placement.

By virtual crystal approximation:

$$E_g^{alloy} = x.E_g^A + (1-x).E_g^B \quad 3.2$$

Figure 13.5

We have quadratic approximation also:

$$E_g^{alloy} = a + b.x + c.x^2 \quad 3.3.$$

Figure 13.6

Equation 3.3 is the same as the Equation given in Table 3.1.

Alloying induced dis-order causes a BOWING Parameter in compound semiconductor Wafer. Equations 3.2 and 3.3 are valid only if the alloy is a good mixture i.e. perfectly random mixing.

In an alloy $A_XB_{(1-X)}$ a good mixing results into the fact that the probability that A is surrounded by B is (1-X) and B is surrounded by A is X. If proportion is different from the stichiometric coefficient then it is clustered or phase repeated.

Test of Eq (3.2):

AlAs has $E_g = 2.75\text{eV}$ and GaAs has $E_g = 1.43\text{eV}$ therefore in $Al_{0.3}Ga_{0.7}As$ has

$E_g = 0.3 \times 2.75 + 0.7 \times 1.43 = 1.826\text{eV}$.

Chapter 14

Chapter 4. Light and Matter – Dielectric Behaviour of Matter¹

Chapter 4. Light and Matter – Dielectric Behaviour of Matter [“OPTICS” by Eugene Hecht, IIIrd Edition, Addison-Wesley-Longman Incorporation, Readings, Massachusetts].

Section 4.1. Brief History of Scientific and Technological Development in the field of Light.

Study of Light and its application in Human Society can be traced back to 1200 BCE. In Exodus 38.8 (a chapter in The Bible) we find the mention of “Looking Glass of the Women”. Early mirrors were made of polished copper and bronze. Evidence of the use of mirrors turned up in excavations of the workers’ quarters near the construction site of Pyramid during the ancient Egyptian Civilization. At that time it was made of Speculum – a copper alloy rich in tin. In Roman Civilization we find the use of convex lens as Magnifying Glass as well as Burning Glass.

After 475CE, with the fall of Western Roman Empire, dark ages descended in Europe and the center of Scientific Enquiry shifted to the Arab World. Islamic scholar Abu Ali al-Hassan Ibn al-Haytham (CE. 965-1041), known in the West as Alhazen, began his career as just another Islamic polymath. He was put in House Arrest by Al-Hakim, the Calipha of Cairo, because he failed to regulate the flow of Nile river. While in House Arrest for 10 years, Alhazen revolutionized the study of optics and laid the foundation for the scientific method. (Move over, Sir Isaac Newton.) Before Alhazen, vision and light were questions of philosophy. Alhazen considered vision and light in terms of mathematics, physics, physiology, and even psychology. In his *Book of Optics*, he discussed the nature of light and color. He accurately described the mechanism of sight and the anatomy of the eye. He was concerned with reflection and refraction. He experimented with mirrors and lenses. He discovered that rainbows are caused by refraction and calculated the height of earth’s atmosphere. In his spare time, he built the first *camera obscura*.

From 1000 CE to 1600 CE, there was only a modest revival of Scientific Enquiry and Research in Europe. The science of vision error correction by the use of Eye Glasses were introduced. Looking Glass or Mirror Technology was revived by the use of liquid amalgam of tin and mercury coated on the back of glasses. Use of multiple mirrors and use of positive and negative lenses were in vogue in this era.

Section 4.1.1. The revival of Scientific Enquiry in 17 th Century in Europe -The Renaissance Period.

Table 1. Time-line of Scientific Research in Application of Light for Human Good.

But there was no consensus about the nature of light-is it a Wave or is it Corpuscular ?

¹This content is available online at <<http://cnx.org/content/m49722/1.1/>>.

But there was no consensus about the nature of light-is it a Wave or is it Corpuscular ?

But there was no consensus about the nature of light-is it a Wave or is it Corpuscular ?

Time	Scientist	Subject
October 2,1608	Hans Lippersley (1587-1619)Dutch Spectacle Maker	Applies for a patent for the Refracting Telescope.
1609	Galileo Galilei (1564-1642), Padua, Italy.	Builds his first Telescope for Astronomical Observ
1609 onward	Astronomical Discoveries of Galileo Galilei.	Four satellites around Jupiter which are Io, Europ
		Observed and analyzed the Sun spots;
		He discovered the poke marked surface of Moon c
		He saw the phases of Venus which lent support to
		He identified Milky Way as our Home Galaxy. Til
		He observed Neptune but could not identify it as
After 1609	Zacharius Jansenn(1588-1632), Dutchman.	Invented Compound Microscope.
After 1609	Willebroed Snell (1591-1626)	Discovered the Law of Refraction and measured F
1657	Pierre de Fermat (1601-1665)	Rederived the Law of Reflection using the Princip
		Interference and diffraction was observed.
		But there was no consensus about the natu

Table 14.1

Within a year of death of Galileo, Sir Issac Newton(1642-1727) was born in England. He studied the dispersion of light into seven rainbow colours (Violet, Indigo, Blue, Green, Yellow, Orange and Red) but he was unable to reconcile the rectilinear propagation of light with the spherical wave-front of light from a point source. Hence Newton favoured Corpuscular Theory of Light.

There was a problem of Chromatic Aberration in Refracting Telescope which Newton was unable to correct. So in its place he built Reflecting Telescope in 1668. This was only 6 inches long and 1 inch in diameter but it had a magnification of 30 timesa.

Christian Huygens (1629 – 1695) extended the Wave Theory of Light and gave the theoretical basis of Reflection, Refraction and Double Refraction. He discovered that there was perpendicular polarized light (perpendicular to the plane of incidence) and parallel polarized light (parallel to the plane of incidence).

Ole Christensen Romer (1644-1710) was the first person to recognize that light was not instantaneous but it had a finite velocity. Based on this reasoning in 1676, Romer predicted that on 9th November Io, a moon of Jupiter, would emerge from Jupiter's shadow 10 minutes later than what would be expected from the yearly average motion. This what happened and this led to the conclusion that light took 22 minutes to cover a distance equal the orbital diameter of Earth around Sun i.e. a distance of 2 Astronomical Unit (A.U.) where 1 A.U. = 1.49598×10^{11} m. Using this data we arrive At $c = 2.2664 \times 10^8$ m/s but the correct value is $c = 3 \times 10^8$ m/s. This error occurred due to underestimation in Jupiter's Orbit size.

Huygen and Newton based on the same reasoning arrived at $c = 2.3 \times 10^8$ m/s and $c = 2.4 \times 10^8$ m/s respectively.

Section 4.1.2. 19 th Century – the emergence of Wave Theory of Light.

Dr. Thomas Young (1773-1829) in England presented a series of papers on Wave Theory of Light in 1801, 1802 and 1803 before the Royal Society of London. He added a new dimension to the existing Wave theory by illustrating the Principle of Interference. He explained the coloured fringes in thin films and determined the wave-length of the seven colours of light.

Augustine Jean Fresnel (1788-1827) in France independently explained the diffraction pattern arising from various obstacles and apertures and he also accounted the rectilinear propagation of Light based on Wave Theory.

In 1725, James Bradley (1693-1762) attempted to measure the distance to star by triangulation method by observing a given star at six months time period. During this experiment he observed Stellar Aberration. This is different from Parallax Error.

The problem of perpendicular and parallel polarization led Young to revise the mode of propagation of Light. Initially it was assumed to be longitudinal much as the sound waves. But detection of polarization forced Young to postulate that Light had Transverse Mode of propagation.

By 1825, Wave Theory of Light was established.

In 1849, Armand Hippolyte Louis Fizeau (1819-1896) did the first terrestrial determination of the speed of light in air. It came to be 315,300 km/s.

Subsequently Foucault measured the velocity of light in water. It turned out to be less than 'c'. This was interoperated as some kind of drag effect by the water medium. This also contradicted Newton's Corpuscular Theory of Light.

In 1845, Michael Faraday (1791-1867) established that a strong magnetic field could change the Polarization of Light Beam.

In 1861 and 1862, James Clerk Maxwell (1831-1879) synthesized the empirical knowledge of Gauss's Divergence Theorem, Faraday Induction Law and Ampere's Circuital Law into four differential equations and he established that Light was Electro-Magnetic Field propagating in all pervading aether as a transverse wave at a velocity c in vacuum:

$$c = \frac{1}{\sqrt{\mu_0 \epsilon_0}} \text{ where } \mu_0 = \text{absolute permeability and } \epsilon_0 = \text{absolute permittivity} \quad 1$$

Figure 14.1

In a dielectric medium the velocity of propagation (v) is:

$$v = \frac{1}{\sqrt{\mu_r \mu_0 \epsilon_r \epsilon_0}} \quad \text{In a non - magnetic Dielectric} = \frac{1}{\sqrt{\mu_r \mu_0 \epsilon_r \epsilon_0}} = \frac{c}{\sqrt{\epsilon_r}} = \frac{c}{n} \quad 1a$$

Figure 14.2

Where n = refractive index of the material.

From (1a) it is evident that n = refractive index = $\sqrt{\epsilon_r}$.

From Maxwell equations it was clear that Light was an Electro-Magnetic disturbance propagating out of a point source with the velocity of light with a spherical wave-front.

The Four Maxwell Equations in differential form are:

$$\nabla \cdot D = \rho \quad \text{or} \quad \nabla \cdot E = \frac{\rho}{\epsilon_0 \epsilon_r} \quad \text{where } D = \epsilon_r \epsilon_0 E \quad \text{Here } \epsilon_r = \text{relative permittivity}$$

= dielectric constant. This is Gauss' sLaw which states that total

Figure 14.3

electric flux coming out of a given volume is equal

Figure 14.4

to the total electric charge enclosed by the volume.

2

Figure 14.5

$$\nabla \times E = -\frac{\delta B}{\delta t} \quad \text{this directly follows from Faraday's Induction Law}$$

Figure 14.6

which states that total induced emf in a Copper Wire Coil is equal

Figure 14.7

to the rate of change of magnetic flux cutting the copper coil.

3

Figure 14.8

$$\nabla \times H = J_c (\text{conduction current density}) + \frac{\delta D}{\delta t} (\text{displacement current})$$

Figure 14.9

this directly follows from Ampere Circuital Law which states that the line integral

Figure 14.10

of Magnetic Field H is equal to the current enclosed by the integral path 4

Figure 14.11

$\nabla \cdot H = 0$ this follows from the fact that there is no Magnetic Monopole 5

Figure 14.12

From (2), (3), (4) and (5) it is evident that:

- i. There is a general perpendicularity of E and H;
- ii. The Maxwell Equations are symmetrical;
- iii. E and H are interdependent.

Time varying E field through (4) produces H field which is perpendicular to the direction of change of E and time varying H field through (3) produces E field which is perpendicular to the direction of change of H. So as an Electro-Magnetic disturbance is produced self sustaining transverse Electro-Magnetic Field travels out from the source of disturbance as shown in Figure 4.1. E and H are coupled in form of a pulse. E generates H farther out and H generates E still farther out. Thus E-M wave travels out in self sustained fashion and there is no need of aether. Still Maxwell assumed that there was an all pervading luminiferous aether which helped the propagation of E-M waves.

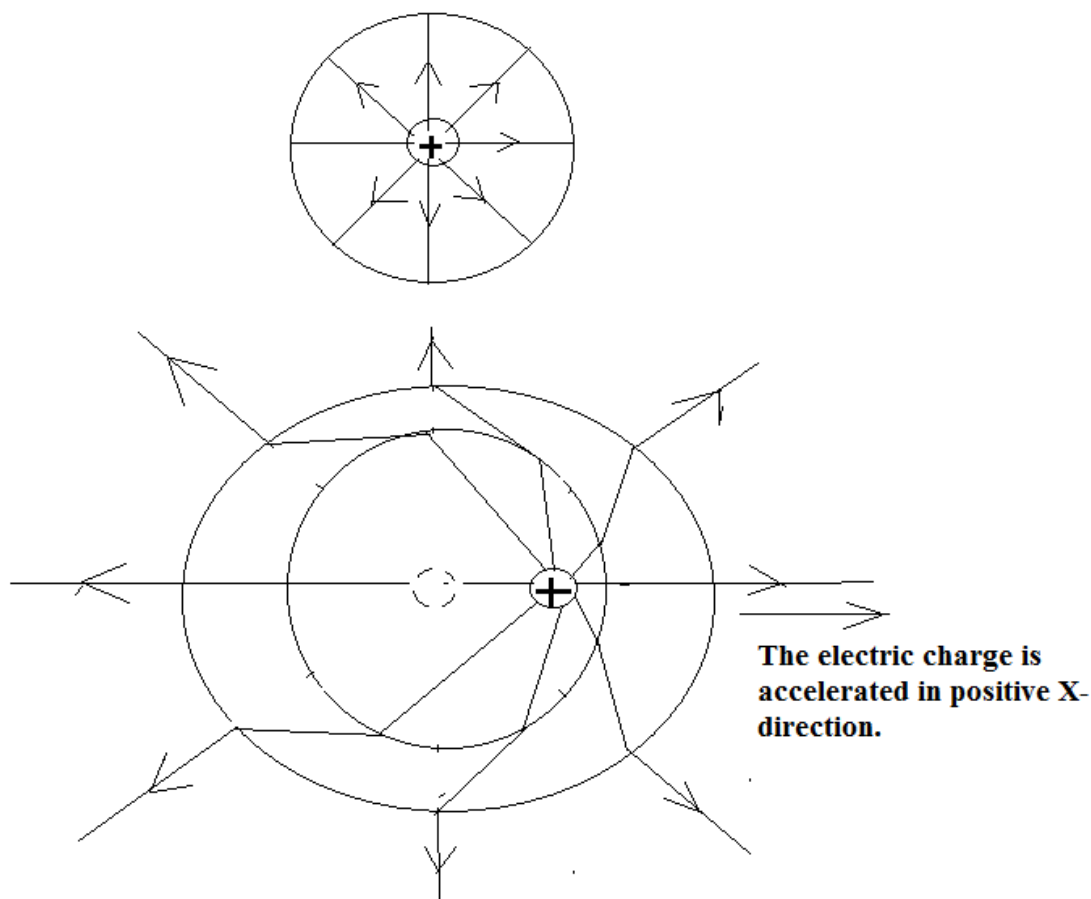


Figure 4.1.A Kink in the E-Field due to acceleration of the charge Q

Figure 14.13

If a charge is accelerated in positive X-direction as shown in Figure 4.1. then a kink is produced in the Electric Field at $(c \cdot dt)$. This kink travels out at 'c'. It has a radial as well as transverse component. Radial Component (electro-static component) diminishes as the square of r while Transverse Component (radiative component) diminishes as 'r'. Hence after some distance r, only Transverse Component remains which detaches from the electric dipole and travels out as self-supporting E-M Radiative Field.

In 1888, Heinrich Rudolf Hertz (1857-1894) generated long E-M waves and published the results in the Philosophical Transactions of Royal Society of London.

In 1881, Michelson-Morley completed the measurement of velocity of light in different frames of reference but could detect no change in the standard value of 'c'. Light velocity seemed to be invariant of the source of emission velocity.

Section 4.1.3. The Conceptual Paradigm Shift at the turn of 19 th and 20 th Century.

The invariance of the velocity of light to the Frame of Reference necessitated a paradigm shift in the theoretical framework given by Newtonian Relativity. Jules Henri Poincare (1854-1912) was the first to grasp this invariance and he expressed an alternative view point:

“Our aether – does it really exist ? I donot believe that more precise observations could ever reveal more than relative displacement.”

In 1905, Albert Einstein introduced his special theory of Relativity in which he showed that,

“the introduction of ‘Luminiferous Aether’ will prove superfluous in as much as the view here to be developed will not require an absolutely stationary space.” E-M wave was now envisaged as a self supporting and self-sustaining process without the need of a sub-stratum.

4.1.3.1. Special Theory of Relativity.

Newtonian Mechanics fails the test of invariance of the speed of light from frame to frame. Einstein resolved this failure of Newtonian Mechanics.

Time measured by a clock in a given frame of reference is called PROPER TIME.

In moving frame, time measured by a clock placed in the same frame of reference is:

$$ds = c.dt' \quad \text{or} \quad dt' = \frac{ds}{c} = dt \sqrt{1 - \frac{v^2}{c^2}}$$

Figure 14.14

Therefore

$$dt(\text{Rest Frame}) = \frac{dt'(\text{Moving Frame})}{\sqrt{1 - \frac{v^2}{c^2}}} = \text{Time Dilation} \quad 6$$

Figure 14.15

Equation (6) implies that time slows down in moving frame as observed from rest frame. That is a person in a moving frame will be seen to age slowly when observed from the rest frame

Some examples of Time Dilation:

Example 1. This experiment was carried out in CERN.

Positive Kaons have a rest lifetime of $\tau_K = 0.1273\mu s$.

In the lab, it is generated at a velocity of $0.927c$.

At this Relativistic Speed its observed life-time = $0.879357\mu s$.

This is the result of Time Dilation.

Distance travelled in the Lab before it decays is = $0.927c \times 0.879357\mu s = 244m$

Example 2.

Cosmic Rays are continuously bombarding our atmosphere. Cosmic Rays consist of PROTONS.

Protons collide with Nitrogen Molecule to form Pions. Pions decay to Muons. This occurs at a height of 45Km. Muons belong to Leptons. Electron and Tau-lepton belong to the same group of the particles.

Velocity of Muons = 99.9943% of c .

Its rest lifetime = $\tau_{\mu 0} = 2.2\mu s$. That is in rest frame the lifetime is $2.2\mu s$.

If it was travel at 99.9943% of c for its rest lifetime of $2.2\mu s$ it would travel only 659.5m and it could never be detected on the ground detectors.

But it is detected.

This is because its observed lifetime from Ground is 0.0192988s and it is travelling at 99.9943% of c . Hence distance travelled as observed from the ground = 5785.3Km. Muon has been generated 45Km above the Ground. Hence it easily reaches our Ground and is readily detected.

l (length measured in moving frame)

$$= l_0(\text{proper length of a body in Rest Frame}) \sqrt{1 - \frac{v^2}{c^2}}$$

$$= \text{Contraction of length} \quad 7$$

Figure 14.16

In a moving frame transverse dimensions remain unchanged.

Let v_x, v_y, v_z be the velocities of a body in rest frame.

Let v'_x, v'_y, v'_z be the velocities of a body in a moving frame. The moving Frame is moving with velocity V in (+)ve x-direction.

Transformation of Velocities from Moving Frame to Rest Frame is given as follows:

$$v_x = \frac{v'_x + V}{1 + \frac{v'_x V}{c^2}}; \quad v_y = \frac{v'_y \sqrt{1 - \frac{v^2}{c^2}}}{1 + \frac{v'_x V}{c^2}}; \quad v_z = \frac{v'_z \sqrt{1 - \frac{v^2}{c^2}}}{1 + \frac{v'_x V}{c^2}} \quad 8$$

Figure 14.17

If the observation is instantaneous then velocity of light ' c ' \rightarrow infinity and (8) reduces to:

$$v_x = v'_x + V; \quad v_y = v'_y; \quad v_z = v'_z \quad \text{therefore } v'_x = v_x - V; \quad 9$$

Figure 14.18

While sitting in a moving train, moving in (+)ve X direction with velocity V , if we measure the velocity of Wind which in rest frame is moving in (+)ve X direction at a velocity v_x then in moving frame the observed or measured value of the velocity of Wind is:

$$v'_x = v_x - V; v'_y = v_y; v'_z = v_z; \quad 10$$

Figure 14.19

But velocity of light is not infinity hence measured value of the velocity of Wind from the moving frame is given by equation (8).

4.3.1.2. Michelson-Morley Experiment and the invariance of the velocity of light.

Velocity of PHOTON from a moving train is given by Equation (8).

$$\text{Therefore } v_x = \frac{v'_x + V}{1 + \frac{v'_x V}{c^2}} \quad 11$$

Figure 14.20

Rearranging the terms we get:

$$v_x \left(1 + \frac{v'_x V}{c^2} \right) = v'_x + V \quad 12$$

Figure 14.21

Open the bracket in (12);

$$\left(v_x + \frac{v_x v'_x V}{c^2} \right) = v'_x + V \quad 13$$

Figure 14.22

Put dashed terms on LHS and undashed terms on RHS:

$$v'_x - \frac{v_x v'_x V}{c^2} = v_x - V \quad \text{or} \quad v'_x \left(1 - \frac{v_x V}{c^2}\right) = (v_x - V) \quad \text{therefore} \quad v'_x = \frac{(v_x - V)}{\left(1 - \frac{v_x V}{c^2}\right)} \quad 14$$

Figure 14.23

But in Rest Frame $v_x = c$ for a photon therefore measured in a moving frame:

$$v'_x = \frac{(v_x - V)}{\left(1 - \frac{v_x V}{c^2}\right)} = \frac{(c - V)}{\left(1 - \frac{cV}{c^2}\right)} = \frac{(c - V)}{\left(1 - \frac{V}{c}\right)} = c \quad 15$$

Figure 14.24

The set of transformations achieved by Equation (8) has to be postulated in order to arrive at the invariance of velocity of light as demonstrated by Michelson-Morley.

Chapter 15

Section 4.2. Dielectric and its Physics.¹

Section 4.2. Dielectric and its Physics.

Non-conducting materials are defined as dielectric. The surrounding sea of air is dielectric. Lenses, prisms and films are dielectric. Once light enters a dielectric we must consider $\mu = \mu_0 \times \mu_r$ and $\varepsilon = \varepsilon_0 \times \varepsilon_r$. That is relative permeability and relative permittivity must be accounted which in vacuum are unity.

Dielectric which are transparent in visible range are non-magnetic. Hence by the definition of Refractive Index $n = c/v = \sqrt{\varepsilon_r}$. This is Equation 1a in Section 4.1.

What does TRANSPARENCY mean in materials science? Light can pass through a transparent material without absorption. This means light does not interact with transparent material. In scientific language it means that light does not interact with the medium it is passing through. If it interacts then the medium is not transparent.

Rewriting Eq 1a we get:

$$n = \sqrt{\varepsilon_r} = \sqrt{K_E}$$

6

Figure 15.1

In Equation 5, Refractive Index 'n' is measured using visible light and the argument of the square root is Static Dielectric Constant which is quite different from High Frequency Dielectric Constant because of the basic physics which causes relative permittivity. Let us examine Water. The Refractive Index of Water is 1.333 but static dielectric constant of water is 80. So it is evident that refractive index is frequency dependent. This was evident some 300 years ago when Newton managed to disperse the Sun-light into seven colours of a Rain-bow. The fact that we can disperse light means that Refractive Index is frequency dependent.

4.2.1. Why is Refractive Index Frequency Dependent ?

In vacuum:

¹This content is available online at <<http://cnx.org/content/m49723/1.2/>>.

$$D = \text{Electric Flux Density} = \epsilon_0 E_{VAC} \quad 7$$

Figure 15.2

In a dielectric material:

$$D = \epsilon_0 \epsilon_r E_{MED} \quad 8$$

Figure 15.3

In (7) and (8), D are the same and relative permittivity of Dielectric is greater than Unity hence the same Electric Flux creates a lower Electric Field in the medium as compared to that in the vacuum. So how is the remaining flux density accounted for. The remaining Flux density is causing Polarization and the scenario is the following:

$$D = P + \epsilon_0 E_{MED} = \epsilon_0 \epsilon_r E_{MED} = \epsilon E_{MED} \text{ therefore } P = (\epsilon - \epsilon_0) E_{MED} \quad 9$$

Figure 15.4

The Application of an Electric Flux Density D in a dielectric medium causes an Electric Field as well as it induces Polarization.

In polar medium such as water, the dipoles get aligned along the line of Electric Field. This is defined as Orientational Polarization = $P_{\text{orientational}}$.

In non-polar medium, applied flux density distorts the electron cloud with respect to the nucleus of the atom as a result center of electron gets displaced with respect to the center of nucleus and a dipole is created temporarily. This is called Electronic Polarization = $P_{\text{electronic}}$.

In ionic crystals such as NaCl, the application of Electric Flux displaces positive and negative ions inducing dipole moments and producing Atomic Polarization or Ionic Polarization = P_{atomic} .

In Table 4.2. we give some examples of polar and non polar dielectric gases.

Table 4.2. Assorted Molecules and their dipole moments.

Molecules	Configuration	Net dipole moment
CO ₂	+ve and -ve charge centers coincident	Zero
H ₂ O	+ve and -ve charge displaced	6.2×10 ⁻³⁰ C-m
HCl	+ve and -ve charge slight displaced	0.40×10 ⁻³⁰ C-m
CO	+ve and -ve charge displaced	3.43×10 ⁻³⁰ C-m

Table 15.1

At low frequency or under DC condition:

$$P = P_{orient} + P_{electronic} + P_{atomic} = \epsilon_0(\epsilon_r - 1)E_{MED} \quad 10$$

Figure 15.5

Due to the contribution of all these factors to polarization depending upon the situation, Static Dielectric Constant is very high. In water it is as high as 80.

But as the sinusoidally varying field's frequency is increased because of appreciable moments of inertia, polar molecules are unable to keep up with the alternating field and their effective contribution to the net polarization decreases. In Water dielectric constant is 80 up to 10^{10} Hz but it rapidly falls off beyond that frequency. At Peta Hz (in visible part of spectrum) it falls of to 1.78.

In electronic polarization, electron cloud has no problem in following the dictates of the harmonically varying electric field. Hence electronic polarization makes its contribution right up to the Peta Hz.

But electronic polarization gives rise to a resonance absorption phenomena.

An atom can be treated as an harmonic oscillator with a central restoring force $F = -kx$ where k = spring constant or restoring force constant and x is the incremental displacement from its equilibrium position. The harmonic oscillator appears as shown in Figure 4.2..

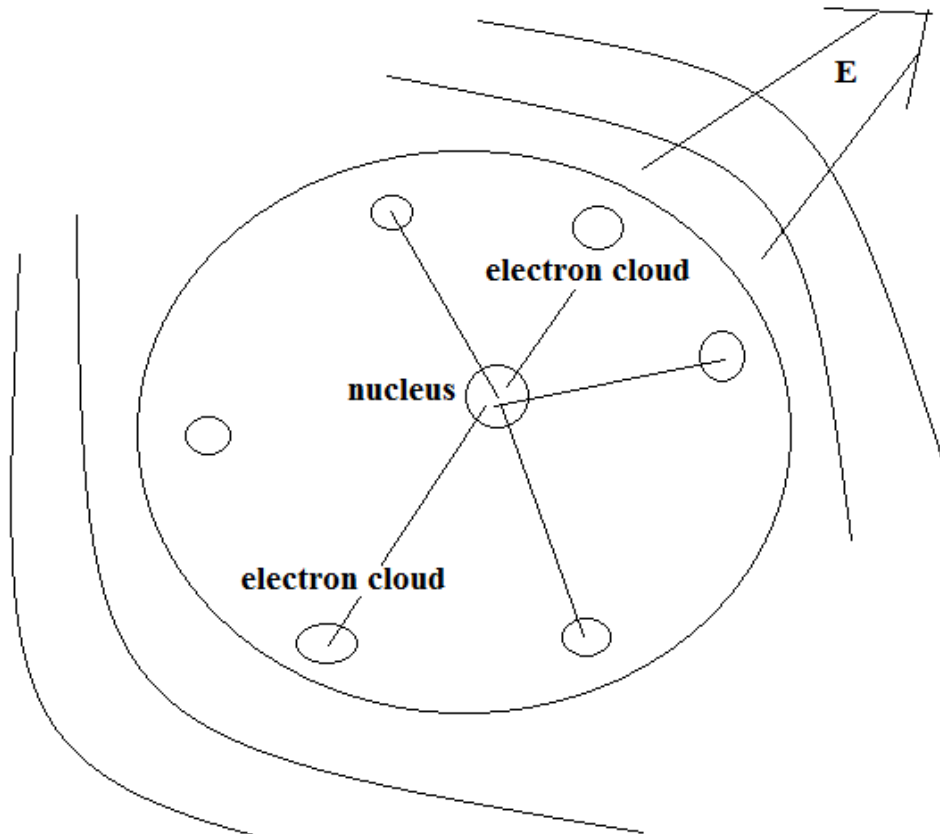


Figure 4.2. The mechanical oscillator model for an atom surrounded by a spherically symmetric electron cloud. The oscillator can vibrate equally in all directions.

Figure 15.6

The equation of motion of this atom with a spherically symmetric electron cloud surrounding the nucleus is as follows:

Perturbing force = $F_E = eE(t)$ = electron cloud is subjected to an electric force

Figure 15.7

The equation of motion of this harmonic oscillator is:

$$eE_0 \cos(\omega t) - kx = m_e \frac{d^2 x}{dt^2} \quad 11$$

Figure 15.8

The first term on L.H.S. is the electric perturbing force. The second term is the restoring force where k is the spring constant. R.H.S. D'Alembert's force due to acceleration of perturbation of electron. (11) is a second order linear differential equation with a Complementary Function + Particular Integral as its total solution.

Under forcing function its harmonic oscillation is as follows:

$$x(t) = \frac{e}{(\omega_0^2 - \omega^2)} E(t) \quad \text{where } \omega_0 = \sqrt{\frac{k}{m_e}} \quad 12$$

Figure 15.9

(12) implies that whenever the incident light has a frequency equal the natural frequency ω_0 resonance occurs and the incident light is completely absorbed by the medium as dissipative absorption.

From (9):

$$\epsilon = \epsilon_0 + \frac{P}{E} \quad \text{but } P = exN = \text{density of dipole moments and } N \\ = \text{contributing electrons per unit volume} \quad 13$$

Figure 15.10

Substituting (12) in (13) we obtain:

$$\varepsilon = \varepsilon_0 + \frac{exN}{E} = \varepsilon_0 + \frac{\frac{e}{m_e}}{(\omega_0^2 - \omega^2)} eN \quad 14$$

Figure 15.11

But we know from (1a) that refractive $n^2 = \varepsilon/\varepsilon_0$. Therefore Dispersion Relation where Refractive Index is expressed as a function of frequency is as follows:

$$\frac{\varepsilon}{\varepsilon_0} = n^2(\omega) = 1 + \frac{Ne^2}{\varepsilon_0 m_e} \left(\frac{1}{\omega_0^2 - \omega^2} \right) \quad 15$$

Figure 15.12

4.2.2. Two cases of Refractive Index – below and above Resonance Frequency (ω_0).

Case 1: $\omega < \omega_0$, P and applied E are in phase and $n(\omega) > 1$. This kind of behaviour is generally observed in the real World around.

Case 2: $\omega > \omega_0$, P and applied E are 180° out of phase and $n(\omega) < 1$.

The plot of Equation 15 is given in Figure 4.3.

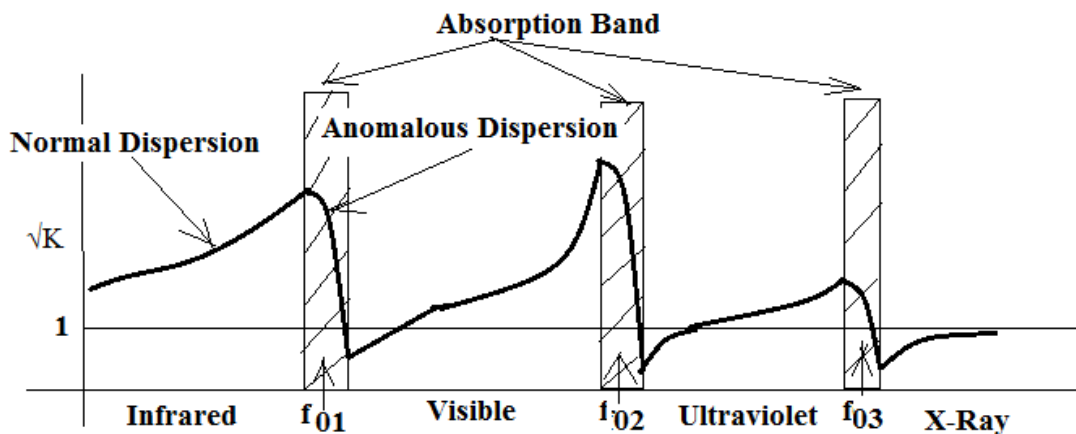


Figure 4.3. Refractive Index versus Frequency.

Figure 15.13

If the incident photon ($h \cdot \text{frequency}$) is not strong enough to excite the crystalline atom then the incident photon is scattered or redirected. This is called Ground State non-resonant scattering.

If the incident photon is equal to excitation energy then the atom will be excited from ground state to one of the permissible higher energy states. Subsequently atom will relax to the ground state and release its excess energy as thermal energy. This is known as dissipative absorption.

If incident photon is less than the excitation energy quanta but matches the natural frequency of the electron cloud system around each atomic nucleus then the alternating Electric Field of the incident photon will set the electron clouds in to oscillation. The crystalline atom continues to be in Ground State but electron cloud in each atom is set into a weak oscillation. This oscillatory vibration has two consequences:

1. Displacement of the center of the electron cloud with respect to the center of the nucleus giving rise to dipole moment qd where q = electronic charge and d = displacement of the center of the negative charge with respect to the center of the positive charge.
2. Due to alternating electric field the dipole moment is also oscillatory.

Oscillatory dipole is accompanied with dipole electro-magnetic radiation in accordance with the classical electro-magnetic Maxwell Laws. The frequency of the secondary radiation is the same as the frequency of the incident radiation. Since electron cloud plus the nucleus form a perfectly elastic system hence coefficient of restitution is Unity. Just as a perfectly elastic steel ball will continue to bounce up to eternity because it is a perfectly conservative system. In exactly the same way the incident photon sets the oscillatory dipole in motion and this oscillatory dipole re-radiates the same energy at the same frequency but with an altered direction. If the incident light is unpolarized then reradiation takes place in random direction. This is known as elastic scattering.

During irradiation, the setting up of dipole oscillators and secondary re-radiation is rapid. If the emission life-time is of the order of 10^{-8} sec then dipole oscillator will re-radiate 10^8 photons per second.

If incident frequency is equal to the natural frequency of the electron cloud system then amplitude of displacement is large leading to a strong dipole moment and causing a large cross-section of absorption. At a modest value of 10^2 W/m^2 incidence 100 million photons will be re-radiated.

When a material with no resonance in visible spectrum is bathed in White Light, non-resonant scattering takes place and this gives each participating atom the appearance of being a tiny source of spherical wavelets.

As the incident frequency becomes closer to the resonance frequency of the electron cloud system the more strongly will the incident photon interact with the dielectric material. In dense medium the strong interaction will lead to dissipative absorption.

It is the selective absorption at resonance frequencies that creates the visual appearance of the multi-colour surrounding- colour of our hair, skin, clothes, colour of leaves, apples and paint.

In real life there are three absorption bands for various dielectric and lie across a broad band of spectrum extending from Infra-red to Visible to Ultra-violet to X-Ray. Below IR these absorption bands can lie in RF band of spectrum also.

Below the absorption band lies the Normal Dispersion Band of frequencies. In this band of Spectrum there is a positive slope of the refractive Index curve as shown in Figure 4.3. Higher frequencies have higher Refractive Index. Therefore in chromatic dispersion of white light by a glass prism, Red Light bends the least and Violet bends the most. Here there is elastic scattering of light. Light is absorbed and re-radiated without any dissipation. Hence the term Elastic Scattering.

In the absorption band, energy of the incident light is absorbed and dissipated in form of heat. This is called Dissipative Absorption. In absorption band the refractive index has a negative slope as shown in Figure 4.3.

After the absorption band, $n < 1$ (as seen in Figure 4.3) meaning by light has a phase velocity greater than light. But the group velocity, the velocity at which energy travels, remains below velocity of light.

It is evident from the discussion that over the visible region of the spectrum, electronic polarization is the operative mechanism determining the refractive index dependence on frequency. When the incident frequency is lower than the resonance frequency/characteristic frequency/natural frequency then oscillations amplitude is very small and incident light is elastically scattered. There is no dissipation. At resonance the amplitude is increased and dissipative absorption sets in. The material becomes opaque in dissipative absorption bands though it remains transparent at other frequencies.

Chapter 16

Section 4.3. Dielectric Loss.¹

Section 4.3. Dielectric Loss.

Theoretically the dielectric constant is real and a capacitor having a dielectric separation of plates always causes a 90° Leading Current with respect to the applied voltage hence loss is zero and an ideal capacitor is always a conservative system. But as we have seen that dissipative absorption can take place at higher frequencies. The relative permittivity at alternating frequency is lower than DC relative permittivity and relative permittivity becomes complex at frequencies where loss occurs.

Thermal agitation tries to randomize the dipole orientations whereas the applied alternating field tries to align the dipole moment along the alternating field. In process of this alignment there is inevitable loss of electric energy. This loss is known as Dielectric Loss. The absorption of electrical energy by a dielectric material subjected to alternating Electric Field is termed as Dielectric Loss.

Under DC condition ϵ_r is real but at high frequencies

Figure 16.1

relative permittivity $\epsilon_r = \epsilon_r' - j\epsilon_r''$ 16

Figure 16.2

The real part is the Relative Permittivity and the imaginary part is the Energy Loss part. Because of Complex Relative Permittivity a loss angle (δ) is introduced.

4.3.1. Loss Angle (δ).

Parallel plate capacitor is given as follows:

¹This content is available online at <<http://cnx.org/content/m49782/1.1/>>.

$$C = \frac{\epsilon_r \epsilon_0 A}{d} \quad \text{where } A = \text{cross - sectional area of the Capacitor and } d$$

$$= \text{distance between the plates} \quad 17$$

Figure 16.3

To account for the lossy nature of the dielectric we assume complex relative permittivity. Hence we get:

$$C = \frac{(\epsilon_r' - j\epsilon_r'')\epsilon_0 A}{d} = C_1 - jC_2 \quad \text{where } C_1 = \frac{\epsilon_r' \epsilon_0 A}{d} \quad \text{and } C_2 = \frac{\epsilon_r'' \epsilon_0 A}{d} \quad 18$$

Figure 16.4

Real part of the Capacitance causes Quadrature Component and Imaginary Part causes In-Phase component. The In-phase component causes the loss angle hence loss angle is defined as:

$$\text{Tan}(\delta) = \frac{\epsilon_r''}{\epsilon_r'} \quad 19$$

Figure 16.5

In the Table 4.3.1, we tabulate some important dielectrics and their loss Tangents. In Figure 4.4 the Relative Permittivity Real Part and Imaginary Part is plotted as frequency.

Table 4.3.1. Some important dielectrics and their loss angle tangent.

Ceramics	Tan (δ)	Dielectric Strength	Applications
Air	0	31.7kV/cm at 60 Hz	Tested in 1cm gap
Al ₂ O ₃	0.002 to 0.01		

continued on next page

SiO ₂	0.00038	10MV/cm at DC	IC Technology MOS-FET
BaTiO ₃	0.0001 to 0.02		
Mica	0.0016		
Polystrene	0.0001		Low loss Capacitance
Polypropylene	0.0002		Low loss Capacitance
SF ₆ Gas		79.3kV/cm at 60 Hz	Used in High Voltage Circuit Breakers To avoid discharge
Polybutane		>138kV/cm at 60 Hz	Liquid dielectric in cable filler
Transformer Oil		128kV/cm at 60 Hz	
Borosilacate Glass		10MV/cm duration 10 μ s 6MV/cm duration 30s	

Table 16.1

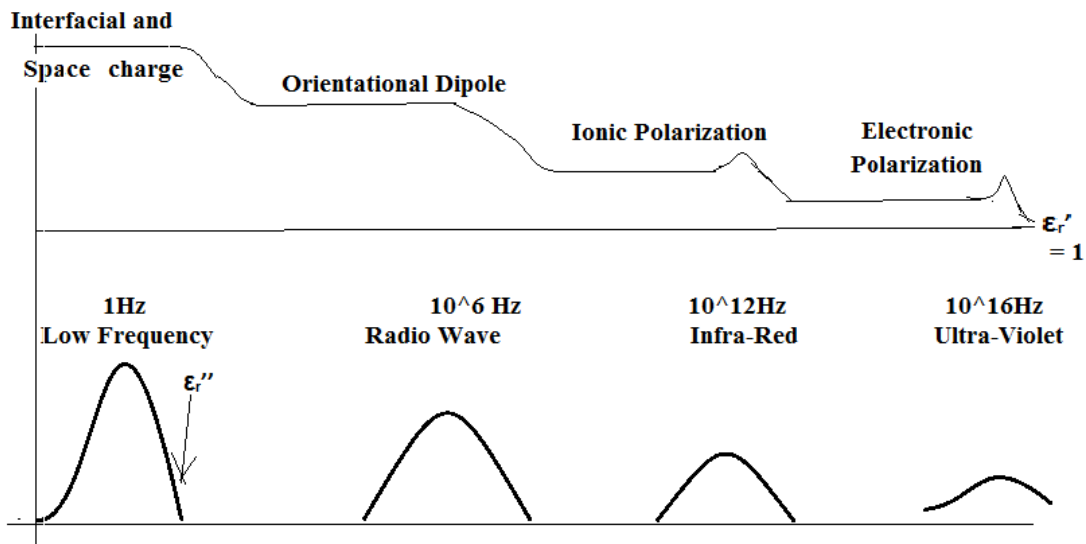


Figure 4.4. Plot of Imaginary Part and Real Part of Relative Permittivity.

Figure 16.6

As seen in Figure 4.4, there is significant loss at low frequency, at Radio-Wave frequency, at Infra-Red frequency and at Ultra-Violet frequency. These correspond to the natural frequencies of the electron cloud system shown in Figure 4.3. For High-Q systems we require capacitance with dielectric material having a very low loss angle. These are generally Poly-sterene Capacitances or Poly-propylene Capacitors.

Section 4.4. Piezoelectric Effect and Piezoelectric Materials.

Electricity resulting from Pressure is known as piezo-electricity. This is called piezo-electric effect.

Electricity causes deformation of such materials. This is known as inverse piezo-electric effect. The most commonly used piezo-electric materials are Quartz, Rochelle Salts, Sodium Potassium Tartarate and tourmaline.

Rochelle Salts are mechanically weak but electrically very sensitive. Hence used in micro-phones, head-phones and loud speakers.

Tourmaline are mechanically the strongest but electrically least sensitive. At frequencies higher than 100MHz, vibrational breakage can take place hence mechanically strongest materials are used namely Tourmaline.

Quartz Wafers are very popular as the stab lest electronic oscillators. These are known as Quartz Crystal Oscillators and to date these are stab lest with only 1part in million drift due to temperature, aging or load. Recently MEMS oscillators have proved to be even more stable. In Quartz Crystal Oscillators, Quartz mechanically oscillates but because of its piezo-electric property it behaves like a LC Tank-circuit with a very high Q Factor. Hence it allows the electronic oscillator to oscillate at its Resonance Frequencies which are critically dependent on the Physical Dimensions. Hence as long as Physical Dimensions are accurately reproduced so long the requisite Oscillation Frequency is accurately generated. The resonance frequencies of some of the standard cut Quartz Wafers are given in Table 4.4.1.

Table 4.4.1. Resonance frequencies and the Q-Factor of standard cut Quartz Wafers.

Frequency(Hz)	32k	280k	525k	2M	10M
Cut	XY Bar	DT	DT	AT	AT
$R_S(\Omega)$	40k	1820	1400	82	5
$L_S(H)$	4800	25.9	12.7	0.52	12mH
$C_s(pF)$	0.0491	0.0126	0.00724	0.0122	0.0145
$C_p(pF)$	2.85	5.62	3.44	4.27	4.35
Q Factor	25,000	25,000	30,000	80,000	150,000

Table 16.2

The electrical analog of the mechanical vibration of Quartz Crystal is as follows:

Electrical Analog of the Mass of the Quartz Wafer is L_S .

Electrical Analog of the spring constant of the Quartz Wafer is C_S .

Electrical Analog of the damping of the Quartz Wafer is R_S .

C_P is the parallel electrode capacitance.

L_S , C_S , R_S comprises the intrinsic series resonance path and C_P is in parallel with this Series Resonance Path as shown in Figure 4.5.

Quartz Crystal Equivalent Model

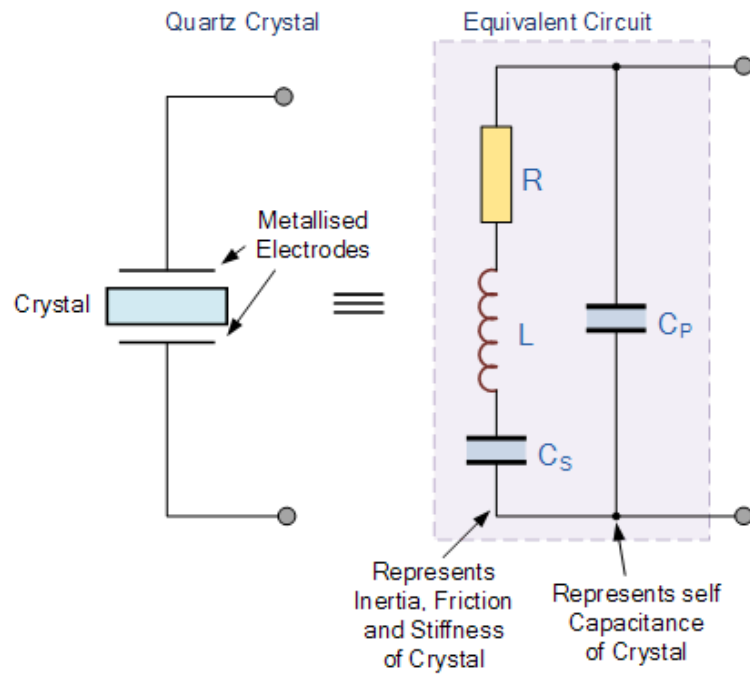


Figure 4.5. Quartz Crystal Electronic Equivalent Circuit

Figure 16.7

Quartz Crystal Reactance

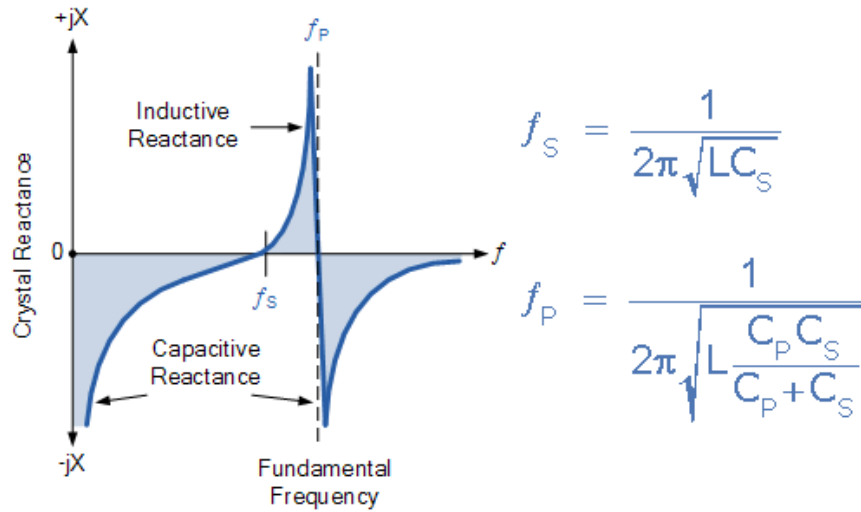


Figure 4.6. Quartz Crystal Reactance Plot and Zero-Pole Pattern.

Figure 16.8

Chapter 17

Section 4.5. Piezo-electricity and Ferro-electricity.¹

Section 4.5. Piezo-electricity and Ferro-electricity.

Piezo-electric effect was discovered by Jacques and Pierri Curie in 1880. They discovered that certain materials like quartz, Rochelle Salt, tourmaline and Sodium Potassium Tartarate exhibited polarization on the application of mechanical stress as shown in Figure 4.6.

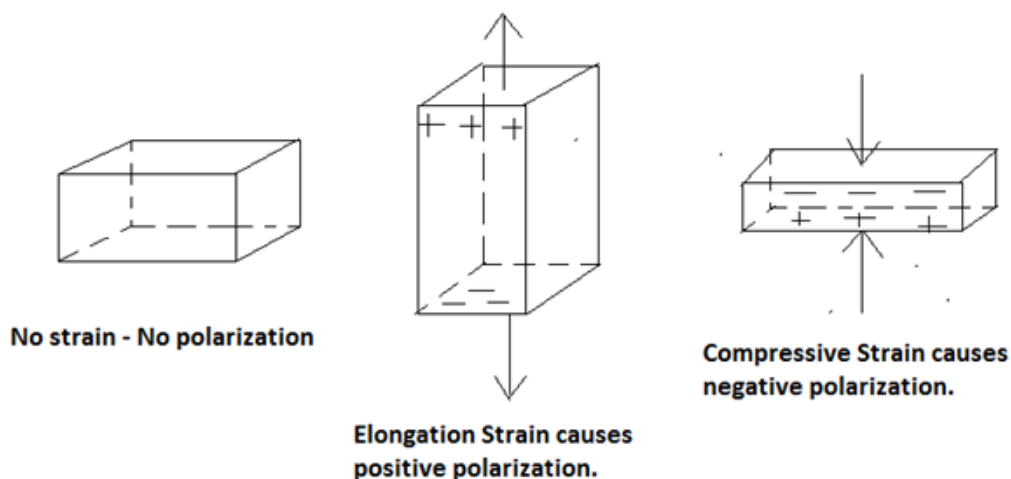


Figure 4.6. Response of Piezo-electric material to Elongation and Compressive Strain.

Figure 17.1

Application of electrical field causes mechanical deformation. This is called Inverse Piezo-electric Effect. Using Inverse Piezo-electric Effect, Ultra-sonic transducers can be built. Alternating Electric field applied in

¹This content is available online at <<http://cnx.org/content/m49792/1.1/>>.

the frequency range 20kHz to 100MHz will set the piezo-crystal in mechanical vibration at the same frequency as long as the frequency happens to be the natural frequency of resonance as determined by the physical dimensions. If the applied alternating electric field is off-resonance then very weak mechanical vibrations will be set.

As seen in Figure 4.6, there is no polarization under zero strain. When tensile or compressive strain is applied to such a crystal, it alters the separation between (+)ve and (-)ve charges in each elementary cell. This leads to a net polarization in each unit cell at the crystal surface. The Polarization is proportional to the applied Stress and its polarity is direction dependent. In the Figure 4.6, Elongation or tensile strain causes positive polarization and Compressive strain causes negative polarization.

Stress creates Electric Field and Electric Field creates Elastic Strain causing the physical dimension to alter in accordance with the electric field.

Besides Quartz, Rochelle Salts, Tourmaline, Sodium Potassium Tartarate we have piezoelectric ceramics. PZT is an example of piezo-electric ceramics. PZT is polycrystalline ferroelectric material with PEROVSKITE crystal structure.

Perovskite has Tetragonal/Rhombohedral structure very close to Cubic Structure. They have a general formula as follows:

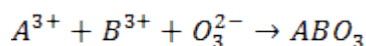


Figure 17.2

Here A is trivalent metal ion such as La.

B is trivalent metal ion such as Al.

Rhombohedral Perovskite is $LaAlO_3$.

PZT is a mass of minute crystallites. Above Curie Temperature it exhibits simple cubic structure with (+)ve charge center and (-)ve charge center being coincident as shown in Figure 4.7.a. Hence the crystal is centro-symmetric with no permanent dipoles. It is found to exhibit paraelectric behavior. Ability for undergoing electronic polarization as discussed in Physics of Dielectric Chapter.

Paraelectricity is the ability of many materials (specifically ceramic crystals) to become polarized under an applied electric field. Unlike Ferroelectricity; this can happen even if there is no permanent electric dipole that exists in the material, and removal of the fields results in the polarization in the material returning to zero. The mechanisms which give rise to paraelectric behaviour are the distortion of individual ions (displacement of the electron cloud from the nucleus) and the polarization of molecules or combinations of ions or defects.

Paraelectricity occurs in crystal phases in which electric dipoles are unaligned (i.e. unordered domains that are electrically charged) and thus have the potential to align in an external electric field and strengthen it. In comparison to the ferroelectric phase, the domains are unordered and the internal field is weak.

The $LiNbO_3$ crystal is ferroelectric below 1430 K, and above this temperature it turns to paraelectric phase. Other perovskites similarly exhibit paraelectricity at high temperatures. Paraelectricity may provide an alternative to the traditional heat pump. A current applied to a paraelectric material will cause it to cool down - which could be useful for refrigeration or for cooling computer chips.

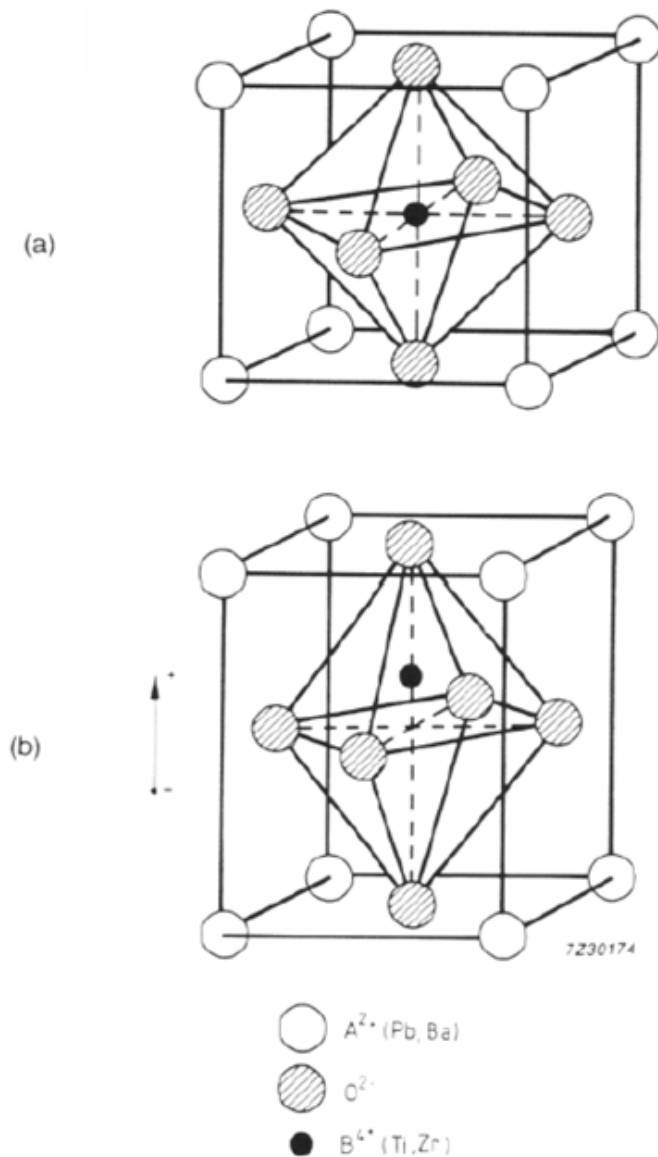


Figure 4.7. Crystal Structure of PZT above and below Curie Temperature.

Figure 17.3

As shown in Figure 4.7.b. below Curie Temperature it takes tetragonal symmetry. Each Unit Cell has built-in electric dipole which may be reversed by the application of electric field. These electric dipoles may be re-oriented in any desired direction by the application of appropriately directed electric field. This is analogous to Ferro-magnetism hence it is called Ferro-electricity.

In PZT, below Curie Temperature, there are domains of polarization known as WEISS DOMAINS as

shown in Figure 4.8.a. Within WEISS DOMAIN, the dipoles are self-aligned hence WEISS DOMAINS has a net polarization measured by dipole moment per unit volume. But WEISS DOMAINS in PZT are randomly oriented as shown in the Figure 4.8.a. Overall polarization or Piezoelectric effect is zero. But this mass of minute crystallites in PZT containing randomly oriented WEISS DOMAINS can be induced to have net polarization by the application of strong electric field. This is called Electric Poling and has been illustrated in Figure 4.8.b.

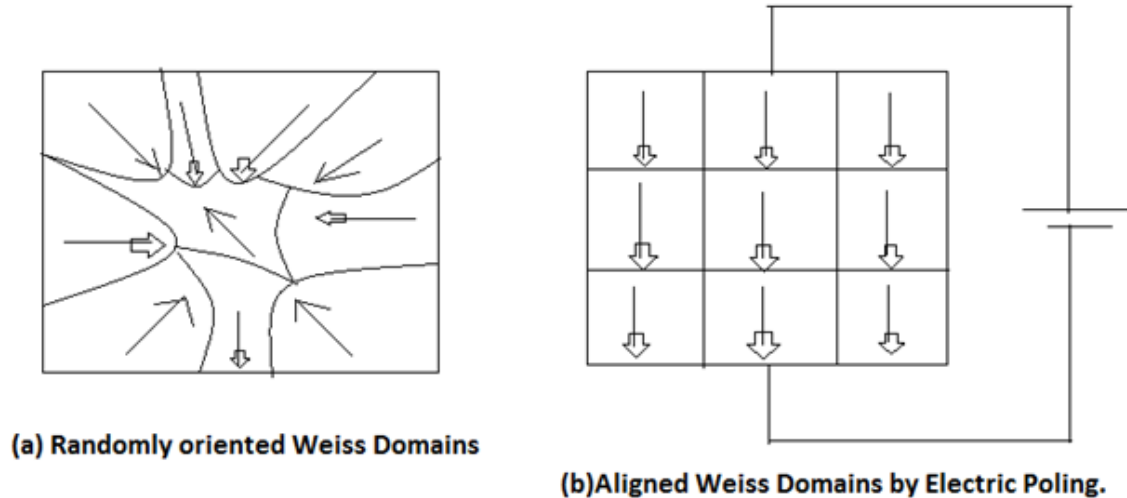


Figure 4.8. PZT material below CURIE TEMPERATURE before electric poling and after poling.

Figure 17.4

As seen in Figure 4.8.b. after Electric Poling all Weiss Domains are forced to be oriented in a given direction by the application of Electric Field in the desired direction below Curie Temperature. The domains most nearly aligned with the applied electric field grow at the expense of the other domains. Even after field is removed the alignment remains locked in the desired direction, giving PZT a remnant electric polarization and a permanent deformation making the material anisotropic. In anisotropic materials the material property depends on the direction of measurement. This is exactly as in Ferro-magnetic Materials. Just as we have B-H Hysteresis Loop in Ferro-Magnet we have Polarization-E Hysteresis Loop in Ferro-electric Materials as shown in Figure 4.9. D closely follows Polarization-E curve.

Remnant Polarization for soft PZT is $P_r = 0.3 \text{ [(C-m)/m}^3] = 0.3\text{C/m}^2 = \text{Dipole Moment per unit Volume.}$

In piezo-electric materials we have Mechanical Deformation versus Applied Electric Field curve. This also shows a hysteresis loop showing plasticity and plasticity loss.

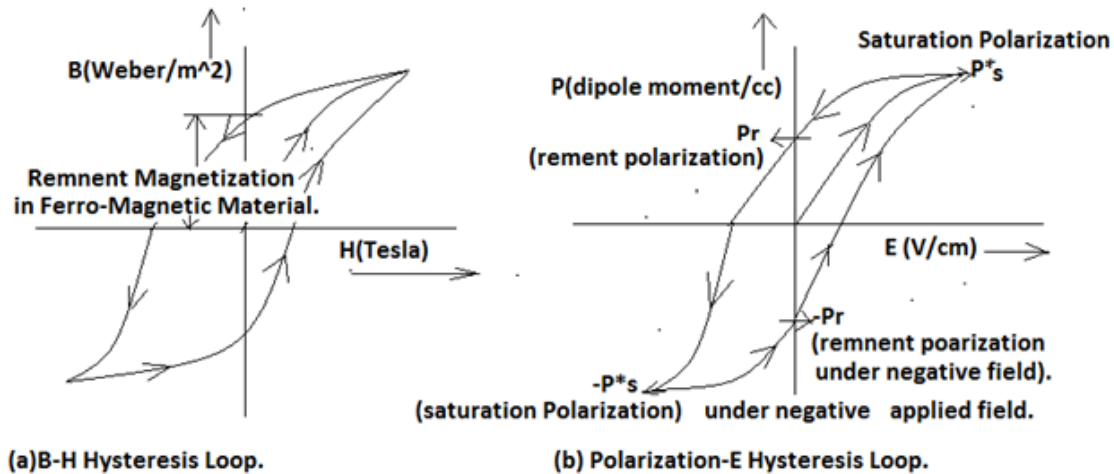


Figure 4.9. Polarization-E curve is analog of B-H Hysteresis Loop.

Figure 17.5

In Table 4.5.1. the main electric parameters of standard Piezo-electric materials are given.
Table 4.5.1. Dielectric Constant and Q-Factor of Quartz, PZT 5A and PZT 4A.

Materials	Quartz	PZT 5A (NAVY II)	PZT 4A (NAVY II)
Dielectric Constant	4.5	1800	1300
Q-factor	$10^4 - 10^6$	80	600

Table 17.1

Section 4.5.1. Applications of Piezo-electric and Ferro-electric Materials.

Quartz are used as high Q, high precision Mechanical Resonators and find wide applications as generating stable electric oscillations for Watches, Clock Waveforms in Computers and for generating Carrier Waves in Radio Broadcast Stations.

To date Quartz Crystal Oscillators (Xtal Oscillator) is the stab lest Frequency Generators. The Frequency of Xtal Oscillator does not drift with temperature , aging or with varying load. The Resonance Frequencies or Natural Frequencies are well defined by the physical dimensions of the crystal and oscillation occurs at natural frequencies. Quartz Xtal Oscillators are very small. It consists of a thin piece of Cut Quartz Wafer with two parallel surfaces metalized to make required electrical connections. The physical dimensions of the crystal are critical in faithfully producing a given frequency.

PZT are generally used as actuating systems in which they operate they operate below natural resonance frequencies and in which the ability to generate high forces and high spatial displacements is more important e.g. in high performance Ultra-sonic Transducers. PZT can be shaped in any fashion and it can be polarized in any direction.

Chapter 18

Chapter 5 _ Introduction-Nanomaterials.¹

Chapter 5 _ Introduction-Nanomaterials.

The Universe ranges from 10^{28} cm to 10^{-33} cm. The first Length is the distance from our Earth to the observable Event Horizon of the Universe which is $13.8\text{blightyears(ly)} = 4.23313 \text{ b parsec(pc)} = 1.30622 \times 10^{26}\text{m}$. The second length is Planck's Length:

$$l_p = \sqrt{\frac{\hbar G}{c^3}} = 1.616199(97) \times 10^{-35} \text{ m}$$

Figure 18.1

Planck's Length sets the fundamental limit on the accuracy of length measurement.

As proto-human-society and human society has developed, its capabilities have developed. Its tool materials improved from flint stones to copper to bronze to iron implements to steel to polymers to Silicon and finally to nano-materials. In Table 5.1, we show the development of Proto-human society due to anatomical changes in homo-species. Once modern humans emerged human society has developed both due to the development of relation of production and due to the development of tools of production.

Relation of production has developed from primitive communism to slavery to feudal and to the capitalist society. The modern Capitalist Society is experiencing the labour pains for delivering a Socialistic Society.

The scale of production has evolved from Small Scale Owner Managed Production to Large Scale Corporate Managed Production.

Table 5.1. Stages of development in Proto Human Society and Human Society based on anatomical changes, based on relation of production and based on the development of means of production.

Hunting & agriculture for fodder

¹This content is available online at <<http://cnx.org/content/m49713/1.1/>>.

9,000 Modern Humans Slavery Native Copper used.Smelted Copper used, Mining, Agriculture for grains, artisans

BRONZE AGE

6,000...5,500...5,500... Modern Humans Feudalism Silver,Tin,Bronze. Mining, Agriculture, artisans

3,400 to1800CE Modern Humans **IRON AGE**

1800CE to 1940CE Modern Humans Capitalism **STEEL AGE**
Industrial Revolution & Large Scale Production

1940-1960CE Modern Humans Capitalism **POLYMER AGE**
Factory production

1960CE to present Modern Humans **SILICON AGE**
Computerization, Automation, Robotization & Miniaturization

1980 to present Modern Humans **NANO AGE**
Miniaturization & System Integration

Hunting & agriculture for fodder

9,000 Modern Humans Slavery Native Copper used. Smelted Copper used, Mining, Agriculture for grains, artisans

BRONZE AGE

6,000...5,500...5,500... Modern Humans Feudalism Silver, Tin, Bronze. Mining, Agriculture, artisans

3,400 to 1800CE Modern Humans **IRON AGE**

1800CE to 1940CE Modern Humans Capitalism **STEEL AGE**
Industrial Revolution & Large Scale Production

1940-1960CE Modern Humans Capitalism **POLYMER AGE**
Factory production

1960CE to present Modern Humans **SILICON AGE**
Computerization, Automation, Robotization & Miniaturization

1980 to present Modern Humans **NANO AGE**
Miniaturization & System Integration

Hunting & agriculture for fodder

9,000 Modern Humans Slavery Native Copper used.Smelted Copper used, Mining, Agriculture for grains, artisans

BRONZE AGE

6,000...5,500...5,500... Modern Humans Feudalism Silver,Tin,Bronze. Mining, Agriculture, artisans

3,400 to1800CE Modern Humans **IRON AGE**

1800CE to 1940CE Modern Humans Capitalism **STEEL AGE**
Industrial Revolution & Large Scale Production

1940-1960CE Modern Humans Capitalism **POLYMER AGE**
Factory production

1960CE to present Modern Humans **SILICON AGE**
Computerization, Automation, Robotization & Miniaturization

1980 to present Modern Humans **NANO AGE**
Miniaturization & System Integration

Date(ya) ¹	Anatomical ³	Relati
4M	AustralopethicusAfarensis	Savage
2.5M	Homo-habilis(handy man)	Savage
1.9M	Homo-erectus(erect man)	Savage
800,000	Homo-sapiens(intelligent man)	Barbar
200,000	Modern humansEmerge in AFRICA	Barbar
70,000(last ice age begins)	Migrate out of Africa and replace all primitive homo-species.	Barbar
50,000	Modern Humans reachAustralia and get isolated as Australian Aborigines.	Barbar
50,000To 40,000	Migration to Asia	Barbar
40,000 to30,000	In;land migration from Asia to Europe	Barbar
	Modern humans push toCentral Asia and arrived in the grassy steppes of Himalaya	Barbar
	From S.E.Asia and China, migration to Japan & Siberia took place.	Barbar
	North Asians migrated to N.America via land bridge across Arctic from Siberia	Barbar
10,000	Great delugeModern Humans	Barbar
9,000	Modern Humans	Slavery
6,000. . .5,500. . .5,500. . .	Modern Humans	Feudal
3,400 to1800CE	Modern Humans	
1800CE to 1940CE	Modern Humans	Capita
1940-1960CE	Modern Humans	Capita
1960CE to present	Modern Humans	
1980 to present	Modern Humans	

Table 18.1

1. Ya = years ago.
2. Hand – grip = hand curves to grip the tool and stiffens at the base of the thumb and in the mid-hands to stabilize the hand and dissipate the force. This complex of traits gives dexterity in tool making and tool handling.
3. “When Early Hominines got a Grip”, Meeting Briefs, American Association of Physical Anthropologists, 9-13 April, 2013, Knoxville Tennessee, Science, Vol. 340, 26th April 2013, pp 426-427.

What is Nano-materials ?

Nanoscience = Study of nanoscale materials, properties and phenomena.

Nanoscale Materials = Specifically: ≤ A material 100 nm along one dimension (Out of three dimention.

Nanotechnology = Applications of nanoscience to industry and commerce.

"Wet" nanotechnology, which is the study of biological systems that exist primarily in a water environment.

"Dry" nanotechnology, which derives from surface science and physical chemistry, focuses on fabrication of structures in carbon (for example, fullerenes and nanotubes), silicon, and other inorganic materials.

Computational nanotechnology, which permits the modeling and simulation of complex nanometer-scale structures.

5.1. Examples of Nanoscience.

The blue color of the butterfly shown in Figure 5.2 is due to Nature's remarkable nanotechnology — the blue color is known as "structural color" (i.e. no pigment) that originates from the nanostructure in the dorsal wing. The structure interferes with certain wavelengths of light to produce an beautiful . The underside of the wing , on the other hand is brown. Why?



Figure 18.2

Figure 5.2. Butterfly *Morpho peleides limpida* is an example of nanoscience.

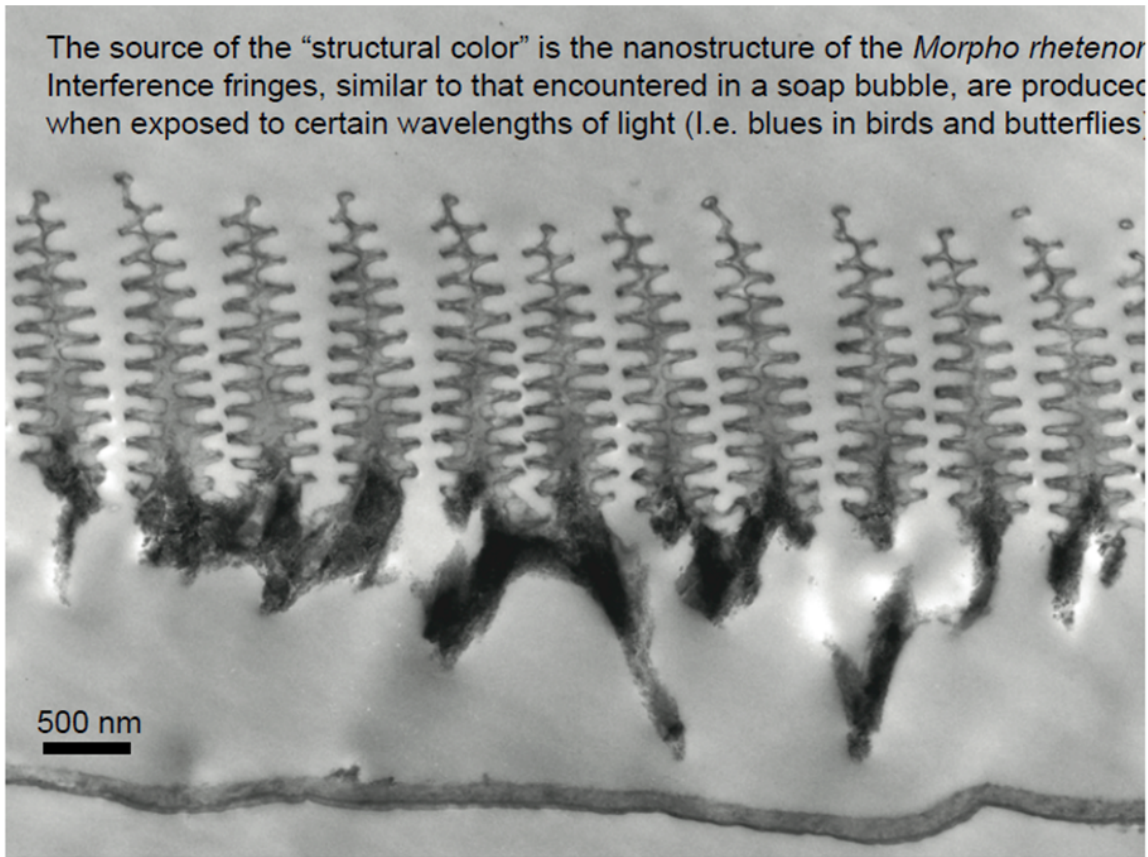


Figure 18.3

Figure 5.3. Nanostructure in Butterfly's wings produces the interference fringes.

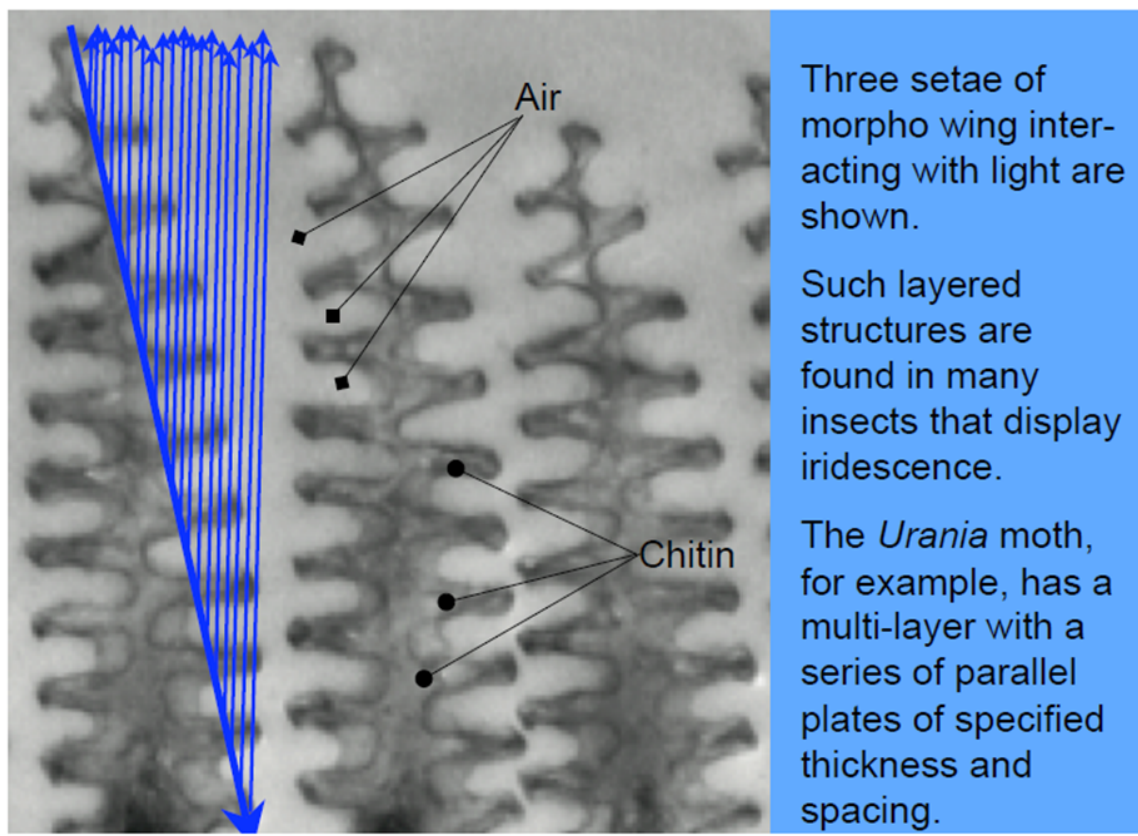


Figure 18.4

Figure 5.4. The layered structure in Butterfly's Wings, through alternate constructive and destructive interference, gives rise to coloured fringes.

In early morning, dew drops curl up to form pearl beads on the lotus leaf in a pond. This is an example of nanoscience. The micro-nanostructure of the lotus leaf exhibits super-hydrophobicity. Superhydrophobicity means repulsion of Lotus Leaf towards Water Dew Drops. Hence dew drops early in the morning curl up as pearl beads.

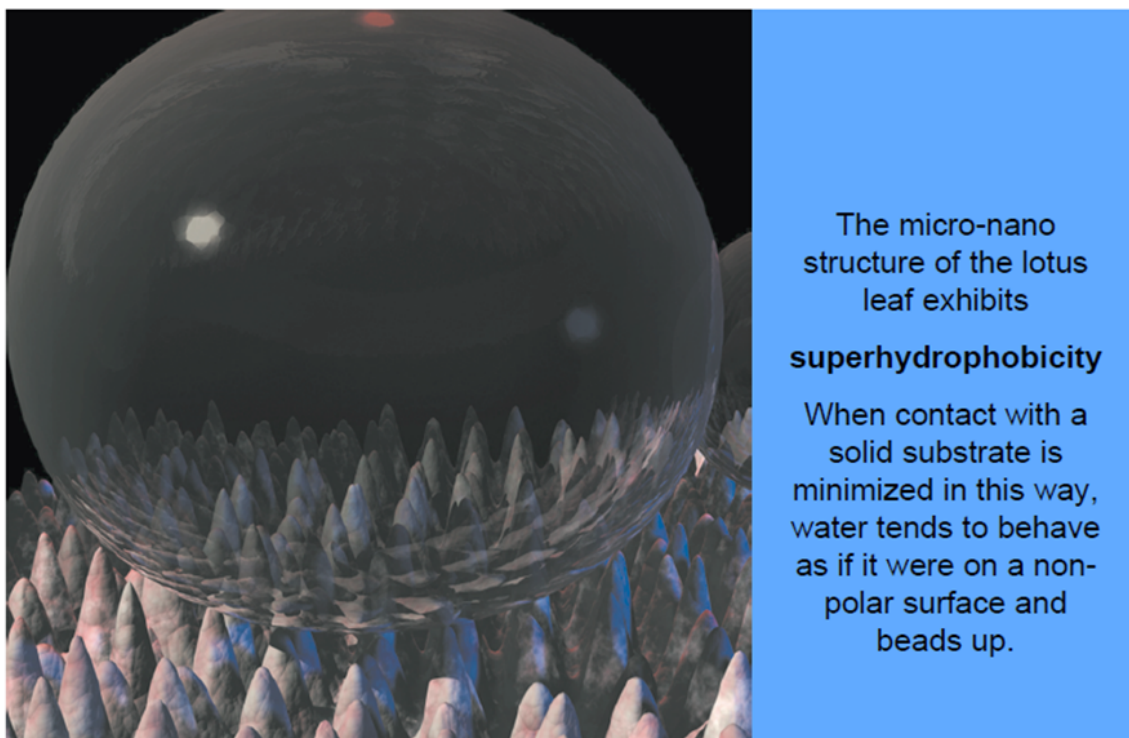


Figure 18.5

Figure 5.5. The water beads formation on lotus leaf is a beautiful example of superhydrophobicity.

5.1.1. Self cleaning in Morpho Aega.

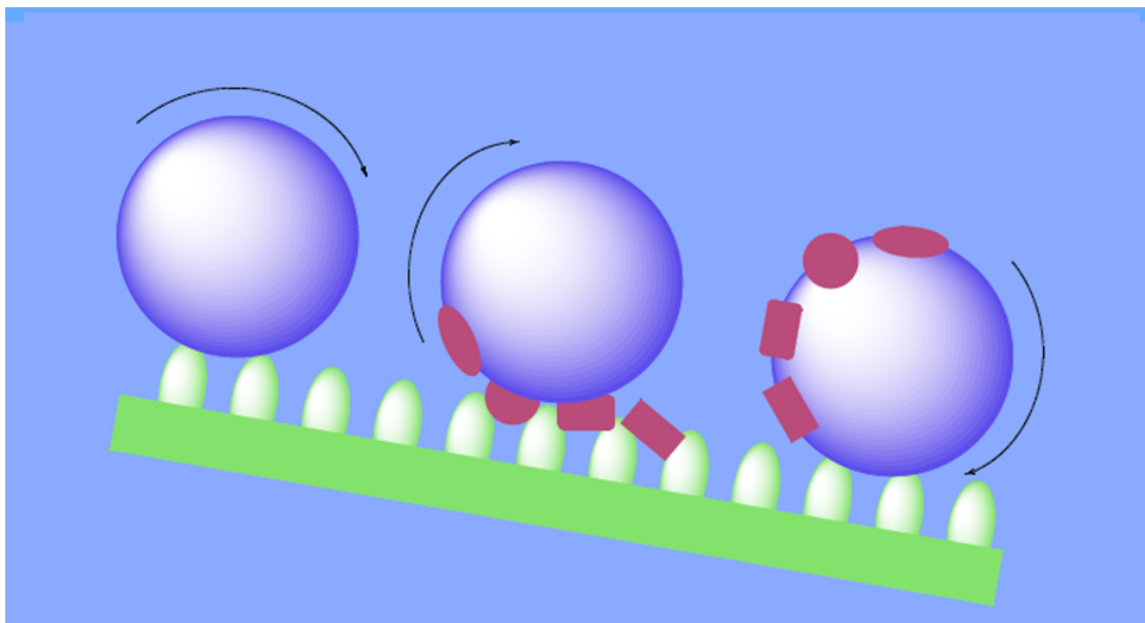


Figure 18.6

Figure 5.6. The attraction to water is higher than the static friction force between the dirty particle(marked in red) and the pointy surface, the dirty particle will be absorbed by the droplet.

Morpho Aega, a species of Butterfly, has the ability to self clean its wings based on nano-science. In Figure 5.6, water-droplets are shown in blue. These water drops roll-off the wing in a “radial out” direction from the central axis of the butterfly body due to directional adhesion of the super-hydrophobic wing. The direction of rolling is tuned by controlling the air-flow by the posture of the wings. The water droplets adsorb the dirt particles by electro-static attraction and these droplets carry away the dirt as the droplets roll off.

5.2. Classification of Nano-materials.

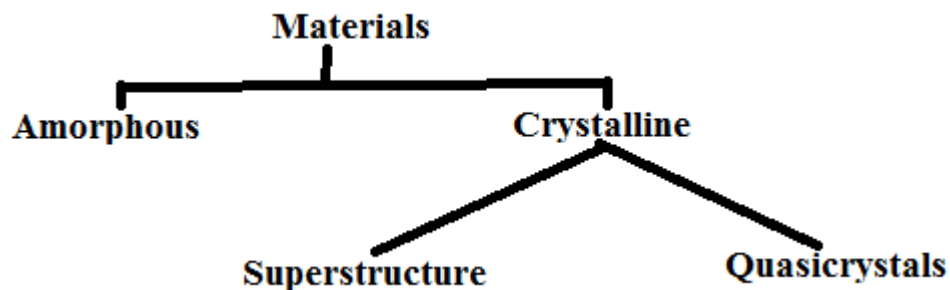


Figure 18.7

Nano-materials are classified in exactly the same manner as Bulk Materials. The crystalline materials have some standard Unit Cells (Cubic Cells, FCC, BCC, Hexagonal Unit Cell, tetrahedral structure) which are repeated in all 3-Dimensions.

A Single Crystal of nanometer size less than 100nm is referred to as nano-crystal. It is a single domain crystal with the diameter of the single domain less than 100nm. In Figure 5.7 the nano-crystals are shown.

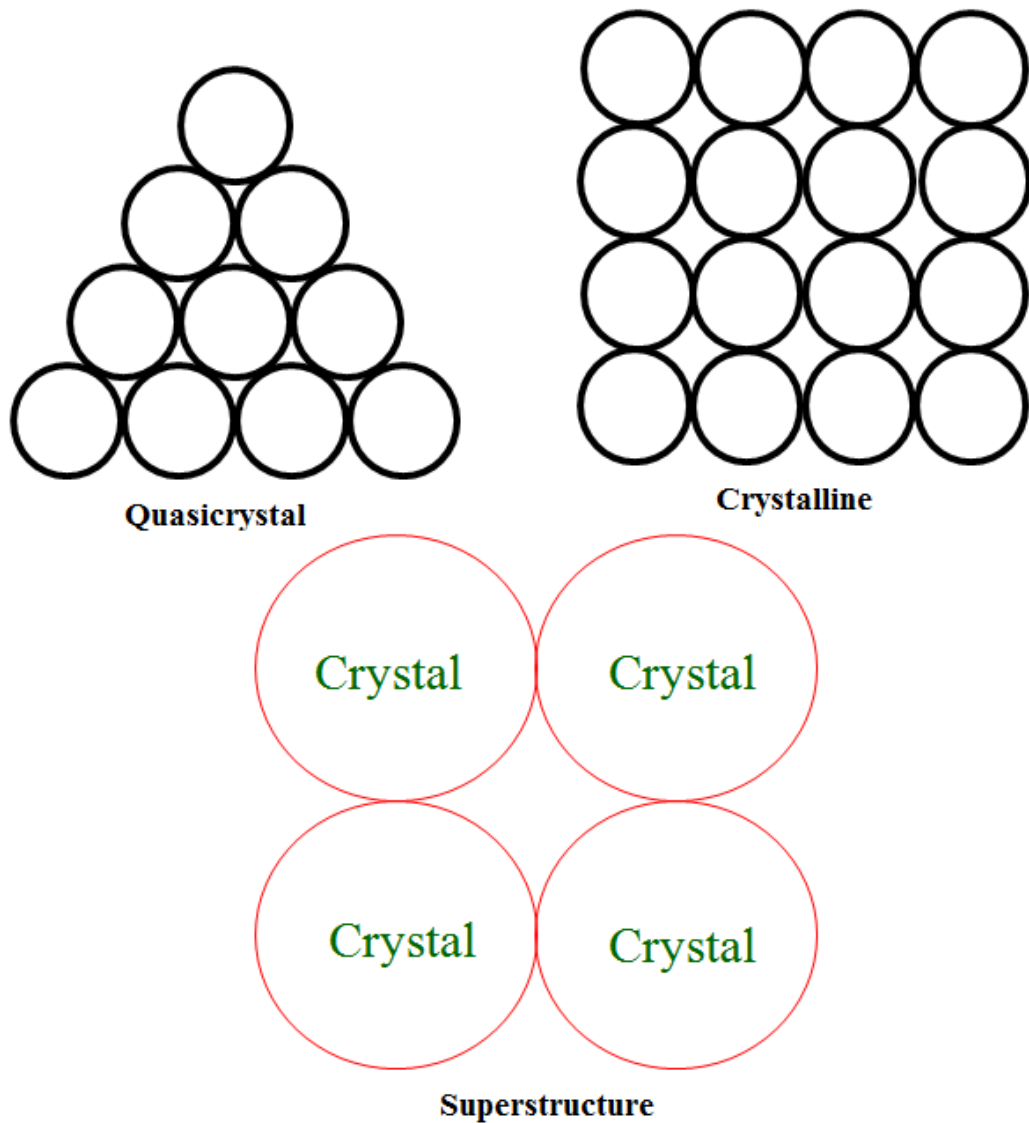


Figure 18.8

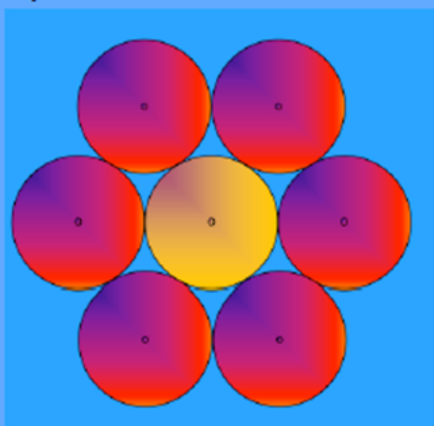
Figure 5.7. A single-crystal of 100nm size or less is a single domain crystal. It is Quasicrystal if in pyramid form. It is Crystalline if in cubic form. It is super structure if single domain crystals are arranged in a regular periodic form.

5.3. Formation of Stable Nano-structure.

A stable nano-structure is the minimum energy configuration and a minimum energy configuration is obtained in the following manner:

Real nanocrystal metals are not perfectly spherical although we stated earlier that the sphere is the most stable structure (one that minimizes surface area and hence, surface energy).

Take one tennis ball and surround it with as many tennis balls as possible. First conduct the two-dimensional experiment:



In the two-dimensional configuration, it takes 6 tennis balls to completely surround the central ball. There are a total of:

$$1 + 6 = 7 \text{ balls.}$$

Figure 18.9

Figure 5.8. One atom surrounded by 6 atoms gives minimum energy configuration hence stable configuration. So a monolayer is stable when we have 7 atoms.

In bulk-materials, minimum energy configuration is spherical. A sphere is a minimum energy configuration from hydro-static equilibrium condition. But this is not true for nano-materials.

In nano materials first stable configuration has 13 atoms as shown in Figure 5.9.

Through inspection it can be shown that stable configuration is achieved by having;

$M^*(K) \text{ atoms} = (1/3)(10K^3 + 15K^2 + 11K + 3)$ for K^{th} configuration where $K = 1, 2, 3, \dots$

For $K = 1$, first stable nano-crystal has 13 atoms.

For $K = 2$, second stable nano-crystal has 55 atoms.

For $K = 3$, third stable nano-crystal has 147 atoms.

For $K = 4$, fourth stable nano-crystal has 309 atoms.

For $K = 5$, fifth stable nano-crystal has 561 atoms.

These configurations are shown in Figure 5.10.

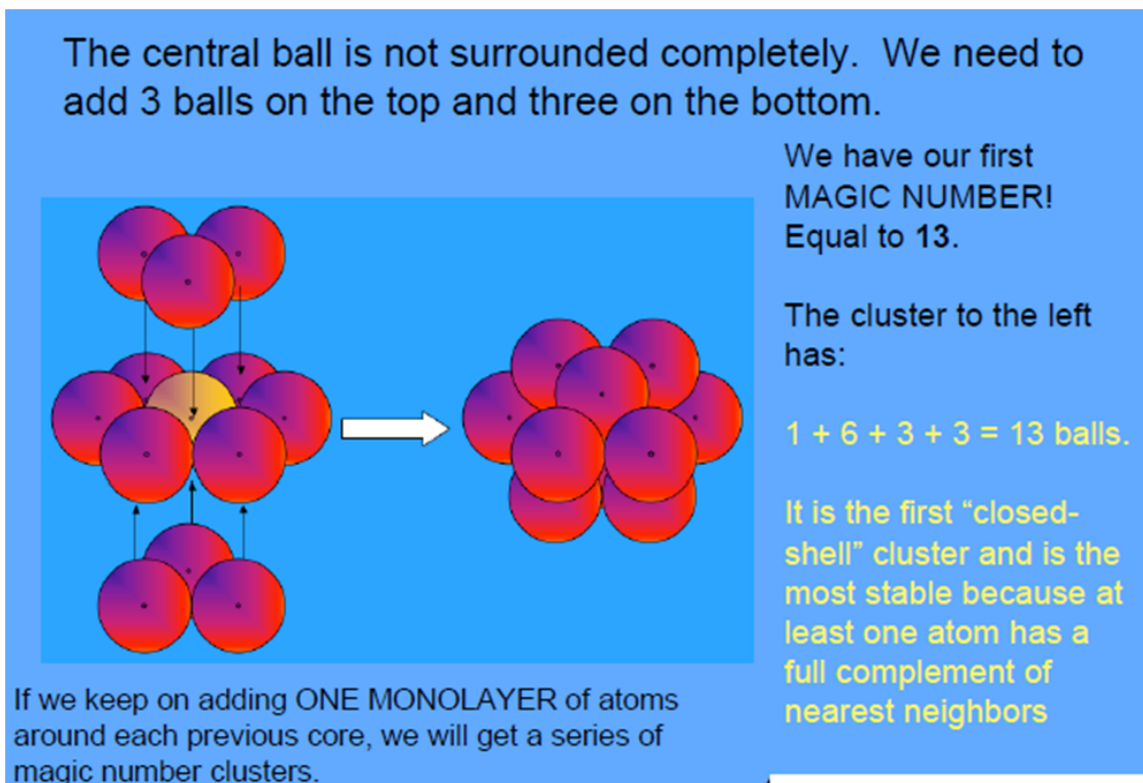


Figure 18.10

Figure 5.9.A 3-D nanocrystal is stable when there are 6 atoms surrounding the core atom and 3-atoms from the top and 3-atoms from the bottom. Meaning by when we have 13 balls then we have first stable 3-D nanocrystal structure though it is not a spherical structure.

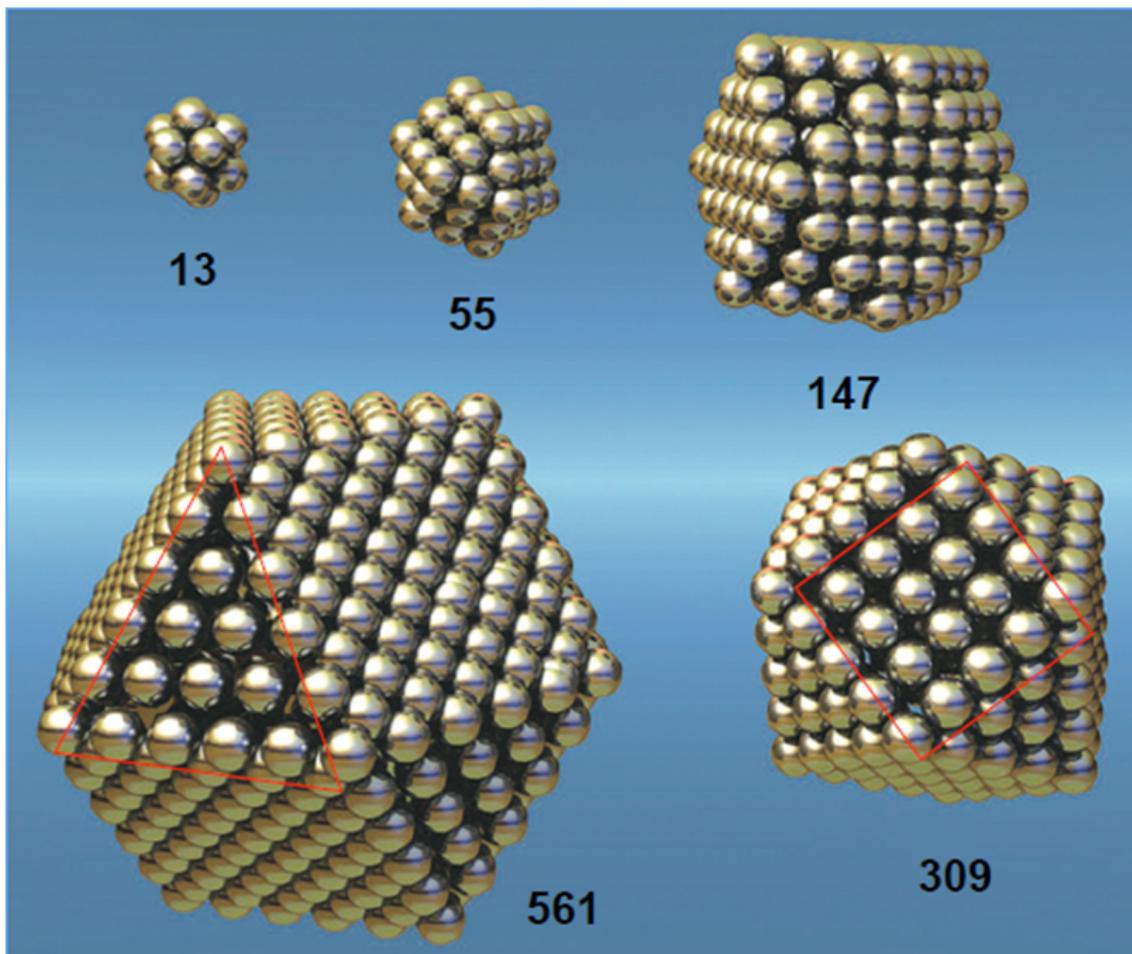


Figure 18.11

Figure 5.10. Stable nano-configuration corresponding to $K = 1, 2, 3, 4$ and 5 are shown.

In Figure 5.11, it is shown that the surface atoms dominate the crystal structure as we move from Bulk configuration to nano-particle configuration. Because of this dominance by surface atoms in nano-crystal configuration, material properties of nano-particle is completely different from those of the bulk crystal.

Surface to volume ratio:-A 3 nm iron particle has 50% atoms on the surface

-A 10 nm particle 20% on the surface

-A 30 nm particle only 5% on the surface

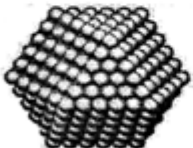
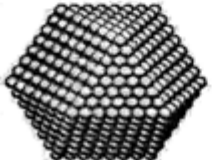
Full-shell Clusters		Total Number of Atoms	Surface Atoms (%)
1 Shell		13	92
2 Shells		55	76
3 Shells		147	63
4 Shells		309	52
5 Shells		561	45
7 Shells		1415	35

Figure 18.12

Figure 5.11. Nano-particle structure for Kth Stable, Minimum Energy, Configuration for K = 1, 2, 3, 4, 5 and 7.

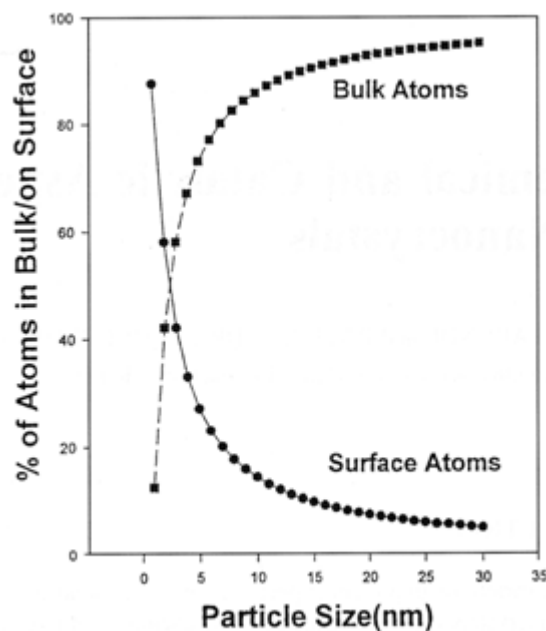


Figure 18.13

Figure 5.12. Calculated Surface Atoms to Bulk Atoms Ratio for Solid Metal Particles vs the Size of Particle (nm). [Curtsey: Kenneth J. Klabunde, Jane Stark, Olga Koper, et al. "Nanocrystal as Stoichiometric Regents with Unique Surface Chemistry", Journal of Physical Chemistry, Vol.100, pp. 12142-12153, (1996)]

As the particle size changes from Bulk – Size to Nano - Size, the overall structure changes and Valence electrons become de-localized. What does this de-localization mean?

We have seen in Band-Theory of Solids that when atoms are far apart the orbital electrons do not interact and the Energy Difference between two consecutive states is at the maximum. But when they are brought close together they start interacting and band gap between consecutive bands reduces. What this means that nano-size particle will have a larger band-gap and as nano-size increases to bulk-size, band-gap asymptotically approaches the bulk band-gap. This leads to different physical and chemical properties continuously graded as size increases from nano to bulk size.

The following properties are affected by nano to bulk-size transition:

Optical properties, Bandgap, Melting point, Specific heat, Surface reactivity, Magnetic property and Electrical conduction.

Chapter 19

Section 5.4. Nano-Size Effect on various opto-electronic-magnetic properties of nano materials.¹

Section 5.4. Nano-Size Effect on various opto-electronic-magnetic properties of nano materials.

A nano-particle or a Quantum Dot Semi-conductor 'Si' is a cluster of large number of atoms arranged in the minimum energy configuration. If there are N atoms there are about N electrons or a few times more in this cluster. Most of these electrons are tightly bound to their host atoms. But there are few carriers electrons and holes which behave like particles in an infinite potential well. The scenario is depicted in Figure 5.12a. These behave just as electrons behave in isolated Hydrogen Atoms. Hence Quantum Dots are Artificial Atoms.

¹This content is available online at <<http://cnx.org/content/m49719/1.1/>>.

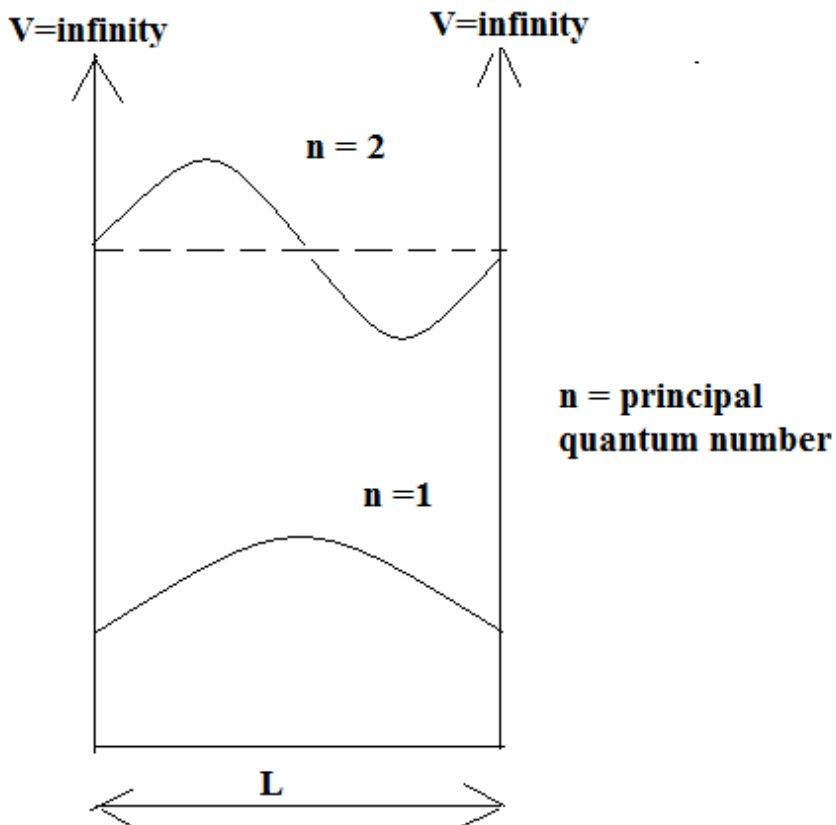


Figure 5.12a. A particle in an infinite Quantum Well of One Dimension

Figure 19.1

The Schrodinger equation of a particle in an infinite potential well is:

$$H\psi = E\psi \text{ where } H \text{ is the Hamiltonian Operator}$$

Figure 19.2

In Quantum Mechanics we have canonical variables: x and p or t and E . Linear Momentum 'p' is equivalent to an operator:

$$p \rightarrow -i\hbar \frac{\delta}{\delta x} \quad \text{and} \quad E \rightarrow i\hbar \frac{\delta}{\delta t}$$

Figure 19.3

Therefore Schrodinger Equation for a particle in an infinite potential well is:

$$H\psi = \left(\frac{p^2}{2m_e} + V \right) \psi = -\frac{\hbar^2}{2m_e} \times \frac{\delta^2 \psi}{\delta x^2} + V\psi = E\psi \quad 5.4.1$$

Figure 19.4

Hamiltonian Operator operates on Matter Wave ψ to yield the eigen value of energy E. (5.4.1) simplifies to Second Order Ordinary Linear Differential Equation with two arbitrary constants determined by the two boundary conditions namely:

$$\psi(L) = \psi(0) = 0$$

Figure 19.5

The simplified Schrodinger Equation is:

$$\frac{\delta^2 \psi}{\delta x^2} + \frac{2m_e(E-V)}{\hbar^2} \psi = 0 \quad 5.4.2$$

Figure 19.6

The Solution is Complementary Function:

$$\psi(x) = B \text{Exp}[-iax] + C \text{Exp}[+iax] \quad \text{where } a = \sqrt{\frac{2m_g(E - V)}{\hbar^2}} \quad 5.4.3$$

Figure 19.7

With the given two boundary condition (5.4.3) simplifies to:

$$\psi(x) = D \text{Sin}[ax] \quad 5.4.4$$

Figure 19.8

To satisfy the given boundary condition:

$$aL = n\pi \quad \text{or} \quad L \sqrt{\frac{2m_g(E - V)}{\hbar^2}} = n\pi \quad \text{or} \quad (E - V) = \frac{n^2 \pi^2 \hbar^2}{2m_g L^2} \quad 5.4.5$$

Figure 19.9

If $V = 0$ then the discrete energy states occupied by a carrier in an infinite 1-D Potential Well are:

$$E_n = \frac{n^2 \pi^2 \hbar^2}{2m_g L^2} = n^2 E_1 \quad 5.4.6$$

Figure 19.10

The energy separation between two adjacent energy states is:

$$E_1 = \frac{\pi^2 \hbar^2}{2m_e L^2} \quad 5.4.7$$

Figure 19.11

The actual energy states in a semiconductor are:

$$E_g^{QD} = E_g^{Bulk} + \frac{\pi^2 \hbar^2}{2m_e L^2} \quad 5.4.8$$

Figure 19.12

In Equation 5.4.8., L is the Radius of the Quantum Dot. By adjusting the size (i.e. R) of the Quantum Dot, it is continuously tunable through all the seven colours of a Rainbow.

The delocalization of electrons and structural changes in nano materials causes band-gap energy change in semi-conductor nano materials as well as changes in the following properties:

- i. Optical properties,
- ii. Melting Point,
- iii. Specific heat,
- iv. Surface reactivity,
- v. Magnetic Properties,
- vi. Electrical conduction.

Table 5.2. gives the Specific Heat of Palladium, Copper and Rubidium in bulk-size and in nano-size.

Table 5.2. Specific Heat of Pd,Cu and Ru in bulk and in nano-size.

Elements	Bulk(J/(mol.K))	Nano(J/(mol.K))	Nano-size	%increase
Pd	25	37	6nm	48
Cu	24	26	8nm	8.3
Ru	23	28	6nm	22

Table 19.1

As the bulk-size moves to nano-size, the Melting Point reduces as given below:

$$\Delta\theta = \frac{2T_0\sigma}{\rho Lr} \text{ where } \Delta\theta$$

= deviation in M.P. from the bulk value and it can be as large as 100°C

Figure 19.13

for particle size $r \sim 10\text{nm}$ and $T_0 = \text{Bulk M.P.}$ and $\sigma = \text{surface tension coefficient for}$

Figure 19.14

*liquid – solid interface and $\rho = \text{particle density}$ and $r = \text{particle radius}$ and L
 $= \text{latent heat of fusion.}$*

Figure 19.15

In Figure 5.13 it is shown that M.P. of gold particles decreases dramatically as the particle size gets below 5nm.

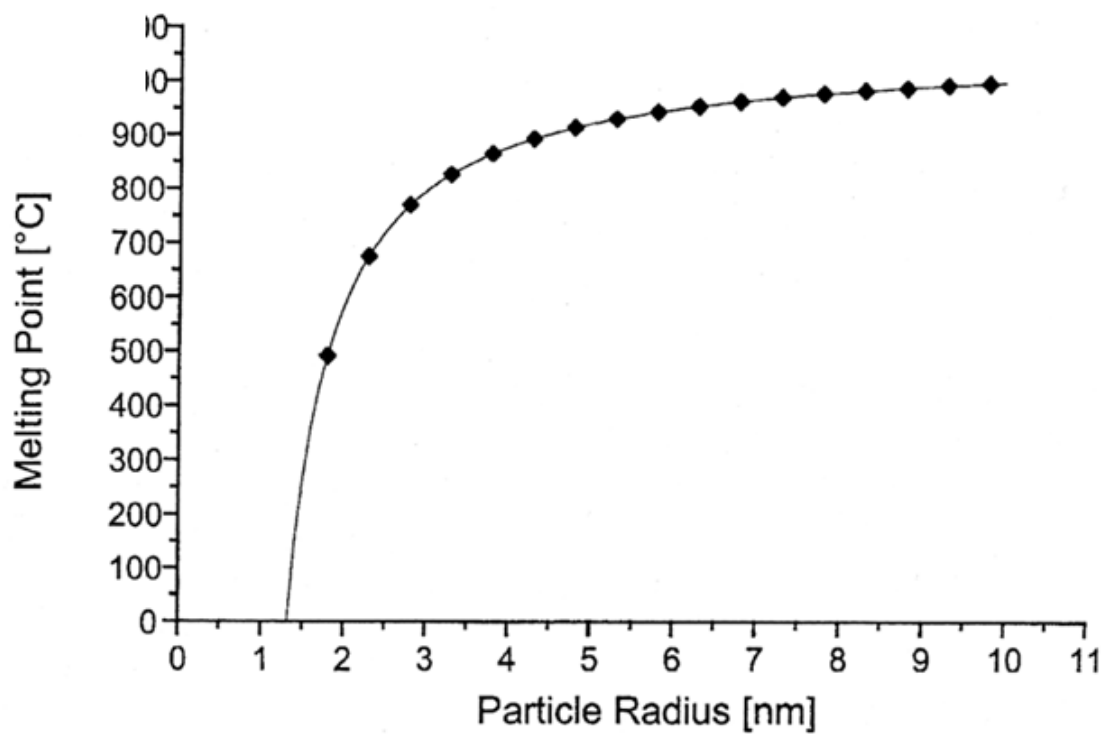


Figure 19.16

Figure 5.13.M.P. of Gold Particles vs Particle Size.

Blue light is used to excite Quantum Dots of reducing size. Progressively shorter wavelengths are emitted as the dot size decreases. The reason is explained in the text.

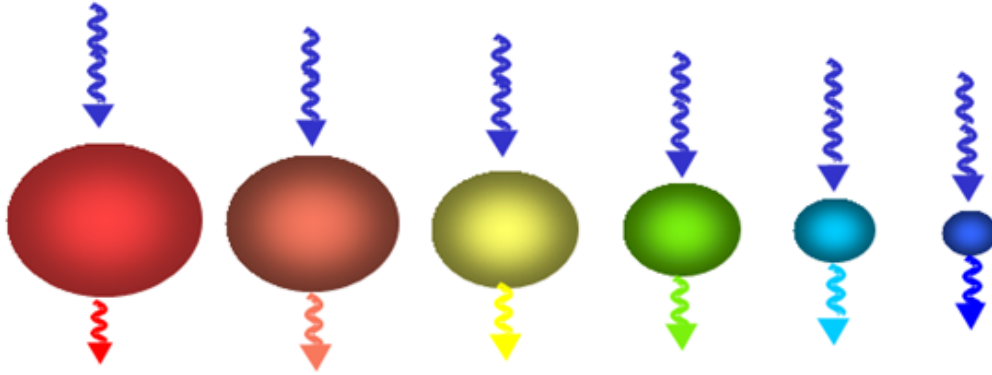


Figure 19.17

Figure 5.14. Quantum Dots of smaller size emit shorter wavelengths.

QD comprises of million atoms and equivalent valence electrons. But QD does have a few free electrons. These electrons behave like particle in an Infinite Potential Well. The Schrodinger Equation has been solved in m33488. That solution tells us electron occupies discrete energy states given by the following equation:

$$E_n = \frac{n^2 h^2}{8mW^2} \text{ where } W = 2r(\text{radius of the dot}) \quad 1$$

Figure 19.18

$$\text{Equation 1, explicitly tells that Energy Gap} = \frac{h^2}{8mW^2} \quad 2$$

Figure 19.19

From (2) it is clear that smaller the dot size larger, larger will be the energy packet absorbed during excitation or larger will be the energy packet radiated when Dot settles to ground state. This is the reason

why in Figure 5.14 as the dot size decreases it is seen to emit shorter wavelengths This emission can be LASER type coherent emission or LED type incoherent emission.

Confining a carrier in atleast one spatial dimension at the scale of the order of de Broglie Wavelength leads to Quantum Size Effect.

In Bulk - 3 degrees of freedoms with 0 degree of Quantum Confinement. So we get bands of permissible energy.

In Quantum Well – 2 degrees of freedom with 1 degree of Quantum Confinement. .

In Quantum Wire - 1 degree of freedom and 2 degrees Quantum Confinement.

In Quantum Dot – 0 degree of freedom with 3 degrees of Quantum Confinement.

Hence in a Quantum Dot, electron behaves as an electron in infinite 1-D Quantum Well. Hence electron behaves as it behaves in a Hydrogen Atom and carriers have discrete energy states. Therefore QD is referred to as an artificial atom.

QD are extremely small semiconductor structures ranging from 2nm to 10nm. At these small dimensions, materials behave differently giving QD unprecedented tunability and enabling never before seen applications in Science & Technology.

The Band-gap of nano-structure:

$$E_g^{nano} = E_g^{bulk} + \frac{\hbar^2 \pi^2}{2R^2} \left(\frac{1}{m_e} + \frac{1}{m_h} \right) \quad 3$$

Figure 19.20

QD LEDs can produce any colour including white light, it is extremely energy efficient giving the highest Lumens per Watt (uses only few watts) whereas CFL uses more than 10W. Its lifetime is 25 times that of incandescent lamp. But these are expensive. As its price falls due high demand and mass-production, these will become affordable.

Section 5.4.1. Electrical Conduction.

In bulk metal, current flow is according to Ohm's Law:

$$I = \frac{V}{R} \quad \text{where } R = \frac{\rho L}{A} \quad \text{and } \rho = \frac{1}{\sigma} = \frac{1}{q\mu_n n}$$

where q = electronic charge, n = density of conducting electron and μ_n = electron mobility

$$= \frac{q\lambda}{4\pi\epsilon_0 m_e v_F} \quad \text{where } v_F$$

= Fermi Velocity and is calculated from the following relationship:

Figure 19.21

$$\frac{1}{2} m_s v_F^2 = \frac{3}{5} (E_F - E_C)$$

Figure 19.22

In nano-material, band theory does not hold good so Ohm's Laws is no longer applicable and special transport equations have to be formulated for accounting for the tunnel currents from nano-particle to nano-particle.

Section 5.5. Electric and Magnetic Properties of matter.

Electron is responsible for two distinct properties:

1- Charge -> It gives all electrical properties of mater.

Conductivity, Paraelectric, ferroelectric, antiferroelectric, diaelectric etc.

2- Spin- > It gives magnetic properties.

Paramagnetic, Ferromagnetic, Antiferromagnetic, Diamagnetic, superparamagnetic, Ferrimagnetic, Canting magnetism, Superferromagnetism.

5.5.1. Charging Energy of nano-particle.

Capacitance of a Sphere is:

$$C = 4\pi\epsilon_0\epsilon_r(a) \quad \text{where } a = \text{radius of the sphere.} \quad 4$$

Figure 19.23

Therefore charging energy U for nanoparticle of radius a is:

$$u = \frac{1}{2} qV = \frac{q^2}{2C} = \frac{q^2}{8\pi\epsilon_0\epsilon_r \times a} = 0.24eV \text{ for } 3nm \text{ diameter nanoparticle with } \epsilon_r = 2$$

Figure 19.24

This is 10 times larger than thermal energy at Room Temperature of 300K which is 25meV.

25meV corresponds to the charging energy of a nano-particle of radius 14.4nm.

So we conclude there is considerable charging energy for nano particle.

5.5.2. Density of States.

It can be shown that Density of permissible Energy States is as follows:

$$D(E) = V \times \frac{1}{2\pi^2} \left(\frac{2m}{\hbar^2}\right)^{3/2} \times \sqrt{E} \quad \text{for 3D Bulk} \quad 5$$

Figure 19.25

$$D(E) = V \times \frac{1}{2\pi} \left(\frac{2m}{\hbar^2}\right) \quad \text{for 2D Quantum Well} \quad 6$$

Figure 19.26

$$D(E) = V \times \frac{1}{2\pi} \left(\frac{2m}{\hbar^2}\right)^{1/2} \times \left(\frac{1}{\sqrt{E}}\right) \quad \text{for 1D Quantum Wire} \quad 7$$

Figure 19.27

Pictorially it is shown in Figure 5.16

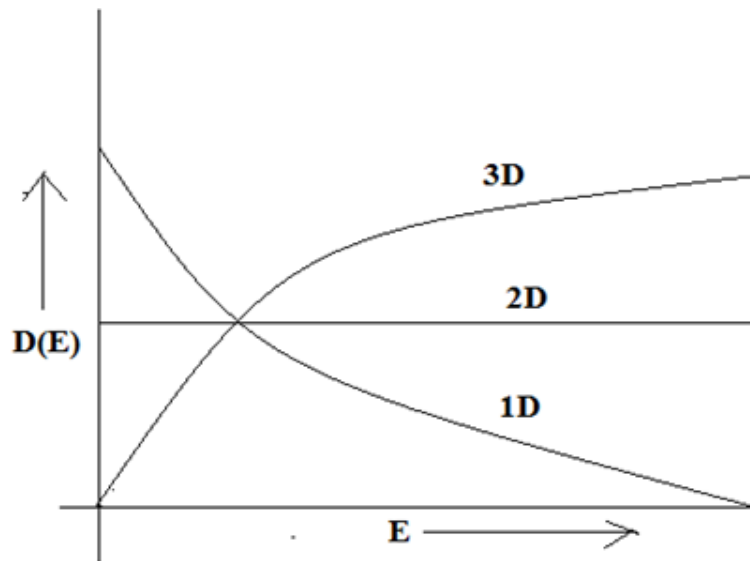


Figure 5.16. Density of States vs Energy for 3D Bulk, 2D Quantum Well and 1D Quantum Wire.

Figure 19.28

Chapter 20

EVEN SEMESTER2014-MidSemester Examination Answers¹

Even Semester Mid-Semester Test

Electronic & Electrical Materials _ EC1419A

Total Marks:30 Duration:2hrs

Question 1 is compulsory and answer any two out of the remaining three.

Question 1.[15 points]

- i. I. What are the MKS units of mass, velocity (v), acceleration (a), force, momentum (p), energy ? **Answer: Kg, m/s, m/s², Newton, Kg-m-s⁻¹, Joules.[1/12+1/12+1/12+1/12+1/12+1/12=1/2Point]**

- i. II. $E = E_0 \exp[j(\omega t - kz)]$ _ This is an equation of a forward travelling wave. Define ω , t, k and z. What is the velocity of propagation ? **Answer: ω =radians/s, t=second, $k=1/m$, z = direction of propagation. Velocity of propagation= ω/k (m/s).[1/10+1/10+1/10+1/10+1/10=1/2Point]**

- i. III. $\psi = \psi_0 \exp[j(\omega t - kz)]$ _ This is also a travelling wave. What is ψ_0 and what is $|\psi^* \psi|$? **Answer: ψ_0 is Probability Amplitude, $|\psi^* \psi|$ is Probability Density.[1/4+1/4=1/2Point]**

- i. IV. $J = I\omega = n[h/(2\pi)]$. This is Bohr's Law of electrons orbiting the nucleus. Define all the terms. **Answer: J→angular momentum, I→moment of inertia, ω →orbital angular velocity, n→principal quantum number, h→ Planck's Constant.[1/10+1/10+1/10+1/10+1/10=1/2Point]**

- i. V. Define the four Quantum Numbers n , L, m, s ? **Answer: n →Principal Quantum Number, L→Azimuthal Quantum Number, m→magnetic Quantum Number, s→Spin Quantum Number.[1/8+1/8+1/8+1/8=1/2Point]**

- i. VI. What is COORDINATION NUMBER=N. Si, Ge have DIAMOND Crystal Structure and GaAs is ZINC-BLENDE Crystal Structure. In both crystal structures N = 8. Justify this statement ? **Answer: N→number of atoms belonging to each Unit Cell of the crystal structure. In Diamond structure there are (8corner atoms)×(1/8)+(6 face centered atoms)×(1/2)+(4 body centered atoms)= 8 atoms per unit cell.[1/8+3/8=1/2Point]**

¹This content is available online at <<http://cnx.org/content/m49733/1.1/>>.

- i. VII. Number density = $N^* = 8/a^3$. What is 'a' ? **Answer : 'a' is the Lattice Parameter.[1/2Point]**
- i. VIII. For Si,Ge and GaAs 'a' = 5.43Å , 5.646Å and 5.6533Å respectively. What is Å ? **Answer: Å is Angstrom =10-10m = 10-8cm .[1/2 Point]**
- i. VIV. Weight of one _____ = (AW gm/mole) ÷ (N_{Avo} atoms/mole). Fill up the BLANK . **Answer: ATOM [1/2 Point]**
- i. X. Wt of one atom × N* = ρ . Define the terms ? **Answer: N*→number density, ρ→weight density.[1/4+1/4=1/2Point]**
- i. XI. In HYDROGEN ATOM, electron occupies discrete energy states given by $E = -13.6/n^2$. What is the unit of energy and what is 'n' ? **Answer: Unit of energy is eV and n→Principal Quantum Number.[1/4+1/4=1/2Point]**
- i. XII. Hydrogen Atoms produce Lyman Series[2→1,3→1,4→1,5→1,6→1], Balmer Series[3→2,4→2,5→2,6→2,7→2] and Paschen Series [4→3,5→3,6→3,7 →3,8 →3] of Spectral lines. What do the square bracket terms mean? **Answer : Square Bracket terms imply transition from Excited States to Ground States.[1/2Point]**
- i. XIII. FCC has 74% parameter and BCC 68% parameter. What is this parameter and what is the full form of FCC and BCC? **Answer: FCC is Face-Centered-Cube and its packing density is 74% and BCC is Body-Centered-Cube and its packing density is 68%. [1/6+1/6+1/6=1/2Point]**

α	Type	Orientation
45°	N	<111>
90°	P	<100>
180°	N	<100>
0°	P	<111>

Table 20.1

- i. XIV. What does the above Table refer to ? Describe the meaning of the terms entered in the boxes ? **Answer: The angle between the Primary Flat of the Si Wafer and the Secondary Flat of the Si Wafer is 'α'. Type tells if Si-Wafer is N-Type or P-Type. Orientation gives the cleavage plane Orientation in Miller Indices.[1/6+1/6+1/6=1/2Point]**

$$n = \int_0^{X_0} N(E)P(E)dE = \left(\frac{8\pi}{3}\right) \left(\frac{2m^*}{h^2}\right)^{3/2} X_0$$

Figure 20.1

XV. What do the different terms refer to in the above Integral Equation? **Answer:** $N(E)$ = density of states per unit volume per unit energy, $P(E)$ → Fermi-Dirac Statistics or the probability of occupancy at energy E by Fermions. dE → elemental energy, m^* → effective mass of electron in the conduction band. X_0 → Fermi Level in Metal with respect to the bottom edge of the Conduction Band i.e. $X_0 = E_F - E_C$. [1/10+1/10+1/10+1/10+1/10=1/2 Points]

XVI.

$$X_0 = \left(\frac{3n}{8\pi}\right)^{\frac{2}{3}} \left(\frac{2m^*}{h^2}\right)$$

Figure 20.2

In the adjacent equation and in Question XV, X_0 is the same parameter. What is this parameter. **Answer:** $X_0 = E_F - E_C$. [1/2 Point]

XVII.

$$E_g(?) = \frac{1.24}{\lambda(?)} ;$$

Figure 20.3

What are the different parameters and what are their units ? **Answer:** E_g is Band-Gap in eV and λ is the wavelength of the photon emitted accompanying the radiative transition from Conduction Band to the Valence Band. [1/4+1/4=1/2]

XVIII. Define the parameters and give the units ?

Semiconductor	E_g	n_i	ϵ_r (DC)	?	ρ_i (300K)	N_C	N_V
Si	1.12	1×10^{10}	11.7	$5 \times 10^{22}/cc$	3.2×10^5	$3.2 \times 10^{19}/cc$	$1.8 \times 10^{19}/cc$
Ge	0.67	2×10^{13}	16.2	$4.4 \times 10^{22}/cc$	48	$1 \times 10^{19}/cc$	$5 \times 10^{18}/cc$
GaAs	1.424	2.1×10^6	12.9	$4.42 \times 10^{22}/cc$	3.3×10^8	$4.7 \times 10^{17}/cc$	$7 \times 10^{18}/cc$

Table 20.2

Answers: E_g (eV) , n_i (#/cc), ϵ_r (DC) rel. permittivity (Dimensionless), #density of atoms in the crystal , ρ_i (300K) Intrinsic Resistivity in Ω -cm, N_C Effective Density of States at EC, N_V Effective Density of States at EV [1/14+1/14+1/14+1/14+1/14+1/14+1/14=1/7]

XIX.

$$v_{drift} = \mu E \text{ where } \mu = \frac{q\tau_{scattering}}{m_e^*}$$

Figure 20.4

Element	E_F	τ (femtosec)	L(Angstrom)	W_F	$v_e^1(\times 10^5 \text{ m/s})$
Li	4.7	9	90		9.96
Na	3.1	31	250	2.3	8.08
K	2.1	44	293	2.2	6.55
Cu	7.0	27	328		12.15
Ag	5.5	41	441.6		10.77
Ge	$E_V + E_G/2$	2217	2106		1.16
Si	$E_V + E_G/2$	767.6	729		1.16
GaAs	$E_V + E_G/2$	4890	4645.5		1.16

Table 20.4

1. This velocity can be thermal velocity or Pauli Velocity.

Answers: Conducting electron is strongly scattering in metallic crystalline lattice but very weakly scattering in Semiconductor as exhibited by short Mean Free Path in metals and by long Mean Free Paths in Semi-conductors.[1/4+1/4=1/2]

XXV. In the Table given in Question XIV which is Pauli Velocity and which is Thermal Velocity?

Answers: Conducting Electron velocities in Metals are Pauli velocities because they arise out of Pauli-Exclusion Principle whereas conducting electron velocities in Semi-conductor are thermal velocities.[1/4+1/4=1/2]

XXVI. In Question XVIII, intrinsic Ge has the least resistivity and intrinsic GaAs has the maximum , Why? **Answers; Ge has the least Band-Gap and GaAs has the widest Band-Gap.[1/4+1/4=1/2]**
XXVII.

$$P(E) = \frac{1}{1 + \exp\left(\frac{E - E_F}{kT}\right)}$$

Figure 20.7

This is what statistics and does it tell. At T= 0 Kelvin what kind of distribution is it? **Answers: This is Fermi-Dirac Statistics, P(E) gives the probability of occupancy of E by Fermions, and Absolute Zero the distribution is RECTANGULAR.[1/6+1/6+1/6=1/2 Points]**

XXVIII.

$$N(E) = 4\pi \left(\frac{2m^*}{\hbar^2}\right)^{3/2} (E - E_C)^{1/2}$$

Figure 20.8

What is this expression ? Define all the terms. **Answers: N(E)→Density of States per unit energy, (E-EC) →kinetic energy of conducting electron in conduction band.[1/4+1/4=1/2]**

XXIX. If Ultra-Violet light of $\lambda = 0.2\mu\text{m}$ is incident on a metal then which of the metals listed in the Table below will respond and emit electrons ? **Answers;UV photon has 6.2eV hence it is powerful enough to cause photo-emission in all the Metals listed in the Table below.All the metals have a work-function less than 6.2eV.[1/2 Point]**

Metal	Work-function	Metal	Work-function
Na	2.3eV	Ca	3.2eV
K	2.2eV	Ba	2.5eV
Cs	1.8eV	Pt	5.3eV
W	4.5eV	Ta	4.2eV

Table 20.5

XXX.

$$n_p^{\wedge} = n_{po}^{\wedge} \text{Exp} \left[-\frac{t}{\tau_n} \right]. \text{What is this expression? Define the terms.}$$

Figure 20.9

Answers: This expression tells how EXCESS CARRIERS decay with respect to time in Semiconductors with excess carrier life-time or excess carrier relaxation time defined as τ_n . Excess carriers exponentially decay with time. If relaxation time is long then excess carriers transient takes a long time to decay.[1/2 points]

Question 2. Describe the step for preparing Electronic Grade Poly-crystal Silicon from sand.

[7.5 marks]

Answer:

Reduction of sand with carbon gives impure polycrystalline Silicon

↓

Reaction of pulverized raw silicon with HCl gaseous vapour to form TriChloroSilane

↓

Multiple distillation of TriChloroSilane to obtain purified electronic grade TriChloroSilane

↓

Thermal decomposition of SiHCl_3 at 1000 degree centigrade in Sieman's reactor to obtain fattened rods of electronic grade Silicon

Question 3. Balmer Series Spectral Lines from Stars are determined to be at 6563\AA , 4862\AA , 4341\AA , 4102\AA and 3970\AA . Determine these spectral lines theoretically.

[By the Red-Shift of these Balmer Spectral Lines the velocity of the receding Galaxy is determined. The recession velocity gives the distance of the Galaxy using Hubble's relationship][7.5 marks]

Answer: $\lambda(\mu\text{m}) = 1.24/E_g(\text{eV})$ here $E_g = (13.6\text{eV}/4 - 13.6/n^2)\text{eV}$. Since the answer is to be obtained in Angstrom therefore the final expression is:

Therefore $\lambda(\text{Angstrom}) = (1.24 / (13.6/4 - 13.6/n^2)) \times 10^4$ Angstrom.

For $n=3$ to $n=2$, $\lambda=6564.71\text{\AA}$;

For $n=5$ to $n=2$, $\lambda=4862.75\text{\AA}$;

For $n=6$ to $n=2$, $\lambda=4341.74\text{\AA}$;

For $n=7$ to $n=2$, $\lambda=4102.94\text{\AA}$;

For $n=8$ to $n=2$, $\lambda=3971.24\text{\AA}$;

Question 4. Determine the temperature at which $E = E_F + kT$ will be occupied by electron with $P(E) = 1\%$. [7.5 marks]

Answer

This question is wrongly stated. At $E = E_F + kT$ the Probability of occupancy is $1/(1+e) = 0.2689$. It can be never 1% irrespective of temperature.

The correct question is: Determine $P(E_F + kT)$ in Fermi-Dirac Statistics. Determine Temperature T at which $P(E_F + 0.5\text{eV}) = 1\%$. [Answers: 0.27, 1262 Kelvin]

You can give either of the answers and fetch full marks.

Chapter 21

Chapter 5. Section 5.6. Metamaterials.¹

Chapter 5. Section 5.6. Metamaterials.

Meta material science is a multidiscipline enterprise which includes applied physics, engineering, material science and nano technology. It aims at designing materials with physical properties beyond those available in nature. In metamaterials we want go beyond the natural materials and fabricate metamaterials with undreamt of properties e.g. invisible cloak.

Metamaterial Science challenges and overcomes the currently held limitations offered by the classical physics. Careful engineering and mixing of meta-atoms has led to completely unconventional standards and yardsticks of classifying the materials.

Metamaterials derive their properties from the structure rather than their constituent components hence they are called super lattices.

For example Photonic Crystals derive their anomalous properties from higher order spatial modes whereas meta materials work with dominant propagation mode and with sub-wavelength spacing between neighboring elements. Macroscopic desired and tailor made properties can be obtained by applying several mixing rates and homogenization principles.

Section 5.6.1. Diffraction Limit of Abbe and its conquest by Xu et.al. Metamaterial Superlens 1

[1. Xu, T.; Agarwal.A.; Abashin, M; Chau, K.J.; Lezec, H.J. “All-angle negative refraction and active flat lensing of Ultra-Violet Light”, *Nature*, **497**, #7450, pp. 470-474 (2013)]

Ernest Abbe(1840-1905) a top Physicist and the CEO of Carl Zeiss Lns Company, had set the resolution of a microscope as follows:

$$2\Delta y(\text{minimum feature size}) = \frac{k \cdot \lambda}{n \sin \alpha} \quad \text{where } \lambda = \text{wavelength of the image light, } n$$

= refractive index of the space in which the image is formed, k = resolution factor, α
= acceptance angle of the lens system 5.6.1.

Figure 21.1

According to this Formula, the wavelength of the light and Numerical Aperture = $n \sin \alpha$ set the resolution limit.

¹This content is available online at <<http://cnx.org/content/m49939/1.1/>>.

Finer feature sizes can be resolved if wavelength is shorter and n (refractive index) is higher.

Present generation of ICs with 40nm node are using Deep Ultra Violet Light with wavelength 193nm and pure water immersion system to achieve the node size of 40nm.

Future Generation IC Lithography is going to use Extreme UV of $\lambda = 100\text{nm}$ with immersion technique.

In 2000 J. B. Pendry made a proposal of synthesizing Negative Refraction Index Meta material which could be used as super lens for perfect lensing to any feature size. [“Negative Refractive Makes a Perfect Lens”, *Physical Review Letter*, **85**, #18, 39th October 2000].

They suggested that electron cloud in a dielectric behaves like a plasma and it has the following dielectric theoretical formulation:

$$\varepsilon = 1 - \frac{\omega_{ep}^2}{\omega^2} \quad \text{here } \omega_{ep} = \text{electronic plasma resonance} \quad 5.6.2.$$

Figure 21.2

When $\omega < \omega_{ep}$ the we have ε is negative.

Similarly we can have loops of conducting wire mimicking magnetic plasma. It will have the following formulation:

$$\mu = 1 - \frac{\omega_{mp}^2}{\omega^2} \quad \text{here } \omega_{mp} = \text{magnetic plasma resonance} \quad 5.6.3.$$

Figure 21.3

When $\omega < \omega_{mp}$ the we have μ is negative.

Xu et al using Ag and TiO_2 layers on glass substrate synthesized negative refraction lens.

Here both $\varepsilon = -1$ and $\mu = -1$.

This results in $n = \pm\sqrt{(\mu\varepsilon)}$. When $\varepsilon = -1$ and $\mu = -1$ then $n = -\sqrt{(\mu\varepsilon)}$

Here the characteristic impedance $Z = \sqrt{(\mu/\varepsilon)} = Z_0 =$ free space characteristic impedance.

Therefore at the interface of the lens there is no reflection and transmission is 100%.

Also it is taken flat with a thickness ‘d’.

The negative refraction index restores the phase of the propagating waves and also the amplitude of the evanescent waves. The device focuses light tuned to the surface plasma frequency of silver and is limited only by the resistive losses. Here both propagation wave and evanescent waves contribute to the perfect resolution of any feature size dimension. Therefore there is no physical obstacle to perfect reconstruction of the image beyond practical limitations of aperture and the lens surface.

The field of meta materials which is emerging shows us how to engineer the refraction of light through metallic composites with nano scale structure so that we get perfect lensing with no diffraction limit as given by (5.6.1).

Section 5.6.2. The diverse field of Metamaterials.

In their short history, metamaterials have been applied to the most diverse areas, including invisibility cloaks, artificial optical black holes, cosmology, high-temperature

superconductors, just to name a few particularly fascinating examples.

It has been used to fabricate Super lens described above.

It has been used in Automotive Industry.

It has been used in THz Time Domain applications.

It has been used in Spectrometers.

It has been used invisibility Cloaks.

In 2002, Lucent Technologies has developed Resonant Antennas.

In 2003, MIT utilized photonic crystals for making metamaterials.

Boeing Company has developed the method for fabricating electromagnetic materials.

In 2004, Lucent Technologies has fabricated Miniature antennae based on negative permittivities.

Boeing Company has developed Metamaterial scanning lens antenna system and methods.

Chapter 22

Chapter 7. Magnetic Materials.¹

Chapter 7. Magnetic Materials.

[All the FIGURES are at the end of the Chapter]

HISTORY: The most popular legend accounting for the discovery of magnets is that of an elderly Cretan shepherd named Magnes. Legend has it that Magnes was herding his sheep in an area of Northern Greece called Magnesia, about 4,000 years ago. Suddenly both, the nails in his shoes and the metal tip of his staff became firmly stuck to the large, black rock on which he was standing. To find the source of attraction he dug up the Earth to find lodestones (load = lead or attract). Lodestones contain magnetite, a natural magnetic material Fe_3O_4 . This type of rock was subsequently named magnetite, after either Magnesia or Magnes himself.

Earliest discovery: The earliest discovery of the properties of lodestone was either by the Greeks or Chinese. Stories of magnetism date back to the first century B.C in the writings of Lucretius and Pliny the Elder (23-79 AD Roman). Pliny wrote of a hill near the river Indus that was made entirely of a stone that attracted iron. He mentioned the magical powers of magnetite in his writings. For many years following its discovery, magnetite was surrounded in superstition and was considered to possess magical powers, such as the ability to heal the sick, frighten away evil spirits and attract and dissolve ships made of iron!

The first paper on Magnetism: Peregrinus & Gilbert Peter Peregrinus is credited with the first attempt to separate fact from superstition in 1269. Peregrinus wrote a letter describing everything that was known, at that time, about magnetite. It is said that he did this while standing guard outside the walls of Lucera which was under siege. While people were starving to death inside the walls, Peter Peregrinus was outside writing one of the first 'scientific' reports and one that was to have a vast impact on the world.

Earth is a huge Magnet: However, significant progress was made only with the experiments of William Gilbert in 1600 in the understanding of magnetism. It was Gilbert who first realized that the Earth was a giant magnet and that magnets could be made by beating wrought iron. He also discovered that heating resulted in the loss of induced magnetism.

Interrelationship between Electricity and Magnetism: In 1820 Hans Christian Oersted (1777-1851 Danish) demonstrated that magnetism was related to electricity by bringing a wire carrying an electric current close to a magnetic compass which caused a deflection of the compass needle. It is now known that whenever current flows there will be an associated magnetic field in the surrounding space, or more generally that the movement of any charged particle will produce a magnetic field.

Birth of Electromagnetic Field: Eventually it was James Clerk Maxwell (1831-1879 Scottish) who established beyond doubt the inter-relationships between electricity and magnetism and promulgated a series of deceptively simple equations that are the basis of electromagnetic theory today. What is more remarkable is that Maxwell developed his ideas in 1862 more than thirty years before J. Thomson discovered the electron in 1897, the particle that is so fundamental to the current understanding of both electricity and magnetism.

The term magnetism was thus coined to explain the phenomenon whereby lodestones attracted iron.

¹This content is available online at <<http://cnx.org/content/m49953/1.1/>>.

Today, after hundreds of years of research we not only know the attractive and repulsive nature of magnets, but also understand MIR scans in the field of medicine, computers chips, television and telephones in electronics and even that certain birds, butterflies and other insects have a magnetic sense of direction.

7.1. Magnetic Circuit – an analog of Electric Circuit.

Just as in an electric circuit , voltage (V) drives current (A) through the electrical circuit resistance R where R is:

$$R = \frac{\rho L}{A} \text{ where } \rho \text{ is resistivity } \Omega - \text{cm}, L \text{ is length of the circuit in cm and } A \text{ is the cross} \\ \text{– sectional area in cm}^2 \text{ and } I(\text{Amp}) = \frac{V(\text{Volts})}{R(\text{ohms})} \quad 7.1.$$

Figure 22.1

In an analogous fashion, transformer's core is a magnetic circuit where Magneto-Motive Force in Amp-Turns(AT) drives magnetic flux in Weber overcoming the reluctance of the magnetic core where Reluctance is defined as follows:

$$R(\text{reluctance}) = \frac{L}{\mu A} \text{ where } \mu = \text{Permeability} \left(\frac{H}{m} \right) \\ = \mu_r \mu_0, A \text{ is the cross} \\ \text{– sectional area of the magnetic path which in this case is the cross} \\ \text{– sectional area of the transformer core and } L \text{ is the Length of the magnetic path and}$$

Figure 22.2

$$\Phi_M (\text{magnetic flux in Weber}) = \frac{MMF(AT)}{R} \quad 7.2.$$

Figure 22.3

7.2. Ampere's circuital Law:

Andre Maria Ampere (1775-1836) gave the Ampere Circuital Law.

In the simplest form it is stated as:

$$H. 2\pi r = I(\text{current enclosed by the circumference of the circle}) \quad 7.3.$$

Figure 22.4

James Clerk Maxwell (1831-1879) stated it as follows:

$$\nabla \times B = \mu J(\text{electronic current}) + \frac{\delta D}{\delta t} (\text{Displacement current}) \quad 7.4.$$

Figure 22.5

(7.4) is Differential Form. In Integral form it is as follows:

$$\oint B \cdot dl = \mu I (\text{total electronic Current enclosed within the line integral path}) +$$

Figure 22.6

$$\frac{\delta D}{\delta t} \times A(\text{total area enclosed within the line integral path}) \quad 7.5.$$

Figure 22.7

7.3. Faraday's Law of electro-magnetic induction.

Whenever the magnetic flux linked with a closed conducting coil changes, an e.m.f. is induced which causes an eddy current to flow through the coil. The direction of eddy current is such as to create a magnetic polarity which opposes the cause of electro-magnetic induction.

If a North Pole approaches the closed coil then eddy current will make the near face of the coil North Pole so that the approaching Pole is opposed and if North Pole is receding then near face will act as South Pole so as to attract the receding Pole.

Mathematically it is:

$$\begin{aligned}
 \text{e.m.f. (induced electro - motive force)} &= -N \frac{d\Phi_M}{dt} \\
 &= -(\text{rate of change of total magnetic flux linkage})
 \end{aligned}
 \tag{7.6}$$

Figure 22.8

Maxwell stated it as follows:

$$\nabla \times E = -\frac{dB}{dt} \tag{7.7}$$

Figure 22.9

(7.7) in integral form is as follows:

$$\oint E dl = -\frac{d\Phi_M}{dt} \tag{7.8}$$

Figure 22.10

7.4. Lorentz Force and Left Hand Rule.

A current in the magnetic field, held transverse to the magnetic field, will experience a mechanical force in the third perpendicular direction. This mechanical force is known as Lorentz Force.

Complete statement of Lorentz Force is as follows:

$$F(\text{Newtons}) = q(E + v \times B) \tag{7.9}$$

Figure 22.11

The first part on R.H.S. is the electro-static force and second is the magneto-static force on a moving electron. J.J. Thomson used this equation to determine q/m of an electron in Cathode Ray Experiment. He balanced the electric force and magnetic force and obtained zero deflection of the electron beam on the CRO screen.

A line of current I Amperes of length L (m) is held in Magnetic Field of B Tesla where I and B are transverse to each other then there is a force f (newtons) acting on the line of current along the third perpendicular direction. If Current is in the direction of Middle finger and Magnetic Field is in the direction of index finger then the Lorentz force is in the direction of the Thumb as shown in Figure 7.2.

This force F (Newtons) = $B \cdot I \cdot L$ It is this force which causes an armature of a motor to rotate.

Two parallel lines carrying I amperes each will experience a magneto-static force of attraction if the current flows are in the same direction and experience a magneto-static repulsion force if they are in opposite direction.

Figure 22.12

7.5. Right Hand Palm Rule.

This rule lets us determine the polarity of a solenoid or a coil of current. If the fingers of right hand clasping the solenoid is in the direction of the current flow as shown in Figure 7.3. then magnetic flux line will be in the direction of the thumb.

North Pole of the Solenoid is the end from where magnetic flux lines come out. The end where they enter the solenoid is defined as South Pole.

7.6. Magnetic Materials.

The materials which are spontaneously magnetized or have a susceptibility to magnetization are referred to as magnetic materials. They are classified as:

i. Ferromagnetic- spontaneously magnetized and have strong, positive susceptibility to magnetization. Ferromagnetic material has been demonstrated in Figure 7.4. Up to a temperature known as Curie Temperature, in this case 1000K, spontaneous magnetization is maintained as shown in the upper part of the Figure but this self alignment of the dipoles gets disrupted due to thermal fluctuations above 1000K.

ii. Paramagnetic materials: these have no spontaneous magnetization and have weak, positive susceptibility to magnetization. As shown in Figure 7.5., there is no spontaneous magnetization but application of Magnetic Field does cause a weak magnetization.

iii. Diamagnetic materials: these have no spontaneous magnetization and they move away from a region of magnetic field and have a negative, weak susceptibility to magnetization. Diamagnetism is the property of an object which causes it to create a magnetic field² in opposition to an externally applied magnetic field, thus causing a repulsive effect. Specifically, an external magnetic field causes eddy currents in such a way that according to Lenz's law³, this opposes the external field. Diamagnets are materials with a magnetic relative permeability⁴ less than 1.

Consequently, diamagnetism is a form of magnetism⁵ that is only exhibited by a substance in the presence of an externally applied magnetic field. It is generally quite a weak effect in most materials, although superconductors⁶ exhibit a strong effect.

²http://www.wikipedia.org/wiki/Magnetic_field

³http://www.wikipedia.org/wiki/Lenz%27s_law

⁴http://www.wikipedia.org/wiki/Magnetic_permeability

⁵<http://www.wikipedia.org/wiki/Magnetism>

⁶<http://www.wikipedia.org/wiki/Superconductor>

Diamagnetic materials cause lines of magnetic flux⁷ to curve away from the material, and superconductors can exclude them completely (except for a very thin layer at the surface).

In Figure 7.6. a comparative study of diamagnetic and paramagnetic material has been made. In paramagnetic there are atomic magnetic dipoles but randomly arranged and application of magnetic field can align them to result in a weak magnetization. But in diamagnetic materials there are no atomic magnetic dipoles. These get induced by the application of external magnetic field but opposed to the external magnetic field in accordance with Lenz's Law.

In Figure 7.7. we show the magnetization curve with respect externally magnetic field.

In Figure 7.8, we show the temperature sensitivity of Ferromagnetic and paramagnetic materials.

$$B = \mu_0 H + \mu_0 M = \mu_0 H + \mu_0 \chi_M H = \mu H \quad \text{therefore } \mu = \mu_0 + \mu_0 \chi_M$$

Figure 22.13

Therefore

$$\frac{\mu}{\mu_0} = \mu_r (\text{relative permeability}) = 1 + \chi_M \quad 7.10$$

Figure 22.14

By rearranging the terms we get:

$$\chi_M = \mu_r - 1 \quad 7.11$$

Figure 22.15

In Table 7.1. the magnetic susceptibilities of paramagnetic and diamagnetic materials are given.

From Figure 7.8 it is evident Ferromagnets have high positive susceptibility right up to Curie Temperature. Only after Curie Temperature susceptibility drastically falls. Where as Paramagnetic material has a graded response. At very low temperatures susceptibility is high and it gradually falls with rise in temperature.

Section 7.6.1. Classifications of Ferromagnets.

Ferromagnets have further sub-classes namely Ferrimagnetic Materials and Anti-ferromagnetic Materials.

⁷http://www.wikipedia.org/wiki/Magnetic_flux

In Figure 7.9 Chromium BCC crystal's Unit Cell is shown. The Body central left directed dipole moment is negated by the right directed dipole moment of 8 corner atoms. This negation results into zero Magnetic Moment because each of the 8 corner atoms make 1/8 contribution to the Unit Cell.

Manganese Oxide is anti-ferromagnetic below Neel Temperature and above Neel Temperature it is Paramagnetic. In Figure 7.10, it is shown below Neel Temperature.

In 1986, high temperature Lanthanite Barium Copper Oxide $[\text{La}(2-x)\text{Ba}(x)\text{CuO}_4]$ were found to exhibit superconductivity at 30K shown in Figure 7.11. Yttrium Barium Copper Oxide ($\text{YBa}_2\text{Cu}_3\text{O}_6$) Superconductors were discovered which exhibited superconductivity at 90K warmer than liquid Nitrogen Temperature. In all these layered compounds it was found that CuO_2 planes had anti-ferromagnetic order. This led to a flurry of activities in CuO_2 based Ceramics for developing Room Temperature Superconductors. A detailed account of the quest for Room Temperature Superconductor is given in Chapter 8.

In Figure 7.12 the dipole alignments in Ferro, Ferri and Antiferro-magnetic materials are shown. Here T_C refers to Curie Temperature and T_N refers to Neel Temperature.

Curie Temperature refers to Ferromagnetic Materials only. Above Curie Temperature, Ferromagnetic Materials loses its spontaneous magnetization.

In Ferrimagnetic and Anti-Ferromagnetic materials below Neel Temperature, the materials retain their Ferrimagnetism or Antiferromagnetism as the case may be. But above Neel Temperature they become paramagnetic. Thermal fluctuations disturbs the order.

Table 7.2. gives the Neel Temperature and Curie Temperature for some important magnetic materials.

Table 7.2. Neel Temperature for some important Ferri and Anti-Ferromagnetic Materials and Curie Temperatures for Ferromagnetic Materials.

FERRI & ANTI-FERRO	NEEL TEMP.	FERRO	CURIE TEMP.
MnO	116K	Fe	1043K
Cr	308K	Co	1400K
MnTe	307K	Ni	631
CoO	291K	Gadolenium	292
NiO	525K	MnBi	630
		Fe ₂ O ₃	948
		FeOFe ₂ O ₃	858

Table 22.1

As is evident from the Table 7.14 , Fe, Co and Ni which are the transition elements and which have uncompensated spin electrons are strongly Ferromagnetic Materials

Section 7.6.2. Domains and Hysteresis.

Like Polycrystals or like Ferrielectric materials, in ferromagnetic and ferrimagnetic materials also there are domains of magnetization. Each domain has its own alignment direction and all dipoles in each domain are aligned but the direction of alignment changes from domain to domain as shown in Figure 7.15.

As we move from one domain to another, orientation of the dipoles only gradually change. Thus there is no abrupt changes across the domain walls as shown in Figure 7.16.

When external magnetic field is applied, favourable domains grow at the expense of unfavourable domains as shown in Figure 7.17. Finally at high fields a domain aligned with external field remains. This is an exact analog of the electric poling of Ferro-electric material.

Figure 7.18 gives B-H curve of a ferro-magnet. Red is the Hysteresis Loop. Blue is the initial magnetization. B_r is the remnance Magnetic Flux Density at $H=0$. H_C is the coercive magnetic field required to completely demagnetize the material.

As is evident from figure 7.19 induced magnetization is perfectly linear in paramagnetic and in diamagnetic materials but is non-linear in ferro/ferromagnetic materials. Hence latter has a hysteresis loop.

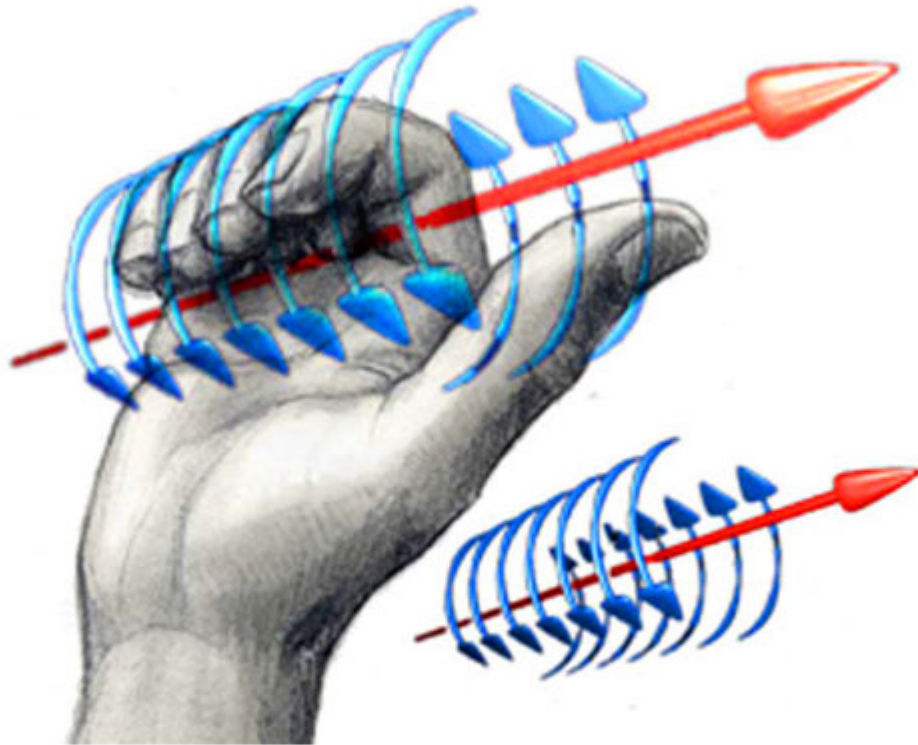


Figure 7.3. Right Hand Palm Rule. Right hand fingers clasp the solenoid in the direction of the current flow and right thumb indicates the direction of magnetic flux.

Figure 22.16

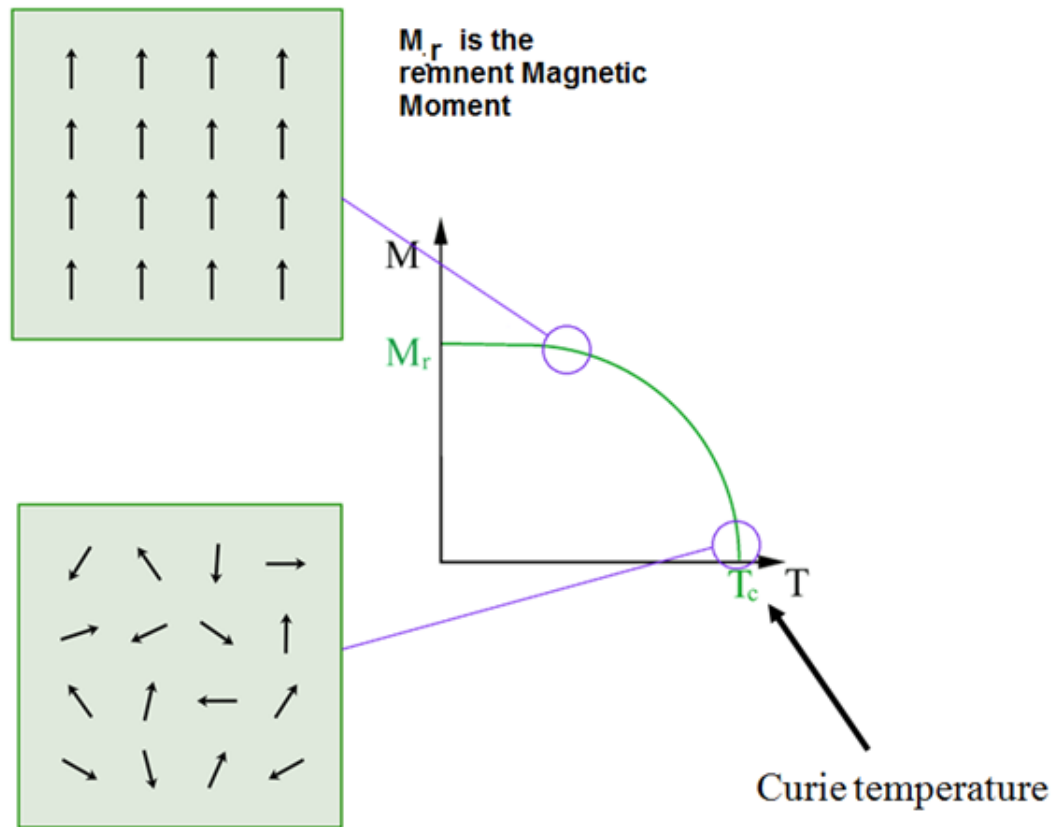


Figure 7.4 In Ferromagnetic materials dipole moments are aligned upto 1000K. Only above Curie Temperature that alignment get disrupted.

Figure 22.17

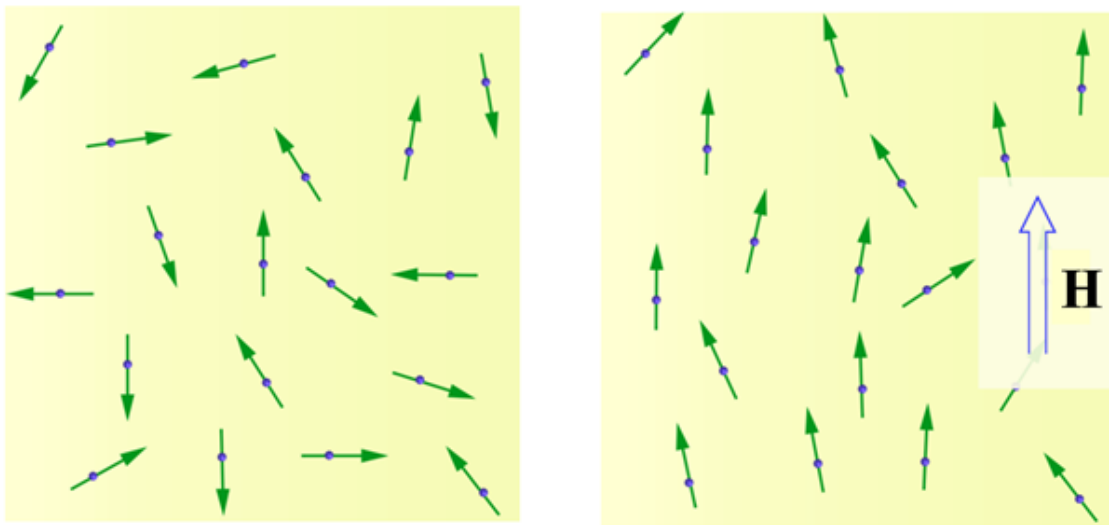


Figure 7.5. In paramagnetic materials an external field has to be applied to generate a small magnetic field at Room Temperature. Room Temperature does not allow alignment of dipole moments.

Figure 22.18

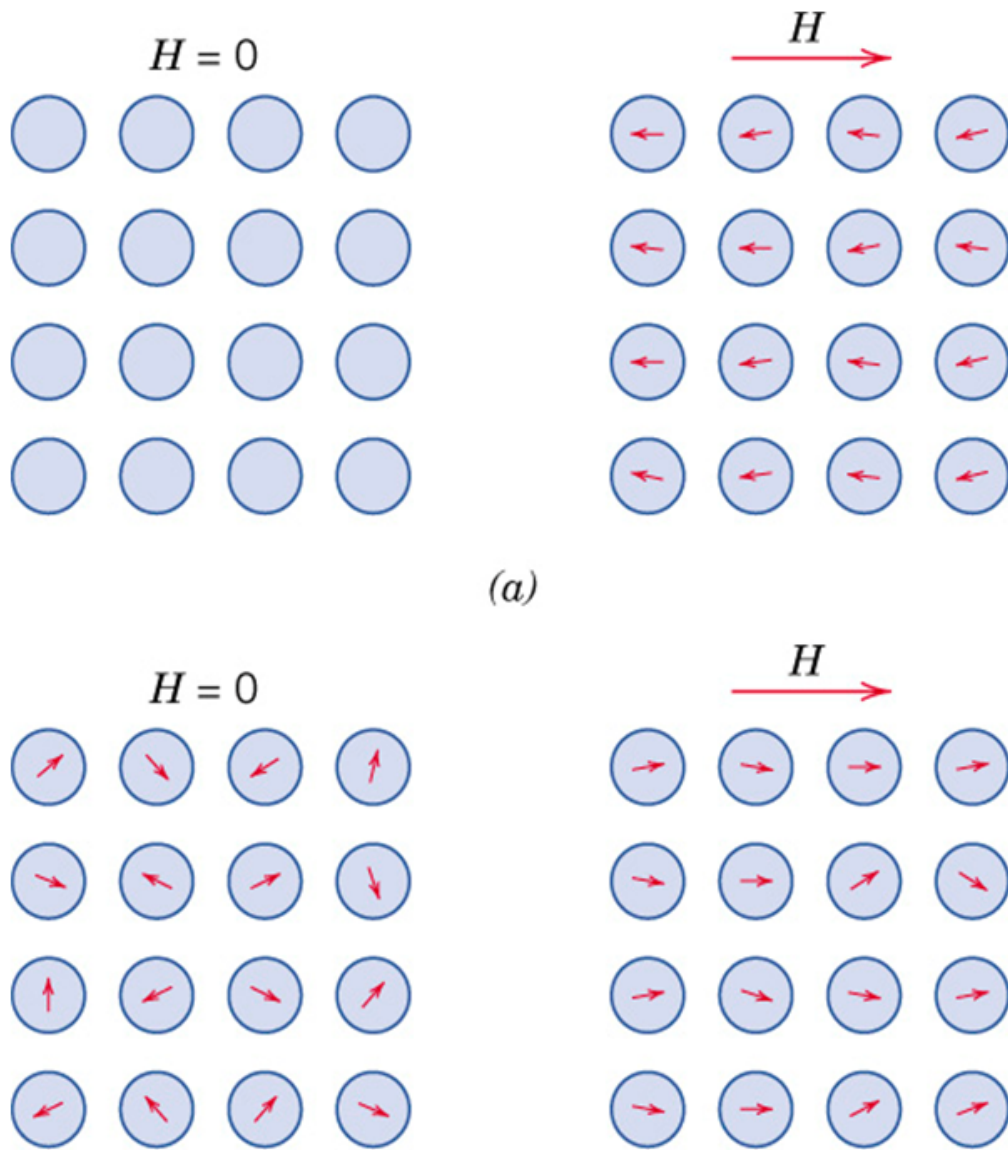


Figure 7.6. Comparative study of Diamagnetic and Paramagnetic materials

Figure 22.19

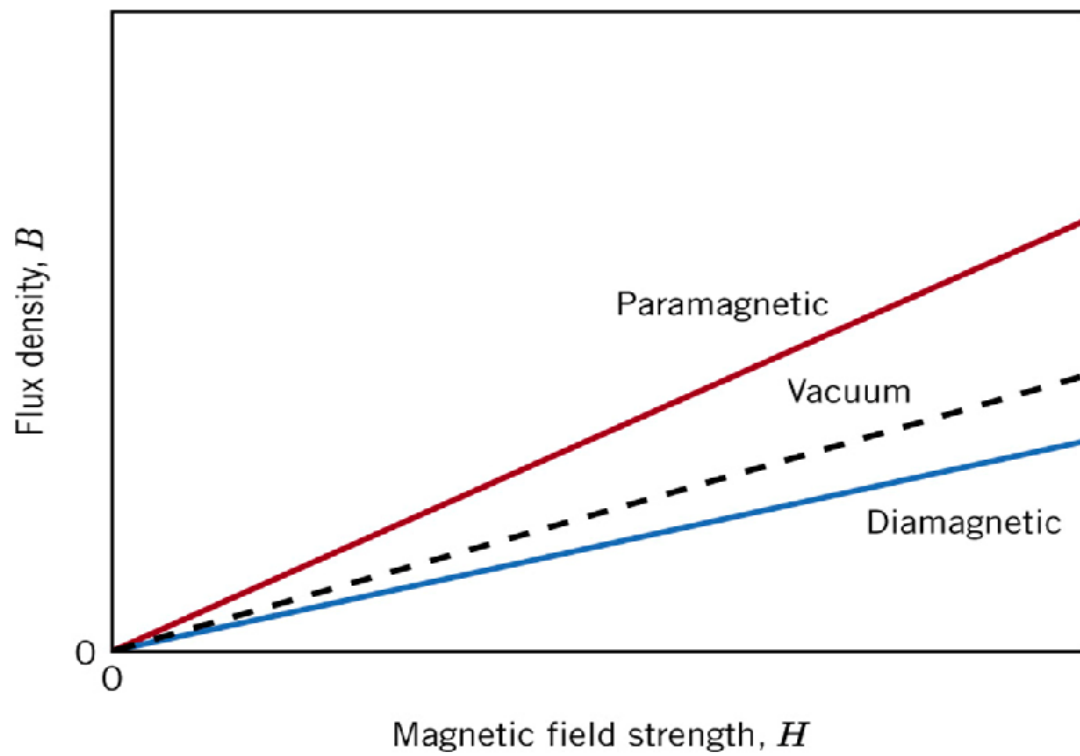


Figure 7.7. Linear Magnetization Curves for Paramagnetic Materials (rel. permeability >1), Vacuum (rel. permeability = 1) and diamagnetic Materials (rel. permeability <1).

Figure 22.20

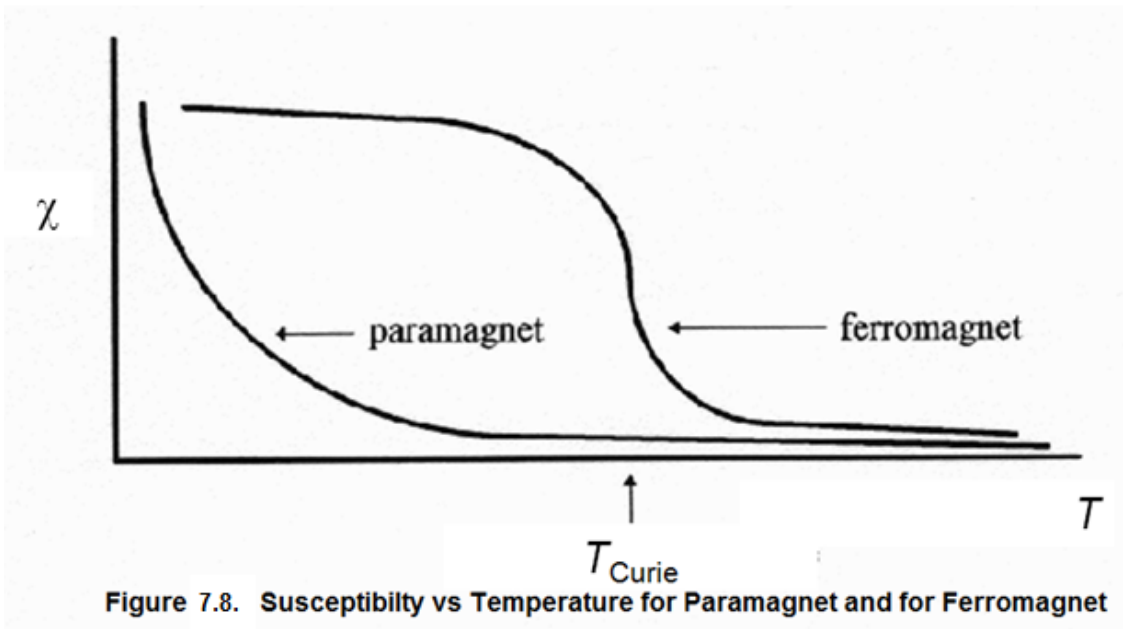


Figure 22.21

Table 7.1 Room-Temperature Magnetic Susceptibilities for Diamagnetic and Paramagnetic Materials

<i>Diamagnetics</i>		<i>Paramagnetics</i>	
<i>Material</i>	<i>Susceptibility</i> χ_m (volume) (SI units)	<i>Material</i>	<i>Susceptibility</i> χ_m (volume) (SI units)
Aluminum oxide	-1.81×10^{-5}	Aluminum	2.07×10^{-5}
Copper	-0.96×10^{-5}	Chromium	3.13×10^{-4}
Gold	-3.44×10^{-5}	Chromium chloride	1.51×10^{-3}
Mercury	-2.85×10^{-5}	Manganese sulfate	3.70×10^{-3}
Silicon	-0.41×10^{-5}	Molybdenum	1.19×10^{-4}
Silver	-2.38×10^{-5}	Sodium	8.48×10^{-6}
Sodium chloride	-1.41×10^{-5}	Titanium	1.81×10^{-4}
Zinc	-1.56×10^{-5}	Zirconium	1.09×10^{-4}

Figure 22.22

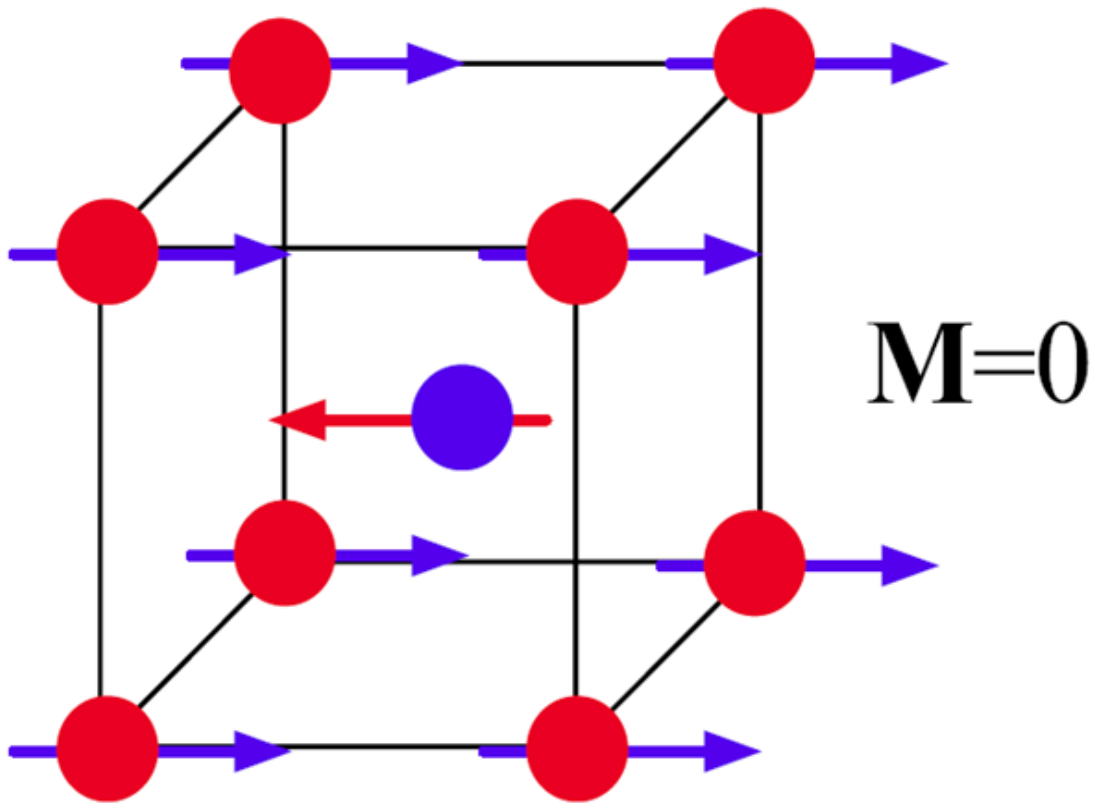


Figure 7.9. Anti-Ferrpmagnetic Material.

Figure 22.23

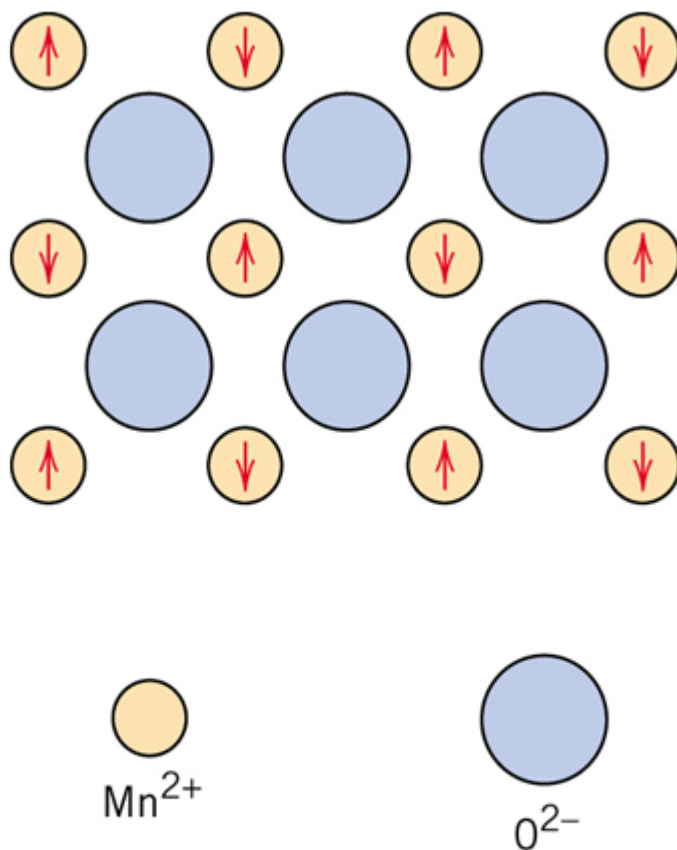


Figure 7.10. Anti parallel alignment of spin magnetic moments for Manganese Oxide (MnO). At low temperature, it is anti-ferromagnetic but above Neel Temperature it becomes paramagnetic.

Figure 22.24

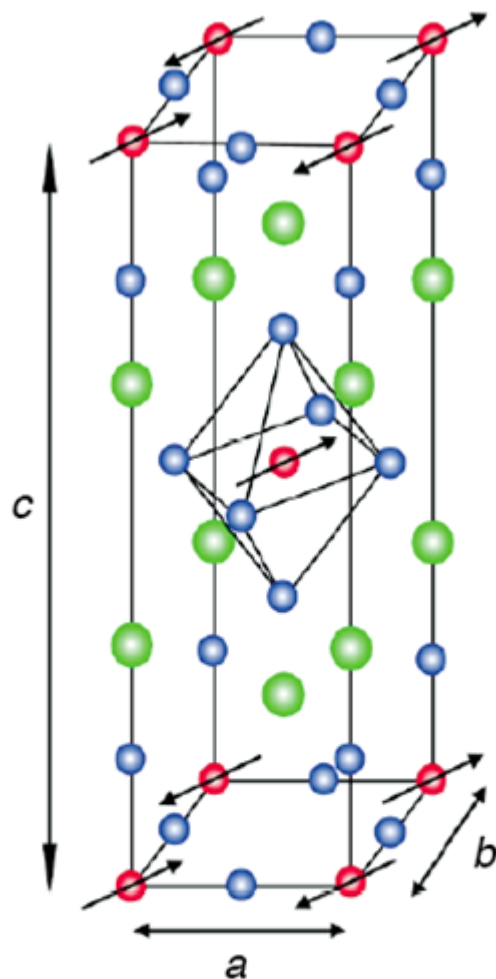


Figure 7.11. Crystal structure of La_2CuO_4 . The CuO_2 planes exhibit anti-ferromagnetic order. Red balls are $\text{Cu}(2+)$ Blue balls are $\text{O}(2-)$ Green balls are $\text{La}(3+)$.

Figure 22.25

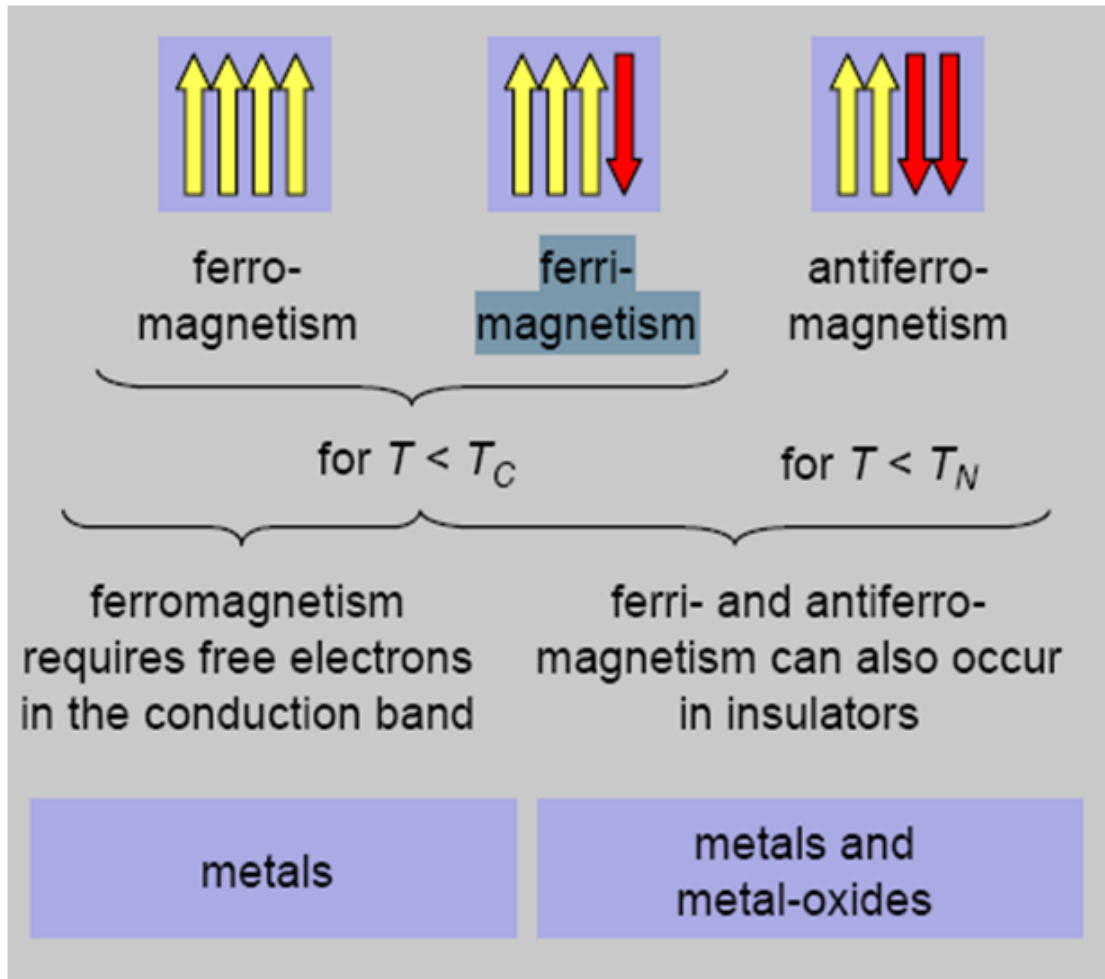


Figure 7.12. Illustration of magnetic dipole alignments in Ferromagnetic materials, in Ferrimagnetic materials and antiferromagnetic materials.

Figure 22.26

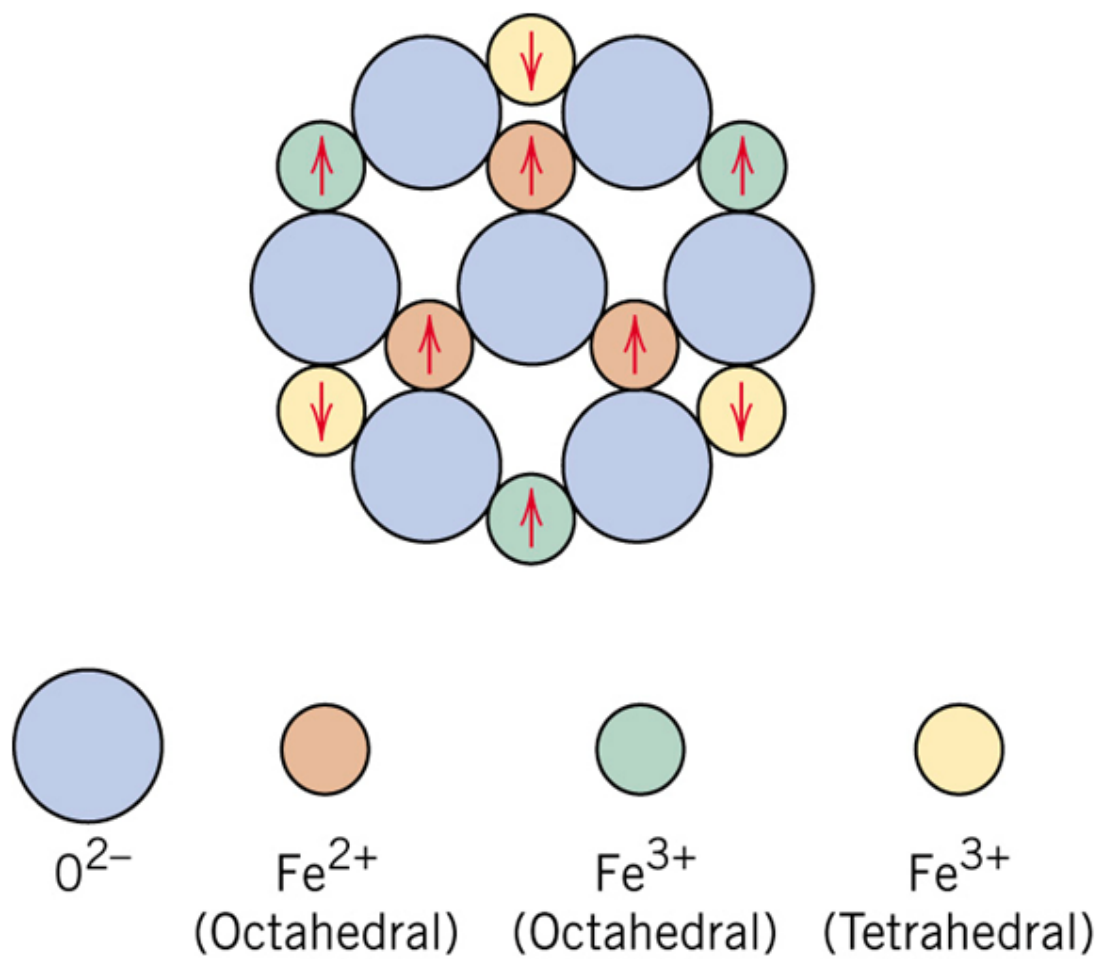


Figure 7.13. Introduction of Magnetic Ions transforms a pure Ferromagnetic into Ferrimagnetic material. Above Curie Temperature it becomes Paramagnetic.

Figure 22.27

magnetic susceptibility χ_m

1	2	3	4	5	6	7	8	9	10	11	12	13	14	15	16	17	18
H (-2,5)	all values given for a temperature of 300 K in case of ferromagnetic materials: saturation polarization																He (-1,1)
Li 24	Be -23											B -19	C -22	N (-6,3)	O 7,9	F	Ne (-4,0)
Na 8,1	Mg 5,7											Al 21	Si -3,4	P -23	S -12	Cl (-22)	Ar (-11)
K 5,7	Ca 21	Sc 264	Ti 181	V 383	Cr 267	Mn 828	Fe 2,16	Co 1,76	Ni 0,61	Cu -9,7	Zn -12	Ga -23	Ge -7,3	As -5,4	Se -18	Br -16	Kr (-16)
Rb 4,4	Sr 36	Y 122	Zr 109	Nb 236	Mo 119	Tc 373	Ru 66	Rh 170	Pd 783	Ag -25	Cd -19	In -8,2	Sn 2,4	Sb -67	Te -24	I -22	Xe (-24)
Cs 5,3	Ba 6,7	La 63	Hf 71	Ta 175	W 78	Re 96	Os 15	Ir 37	Pt 264	Au -34	Hg -28	Tl -36	Pb -16	Bi -153	Po	At	Rn

diamagnetic
paramagnetic
ferromagnetic
numbers without (): $\cdot 10^{-6}$
numbers with (): $\cdot 10^{-9}$

Table-Figure 7.14. Magnetic Properties are determined by the position of the Element in the Periodic Table.

Figure 22.28

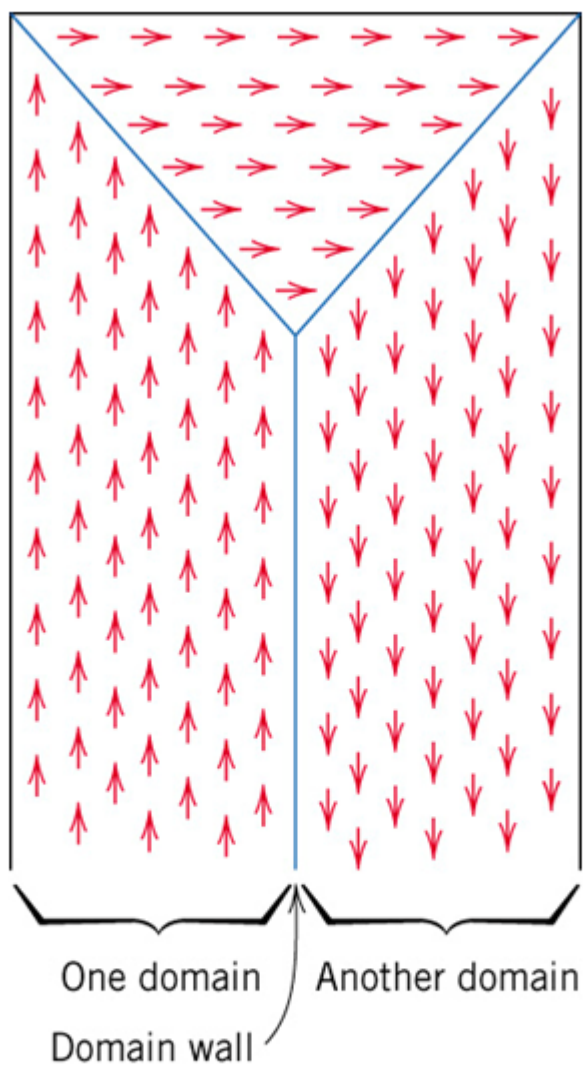


Figure 7.15. Domains in Ferromagnetic/Ferrimagnetic materials. Within each domain all the dipoles are aligned but direction of alignment changes from domain to domain.

Figure 22.29

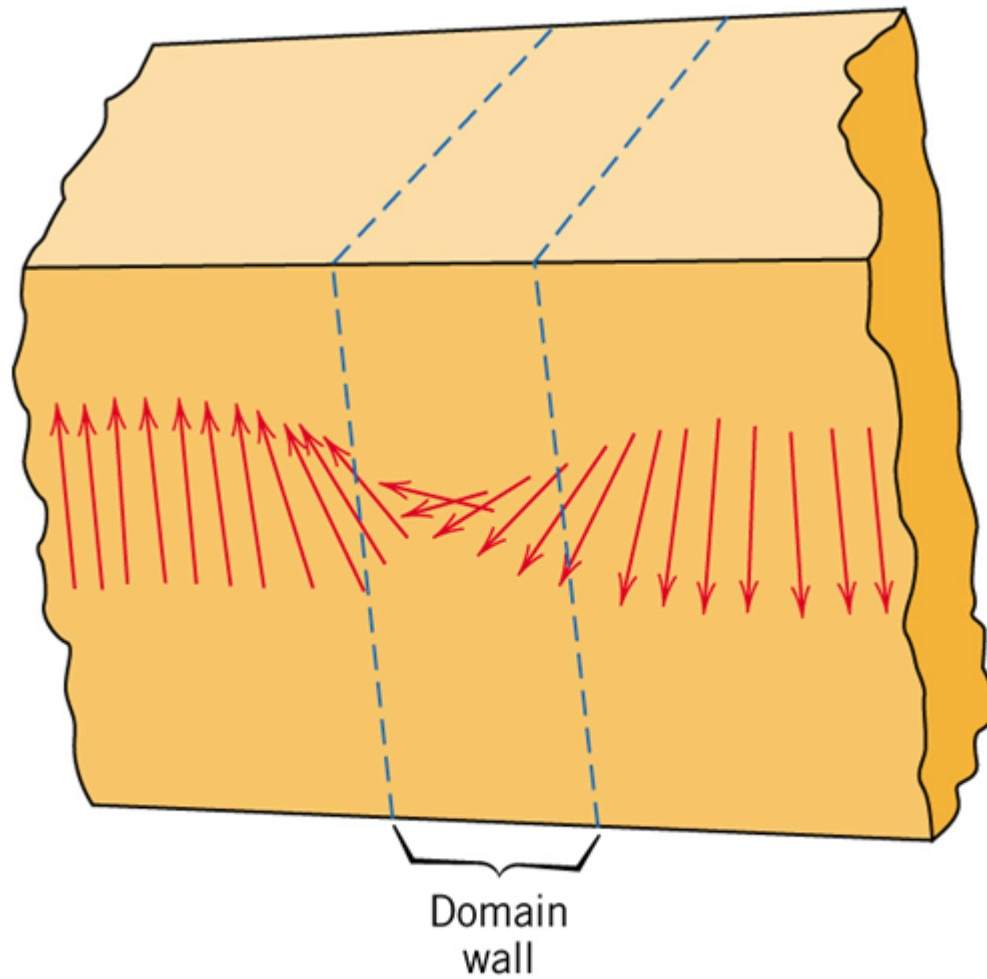


Figure 7.16. Gradual change in dipole orientation across a domain wall.

Figure 22.30

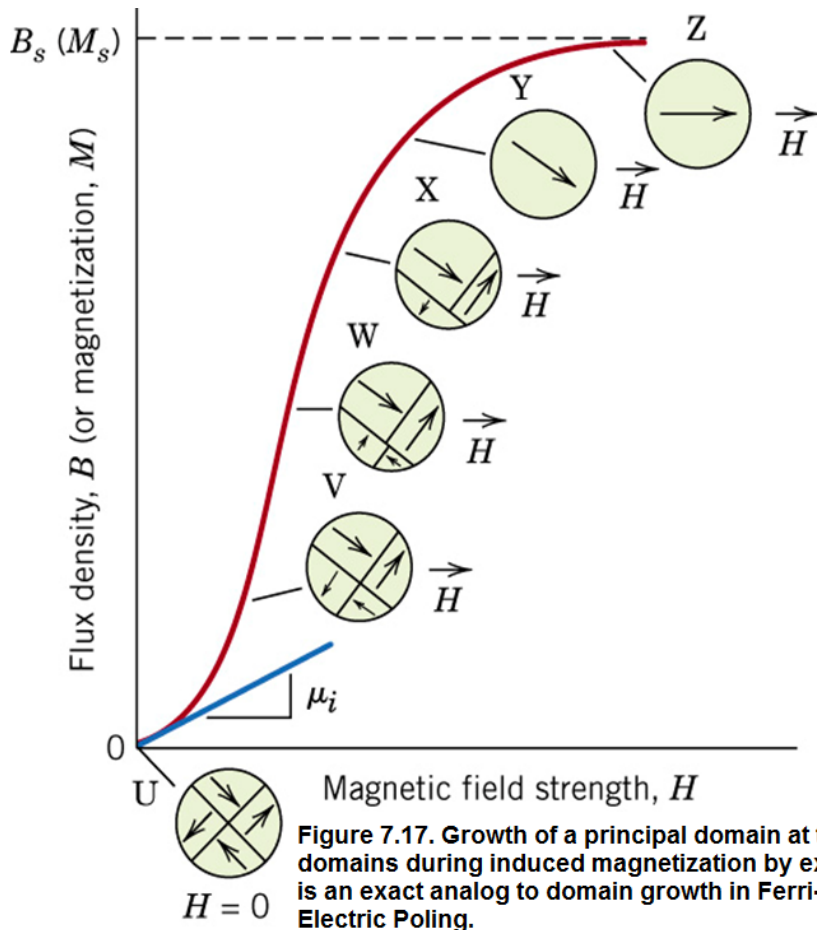


Figure 22.31

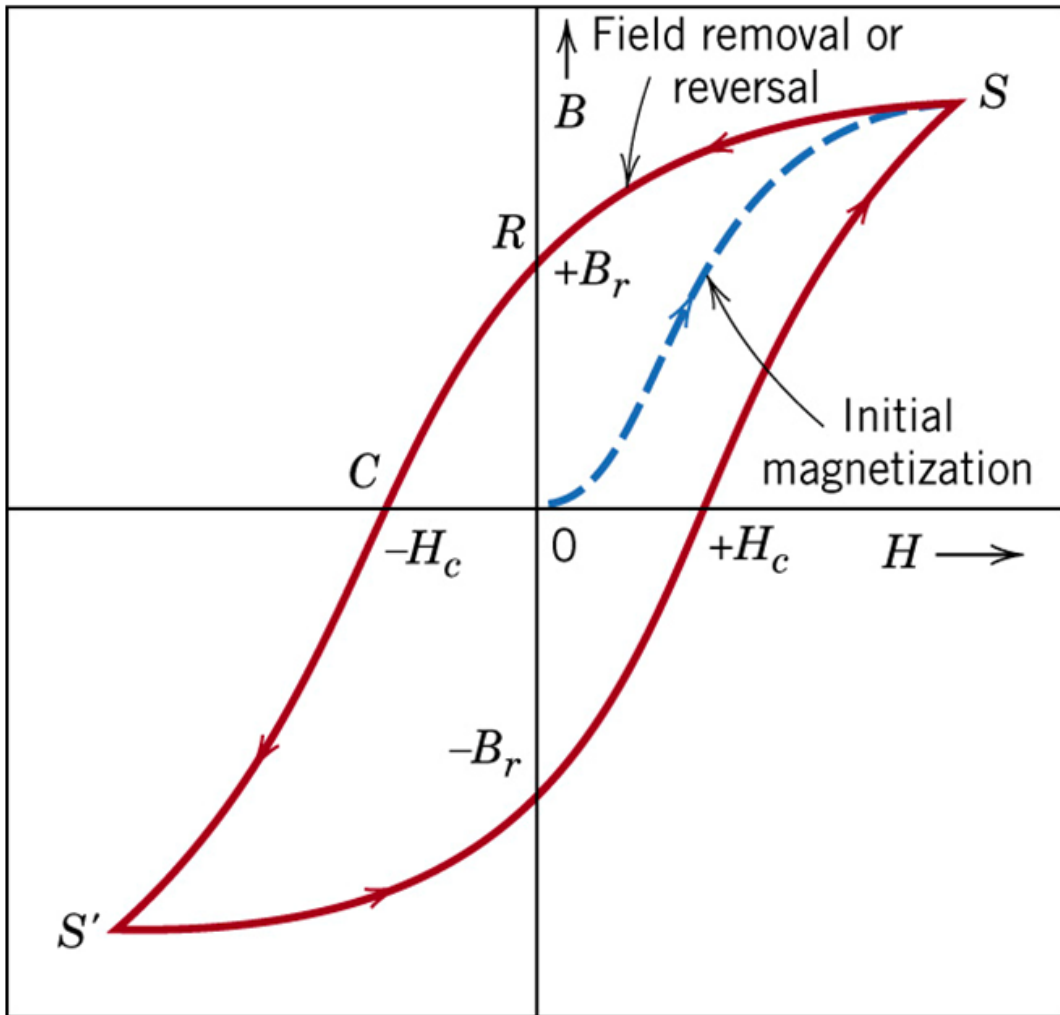


Figure 7.18. The Hysteresis Loop in a Ferromagnetic Material.

Figure 22.32

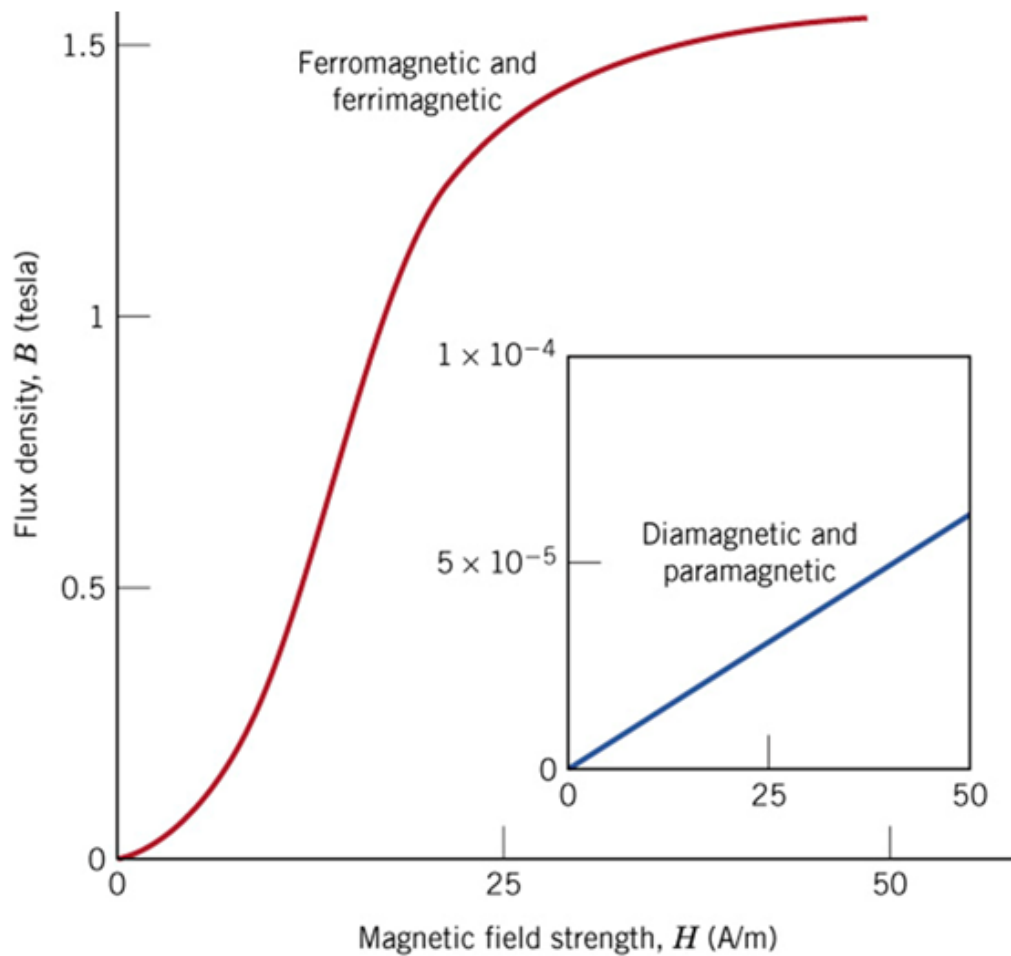


Figure 7.19. B-H curve for Ferromagnetic, Paramagnetic and diamagnetic materials.

Figure 22.33

Chapter 23

Chapter 7. Section 7.6.3. Hysteresis Loops of Hard Iron and Soft Iron.¹

Chapter 7. Section 7.6.3. Hysteresis Loops of Hard Iron and Soft Iron.

Figures are at the end of the module

In Figure 7.18. given in the previous module, the magnetization curves of Ferromagnetic materials, Paramagnetic Materials and Diamagnetic Materials are given. Para or Diamagnetic materials have linear magnetization curve hence there are no hysteresis loops and Ferromagnetic Materials have non-linear curves hence they have hysteresis loops. Hysteresis loop implies hysteresis loss.

This means in magnetizing or demagnetizing a ferromagnetic material, some energy is expended. The energy expended will depend on the ease with which we can magnetize a ferromagnetic material.

Soft irons are used in electro-mechanical relay switches as shown in Figure 7.19. An actuating current easily magnetizes the soft iron core and attracts the spring-loaded switch. In this process the electro-mechanical relay is closed. As the current is turned off the switch is immediately opened by spring action. The hysteresis loop of Soft Iron along side the hysteresis loop Hard Iron is shown in Figure 7.20.

As seen in Figure 7.20, soft iron has a much higher saturation Magnetization (B_{S2}) but hard iron has a much higher remnant Magnetization (B_r) as well as a much higher Coercive Magnetic Field (H_C).

Soft iron gives rise to temporary magnet whereas hard iron gives a permanent magnet. Because of high remnant Magnetization as well as a much higher Coercive Magnetic Field that hard iron becomes a permanent magnet.

Section 7.7. Theoretical basis of spontaneous Magnetization in Ferromagnets.

The theoretical basis of magnetism is the Orbital Angular Momentum of the orbital electrons in an atom and the Spin Angular Momentum of the spinning electron circulating around the nucleus of the atom.

Just as our Earth has orbital period of 365.25 days around the Sun but it has a spin period of 24 hours around its spin axis. In a similar fashion orbital electrons have orbital angular momentum J_L as well as it has J_S spin angular momentum.

Both these angular momentums give rise to dipole moments. Their parallel alignment can give rise to strong spontaneous magnetization as we find in magnetic materials such as FERRO-MAGNETIC Materials.

Their random alignment can give rise to weak spontaneous magnetization as we find in PARAMAGNETIC materials. Diamagnetic materials have no magnetization.

In 1915, Albert Einstein in team with W.J. de Hass (the son-in-law of the great Dutch physicist H.A.Lorentz) demonstrated that magnetism was a result of the alignments of electron's orbital magnetic moment and spin magnetic moment. As shown in Figure 7.21. they attached a soft iron cylinder from a friction less pivot. The soft iron was surrounded by solenoid. Whenever a impulsive current was passed through the solenoid, the soft iron got magnetized and experienced a rotary motion so as to keep the overall Angular momentum equal to zero.

¹This content is available online at <<http://cnx.org/content/m49954/1.1/>>.

This amply demonstrated that ferromagnetism is a result of the alignment of magnetic dipole moments due to orbital angular momentum and due to spin angular momentum.

But as we will see shortly that the spontaneous magnetization is primarily due to the spin angular momentum.

Section 7.7.1. Electron's orbital magnetic moment and spin magnetic moment.

By definition, a loop of orbiting electron has a dipole moment:

$$\mu = \text{Loop current} \times \text{loop cross-sectional area} = I \times \pi r^2 \quad (\text{A.m}^2) \quad 7.1$$

Figure 23.1

$$I = \text{loop current due to circulating electron} = -q \times \frac{v}{2\pi r} \quad 7.2$$

Figure 23.2

$$L(\text{orbital angular momentum of electron}) = \text{Moment of Inertia} \times \text{Angular Velocity}$$

Figure 23.3

Therefore

$$L = m_e r^2 \times \frac{v}{r} = m_e v r \quad 7.3$$

Figure 23.4

Substituting (7.2) and (7.3) into (7.1)

$$\mu_L = -q \times \frac{v}{2\pi r} \times \pi r^2 = -\frac{qvr}{2} = -\frac{q}{2m_e} \cdot L \quad 7.4$$

Figure 23.5

Magnetic Moment (μ) of Orbiting Electron is anti-parallel to Orbital Angular Momentum (L) as shown in Figure 7.22..

Similarly:

$$\mu_S = -\frac{q}{2m_e} \cdot S \text{ where } S = \text{Spin Angular Momentum} \quad 7.5.$$

Figure 23.6

In a preferred direction say Z-direction we have the projection of L and S on Z-axis.
We have seen in Quantum Mechanics that :

$$\mu_{LZ} = -\frac{q}{2m_e} \cdot m_l \hbar = -\frac{qh}{4\pi m_e} m_l \text{ where } m_l = 0, \pm 1, \pm 2 \dots \dots \pm l \text{ where } l = (n - 1) \quad 7.6$$

Figure 23.7

$$\mu_{SZ} = -\frac{q}{2m_e} \cdot \pm \left(\frac{1}{2}\right) \hbar = -\frac{qh}{4\pi m_e} \left(\pm \frac{1}{2}\right) \quad 7.5.$$

Figure 23.8

Here:

$$\mu_B(\text{Bohr Magnetron}) = \frac{qh}{4\pi m_e} = 9.274 \times 10^{-24} \frac{J}{T} = 5.788 \times 10^{-5} \frac{eV}{T} \quad 7.6.$$

Figure 23.9

Both spin and orbital angular momentum have a role to play as shown in Figure 7.23.

After detailed investigation it was found that in ferro-magnetic materials, spin angular momentum rather than orbital is the main contributor to Ferro-magnetism. The orbital angular momentum have a role to play but when there are uncompensated spins as in the case of transition elements the orbitals have negligible role to play.

Ferromagnetism occurs because of coupling of uncompensated spins in parallel direction. This coupling occurs directly and is called DIRECT EXCHANGE COUPLING or through intermediate anions usually Oxygen molecule through SUPER EXCHANGE.

In crystals this results in a net magnetic moments even at 300K. This is purely a Pauli-Exclusion Phenomena and Coulombic Interaction phenomena.

As shown in Figure 7.24., uncompensated spins of two atoms in an overlapping electron clouds have preference for parallel alignment (which contributes to net magnetic moment) rather than anti-parallel alignment (which is zero magnetic moment). Parallel alignment corresponds to lower energy level E_2 because of less columbic repulsion and anti-parallel alignment corresponds to higher energy level E_1 because of stronger columbic repulsion due to closer spatial proximity. So obviously the lower energy state is preferred hence there is spontaneous magnetization in elements with uncompensated spin electrons. This is the case for Transition Elements hence Fe,Co and Ni are the strongest ferromagnetic materials.

$$\Delta E = E_1 - E_2 = \text{exchange energy} \quad 7.7$$

Figure 23.10

At room temperature:

$$\Delta E \gg k_B 300K$$

Figure 23.11

Hence spontaneous magnetization is high up to Curie Temperature. At Curie Temperature exchange coupling is disrupted by thermal fluctuations and material becomes paramagnetic.

In Table 7.7.1. the Curie Temperatures of important Ferro-magnets are listed.

Table 7.7.1. Curie Temperatures of typical Ferromagnetic materials.

Materials	Curie Temperature (K)
Fe	1043
Co	1388
Ni	627
Gd	293

Table 23.1

Section 7.8. Magneto-crystalline Anisotropy.

In Figure 7.25. M-H curve for a single iron crystal is given. M-H depends on the crystal direction. As seen from the Figure 7.25, it is the easiest along [100] direction and hardest along [111] direction.

Section 7.9. Magnetostriction.

In Figure 7.26. magnetostriction is defined. The Iron crystal elongates along the easy X-direction but contracts along the Y-direction.

Section 7.10. Giant Magneto-Resistance used in hard discs of Computers.

Giant Magneto-Resistance(GMR) is widely used in hard disc memories of computers. It made its mass market debut when IBM commercialized its record breaking 16.8GB hard disc in computer market. IBM called it SPIN VALVE based on electronic spin.

In 1980, Peter Gruenberg of KFA Research Institute in Julich, Germany, and Albert Fert of the University of Paris-Sud saw large resistance change of 6% and 50% in Spin Valves.

In IBM, using sputtering, scientists built trilayer GMR as shown in Figure 7.27. and demonstrated a large resistance change.

As shown in the Figure 7.27 there are two Ferromagnetic Layers of Co separated by non-magnetic Cu layer.

A current flow through GMR experiences a Spin Valve effect.

What does this mean?

The tri-layer can have its ferromagnetic layer anti-parallel or parallel.

Anti-parallel FM layers behaves like a open valve offering large resistance and parallel FM layers behave like a close valve offering small resistance.

This is better clarified by the Figure 7.28.

The scattering of electron depends on the spin of the conducting electron. There are two cases:

Case 1: conducting electron spin is the same as the spin of the FM layer. This will undergo very weak scattering. Hence low resistance.

Case 2: conducting electron spin is opposite the spin of the FM layer. This will undergo very strong scattering Hence high resistance.

Now you examine the Figure 7.28.

We have two cases: Left Hand is parallel FM and right is anti-parallel FM. Its equivalent electrical circuit, considering all permutation of spins, are given below.

It is evident that Parallel FM has a much lower resistance and antiparallel FM offers a very high resistance path. We study GMR in the case when the current flows in the direction perpendicular to the layers. The GMR effect is exploited in magnetic field sensors and its applications range from automotive to information storage technology.

In Figure 7.29. the principle of longitudinal recording is illustrated.

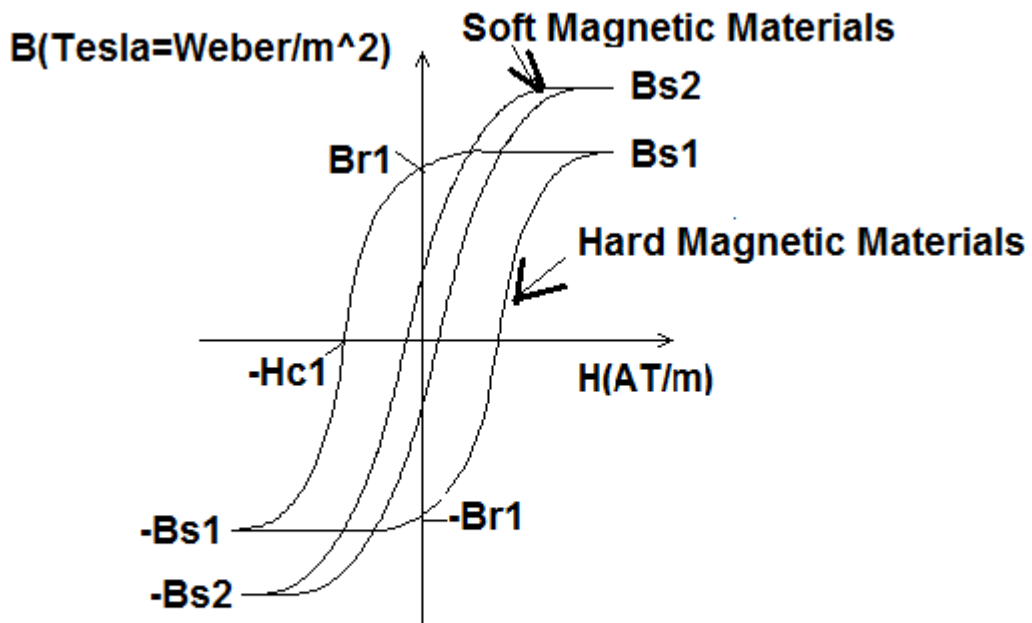


Figure 7.20. Hysteresis curves of soft magnetic material and hard magnetic material.

Figure 23.12

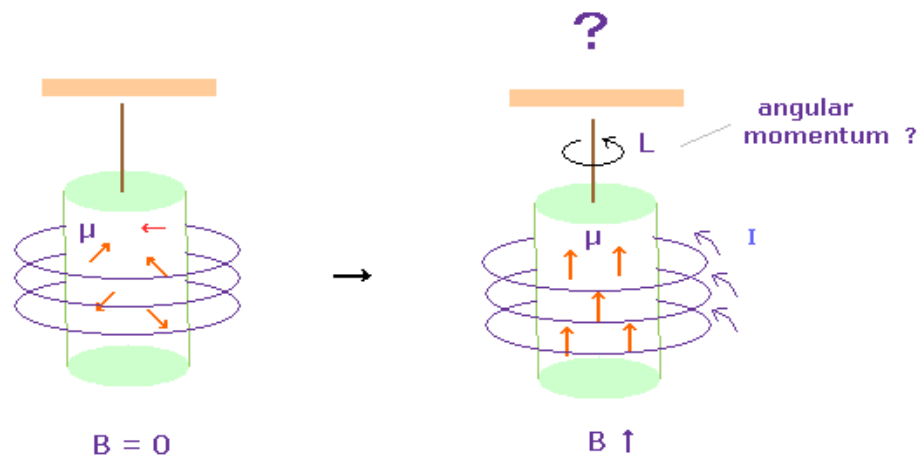


Figure 7.21. Experimental set-up for demonstrating Einstein-de Haas effect.

Figure 23.13

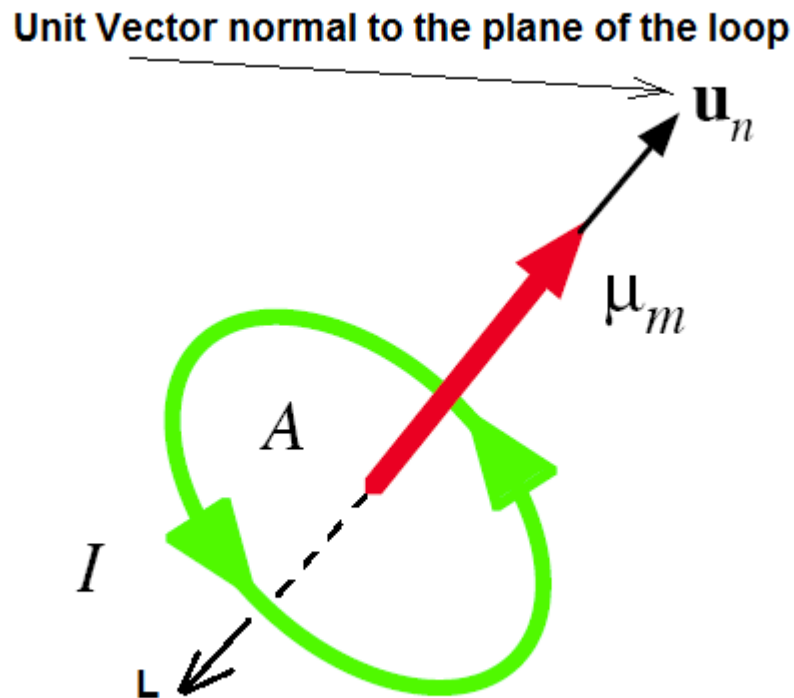
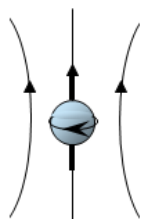
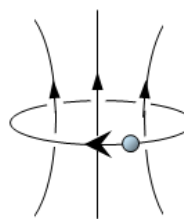


Figure 7.22. Magnetic dipole Moment due to a loop of current I and loop cross-sectional area A

Figure 23.14



Mysterious : Spin moment



Intuitive : Orbital moment

Figure 7.23. Contribution to magnetic dipole moment due to spin on the left and due to orbital motion on the right.

Figure 23.15

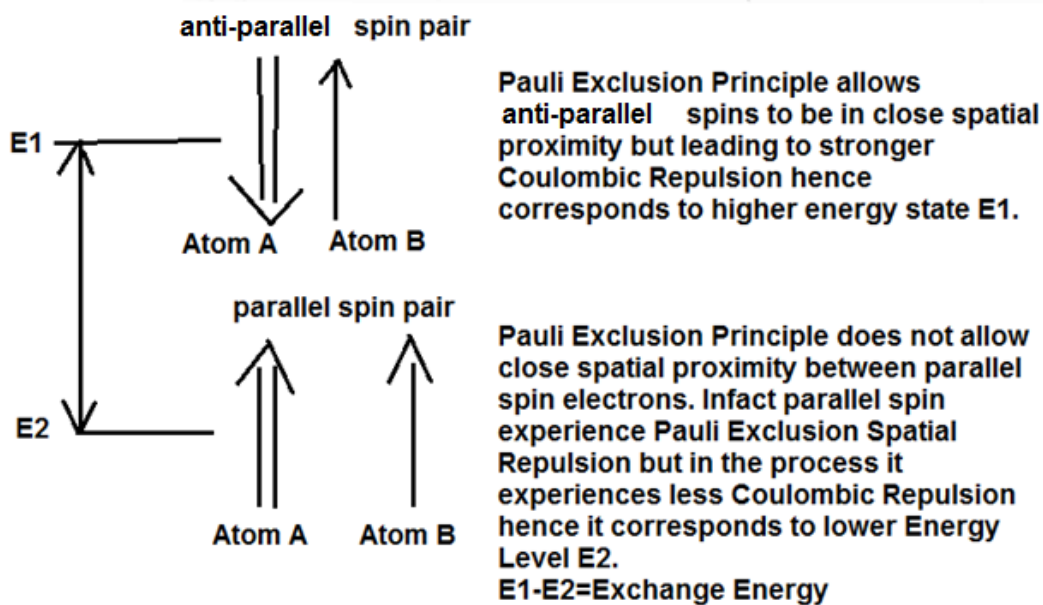


Figure 7.24 Illustration of Exchange Energy due to overlapping orbitals of two adjacent Atoms A and B.

Figure 23.16

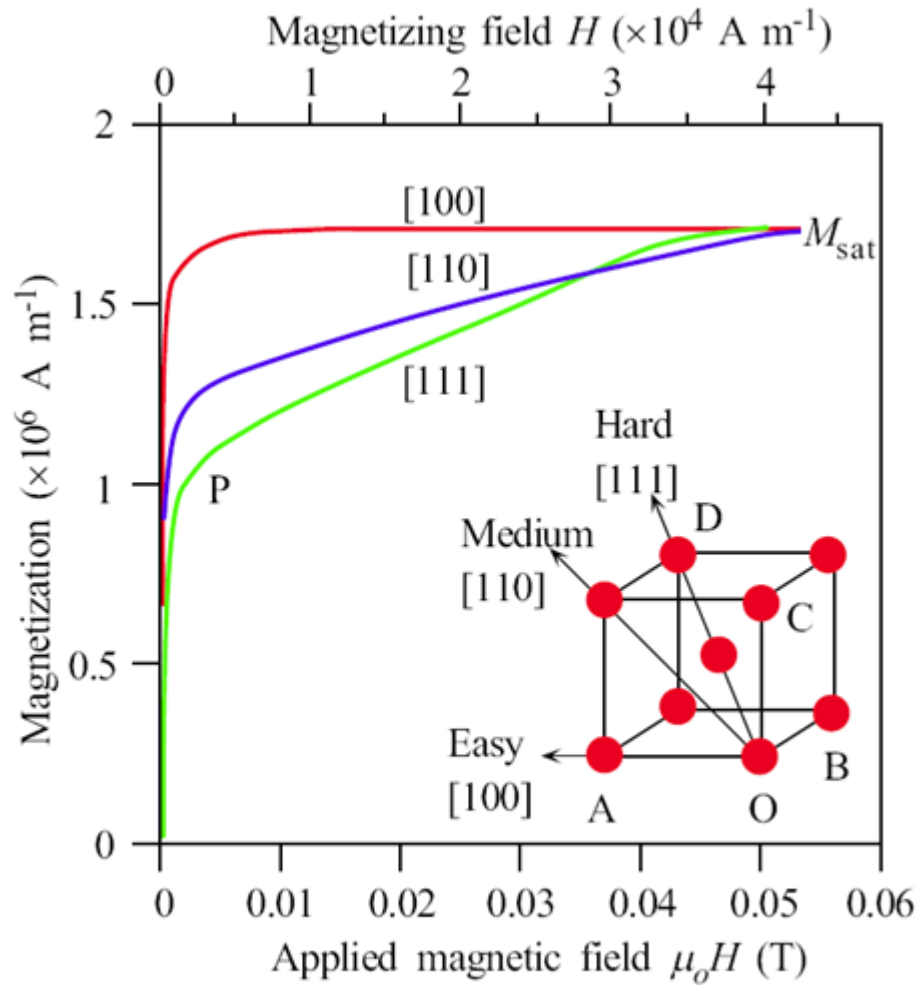


Figure 7.25. Magnetocrystalline anisotropy in single iron crystal

Figure 23.17

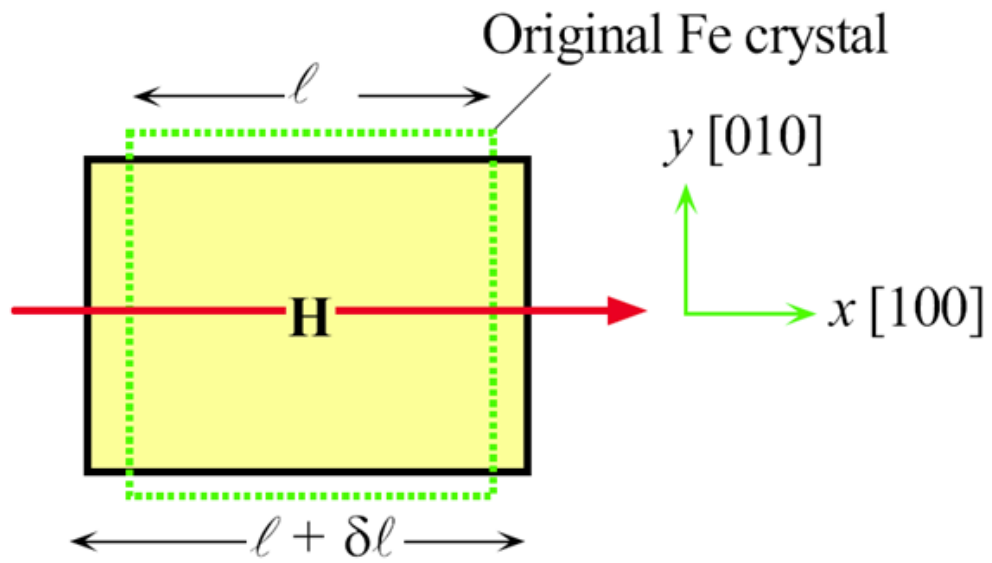


Figure 7.26. Illustration of Magnetostriction.

Figure 23.18

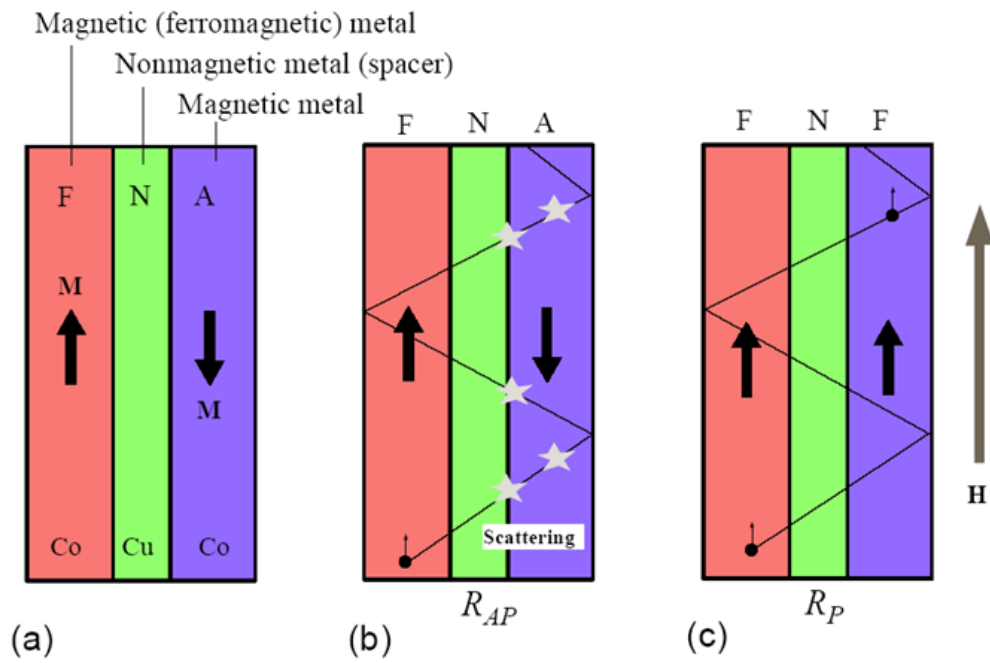


Figure 7.27. The structure of multi-layered Giant Magneto-Resistance (GMR) used in hard discs of a computer.

Figure 23.19

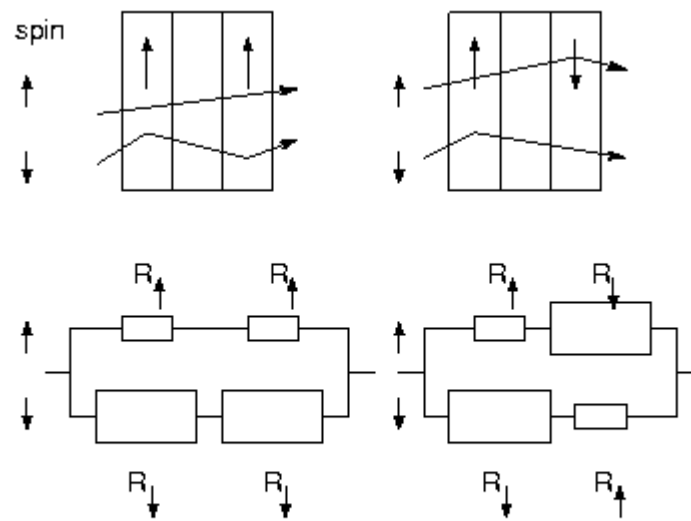


Figure 7.28. Parallel FM layers offer low resistance whereas antiparallel FM layers offer high resistance path.

Figure 23.20

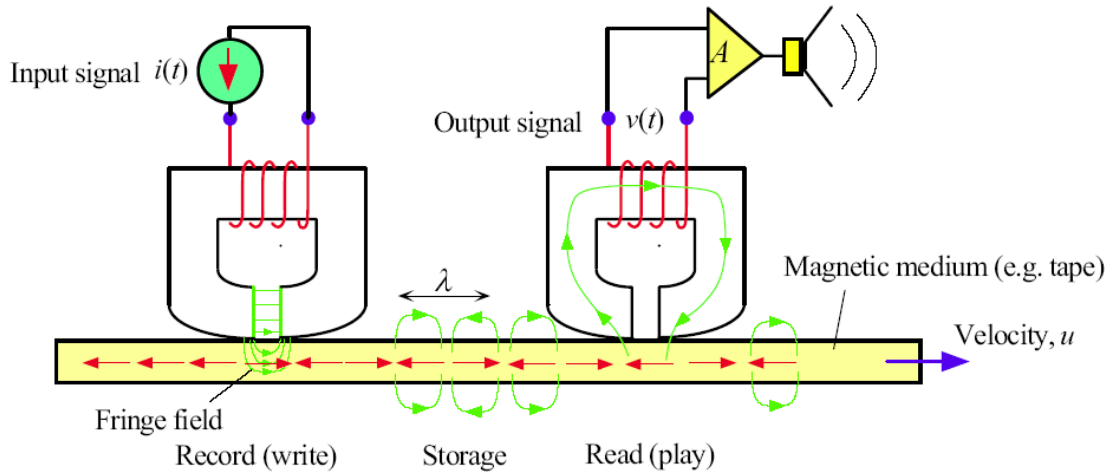


Figure 7.29. The principle of longitudinal magnetic recording on a flexible medium, e.g. magnetic tape in an audio cassette

Figure 23.21

Chapter 24

Chapter 8. Superconductors.¹

Chapter 8. Superconductors.[curtsey: <http://superconductors.org/history.htm>²]
[Figures are at the end of the Module]

Superconductors, materials that have no resistance to the flow of electricity, are one of the last great frontiers of scientific discovery. Not only have the limits of superconductivity not yet been reached, but the theories that explain superconductor behavior seem to be constantly under review. In 1911 superconductivity was first observed in mercury by Dutch physicist Heike Kamerlingh Onnes of Leiden University³. When he cooled it to the temperature of liquid helium, 4 degrees Kelvin (-452F, -269C), its resistance⁴ suddenly disappeared. The Kelvin scale represents an "absolute" scale of temperature. Thus, it was necessary for Onnes to come within 4 degrees of the coldest temperature that is theoretically attainable to witness the phenomenon of superconductivity. Later, in 1913, he won a Nobel Prize in physics for his research in this area.

The next great milestone in understanding how matter behaves at extreme cold temperatures occurred in 1933. German researchers Walther Meissner (above left) and Robert Ochsenfeld (above right) discovered that a superconducting material will repel a magnetic field (below graphic). A magnet moving by a conductor induces currents in the conductor. This is the principle on which the electric generator operates. But, in a superconductor the induced currents exactly mirror the field that would have otherwise penetrated the superconducting material - causing the magnet to be repulsed. This phenomenon is known as strong diamagnetism and is today often referred to as the "Meissner effect" (an eponym). The Meissner effect is so strong that a magnet can actually be levitated⁵ over a superconductive material.

In subsequent decades other superconducting metals, alloys and compounds were discovered. In 1941 niobium-nitride was found to superconduct at 16 K. In 1953 vanadium-silicon displayed superconductive properties at 17.5 K. And, in 1962 scientists at Westinghouse developed the first commercial superconducting wire, an alloy of niobium and titanium (NbTi). High-energy, particle-accelerator electromagnets made of copper-clad niobium-titanium were then developed in the 1960s at the Rutherford-Appleton Laboratory in the UK, and were first employed in a superconducting accelerator at the Fermilab Tevatron⁶ in the US in 1987.

The first widely-accepted theoretical understanding of superconductivity was advanced in 1957 by American physicists John Bardeen, Leon Cooper, and John Schrieffer (above). Their *Theories of Superconductivity* became known as the BCS theory⁷ - derived from the first letter of each man's last name - and won them a Nobel prize in 1972⁸. The mathematically-complex BCS theory explained superconductivity at temper-

¹This content is available online at <<http://cnx.org/content/m49955/1.1/>>.

²<http://superconductors.org/history.htm>

³<http://www.leiden.edu/>

⁴<http://superconductors.org/history.htm#resist>

⁵<http://superconductors.org/history.htm#meiss>

⁶<http://www.fnal.gov/>

⁷<http://superconductors.org/terms.htm#BCS>

⁸<http://www.nobel.se/physics/laureates/1972/>

atures close to absolute zero for elements⁹ and simple alloys¹⁰. However, at higher temperatures and with different superconductor systems, the BCS theory has subsequently become inadequate to fully explain how superconductivity is occurring.

Another significant theoretical advancement came in 1962 when Brian D. Josephson, a graduate student at Cambridge University¹¹, predicted that electrical current would flow between 2 superconducting materials - even when they are separated by a non-superconductor or insulator. His prediction was later confirmed and won him a share of the 1973 Nobel Prize in Physics. This tunneling phenomenon is today known as the "Josephson effect"¹² and has been applied to electronic devices such as the SQUID¹³, an instrument capable of detecting even the weakest magnetic fields.

The 1980's were a decade of unrivaled discovery in the field of superconductivity. In 1964 Bill Little of Stanford University had suggested the possibility of organic (carbon-based) superconductors. The first of these theoretical superconductors was successfully synthesized in 1980 by Danish researcher Klaus Bechgaard¹⁴ of the University of Copenhagen and 3 French team members. $(\text{TMTSF})_2\text{PF}_6$ had to be cooled to an incredibly cold 1.2K transition temperature (known as T_c) and subjected to high pressure¹⁵ to superconduct. But, its mere existence proved the possibility of "designer" molecules - molecules fashioned to perform in a predictable way.

Then, in 1986, a truly breakthrough discovery was made in the field of superconductivity. Alex Müller and Georg Bednorz, researchers at the IBM Research Laboratory in Rüschlikon, Switzerland, created a brittle ceramic compound that superconducted at the highest temperature then known: 30 K. What made this discovery so remarkable was that ceramics are normally insulators. They don't conduct electricity well at all. So, researchers had not considered them as possible high-temperature superconductor candidates. The Lanthanum, Barium, Copper and Oxygen compound that Müller and Bednorz synthesized, behaved in a not-as-yet-understood way. (Original article printed in *Zeitschrift für Physik Condensed Matter*, April 1986.)¹⁶ The discovery of this first of the superconducting copper-oxides (cuprates) won the 2 men a Nobel Prize the following year. It was later found that tiny amounts of this material were actually superconducting at 58 K, due to a small amount of lead having been added as a calibration standard - making the discovery even more noteworthy.

Müller and Bednorz' discovery triggered a flurry of activity in the field of superconductivity. Researchers around the world began "cooking" up ceramics of every imaginable combination in a quest for higher and higher T_c 's. In January of 1987 a research team at the University of Alabama-Huntsville substituted Yttrium for Lanthanum in the Müller and Bednorz molecule and achieved an incredible 92 K T_c . For the first time a material (today referred to as YBCO) had been found that would superconduct at temperatures warmer than liquid nitrogen - a commonly available coolant. Additional milestones have since been achieved using exotic - and often toxic - elements in the base perovskite¹⁷ ceramic. The current class (or "system") of ceramic superconductors with the highest transition temperatures are the mercuric-cuprates. The first synthesis of one of these compounds was achieved in 1993 at the University of Colorado and by the team of A. Schilling, M. Cantoni, J. D. Guo, and H. R. Ott of Zurich, Switzerland. The world record T_c of 138 K is now held by a thallium-doped, mercuric-cuprate comprised of the elements Mercury, Thallium, Barium, Calcium, Copper and Oxygen. The T_c of this ceramic superconductor¹⁸ was confirmed by Dr. Ron Goldfarb at the National Institute of Standards and Technology-Colorado in February of 1994. Under extreme pressure its T_c can be coaxed up even higher - approximately 25 to 30 degrees more at 300,000 atmospheres.

The first company to capitalize on high-temperature superconductors was Illinois Superconductor

⁹<http://superconductors.org/type1.htm>

¹⁰<http://superconductors.org/type2.htm#alloys>

¹¹<http://www.cam.ac.uk/>

¹²<http://superconductors.org/terms.htm#josephsn>

¹³<http://superconductors.org/history.htm#squid>

¹⁴http://superconductors.org/history.htm#klaus_b

¹⁵<http://superconductors.org/terms.htm#pressure>

¹⁶<http://superconductors.org/condmatt.htm>

¹⁷<http://superconductors.org/terms.htm#pero>

¹⁸<http://superconductors.org/type2.htm#record>

(today known as ISCO International¹⁹), formed in 1989. This amalgam of government, private-industry and academic interests introduced a depth sensor for medical equipment that was able to operate at liquid nitrogen temperatures ($\sim 77\text{K}$).

In recent years, many discoveries regarding the novel nature of superconductivity have been made. In 1997 researchers found that at a temperature very near absolute zero an alloy of gold and indium was both a superconductor and a natural magnet. Conventional wisdom held that a material with such properties *could not exist!* Since then, over a half-dozen such compounds²⁰ have been found. Recent years have also seen the discovery of the first high-temperature superconductor that does NOT contain any copper²¹ (2000), and the first all-metal perovskite superconductor²² (2001).

Also in 2001 a material that had been sitting on laboratory shelves for decades was found to be an extraordinary new superconductor. Japanese researchers measured the transition temperature of magnesium diboride at 39 Kelvin - far above the highest T_c of any of the elemental²³ or binary alloy²⁴ superconductors. While 39 K is still well below the T_c 's of the "warm" ceramic superconductors²⁵, subsequent refinements in the way MgB_2 is fabricated have paved the way for its use in industrial applications. Laboratory testing has found MgB_2 will outperform²⁶ NbTi and Nb_3Sn wires in high magnetic field applications like MRI²⁷.

Though a theory to explain high-temperature superconductivity still eludes modern science, clues occasionally appear that contribute to our understanding of the exotic nature of this phenomenon. In 2005, for example, Superconductors.ORG discovered that increasing the weight ratios of alternating planes within the layered perovskites can often increase T_c significantly²⁸. This has led to the discovery of more than 70 new high-temperature superconductors²⁹, including a candidate for a new world record³⁰.

The most recent "family" of superconductors to be discovered is the "pnictides". These iron-based superconductors were first observed by a group of Japanese researchers in 2006. Like the high- T_c copper-oxides, the exact mechanism that facilitates superconductivity in them is a mystery. However, with T_c 's over 50K ³¹, a great deal of excitement has resulted from their discovery.

Researchers do agree on one thing: discovery in the field of superconductivity is as much serendipity as it is science.

Section 8.1.Meissner Effect in Superconductors.

As the temperature falls below a critical temperature there is phase change and the metal under consideration becomes super-conductor as shown in Figure 8.1. In normal metal no such sudden drop in resistance is observed or measured.

In Figure 8.2. a long cylindrical YBCO bar is shown kept in an external magnetic field. Below critical temperature, as the metal becomes superconductor it becomes strongly diamagnetic. In presence of an external magnetic field, strong eddy currents are set up within the body which in accordance with Lenz's law completely excludes the external magnetic field from the interior of the body as shown in Figure 8.2.b. As the metal returns to normal condition above the critical temperature, external magnetic field passes through the body but causes no induced magnetization as shown in Figure 8.2.a.

Table 8.1. tabulates some well known superconductors and some recently discovered high temperature ceramics of cuprate variety. The record high critical temperature to date is 153K . It also tabulates the critical magnetic field above which superconductivity gets killed. For ceramic YBCO type superconductors also there is a critical Magnetic Field H_{C2} and H_{C1} but it has not been shown in the Table.

¹⁹<http://www.iscointl.com/>

²⁰<http://superconductors.org/type2.htm#shortlst>

²¹<http://superconductors.org/91k.htm>

²²<http://www.princeton.edu/%7Eppcm/past/Nugget%202001-IRG1-Superconductivity.htm>

²³<http://superconductors.org/Type1.htm>

²⁴<http://superconductors.org/type2.htm#alloys>

²⁵<http://superconductors.org/type2.htm>

²⁶http://superconductors.org/39K_updt.htm

²⁷<http://superconductors.org/Uses.htm>

²⁸<http://superconductors.org/32121212.htm>

²⁹<http://www.superconductors.org/50plus.htm>

³⁰<http://www.superconductors.org/77C.htm>

³¹<http://www.iop.org/EJ/abstract/0953-2048/21/8/082001>

Section 8.2. BCS theory of Superconductivity.

In 1957, John Bardeen, Leon Cooper and John Schriffer proposed the cooper pair theory. According to this theory electrons are Fermions and real particles with J_S (Spin Angular Momentum) = $\pm(1/2)$ hence susceptible to photon and defect scattering resulting in resistive metals.

But as temperature falls, electrons couple to form virtual particles with $J_S = 0$. These are Bosons which are virtual particles and hence not susceptible to photon and defect scattering. This leads to sudden drop in resistance as shown in Figure 8.1.

This theory came to be known as BCS Theory.

BCS Theory predicts isotope effect in the following manner:

$$M^{0.5}T_c = \text{Constant} \quad \text{here } M = \text{molar mass of the isotope} \quad 8.1$$

Figure 24.1

This equation predicts that for lighter isotopes super-conductivity can be maintained till higher temperatures.

BCS Theory predicts a critical Magnetic Field also. External Magnetic Fields greater than B_C (the critical magnetic flux density) kills the superconductivity phase of the given metal.

BCS theory is strictly for metals. It completely fails to explain the superconductivity in Cuprate Ceramics.

Table 8.1 Critical Temperatures and Magnetic Fluxes for Selected Superconducting Materials

<i>Material</i>	<i>Critical Temperature T_C (K)</i>	<i>Critical Magnetic Flux Density B_C (tesla)^a</i>
Elements^b		
Tungsten	0.02	0.0001
Titanium	0.40	0.0056
Aluminum	1.18	0.0105
Tin	3.72	0.0305
Mercury (α)	4.15	0.0411
Lead	7.19	0.0803
Compounds and Alloys^b		
Nb–Ti alloy	10.2	12
Nb–Zr alloy	10.8	11
PbMo ₆ S ₈	14.0	45
V ₃ Ga	16.5	22
Nb ₃ Sn	18.3	22
Nb ₃ Al	18.9	32
Nb ₃ Ge	23.0	30
Ceramic Compounds		
YBa ₂ Cu ₃ O ₇	92	—
Bi ₂ Sr ₂ Ca ₂ Cu ₃ O ₁₀	110	—
Tl ₂ Ba ₂ Ca ₂ Cu ₃ O ₁₀	125	—
HgBa ₂ Ca ₂ Cu ₂ O ₈	153	—

^a The critical magnetic flux density ($\mu_0 H_C$) for the elements was measured at 0 K. For alloys and compounds, the flux is taken as $\mu_0 H_{C2}$ (in teslas), measured at 0 K.

^b **Source:** Adapted with permission from *Materials at Low Temperatures*, R. P. Reed and A. F. Clark (Editors), American Society for Metals, Metals Park, OH, 1983.

Figure 24.2

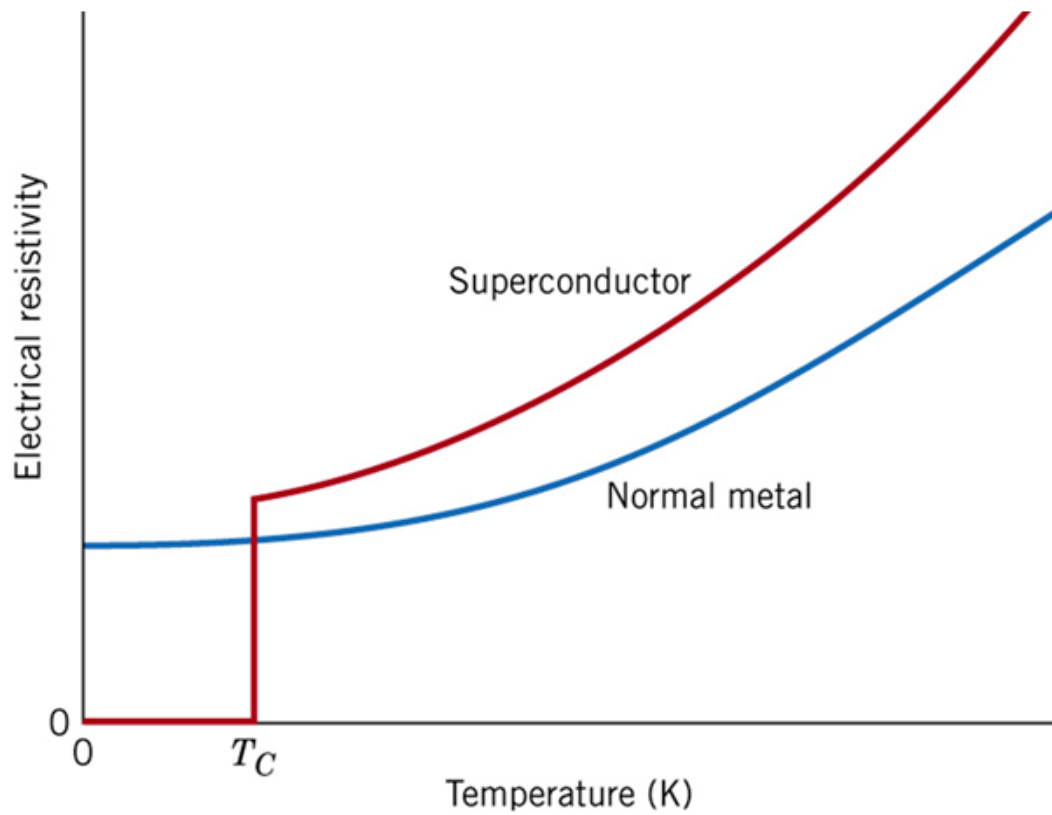


Figure 8.1 Electrical Resistivity vs Temp. curve shows a sharp drop in resistance of a superconductor below T_C (critical temperature). In normal metal no such critical temperature exists.

Figure 24.3

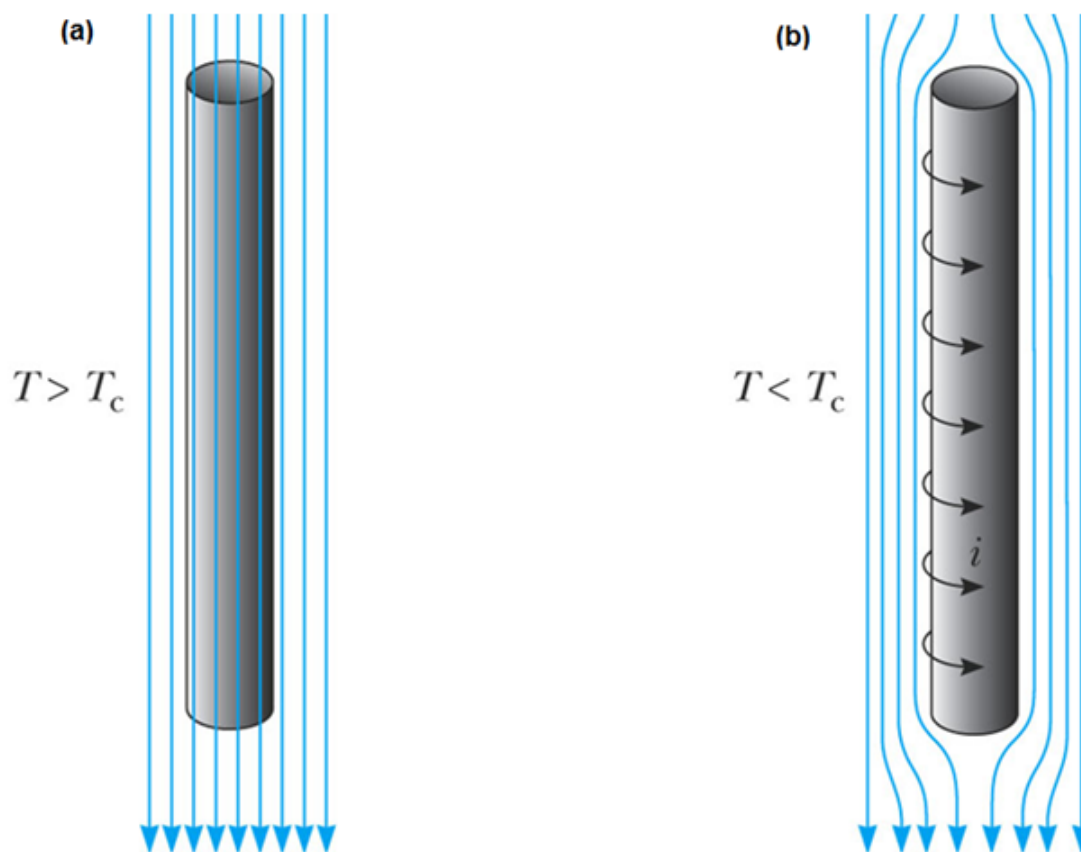


Figure 8.2. A superconductor bar is kept in an external magnetic field. When the temperature of the bar is below T_c , the field lines are undisturbed and pass normally through the metallic cylinder. But as soon as it is cooled below T_c , it abruptly excludes the external field as shown in (b). This drastic exclusion is because of strong eddy currents set up in the cylinder. These eddy currents in accordance with LENZ's Law oppose the external field and hence exclude it from the interior.

Figure 24.4

Index of Keywords and Terms

Keywords are listed by the section with that keyword (page numbers are in parentheses). Keywords do not necessarily appear in the text of the page. They are merely associated with that section. *Ex.* apples, § 1.1 (1) **Terms** are referenced by the page they appear on. *Ex.* apples, 1

- B** Bloch waves, six states of matter, effective density of states, § 12(91)
Bohr's Postulates, Synchrotron Radiation, Malmer Series, § 9(63)
- C** Czochralski method, crystal, § 1(1)
- E** Elastic Scattering, dissipative absorption, natural frequency, normal dispersion, § 15(119)
Ero-magnetic, Ferri-magnetic, Anti-ferro magnetic, Paramagnetic, Dia-magnetic materials., § 22(181)
- F** float zone method,, § 1(1)
- H** Hystersis, Exchange Energy, Magnetostriction, Giant Magneto Resistance., § 23(207)
- I** intrinsic carrier concentration, § 12(91)
Ionic Bonding, Crystalline Bonding, Metallic Bonding, Van-der Waal weak force bonding, § 8(53)
- L** Loss Angle, Piezoelectric Effect, Electrical Analog, Series Resonance Path., § 16(127)
- M** MBE, LPE, CVPD, Ultra High Vacuum, Ion Pump, § 4(17)
Mean Free Time, Relaxation Time, Mobility, Fermi Level., § 10(75)
Metamaterials, negative refractive index, characteristic impedance, diffraction limit of Abbe, § 21(177)
- N** nanoscience, nanotechnology, iridescent blue, carbon-nano tubes, fullerenes, § 18(139)
- O** orientation,, § 1(1)
- P** Photonics, Band-gap Engineering, Ternary Alloys, Quaternary Alloys, § 13(101)
Piezo-electricity, ferro-electricity, paraelectricity., § 17(133)
Primary Flat, Secondary Flat, Major Flat, Miller Index, Crystal Orientation, § 3(13)
- Q** Quantum Dots, Tunability, Potential Well, § 19(157)
Quantum Numbers, Coordination Number, Avogadro's Number., § 20(169)
- R** Random Thermal Motion, net displacement, mean free time, mean free path, § 11(79)
- S** Semiconductor, Metals and Insulators., § 6(35)
Solid, liquid, gaseous, plasma, bose-einstein condensate, § 7(37)
Superconductor, Meissner effect, Cuprates, high temperature ceramic superconductor, § 24(221)
- T** Taper, Flatness, Circular Saw Blade, Diamond impregnation, § 2(9)
Tutorial, worked out example, chart, § 5(27)
- W** Wave Theory of Light, Corpuscular Theory of Light, Maxwell, Aether., § 14(107)

Attributions

Collection: *Electrical and Electronic Materials Science*

Edited by: Bijay_Kumar Sharma

URL: <http://cnx.org/content/col11615/1.14/>

License: <http://creativecommons.org/licenses/by/4.0/>

Module: "Crystal Growth-Bulk and Epitaxial Film-Part 1"

By: Bijay_Kumar Sharma

URL: <http://cnx.org/content/m34199/1.1/>

Pages: 1-8

Copyright: Bijay_Kumar Sharma

License: <http://creativecommons.org/licenses/by/3.0/>

Module: "Crystal Growth-Bulk and Epitaxial Film-Part 2"

By: Bijay_Kumar Sharma

URL: <http://cnx.org/content/m34200/1.2/>

Pages: 9-12

Copyright: Bijay_Kumar Sharma

License: <http://creativecommons.org/licenses/by/3.0/>

Module: "Crystal Growth-Bulk and Epitaxial Film-Part 3"

By: Bijay_Kumar Sharma

URL: <http://cnx.org/content/m34202/1.4/>

Pages: 13-16

Copyright: Bijay_Kumar Sharma

License: <http://creativecommons.org/licenses/by/3.0/>

Module: "Crystal Growth-Bulk and Epitaxial Film-Part 4"

By: Bijay_Kumar Sharma

URL: <http://cnx.org/content/m34203/1.1/>

Pages: 17-26

Copyright: Bijay_Kumar Sharma

License: <http://creativecommons.org/licenses/by/3.0/>

Module: "Tutorial on Chapter 1-Crystal and Crystal Growth."

By: Bijay_Kumar Sharma

URL: <http://cnx.org/content/m48918/1.1/>

Pages: 27-33

Copyright: Bijay_Kumar Sharma

License: <http://creativecommons.org/licenses/by/3.0/>

Module: "Syllabus of EC1419A_Electrical and Electronic Materials Science"

By: Bijay_Kumar Sharma

URL: <http://cnx.org/content/m48856/1.1/>

Page: 35

Copyright: Bijay_Kumar Sharma

License: <http://creativecommons.org/licenses/by/3.0/>

Module: "Chapter 2. Solid State of Matter."

By: Bijay_Kumar Sharma

URL: <http://cnx.org/content/m49804/1.1/>

Pages: 37-52

Copyright: Bijay_Kumar Sharma

License: <http://creativecommons.org/licenses/by/4.0/>

Module: "Chapter 2. Section 2.3.2. Application of Inert Gases."

By: Bijay_Kumar Sharma

URL: <http://cnx.org/content/m49811/1.1/>

Pages: 53-61

Copyright: Bijay_Kumar Sharma

License: <http://creativecommons.org/licenses/by/4.0/>

Module: "Chapter 2. Solid State of Matter. Section.2.5. Bohr Model of Hydrogen Atom."

By: Bijay_Kumar Sharma

URL: <http://cnx.org/content/m49815/1.1/>

Pages: 63-74

Copyright: Bijay_Kumar Sharma

License: <http://creativecommons.org/licenses/by/4.0/>

Module: "Tutorial on Chapter 2: Insulator, Semi-conductor and Metal."

By: Bijay_Kumar Sharma

URL: <http://cnx.org/content/m49555/1.2/>

Pages: 75-78

Copyright: Bijay_Kumar Sharma

License: <http://creativecommons.org/licenses/by/4.0/>

Module: "SSPD_Chapter 1_Part 12_Quantum Mechanical Interpretation of Resistance"

By: Bijay_Kumar Sharma

URL: <http://cnx.org/content/m34450/1.1/>

Pages: 79-90

Copyright: Bijay_Kumar Sharma

License: <http://creativecommons.org/licenses/by/3.0/>

Module: "SSPD_Chapter 1_Part 11_Solid State of Matter"

By: Bijay_Kumar Sharma

URL: <http://cnx.org/content/m34343/1.1/>

Pages: 91-100

Copyright: Bijay_Kumar Sharma

License: <http://creativecommons.org/licenses/by/3.0/>

Module: "Chapter 3. Special Classification of Semiconductors.Sec3.1.Compund Semiconductors"

By: Bijay_Kumar Sharma

URL: <http://cnx.org/content/m49543/1.1/>

Pages: 101-106

Copyright: Bijay_Kumar Sharma

License: <http://creativecommons.org/licenses/by/4.0/>

Module: "Chapter 4.Light and Matter – Dielectric Behaviour of Matter"

By: Bijay_Kumar Sharma

URL: <http://cnx.org/content/m49722/1.1/>

Pages: 107-117

Copyright: Bijay_Kumar Sharma

License: <http://creativecommons.org/licenses/by/4.0/>

Module: "Section 4.2. Dielectric and its Physics."

By: Bijay_Kumar Sharma

URL: <http://cnx.org/content/m49723/1.2/>

Pages: 119-126

Copyright: Bijay_Kumar Sharma

License: <http://creativecommons.org/licenses/by/4.0/>

Module: "Section 4.3. Dielectric Loss."

By: Bijay_Kumar Sharma

URL: <http://cnx.org/content/m49782/1.1/>

Pages: 127-132

Copyright: Bijay_Kumar Sharma

License: <http://creativecommons.org/licenses/by/4.0/>

Module: "Section 4.5. Piezo-electricity and Ferro-electricity."

By: Bijay_Kumar Sharma

URL: <http://cnx.org/content/m49792/1.1/>

Pages: 133-137

Copyright: Bijay_Kumar Sharma

License: <http://creativecommons.org/licenses/by/4.0/>

Module: "Chapter 5_ Introduction-Nanomaterials."

By: Bijay_Kumar Sharma

URL: <http://cnx.org/content/m49713/1.1/>

Pages: 139-155

Copyright: Bijay_Kumar Sharma

License: <http://creativecommons.org/licenses/by/4.0/>

Module: "Section 5.4. Nano-Size Effect on various opto-electronic-magnetic properties of nano materials."

By: Bijay_Kumar Sharma

URL: <http://cnx.org/content/m49719/1.1/>

Pages: 157-168

Copyright: Bijay_Kumar Sharma

License: <http://creativecommons.org/licenses/by/4.0/>

Module: "EVEN SEMESTER2014-MidSemester Examination Answers"

By: Bijay_Kumar Sharma

URL: <http://cnx.org/content/m49733/1.1/>

Pages: 169-175

Copyright: Bijay_Kumar Sharma

License: <http://creativecommons.org/licenses/by/4.0/>

Module: "Chapter 5. Section 5.6. Metamaterials."

By: Bijay_Kumar Sharma

URL: <http://cnx.org/content/m49939/1.1/>

Pages: 177-179

Copyright: Bijay_Kumar Sharma

License: <http://creativecommons.org/licenses/by/4.0/>

Module: "Chapter 7. Magnetic Materials."

By: Bijay_Kumar Sharma

URL: <http://cnx.org/content/m49953/1.1/>

Pages: 181-205

Copyright: Bijay_Kumar Sharma

License: <http://creativecommons.org/licenses/by/4.0/>

Module: "Chapter 7. Section 7.6.3. Hysteresis Loops of Hard Iron and Soft Iron."

By: Bijay_Kumar Sharma

URL: <http://cnx.org/content/m49954/1.1/>

Pages: 207-220

Copyright: Bijay_Kumar Sharma

License: <http://creativecommons.org/licenses/by/4.0/>

Module: "Chapter 8. Superconductors."

By: Bijay_Kumar Sharma

URL: <http://cnx.org/content/m49955/1.1/>

Pages: 221-227

Copyright: Bijay_Kumar Sharma

License: <http://creativecommons.org/licenses/by/4.0/>

Electrical and Electronic Materials Science

This is a full semester course having 42 lecture classes. This covers the materials being used in Solid State Devices.

About OpenStax_{CNX}

Rhaptos is a web-based collaborative publishing system for educational material.